



HAL
open science

New supramolecular assemblies based on Cu(I) ion bearing an irreversible thermal transition of their solid state luminescence

Florent Moutier

► **To cite this version:**

Florent Moutier. New supramolecular assemblies based on Cu(I) ion bearing an irreversible thermal transition of their solid state luminescence. Chemical engineering. INSA de Rennes, 2022. English. NNT: 2022ISAR0022 . tel-04513144

HAL Id: tel-04513144

<https://theses.hal.science/tel-04513144>

Submitted on 20 Mar 2024

HAL is a multi-disciplinary open access archive for the deposit and dissemination of scientific research documents, whether they are published or not. The documents may come from teaching and research institutions in France or abroad, or from public or private research centers.

L'archive ouverte pluridisciplinaire **HAL**, est destinée au dépôt et à la diffusion de documents scientifiques de niveau recherche, publiés ou non, émanant des établissements d'enseignement et de recherche français ou étrangers, des laboratoires publics ou privés.

THESE DE DOCTORAT DE

L'INSTITUT NATIONAL DES SCIENCES
APPLIQUEES RENNES

ECOLE DOCTORALE N° 596
Matière, Molécules, Matériaux
Spécialité : Chimie Moléculaire et Macromoléculaire

Par

Florent Moutier

New supramolecular assemblies based on Cu(I) ion bearing an irreversible thermal transition of their solid state luminescence

Thèse présentée et soutenue à Rennes, le 23 Novembre 2022
Unité de recherche : Institut des Sciences Chimiques de Rennes, INSA Rennes
Thèse N° : 22ISAR 28 / D22 - 28

Rapporteurs avant soutenance :

Sandrine PERRUCHAS
Igor KOSHEVOY

Chargée de recherche, CNRS, Institut des Matériaux de Nantes Jean Rouxel
Professor, University of Eastern Finland

Composition du Jury :

Présidente : Karine COSTUAS
Examineurs : Sandrine PERRUCHAS

Igor KOSHEVOY
Manfred SCHEER

Directrice de Recherche, CNRS, ISCR Université de Rennes 1
Chargée de recherche, CNRS, Institut des Matériaux de Nantes Jean Rouxel
Professor, University of Eastern Finland
Professor Doctor, Universität Regensburg

Dir. de thèse : Christophe LESCOP

Directeur de recherche, CNRS, ISCR Institut National des Sciences Appliquées de Rennes

Co-encadrant de thèse : Guillaume CALVEZ

Maître de conférences, ISCR, Institut National des Sciences Appliquées de Rennes

Acknowledgments :

I would first like to thank my supervisor during these years, Christophe LESCOP, for offering me this opportunity, and for supporting and guiding me toward the completion of my thesis. It was three long years, yet they flew by rapidly especially because of covid, starting halfway through the first year, and continuing during the better part of the second year. Despite this major hardship, we were, with a bit of luck, able to go on an exchange with the City University of Hong-Kong and numerous exchange with Universität Regensburg, from which I keep very good memories. I deeply appreciate the energy you put in your work and I think I will start to miss hearing you calling out my name across the corridor to discuss about a reaction or a result.

Once again, I thank you Christophe, for having given me this chance, and I hope to be able to continue to read about your chemistry, to which I have brought my modest contribution, for many years to come. Thank you.

I would like to express my gratitude to the jury members for accepting to participate in the evaluation of this work. I would like to thank Lucie Norel and Khalil Hanna for following my work through the different CSI reports. I would like to deeply thank Sandrine Perruchas and Igor Koshevoy, which agreed to review this thesis before the defense. As I am writing these lines, the defense is still a month away, but I eagerly look forward the discussion with them concerning my research works as well as with the other members of my jury, Karine Costuas and Manfred Scheer, which I also deeply thank.

I would then like to thank all the wonderful people of the CSM INSA team which I worked with during these years. First, the permanent members, some of which I shared practical work tutoring for the INSA students with, Yan, Valérie, Carole, Olivier, Kevin and Nathalie, which I had the pleasure to work under her supervision during an internship in my first year of master studies. I would like to thank in particular Guillaume Calvez, who trained me and helped for the multiple luminescent measurements that I had to conduct during my thesis. Lastly, I would like to thank Isabelle and Stéphane, for being the pillars of the lab. Their help is invaluable to keeping the lab working smoothly on a day to day basis.

Next, I would like to thank the other PhD and Post Doc students that I shared the office with. First, Ali which was here during the beginning of the works all the way back in 2017. Then, Chendong, which started his PhD studies at the same time as me : Thank you for the discussions in the lab, and good luck for your defense wich will not be long after mine. I would like to express my thanks toward Jana, Constance and Adrien, the post doc students which worked with me during these years and to which I had great pleasure to discuss and interact with everyday. Adrien especially helped, almost as soon as he arrived, to organize the weekly students' trip to the bar. We now know where we go and when we depart at least few hours in advance.

Deep thanks to all the other students in the office, Félix, Chloé, Thibaut and Lowik, as well as all the numerous internship students that were present at some point in the rooms of the lab. I wish to all of you great success in all your future endeavors.

Finally, I would like to thank the people that supported me from outside the walls of the INSA, and to do so, I will switch to french.

Un profond merci à mes amis de longue date : Thibault, Médéric et Gabriel. Une amitié aussi longue qui remonte à l'école primaire et au collège, c'est assez rare et je l'apprécie fortement, et même si nous ne sommes pas souvent physiquement ensemble, nos discussions et parties en ligne aident grandement à libérer du stress et à penser à autre chose. J'espère que je ne vous bassine pas trop avec mes inepties scientifiques ! Merci beaucoup les gars.

Enfin, je tiens à remercier profondément les membres de ma famille, mon père Thierry, ma mère Christèle et mon frère Guillaume, pour m'avoir soutenu durant ces longues années d'études et je sais que je peux compter sur vous dans les moments d'incertitude ou de doute. Cela fait maintenant six ans que je suis à Rennes, et même si je ne rentre pas souvent à la maison, les appels réguliers du samedi sont un moment que j'affectionne particulièrement. Merci.

To all of you and many others, thank you very much.

Table of contents :

Table of abbreviations	5
Résumé en français.....	7
Références	20
Chapter I Introduction to the context of the study	21
I-1 Generalities on copper	22
I-1.a History of copper metal	22
I-1.b Copper as an element in chemistry	23
I-2 Generalities on luminescence	24
I-2.a Origin of luminescence	24
I-2.b Different kind of luminescent processes	25
I-2.c Luminescent properties of heavy transition metals and copper.....	27
I-3 Thermally activated delayed fluorescence.....	31
I-4 Cu(I) complexes presenting TADF properties	33
I-4.a History of Cu(I) based TADF complexes.....	33
I-4.b Organic versus Cu(I) based TADF emitters.....	35
I-5 Synthesis strategies for designing polymetallic Cu(I) complexes.....	38
I-5.a Supramolecular chemistry, history and interest.....	38
I-5.b Coordination Driven Supramolecular chemistry	39
I-5.c Use of CDS in the context of Cu(I) compounds	39
I-5.d Development of « U-shape » bimetallic Cu(I) precursors for usage in CDS chemistry	41
References of chapter I.....	45
Chapter II Preparation of a series of Cu(I) based 1D coordination polymers and study of their solid-state and luminescence properties.....	51
II-1 Presentation of the Cu(I) bimetallic precursor used.....	51
II-2 Synthesis of a series of Cu(I) one dimensional coordination polymers	55

II-3 Infrared spectroscopic characterization of the compounds C_n	56
II-4 Structural characterization of compounds C_n by single crystal X-ray diffraction studies	60
II-5 Photophysical studies of the compounds C_n	64
II-5.a Solid-state UV-visible absorption study of the polymers C_n	64
II-5.b Solid-state excitation spectra of the polymers C_n	66
II-5.c Solid-state emission spectra of the polymers C_n	67
II-5.d Measurements of the lifetime of the excited states of the polymers C_n	72
II-5.e Quantum yield measurements of the polymers C_n	76
II-5.f Tentative assignment of the photophysical properties of polymers C_n	76
II-5.g Luminance measurements of the polymers C_n	77
II-6 Thermal properties of the polymers C_n	79
II-7 Conclusion.....	83
References of chapter II	85
Chapter III Study of irreversible thermal transition occurring in the solid-state for the polymers C_n.....	87
III-1 Study of the high temperature behavior in the solid-state of the precursor A	87
III-1.a TGA-DTA measurements of precursor A.....	87
III-1.b Infrared spectroscopy of transited phase A'	89
III-1.c Powder X-ray diffraction of transited precursor A'	90
III-1.d Luminescence properties of thermally transited precursor A'	93
III-1.e Thermal behavior of the transited phase A'	98
III-2 Effect of the transition on the polymers C_n	100
III-2.a Infrared measurements of the transited compounds C_n'	100
III-2.b Hypothesis of the nature of the thermal transition.....	104
III-2.c Photophysical properties of the thermally transited C_n' compounds	105
III-2.c.i Solid-state UV-visible absorption spectra.....	107
III-2.c.ii Luminescent properties of transited compounds C_n'	109

III-2.c.iii Lifetime measurements of the transited compounds C_n'	111
III-2.c.iv Quantum yields and luminance of the transited compounds C_n'	111
III-2.d Powder X-ray diffraction of transited phases C_n'	112
III-2.e Thermal properties of the transited phase C_n'	116
III-3 Recovering the initial luminescence post thermal transition	118
III-3.a Solid-state infrared spectroscopy measurements on the C_6' DCM phase	118
III-3.b Powder X-ray diffraction on the regenerated phase C_6' DCM	120
III-3.c Photophysical properties of the regenerated polymer C_6' DCM	122
III-3.c.i Solid-state UV-visible absorption spectrum	123
III-3.c.ii Luminescence properties of the C_6' DCM phase	124
III-3.c.iii Thermal behavior of the C_6' DCM phase	127
III-4 Conclusion on the irreversible thermal transition of the polymers C_n	128
References of chapter III	130
Chapter IV Toward the obtention of alternative self-assembled luminescent Cu(I) multimetallic species	131
IV-1 Synthesis and structural characterization of the metallacycles D_x	132
IV-2 Photophysical measurements of the tetrametallic metallacycles D_x	138
IV-2.a Solid-state UV-visible absorption spectrum	138
IV-2.b Solid-state luminescence of the metallacycles D_x	139
IV-3 Thermal stability study of the D_x tetrametallic metallacycles	146
IV-4 Conclusion	149
References to chapter IV	151
General conclusion	153
Appendix	156
I-General appendix	156
II-Appendix to chapter II	159
III-Appendix to chapter III	196

IV-Appendix to chapter IV	234
References	249

Table of abbreviations :

1D	One-Dimensional
2D	Two-Dimensional
Å	Angstrom
Cd	Candela
CDS	Coordination Driven Supramolecular (chemistry)
CH₂Cl₂/DCM	Dichloromethane
CH₃CN	Acetonitrile
CuBr	Copper Bromide
CuCl	Copper Chloride
CuI	Copper Iodide
dppm	Bis(diphenylphosphino)methane
eV	Electron Volt
EQY	Emission Quantum Yield
EQE	External Quantum Efficiency
FWHM	Full Width at Half Maximum
HMI	Heavy Metal Ions
HOMO	Highest Occupied Molecular Orbital
I₈₀/I_{RT}	Ratio of the intensity of emission at 80 K and the intensity at room temperature
IC	Internal Conversion
ILCT	IntraLigand Charge Transfer
IR	InfraRed
ISC	InterSystem Crossing
k_r / k_{nr}	Radiative and Non-Radiative rate constants

LUMO	Lowest Unoccupied Molecular Orbital
MLCT	Metal to Ligand Charge Transfer
MOF	Metal-Organic Framework
NMR	Nuclear Magnetic Resonance
OLED	Organic Light Emitting Diode
PXRD	Powder X-Ray Diffraction
RISC	Reverse InterSystem Crossing
RT	Room Temperature
SOC	Spin-Orbit Coupling
TD-PXRD	Temperature Dependant Powder X-Ray Diffraction
TADF	Thermally Activated Delayed Fluorescence
TDA	Thermal Derivative Analysis
TD-DFT	Time Dependant Density Functional Theory
TGA	ThermoGravimetric Analysis
UV	UltraViolet
W	Watt
τ	Lifetime
μ	Micro
Φ	Quantum Yield
ξ	Spin-Orbit Coupling
λ	Wavelength

Résumé en français

Introduction Générale

Durant les années 80, une grande attention a été portée vers le développement de nouvelles méthodes plus efficaces de génération d'énergie et de lumière, dû à la menace toujours plus pressante du réchauffement climatique. Les matériaux luminescents sont parmi les plus impactés par ces développements car ces derniers étaient alors basés sur des technologies très consommatrices en énergie. C'est dans ces années que les premières *Organic Light Emitting Diodes* (OLEDs) virent le jour, permettant une génération beaucoup plus efficace en énergie comparativement par exemple aux ampoules incandescentes et tubes fluorescents alors en utilisation.¹

Ces technologies efficaces ont été basées initialement sur l'utilisation de matériaux construits autour de ligands π -conjugués et d'ions de métaux lourds comme Pt(II), Au(I), Ir(III), Os(II)... Ces ions métalliques sont rares et coûteux, entraînant des tensions entre pays en terme d'accès à ces ressources stratégiques (Figure 1). De plus, ces ressources métalliques sont déjà utilisées dans des industries très demandeuses comme par exemple les pots catalytiques pour la réduction de la nocivité des gaz d'échappements des automobiles.

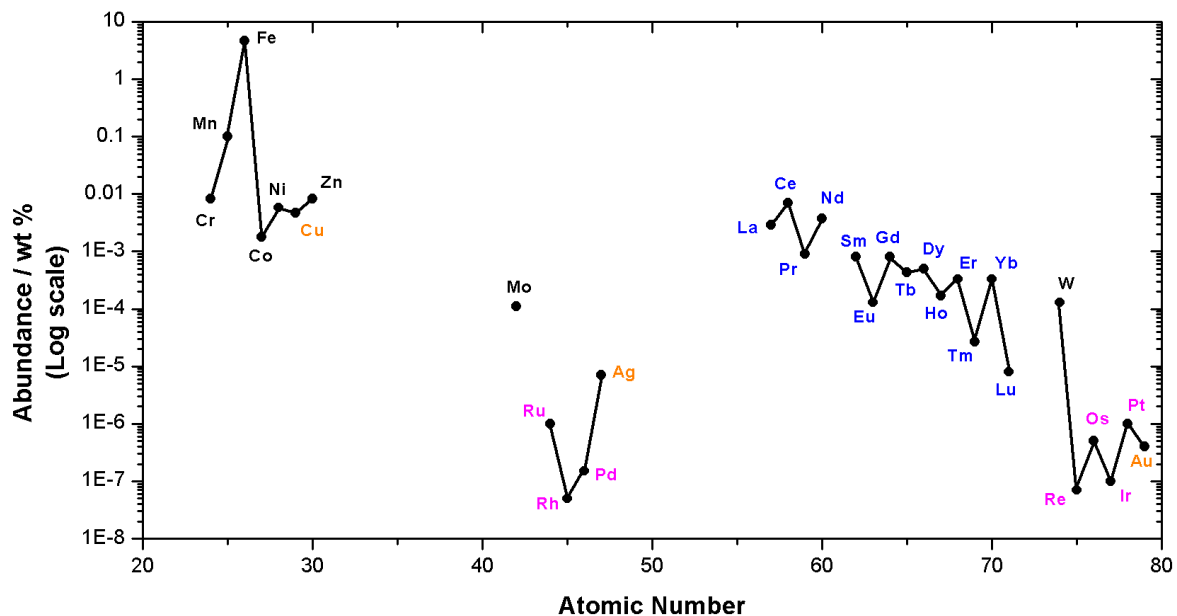


Figure 1 : Distribution en pourcentage massique d'une sélection d'éléments dans la croûte terrestre. L'or, l'argent et le cuivre sont surlignés en orange, les terres rares en bleu et les métaux lourds en violet. Données obtenues depuis les références^{2,3,4}.

Ce coût et cette rareté ont mené à la recherche de moyens d'utiliser des éléments plus abondants dans la croûte terrestre, tel que le fer ou le cuivre. Les travaux présentés dans cette thèse s'inscrivent dans l'optique du développement de matériaux luminescent efficaces basés sur l'utilisation de l'ion Cu(I).

L'ion Cu(I) présente un intérêt particulier pour les applications luminescentes dû à sa configuration électronique $3d^{10}$, empêchant la présence de chemins de relaxation non-radiatif dus à des transition d-d centrées sur le métal. Cette configuration permet à l'ion Cu(I) d'être un élément abondant sur lequel sont basés un grand nombre de matériaux luminescents.⁵

Cette attractivité de l'ion Cu(I) est renforcée par la possibilité offerte de voir plusieurs types de processus de relaxation radiatif présent dans les complexes obtenus. Parmi ces processus, la fluorescence retardée thermiquement ou le *Thermally Activated Delayed Fluorescence* (TADF) a été l'objet dans les dernières décennies d'une forte attention. D'abord découvert dans l'eosin-Y en 1961⁶, ce mécanisme permet en théorie la récupération potentielle de l'intégralité des électrons excités pour l'émission de lumière de par la présence d'un mécanisme de *Reverse Intersystem Crossing* (RISC) entraînant, à haute température, la population du premier état singulet depuis le premier état triplet. Un complexe présentant ce mécanisme de TADF possède généralement un important rendement quantique d'émission à température ambiante.

Cependant, l'écart entre les états excités pour que ce mécanisme puisse avoir lieu doit être assez faible, de l'ordre de $1\ 000\ \text{cm}^{-1}$ (0.12 eV), ce qui nécessite l'utilisation de concepts de synthèse permettant le design de complexes répondants à ce critère.

Parallèle à ces développements, un travail sur l'obtention de complexes luminescents efficaces basés sur l'ion Cu(I) a eu lieu. En effet, l'ion Cu(I) peut accommoder un certain nombre de sphères de coordination, notamment linéaire, trigonale et tétraédrique, et cette sphère de coordination est de plus considérée comme étant très labile et flexible. Ces éléments, en plus du caractère peu directionnel de la liaison entre le ligand et l'ion Cu(I), rendent la synthèse de complexes intéressants difficiles.

Une approche explorée dans les années récentes consiste à utiliser des ligands possédants une géométrie spécifique qui apporteraient une limite contrôlée à la flexibilité de la sphère de coordination de l'ion Cu(I).

Résultats Obtenus

C'est dans cette optique qu'a été développé en 2016 dans notre groupe, un métallacycle tétramétallique basé sur l'ion Cu(I) et constitué de deux unités bimétalliques $[\text{Cu}_2(\mu_2\text{-dppm})_2]^{2+}$ reliées entre-elles par deux ligands cyanure (Figure 2).

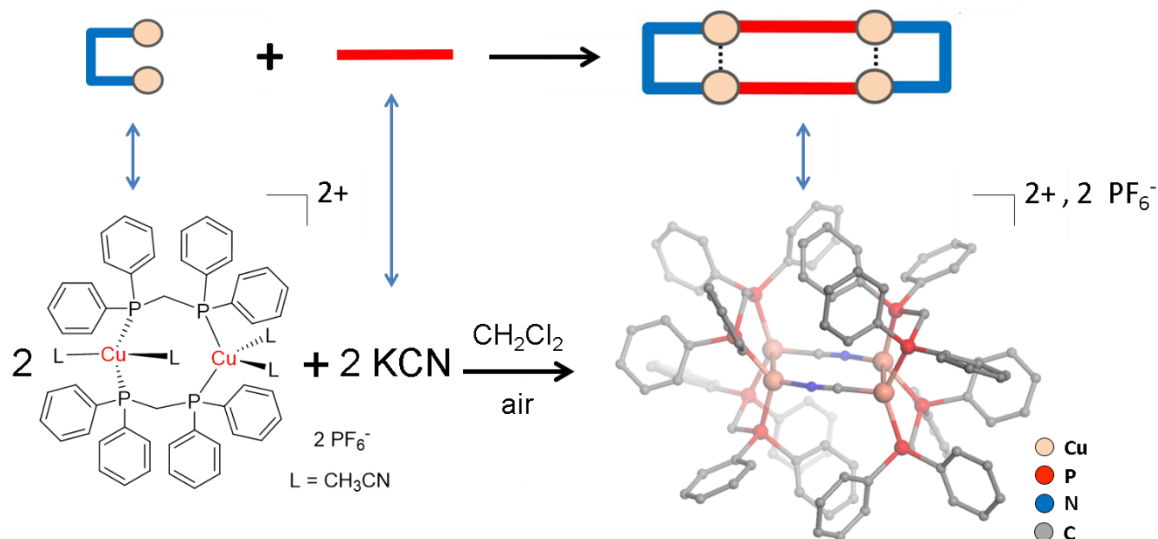


Figure 2 : Schéma de synthèse entre les unités bimétalliques $[\text{Cu}_2(\mu_2\text{-dppm})_2(\text{CH}_3\text{CN})_4]^{2+}$ et le cyanure de potassium. Structure moléculaire obtenue par diffraction des rayons X sur monocristal du composé **A**. Les atomes d'hydrogène, molécules de solvant et les contre-ions PF_6^- sont omis pour clarté.

Dans ce métallacycle, désigné **A**, les ions Cu(I) ont une sphère de coordination planaire trigonale distordue, différentes de la sphère de coordination tétraédrique adoptée par les unités bimétalliques avant réaction avec le ligand cyanure. Ce changement de sphère de coordination est accompagné d'un raccourcissement de la distance intermétallique entre les ions Cu(I) qui n'est plus que de l'ordre de 2.87 Å, se trouvant alors dans la plage de distances communément acceptées comme permettant la présence d'interactions cuprophiles.

Ce composé **A** présente une forte luminescence à l'état solide sous lumière UV avec l'émission d'une lumière perçue à l'œil comme étant bleue ($\lambda_{\text{ex}} = 365 \text{ nm}$). Cette luminescence est caractérisée par une large bande dans le spectre d'émission à l'état solide et à température ambiante, centrée à 457 nm. Le métallacycle **A** présente un caractère bathochrome de son émission avec un décalage vers le rouge lors du refroidissement, et une émission caractérisée par une large bande centrée à 485 nm dans son spectre d'émission à 80 K. L'étude de la variation du temps de vie de l'état excité en fonction de la température de **A** a permis mettre en lumière

la présence du mécanisme de TADF, associé avec un fort rendement quantique en émission observé à l'état solide et à température ambiante de 72 %.

Ce métallacycle tétramétallique **A** a été utilisé en tant que précurseur pour l'obtention de nouveaux matériaux luminescents et sa réaction avec différents ligands polytopiques à terminaison 3- ou 4-pyridyle a été étudiée. La réaction avec ces ligands polytopiques, désignés **B_n**, a permis l'obtention systématique de monocristaux et la structure moléculaire des complexes ainsi obtenus a été étudiée par diffraction des rayons X sur monocristaux. Cette étude a permis de révéler que les complexes ainsi obtenus de part la réaction entre le précurseur **A** et les ligands **B_n** sont des polymères de coordination monodimensionnels. Ces polymères **C_n** consistent en une alternance entre les métallacycles tétramétalliques du précurseur **A** et du ligand **B_n** utilisés lors de la synthèse. Un des ions Cu(I) des unités bimétalliques du métallacycle est coordonné à l'atome d'azote d'un des sites pyridine du ligand. Cela entraîne un changement de la sphère de coordination de cet ion Cu(I), de trigonal planaire distordue à tétraédrique. Une situation où les ions Cu(I) des unités bimétalliques du précurseur **A** possèdent des sphères de coordination différentes est alors observée. Avec ce changement de sphère de coordination, la distance intermétallique au sein des unités bimétalliques est nettement augmentée, avec une moyenne de 3.2 Å pour la série **C_n**, excluant ainsi la possibilité d'interactions cuprophiles (Figure 3).

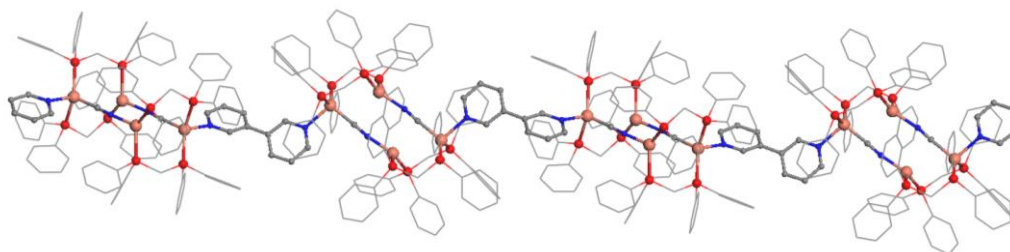


Figure 3 : Structure moléculaire obtenue par diffraction des rayons X sur monocristaux du polymère **C₃**. Les atomes d'hydrogène, molécules de solvant et les contre-ions PF_6^- sont omis pour clarté.

Les polymères de coordination **C_n** ont été caractérisés par spectroscopie infrarouge en particulier en considérant la bande de vibration du fragment cyanure, présente à 2117 cm^{-1} dans le précurseur **A**, et où un décalage vers les plus petits nombres d'ondes dans les polymères **C_n**, entre 2105 et 2088 cm^{-1} pour cette bande est observé.

Les polymères C_n se présentent comme des poudres polycrystallines luminescentes à l'état solide et à température ambiante, avec des lumières d'émission sous excitation UV perçues à l'oeil comme parcourant le spectre lumineux, du bleu au rouge (Figure 4).

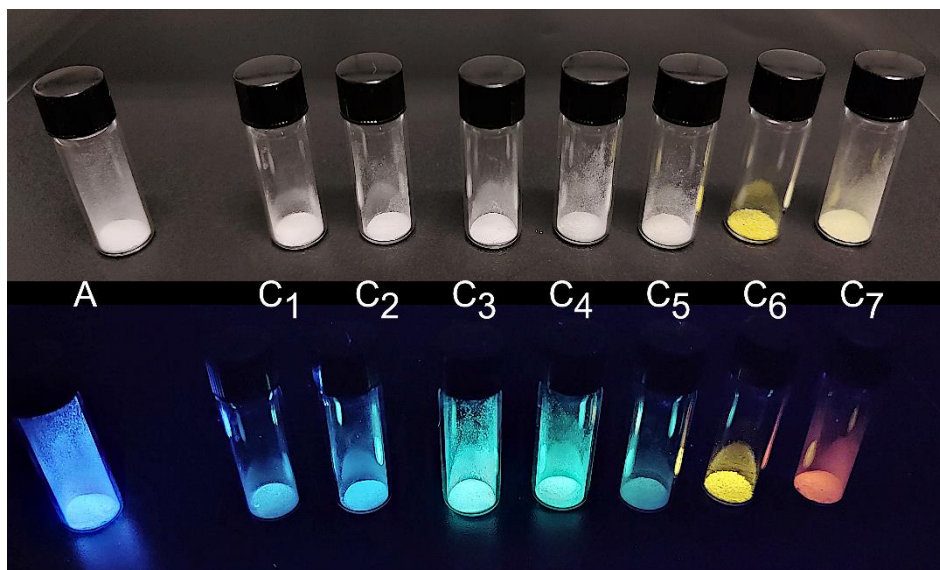


Figure 4 : Photographie sous lumière visible (haut) et lumière UV (bas) ($\lambda_{ex} = 365$ nm) des polymères de coordination C_n obtenus.

Cette luminescence est caractérisée à l'état solide et à température ambiante par la présence d'une large bande dans le spectre d'émission des polymères C_1 - C_3 et C_6 . Le polymère C_5 est très peu émissif à température ambiante tandis que les polymères C_4 et C_7 présentent une sous-structure vibronique de leurs spectres d'émissions. L'analyse de la variation thermique des spectres d'émissions des polymères C_n révèle une grande variété dans les propriétés photophysiques de ces polymères : la présence de bathochromisme dans le spectre d'émission lors du refroidissement est observée pour certains polymères tandis que d'autres ont un comportement hypsochrome, et enfin certains ne présentent pas de déplacement de leur spectre de luminescence lors du refroidissement. La variation thermique du temps de vie de l'état excité des polymères C_n présente aussi une grande diversité dans les comportements de ces polymères, certains allant jusqu'à plusieurs centaines de millisecondes, tandis que d'autres ne dépassent pas la dizaine de microsecondes.

Enfin, l'étude du rendement quantique à température ambiante à l'état solide des polymères C_n révèle ici aussi une grande variation dans la série, avec des valeurs qui vont de 50 % pour les plus émissifs, à seulement quelques pourcents pour d'autres et moins de 1 % pour le polymère C_5 . Ces études montrent la grande variété de chemins de relaxation radiatifs présents dans les

polymères C_n . Une analyse de ces propriétés assigne aux polymères C_1 et C_2 un caractère de phosphorescence 3MLCT , tandis que les polymères C_4 , C_5 et C_7 présentent quant à eux un caractère de phosphorescence centrée sur le ligand connecteur perturbée par la coordination sur le le métal de part leur faible valeur de taux de relaxation radiatif et de la présence d'une forte sous-structure vibronique observée dans les spectres d'émission. Enfin, les polymères C_3 et C_6 semblent conserver le comportement TADF du précurseur **A**, fait étayé par l'allure sigmoïdale de leur courbe de variation du temps de vie de l'état excité ainsi que de leur taux de relaxation radiatif élevés. Il est cependant encore difficile de se prononcer avec certitude et des mesures supplémentaires en température, accompagnées par des calculs TD-DFT demeurent nécessaires pour trancher.

La stabilité thermique des polymères C_n a été étudiée, d'abord avec des mesures d'ATG-ATD jusqu'à 950 °C. Cette mesure révèle que les polymères C_n sont stables thermiquement jusqu'à 350 °C, une fois cette température atteinte, une décomposition du composé est observée.

Cette mesure révèle aussi la présence d'un pic exothermique dans les polymères C_n , à une température d'environ 200 °C. Pour analyser en profondeur cet événement, une mesure ATG-ATD jusqu'à 270 °C avec une mesure du retour à température ambiante est effectuée (Figure 5).

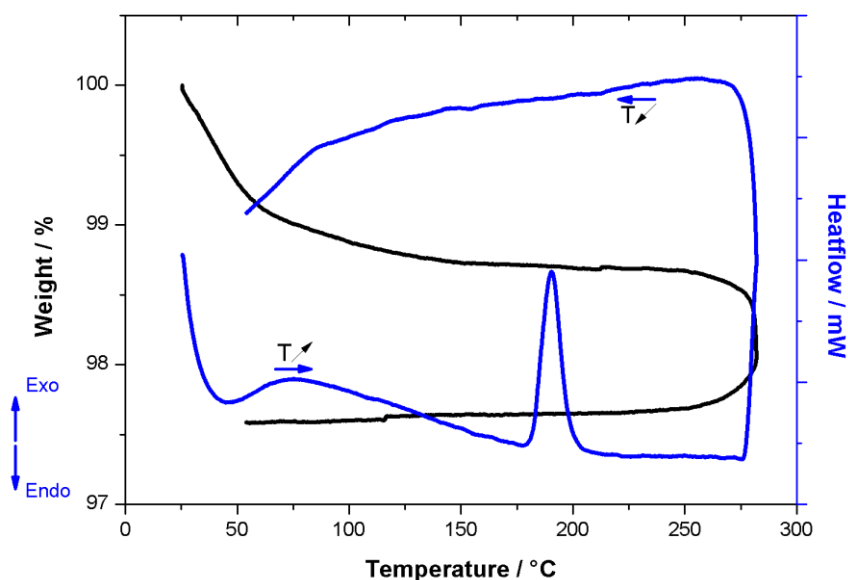


Figure 5 : Mesure ATG-ATD du polymère C_6 jusqu'à 270 °C, avec mesure du retour à température ambiante.

Cette nouvelle mesure révèle effectivement la présence d'un pic exothermique dans la courbe ATD des polymères C_n , non présente lors du retour à température ambiante, indiquant qu'un événement irréversible a eu lieu à une température de *ca.* 200 °C. Ce pic exothermique est accompagné dans plusieurs polymères par l'observation d'une perte de masse simultanée ou ayant lieu immédiatement après ce pic exothermique.

Après cette mesure, une fois les échantillons revenus à température ambiante, et parce que les polymères C_n n'ont pas subis de décomposition, une évolution inattendue a pu être observée.

En effet, les polymères C_n ainsi chauffés, désignés C_n' , présentent sous lumière UV à l'état solide, l'émission d'une lumière perçue à l'oeil comme étant bleue, très similaire à la lumière émise par le précurseur **A** (Figure 6) et très différente de celle présentée par les polymères initiaux C_n .

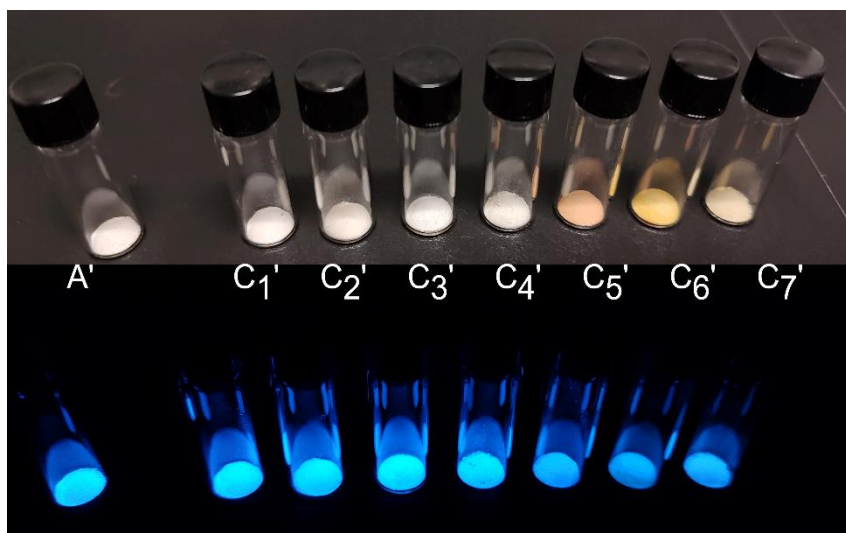


Figure 6 : Photographie sous lumière visible (haut) et lumière UV (bas) des phases transitées thermiquement C_n' ainsi que du précurseur transité **A'** ($\lambda_{\text{ex}} = 365 \text{ nm}$).

Ces phases transitées C_n' ont été caractérisées par spectroscopie infrarouge, révélant un déplacement de la bande de vibration associée au fragment cyanure, maintenant située à 2127 cm^{-1} pour la totalité de la série. Une étude thermique similaire, suivie d'une spectroscopie infrarouge sur le précurseur **A** révèle que ce dernier subit une transition à 233 °C, avec la présence dans la courbe ATD d'un pic exothermique, et un déplacement de la bande de vibration du fragment cyanure à 2127 cm^{-1} , à comparer à la valeur de 2117 cm^{-1} initialement obtenue pour le précurseur **A**.

Les propriétés de luminescence du précurseur transité **A'** ainsi que des phases transitées **C_n'** ont été étudiées, permettant de mettre en lumière des propriétés proches de celles du précurseur initial **A**. La luminescence des composés transités à l'état solide et à température ambiante est caractérisée par une large bande non-structurée dans leur spectre d'émission, centrée à 455 nm, très similaire à la valeur obtenue pour le précurseur **A**. Les composés transités thermiquement présentent aussi un comportement bathochrome très similaire lors de l'étude de la variation de leur émission en fonction de la température. Une fois refroidi à 80 K, les composés transités présentent une large bande non-structurée dans leur spectre d'émission, centrée à 495 nm.

L'analyse de la variation du temps de vie en fonction de la température des phases transitées **C_n'** révèle un comportement très proche entre celles-ci et le précurseur transité **A'** avec un temps de vie de l'état excité à l'état solide et à température ambiante ayant une valeur moyenne d'environ 40 μ s. Une fois les échantillons refroidis à la température de l'azote liquide, ce temps de vie est nettement augmenté, atteignant *ca.* 200 μ s dans le précurseur transité **A'** et 250 μ s pour les phases transitées **C_n'**. L'allure des courbes obtenues ainsi que des valeurs de temps de vie laissent supposer de la présence d'un mécanisme de TADF dans les composés transités thermiquement. Le rendement quantique à température ambiante à l'état solide des composés transités montre des valeurs élevées atteignant une valeur moyenne de 65 % pour la série **C_n'**. Une analyse à haute température du temps de vie de l'état excité du précurseur transité **A'** a permis de fitter la courbe obtenue selon l'équation du TADF avec de bons paramètres, confirmant ainsi les propriétés très similaires entre la phase transitée **A'** et le précurseur initial **A**.

Les propriétés thermiques des phases **C_n'** ainsi que du précurseur transité **A'** ont été explorées. Ces mesures ATG-ATD montrent qu'aucune autre transition thermique n'est observée dans ces composés, une fois la première transition ayant eu lieu, confirmant que les phases transitées sont stables thermiquement jusqu'à leur température de décomposition.

La perte de masse observée lors de la transition thermique des polymères de coordination **C_n**, coïncidant avec le pic exothermique présent dans les courbes ATD, ainsi que les mesures de spectroscopies infrarouges semblent pointer vers la décooordination du ligand connecteur **B_n** du métallacycle tétramétallique. Dans les polymères **C₁-C₄**, le ligand est alors possiblement sublimé, et des expériences de chauffage menées dans un appareil de sublimation ont permis de récolter sur le doigt froid de l'appareil des résidus qui sont caractérisés comme étant les ligands **B_n**. Cette décooordination du ligand laisse ainsi le métallacycle tétramétallique dans une configuration proche de celle observée pour le précurseur transité **A'**. Cette hypothèse

concernant la nature de la transition thermique est étayée par l'absence de bandes de vibrations caractéristiques des ligands B_n dans l'étude par spectroscopie infrarouge des phases transitées C_1' - C_4' et C_7' et permet de mieux comprendre la luminescence bleue observée pour ces phases transitées.

Les polymères de coordination C_5 et C_6 font exception. En effet, lors de l'analyse thermique de ces polymères, le pic exothermique n'est pas accompagné ou suivi d'une perte de masse. De plus, l'étude du spectre infrarouge des phases transitées C_5' et C_6' montre la présence de bandes de vibration caractéristiques des ligands B_5 et B_6 respectivement. Dans ce cas, il est vraisemblable que les phases transitées C_5' et C_6' consistent en un mélange intime du métallacycle tétramétallique et du ligand B_n décoordiné.

Une étude sur la possibilité de régénérer le polymère C_6 initial à partir de la phase transitée C_6' a été entreprise. Il a été observé que la phase C_6' recouvre une luminescence perçue par l'oeil comme étant similaire à celle du polymère initial C_6 après avoir été mis en contact de quelques gouttes du solvant de synthèse (dichlorométhane) ou bien de vapeurs de ce solvant. Cette phase régénérée, désignée C_6' _{DCM}, a été analysée par spectroscopie infrarouge et ses propriétés photophysiques ont été étudiées. Ces études ont révélé des propriétés très similaires entre la phase initiale et la phase régénérée avec la bande de vibration du fragment cyanure observée à une même valeur de nombre d'ondes (2102 cm^{-1}) et avec des valeurs proches du maximum de la bande de leur spectre d'émission et du temps de vie de l'état excité, à l'état solide. Aussi cette phase régénérée présente un comportement proche du polymère initial lors de l'étude de la variation des propriétés photophysiques en fonction de la température. Le rendement quantique d'émission à l'état solide et à température ambiante de la phase régénérée et aussi très similaire à la valeur obtenue pour la phase initiale C_6 (Figure 7).

Enfin, l'étude de la stabilité thermique de la phase régénérée C_6' _{DCM} révèle la présence à 190 °C d'un pic exothermique non accompagné d'une perte de masse dans la mesure ATG-ATD, un comportement thermique identique à celui observé pour le polymère initial C_6 . L'observation sous lumière UV ($\lambda_{\text{ex}} = 365\text{ nm}$) de l'échantillon après retour à température ambiante révèle l'émission d'une lumière perçue à l'oeil comme étant bleue, affirmant la présence de la transition thermique irréversible dans la phase régénérée. Cette observation montre le caractère circulaire de la transition thermique irréversible présente dans les polymères de coordination monodimensionnels C_n où il est possible pour certains polymères de régénérer la phase initiale après transition par mise en contact avec de faibles quantités du solvant de synthèse.

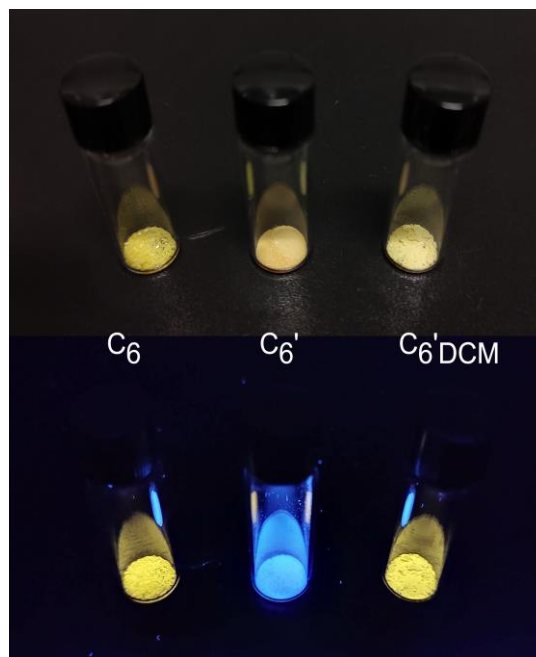


Figure 7 : Photographie sous lumière visible (haut) et lumière UV (bas) des phases C_6 , C_6' et $C_6'DCM$ ($\lambda_{ex} = 365$ nm).

Cette étude des propriétés thermiques des polymères de coordination C_n a permis de mettre en lumière la présence d'une propriété originale de transition impactant leur luminescence. Cette propriété rend les polymères C_n attractifs dans l'optique d'une application en tant que marqueurs d'un historique thermique de leur environnement. Cependant, un frein à l'emploi de ces polymères dans des applications est la présence de fragments cyanure au sein de l'unité tétramétallique présente dans les polymères. En effet, le cyanure présente une toxicité importante, tant pour la santé que pour l'environnement.

Ainsi, une recherche pour obtenir de nouveaux assemblages supramoléculaires basés sur l'ion Cu(I) a été entreprise et le clip bimétallique $[Cu_2(\mu_2-dppm)_2]^{2+}$ a été réagi avec le ligand ditopique 3,3' bipyridine **B3**. Cette synthèse a permis d'obtenir un nouveau composé qui a été caractérisé par diffraction des rayons X sur monocristal comme étant un métallacycle tétramétallique composé de deux sous-unités bimétalliques pontées par un ion chlorure et reliées entre elles par le ligand **B3**. Cette synthèse a alors été étendue à d'autres anions halogénures, menant à la formation d'une nouvelle série de métallacycles tétramétalliques dénomés D_x où X peut être Cl, Br ou I.

La distance intermétallique au sein des clips bimétalliques $[Cu_2(\mu_2-X)(\mu_2-dppm)_2]^+$ dans les composés D_x est supérieur à 3.2 Å ce qui est très supérieur à la distance à laquelle des

interactions cuprophiles peuvent avoir lieu. Les ligands **B3**, reliant les deux clips bimétalliques et permettant de fermer le métallacycle, présentent une planarité prononcée avec un angle de torsion moyen de 15° dans les composés **D_x**, une valeur bien plus faible que pour d'autres composés possédant ce ligand, comme par exemple le polymère de coordination **C3** dans lequel les ligands **B3** présentent alors un angle de torsion de 42° (Figure 8).

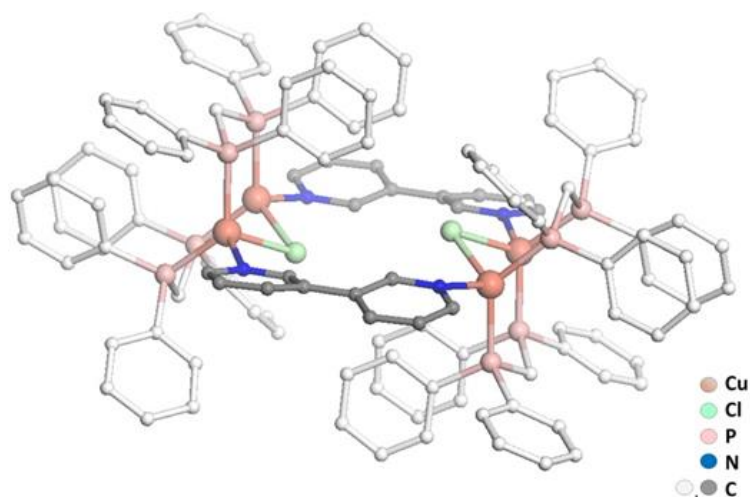


Figure 8 : Structure moléculaire du métallacycle **D_{Cl}** obtenue par diffraction des rayons X sur monocristaux. Les atomes d'hydrogène, molécules de solvant et les contre-ions PF_6^- sont omis pour causes de clarté.

Les mesures infrarouges de ces composés **D_x** sont en accord avec les similarités observées dans les structures moléculaires. Les bandes caractéristiques du ligand dppm sont principalement présentes dans les spectres infrarouges, et il peut être noté que la bande caractéristique du ligand **B3** ne peut pas être observée.

Les propriétés photophysiques des métallacycles tétramétalliques **D_x** ont été étudiées en détail. Ils présentent une large bande centrée à *ca.* 470 nm dans leur spectre d'émission à l'état solide, à température ambiante. Cette bande large est accompagnée à l'état solide par des valeurs de temps de vie de l'état excité à température ambiante de l'ordre de 80 μs . L'analyse de la variation thermique des propriétés photophysiques des composés **D_x** révèle l'apparition d'une sous-structure vibronique dans les spectres d'émissions lors du refroidissement, accompagnée par une forte hausse de la valeur du temps de vie de l'état excité, atteignant plusieurs millisecondes à 80 K. Enfin, les métallacycles **D_x** présentent des fortes valeurs de rendement quantique d'émission à l'état solide à température ambiante, atteignant 80% pour **D_{Cl}**.

Concernant l'attribution de l'origine de ces propriétés photophysiques, les valeurs observées de temps de vie de l'état excité dans les métallacycles **D_x** et la variation thermique des spectres

d'émissions empêchent de suggérer un processus de TADF, malgré les fortes valeurs de rendement quantique d'émission à température ambiante.

Les valeurs des constantes de relaxation radiative k_r sont en accords avec une phosphorescence $^3\text{MLCT}$ à des températures proches de la température ambiante qui peut être assignée à des densités électroniques vraisemblablement localisées sur le ligand 3,3' bipyridine **B₃**. L'apparition d'une structuration vibronique de la bande d'émission à basse température suggère une phosphorescence $^3\pi\text{-}\pi^*$ $^3\text{ILCT}$ à basse température centrée sur les ligands connecteurs **B₃**.

Finalement, la stabilité thermique de ces métallacycles **D_x** a été étudiée, révélant une stabilité jusqu'à environ 300 °C, température à laquelle les composés commencent à se décomposer thermiquement. Contrairement aux polymères de coordination **C_n**, aucun événement dans la courbe ATD n'a lieu, et la présence d'une transition thermique des propriétés de luminescence n'est pas observée (Figure 9).

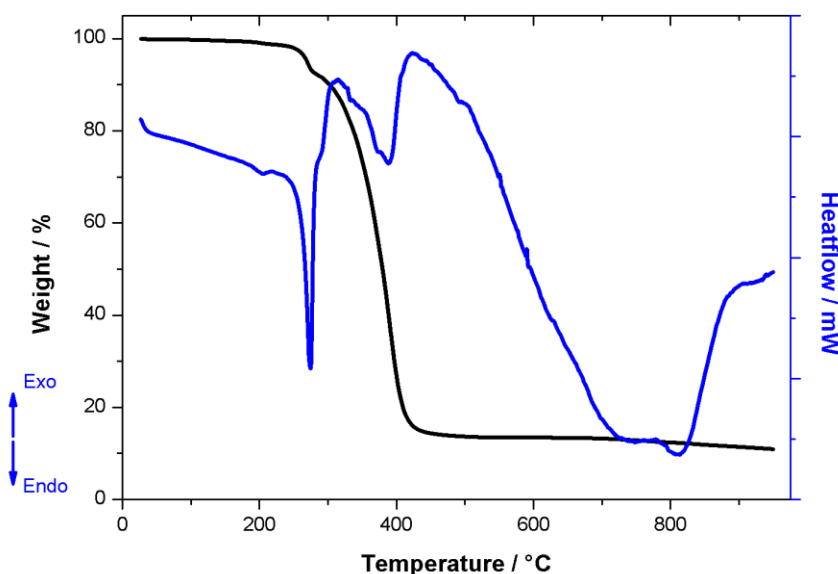


Figure 9 : Mesure ATG-ATD du composé **D_{Cl}** jusqu'à 950 °C.

En conclusion, l'analyse des propriétés photophysiques des métallacycles tétramétalliques **D_x** révèle des propriétés intéressantes, centrées sur le ligand connecteur **B₃**, et améliorées par la planarité de ce ligand, imposée par une rigidification exercée par le métallacycle. En revanche, ces métallacycles ne présentent pas la propriété originale de transition thermique de leur luminescence à haute température observée dans les polymères **C_n**.

En conclusion, ces travaux de thèse ont permis de montrer l'intérêt de l'utilisation d'un précurseur basé sur l'ion Cu(I) possédant des propriétés de luminescences intéressantes pour l'obtention de polymères de coordination monodimensionnels présentant des propriétés photophysiques variées. Une propriété nouvelle et originale de transition thermique irréversible de la luminescence de ces polymères a été découverte, créant un intérêt pour l'utilisation de ces polymères pour des applications industrielles. Un frein à cette utilisation est la présence du fragment cyanure au sein du précurseur, limitant les applications potentielles. La recherche de l'obtention de nouveaux assemblages supramoléculaires a mené à l'obtention d'une série de métallacycles tétramétalliques possédant des propriétés de luminescence centrées sur le ligand connecteur, exacerbées par la planarité de ce ligand imposée par une structure supramoléculaire rigide. Ces métallacycles ne présentent cependant pas de propriété de transition thermique de la luminescence. Des études approfondies sont en cours sur ces nouveaux polymères de coordination monodimensionnels pour une caractérisation de cette transition thermique.

Références :

1. Hong, G.; Gan, X.; Leonhardt, C.; Zhang, Z.; Seibert, J.; Busch, J. M.; Brase, S., A Brief History of OLEDs-Emitter Development and Industry Milestones. *Advanced Materials* **2021**, *33* (9), e2005630.
2. Holleman, A. F.; Wiberg, N., *Lehrbuch der Anorganischen Chemie, 102th ed.* Walter de Gruyter: Berlin, 2007.
3. Yaroshevsky, A. A., Abundances of chemical elements in the Earth's crust. *Geochem. Int.* **2006**, *44* (1), 48-55.
4. Haynes, W. M.; Lide, D. R.; Bruno, T. J., *CRC Handbook of Chemistry and Physics.* 97 ed.; CRC Press: Boca Raton, 2016; p 2670.
5. Barbieri, A.; Accorsi, G.; Armaroli, N., Luminescent complexes beyond the platinum group: the d10 avenue. *Chem. Commun.* **2008**, (19), 2185-2193.
6. Parker, C. A.; Hatchard, C. G., Triplet-singlet emission in fluids solutions. Phosphorescence of eosin. *Trans. Faraday Soc.* **1961**, *57*, 1894-1904.

Chapter I Introduction to the context of the study

With the proof of global warming being underway during the 1970s and the apparitions of clear increase in global temperatures during the 1980s, a lot of attention was turned toward the development of new and more efficient ways to generate energy, products and light. This need was especially felt in the field of light emissions as technologies of the time were incredibly wasteful in energy : Incandescent bulbs and fluorescent tubes converting most of the energy supplied in heat instead of light. This changed with the developement in the 1980s of the first organic light emitting diodes (OLEDs), providing a more energy friendly source of light emission. OLEDs became an efficient and sustainable method of light emissions in the fields of displays and general lighting.¹ It was during this period and in the following decades that a huge focus was geared toward the development of new light emitting systems for a number of different applications. The best results obtained in earlier years and up until recently were achieved with light emitting materials based on π -conjugated systems and rare earth and heavy transition metals complexes such as Pt(II), Au(III), Ir(III), Os(II), Ru(III) ions...^{2,3,4} Such complexes were used in a large variety of applications such as opto-electronic devices, including organic light emitting diodes (OLEDs) and photovoltaic cells, but also chemical and biological sensors and probes.

Heavy metal ions (HMI), including Ruthenium, Rhodium, Palladium, Rhenium, Osmium, Iridium and Platinum, display efficient radiative relaxation processes after photo excitation, which results in high intensity light emissions.⁵ However, there is a disadvantage in using such HMIs. Indeed, such metals are rare, being present in low abundance in the earth's crust (Figure I-1). They are a source of tension between countries possessing the natural resources and countries needing the metals for their strategic manufacturing. The vast majority of HMIs produced worldwide are from South Africa and Russia, amounting for *ca.* 80 % of the global supply. The principal use of HMIs are for the production of highly technological goods such as chemical catalysts, coatings, alloys, and electronic alloys. For platinum and palladium, their main usage at the beginning of the 21st century were jewelry and catalytic converters for reducing cars emissions.⁶ In this regard, it is interesting to change the focus of attention toward more abundant elements, such as iron and copper, in order to develop more affordable luminescent materials, provided by easier synthesis methods.

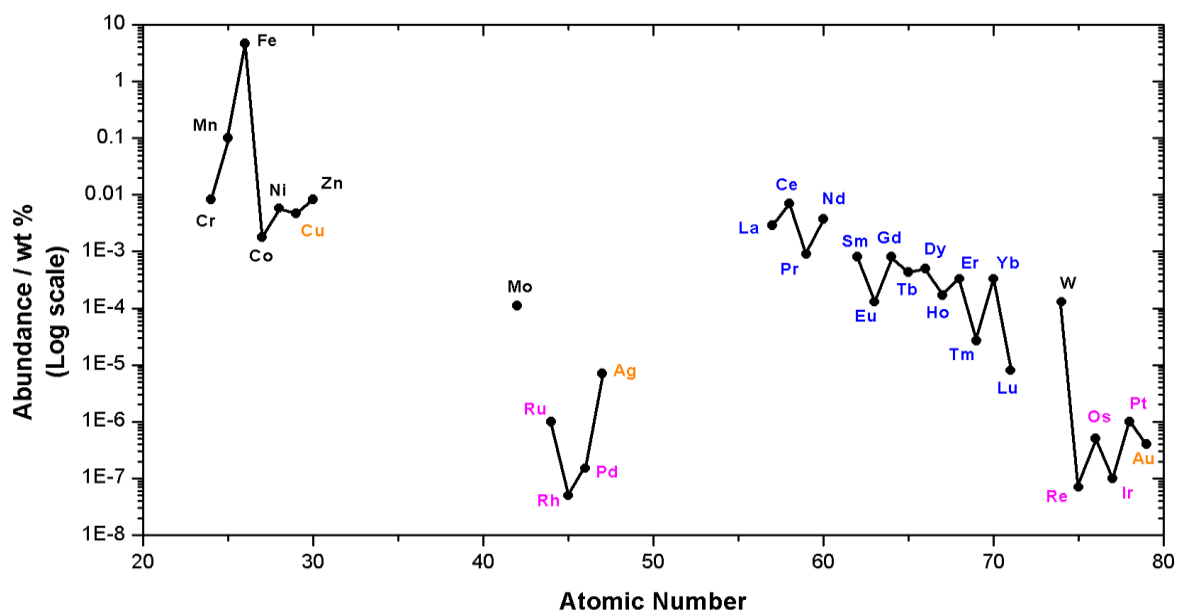


Figure I-1: Distribution, in mass percent, of a selection of metals in earth's crust. The three coinage metals are highlighted in orange, rare earth elements are highlighted in blue and heavy metal ions (HMIs) are highlighted in purple. Data obtained from^{7,8,9}.

In this context, this PhD study will focus on the synthesis and study of luminescent materials based on affordable and abundant Cu(I) ions centers. Indeed, this ion offers the access to a large number of coordination complexes, including emissive derivative bearing a variety of radiative relaxation processes.

I-1 Generalities on copper

I-1.a History of copper metal

Copper, as a metal, was among the first metal used by early humans, before other metals such as gold or silver. Its availability and ease of processing made it so that evidences of copper usage trace back to 10.000 BC. With copper being combined with zinc to form brass and with tin to form bronze, during the so called « bronze age », copper was used by humans ever since its discovery (Figure I-2).



Figure I-2 : Photography of a ritual cauldron in bronze (copper and tin alloy), originating from the Shang dynasty, in today's China; Dated *ca.* 13th century BC.

With the discoveries of new techniques, other, more durable metals and alloys were started to be used, such as iron and steel. During the 18th and 19th century, copper was mainly used in roofs, coinage and art. Toward the end of the 19th century, copper was once again used in an industrial process with the recently mastered electricity. Finally, in recent decades, copper was, and is, still in use under different forms for a large variety of applications, due to it being a cheap and readily accessible transition metal. The annual production of copper in 2000 was as high as 15.000.000 tons and has been growing ever since.

I-1.b Copper as an element in chemistry

Copper in solution is found as ion in two oxydation states : +I and +II. Since the electronic structure of copper is $[\text{Ar}]3d^{10}4s^1$, Cu(I) ions displays a $3d^{10}$ electronic structure, while Cu(II) displays a $3d^9$ configuration. This configuration of Cu(I) permits the presence of intense d-d metal-centered (MC) absorption bands in the visible/near-IR region of the spectrum for Cu(II) complexes which are usually highly colored in solution or in the solid-state. This configuration enables fast non-radiative pathways to take place which in turns render Cu(II) complexes uninteresting for luminescence-related applications. Conversely, this is not the case in the d^{10} Cu(I) ion that carries a closed-shell d orbital configuration.

On the other hand, Cu(I) complexes represent a high number of luminescent systems.¹⁰ With the properties typically displayed by Cu(I) complexes such as flexible structure, versatile

luminescence and electronic behaviors, such derivatives attracted a lot of attention in a number of different fields : spectroscopy, catalysis, luminescence, solar energy conversion, supramolecular chemistry...

I-2 Generalities on luminescence

I-2.a Origin of luminescence

Luminescence can be defined as the emission of a photon from a material resulting from an external stimuli. This phenomenon occurs after a system in an excited state emits a photon to reach a more stable state. The term « luminescence » is attributed to the German scientist Eilhard Wiedemann in 1888,¹¹ derived from the latin word « lumen » which means light, even though the phenomenon has been observed since the antiquity. A distinction need to be made however, between thermoluminescence which is induced by absorption of heat, and photoluminescence, which is induced *via* the absorption of light. Other kind of luminescence includes piezo-, electro- and triboluminescence for example, which are induced by deformation, the influence of an electric field and grinding or breaking, respectively. In this work, the focus will mainly be on photoluminescence. As previously stated, photoluminescence start with the absorption of light.

If this light is absorbed, there is an excitation of an electron in the electronic structure of the molecule, from a low energy ground state, to a high energy excited state. The energy gap between the low level fundamental state and the excited state matches the energy of the excitation. Once in this high level excited state, there are several possibilities of de-excitation processes in order to return to the fundamental ground state. Mainly, there is the possibility of non-radiative de-excitation *via* phonon emission, and radiative de-excitation *via* photon emission, which is in other words, luminescence.

A distinction can be made between two type of photoluminescence : fluorescence and phosphorescence. The difference between the two resides in the electronic state from which the de-excitation process occurs (Figure I-3).

If the de-excitation occurs from an excited singlet state directly to the singlet ground state, then the process is called fluorescence. If the de-excitation occurs instead from an excited triplet state to the ground state, the process is then called phosphorescence. Due to the difference in

multiplicity between the ground state, usually a singlet state, and the first excited triplet state, the excited electron will generally populate the excited singlet states. After very fast internal conversion (IC) to the lowest energy excited singlet state, a non-radiative transition is necessary in order to populate the lowest energy excited triplet state rendered difficult due to the forbidden nature of such transition. This transition is rendered possible due to the spin-orbit coupling (SOC), leading to the possibility of Intersystem Crossing (ISC) between the two excited states. This spin-orbit coupling stems from the interaction between an electron and its orbital angular momentum with the core of the atom. This spin-orbit coupling is proportionally linked to the Z atomic number of an atom, leading to heavy atoms, with high Z number, having very high spin-orbit coupling. This is called the heavy atom effect, and it is the effect granting the heavy transition metals such as Pt(II) or Ir(III) a certain affinity toward luminescent applications.

I-2.b Different kind of luminescent processes

Typically, processes found in a luminescent system are explained *via* a Jablonski diagram (Figure I-3), first represented in 1933.¹² At first, the system is in the ground state S_0 . If a photon which possesses an energy that matches the gap between the ground state and the first excited state S_1 is absorbed, then the system reaches the excited state S_1 (or subsequent S_{1+n} states if the energy of the photon is higher, but rapidly relaxes non-radiatively to the S_1 state). In this state there are multiple relaxation possibilities. The system can relax *via* non-radiative phonon production. There is also the possibility of direct relaxation from the S_1 to the S_0 state with the emission of a photon (fluorescence). And finally there is the possibility of an intersystem crossing taking place between the excited singlet state S_1 and the excited triplet state T_1 , after which a generally slower relaxation to the ground state S_0 is possible (phosphorescence). A photon emitted during the phosphorescence process possesses a lower energy than the absorbed photon as the lower energy states are stabilized, and this results in a shift of the emission towards longer wavelengths. A distinction between fluorescence and phosphorescence can be found in the typical decay times of the different processes : fluorescence decay times range from 10^{-7} s to 10^{-10} s and phosphorescence decay times range from 10^{-6} s to 10^1 s.

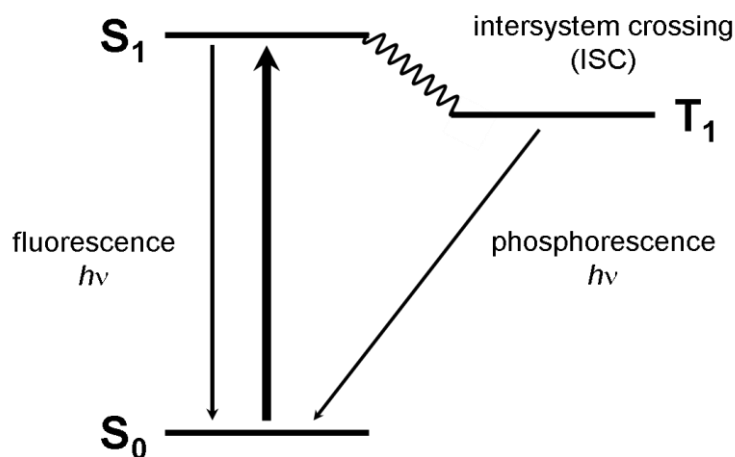


Figure I-3 : Jablonski-type diagram, the higher level excited states S_{1+n} and T_{1+n} are not represented for simplicity.

Coordination complexes of transition metals offer a number of excited states transitions, in which the ligands can play an important part. The different transitions can be classified in 3 types :

- Metal Centered transitions (MC) : This kind of transitions are found to occur between the d orbitals of the metal center, especially in metals having incomplete d^1 to d^9 orbitals. Such transitions are generally located in the visible to near-IR region of the spectrum.
- Metal to Ligand Charge Transfer (MLCT) and Ligand to Metal Charge Transfer (LMCT) : This kind of transitions occurs between a metal centered orbital and a ligand centered orbital. This transition results in intense emission bands that can be observed in the visible and UV region. MLCT transitions are typically found in d^6 , d^8 and d^{10} and in low oxidation state transition metals, especially coordinated to π -acceptor ligands.
- Ligand to Ligand Charge Transfer (LL'CT) : This transition typically occurs between a donor ligand and an acceptor ligand, both coordinated to the same metallic center. This transition originates from the electron rich ligand and transfer toward the electron poor ligand.

I-2.c Luminescent properties of heavy transition metals and copper.

As previously stated, one of the focus of luminescent research in the past decades has been second and third row transition metals complexes.^{13,14} The heavy metal effect found in complexes bearing d^6 and d^8 heavy transition metals ions such as Pt(II), Au(I), Ir(III), Os(II) or Ru(III) create appealing electronic properties. The heavy atom effect is due to the high SOC value of these ions and results in efficient intersystem crossing in the complexes, as well as a strong metal to ligand charge transfer behavior, resulting in high intensity emissions. They tend to display far longer excitation lifetimes than purely fluorescent compounds with phosphorescence decay times ranging from hundreds of nanoseconds to hundreds of microseconds.

Cu(I) based complexes are interesting with the presence of strong MLCT transition as well as a lack of d-d transition due to the $3d^{10}$ electronic configuration of the Cu(I) center. In spite of the properties described earlier and the fact that copper is cheap, the research on luminescent materials based around Cu(I) complexes was not up to the work done on other transition metals, such as Ir(III) and Pt(II). This was due to the fact that the properties of Cu(I) complexes were probably underestimated initially. It was believed that Cu(I) complexes would display long phosphorescence decay times because of low SOC values ($\xi_{Cu} = 857 \text{ cm}^{-1}$ versus $\xi_{Pt} = 4481 \text{ cm}^{-1}$, $\xi_{Ir} = 3909 \text{ cm}^{-1}$, with the spin-orbit coupling constant ξ)¹⁵ which results in relatively weak intersystem crossing. This should lead to longer ISC rates in Cu(I) complexes compared to heavy transition metals equivalents and lower luminescence intensities.

Initially, a large portion of the studied Cu(I) complexes exhibited the general formula $[Cu(N^N)_2]^+$ where N^N is a bisimine ligand. However, an increasing number of heteroleptic complexes such as $[Cu(N^N)(P^P)]^+$ (where P^P are bisphosphine ligand) has been reported, bearing enhanced luminescence properties.

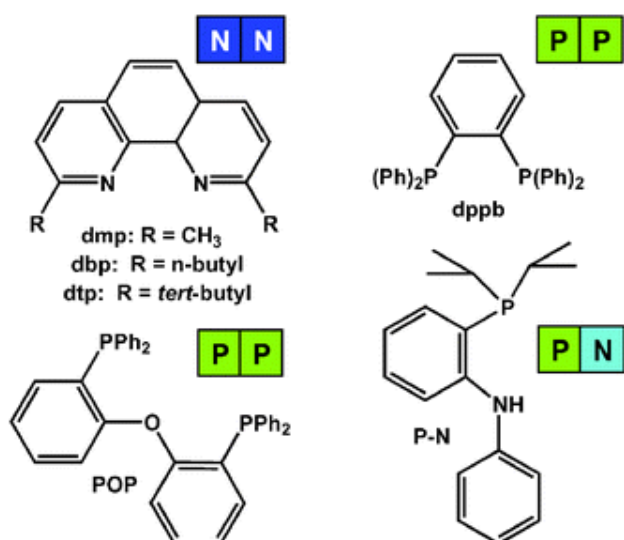


Figure I-4 : Examples of ligands used in Cu(I) complexes with N[^]N, P[^]P or P[^]N formulas. dmp : 2,9-dimethyl-1,10-phenanthroline, dbp : 2,9-di-n-butyl-1,10-phenanthroline, dppb : 1,2-bis(diphenylphosphino)-benzene, POP : bis[2-diphenylphosphino)-phenyl]ether, P-N : 2-(diisopropyl-phosphino)diphenylamide. Reproduced from¹⁰.

Finally, [Cu(P[^]P)₂]⁺ complexes were reported^{16,17} which exhibited, in several cases, even better electroluminescent properties. However, Cu(I) complexes were still suffering from diverse issues, mainly their highly flexible coordination sphere which would hinder their luminescence properties since it eases non radiative de-excitation pathways.

In recent years, however, such derivatives became increasingly attractive, due to the possibility of their radiative relaxation properties being governed by thermally activated delayed fluorescence, which was in particular showed by Hartmut Yersin, as well as the demonstration of their propensity toward stimuli sensitive behavior.

One such example of stimuli responsive behaviors found in Cu(I) complexes are cubane like structures [Cu₄I₄L₄] where L is a ligand, typically phosphine or pyridine terminated. This kind of structure was known since the early times of the 20th century. The early compounds, such as Cu₄I₄(py)₄ (Figure I-5), gave rise, through their interesting luminescent properties to a plethora of stimuli responsive complexes, especially to temperature, in a phenomenon coined as « Luminescence thermochromism ». First explored by the group of Ford¹⁸, recent work was conducted by the group of Perruchas¹⁹ and put in the spotlight new stimuli responsive behaviors for this family of compounds.



Figure I-5 : Molecular structure of $\text{Cu}_4\text{I}_4(\text{py})_4$. Reproduced from¹⁸.

The first notable work on the luminescent thermochromism properties of such cubane-like $\text{Cu}_4\text{I}_4\text{L}_4$ structure was conducted in 2011, by replacing the early pyridine ligands by triphenylphosphine and its derivatives. The obtained compounds presented a significant thermochromism behavior with for example a recorded shift of 45 nm in the case of $\text{Cu}_4\text{I}_4(\text{PPh}_3)_4$, from 545 nm in the solid-state at room temperature up to 587 nm at 77 K.²⁰ The luminescence observed at RT for these clusters stems from a combination of an iodide to copper charge transfer transition (XMCT) and a copper centered 3d to 4s,4p transition. This results in a « Cluster Centered » ³CC emission, mainly based on the $[\text{Cu}_4\text{I}_4]$ cluster core. The emission observed at low temperature is assigned to a transition from the LUMOs which are a combination of the π^* orbitals of the phenyl groups of the ligands to the HOMOs which are of a mixed iodide/copper to ligand charge transfer transitions ³XLCT/³MLCT character.

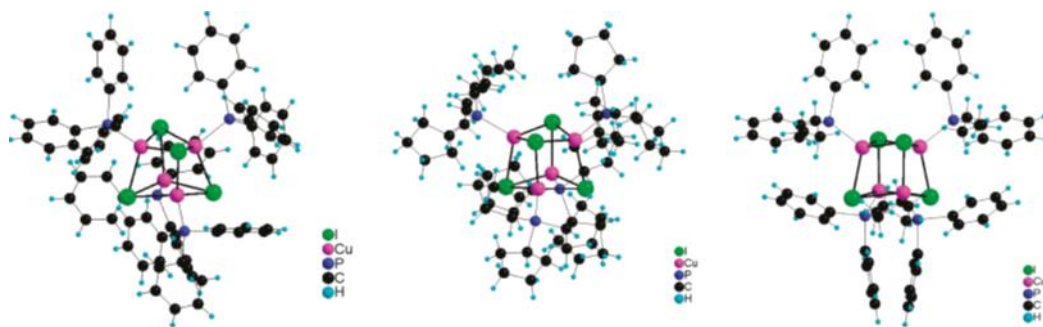


Figure I-6 : Molecular structure of 3 clusters of $\text{Cu}_4\text{I}_4\text{L}_4$ presenting a net thermochromism behavior. Reproduced from²⁰.

The attention of the group was then ported toward the study of a different cubane like cluster $[\text{Cu}_4\text{I}_4(\text{PPh}_2(\text{CH}_2\text{CHCH}_2))_4]$ presenting a more interesting behavior. This cluster, obtained as a white crystalline powder under visible light and emitting a weak green luminescence under UV-

light ($\lambda_{\text{ex}} = 365 \text{ nm}$), present a noticeable thermochromic behavior. Indeed, once cooled down to the temperature of liquid nitrogen (77 K), the cluster now emits a bright blue emission under the same excitation. Additionally to this thermochromic behavior, this cluster exhibits a mechanochromic behavior upon grinding, where its luminescence shift in the solid-state at room temperature from a weak green to a more intense yellow emission. Once cooled down to 77 K, the ground phase of this cluster continues to exhibit a thermochromic behavior where the yellow luminescence is shifted to a purple one. The initial cluster $[\text{Cu}_4\text{I}_4(\text{PPh}_2(\text{CH}_2\text{CHCH}_2))_4]$ and its weak green luminescence can be restored by either dissolution in dichloromethane and evaporation of the solvent or by heating the sample at 100 °C for 30 minutes, demonstrating both complete reversible thermo- and mechanochromic luminescence mechanisms.²¹

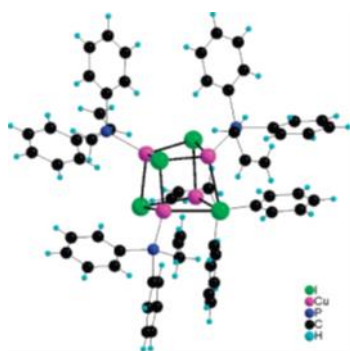


Figure I-7 : Molecular structure of $[\text{Cu}_4\text{I}_4(\text{PPh}_2(\text{CH}_2\text{CHCH}_2))_4]$. Reproduced from²¹.

In the following years, the group of Perruchas has continued to develop copper iodide clusters presenting both thermochromic and mechanochromic behaviors as well as polymorphism, by switching to using alkoxy silane phosphine-based ligand, and exploring in details the different parameters governing this behavior.²² Few years later, they also explored the shaping of such compounds and develop functional mechano responsive coatings.²³

Finally, a few years ago, the same group developed a smaller copper iodide cluster of $[\text{Cu}_2\text{I}_2(\text{Ph}_2\text{PC}_2(\text{C}_6\text{H}_4)\text{C}_2\text{PPh}_2)_3]$ displaying significant solvato- and vapochromic behaviors, making it a good candidate for solvent sensing applications.²⁴

I-3 Thermally activated delayed fluorescence

Cu(I) based complexes exhibit a number of different photophysical properties. Among the possible properties, is the Thermally Activated Delayed Fluorescence (TADF) mechanism, currently gathering an increasing interest. First discovered in eosin, and described as E-type fluorescence in 1961 (Figure I-9)²⁵, this mechanism has been studied with great interest in the fields of organics and inorganics materials, by several groups.^{26,27}

The mechanism of thermally activated delayed fluorescence stems from the possibility of a low energy gap to exist between an excited singlet state and an excited triplet state. This mechanism is interesting because it effectively enables the possible use of all singlet and triplet excitons in radiative relaxations (Figure I-8). In a system in which TADF is exhibited, upon absorption of a photon, there is an excitation of the electronic structure from the ground state to excited singlet states S_n , immediately followed by a fast non-radiative relaxation to the lowest energy singlet state S_1 . An effective intersystem crossing takes place and populates the lowest energy triplet state T_1 . At low temperature, a long-lived phosphorescence can be observed, and no S_1 to S_0 fluorescence is observed.

With an increase of temperature arises the possibility of a thermal population of the lowest excited singlet state S_1 from the lowest excited triplet state T_1 *via* reverse intersystem crossing (RISC). This RISC process is governed by the temperature and the energy gap between the two excited states. Once the lowest energy singlet state is populated, there is a long-lived fluorescence taking place, albeit delayed from a direct S_1 - S_0 fluorescence process. In order for the TADF mechanism to take place the energy gap between the two excited states needs to be in a certain range, and quite small. In eosin, when first discovered, the energy gap $\Delta E_{(S_1-T_1)}$ was calculated to be as large as $\sim 3500 \text{ cm}^{-1}$ ($\sim 0,43 \text{ eV}$).²⁸ However, it was found that the gap generally needed to be substantially lower in order TADF to take place in transition metal complexes. For example, a typical value for the energy gap is around 10^3 cm^{-1} or 0.12 eV .²⁹ Systems displaying TADF behavior possess high emission quantum yields at room temperature, along decay times in the range of few microseconds. However, at low temperature, the S_1 state cannot be populated, which leads to phosphorescence with decay times around hundreds of microseconds.³⁰

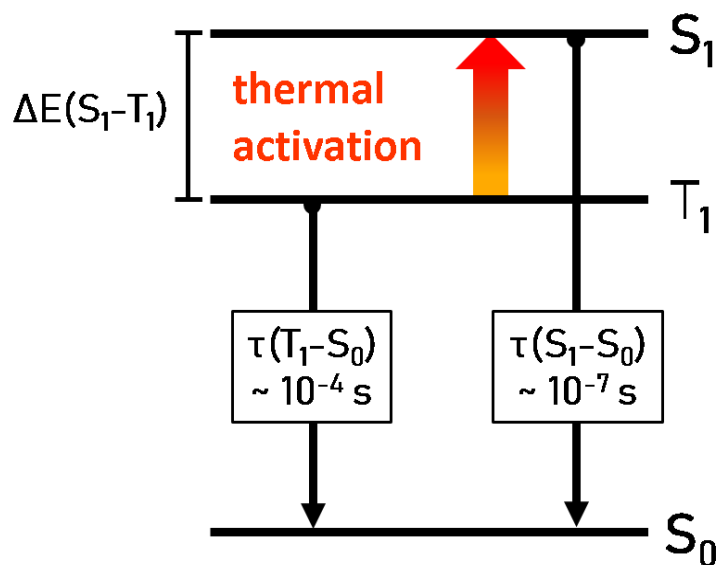


Figure I-8 : Simplified mechanism of the TADF process.

The parameters that need to be taken into account are put in relation in the following equation :

$$\tau(obs) = \frac{3 + \exp\left(-\frac{\Delta E_{ST}}{k_B T}\right)}{3k(T_1) + k(S_1)\exp\left(-\frac{\Delta E_{ST}}{k_B T}\right)}$$

Equation I-1 : Equation of the lifetime variation following a function of temperature where $\tau(obs)$ is the lifetime, $k(T_1)$ is the decay rate associated with T_1 , $k(S_1)$ is the decay rate associated with S_1 , k_B is the Boltzmann constant, T is the temperature and ΔE_{ST} is the energy gap between the two excited states.

It is possible to fit the curve of the evolution of the decay times depending of the temperature with this equation, which in turn, gives access to the intrinsic properties of the studied system, the energy gap, and the decay rate of the two excited states, S_1 and T_1 .

In contrast to materials based on expensive heavy atoms such as Ir(III) or Pt(II), purely organic compound or copper(I) complexes does not possess high spin-orbit coupling, leading to a slow intersystem crossing and a forbidden T_1 to S_0 transition. This is, in the context of TADF emitter, beneficial, as the long lived triplet excited state facilitates the population of the lowest energy singlet state *via* RISC process.

I-4 Cu(I) complexes presenting TADF properties

I-4.a History of Cu(I) based TADF complexes

The TADF phenomenon constitutes an attractive luminescence mechanism that, when applied to Cu(I) complexes, allows for short decay times and high quantum yields at room temperature, *via* the harvesting of both singlet and triplet excitons. The main interest behind this mechanism is that it does not require the use of low abundance and expensive heavy metals such as iridium or platinum. Indeed, the TADF mechanism can be achieved *via* the use of more affordable and cheaper metal alternatives, such as silver or copper and can also be achieved in purely organic molecules.

And in fact, as it stands, the first reported study featuring such a mechanism was done on eosin-Y in 1961, by Parker and Hatchard²⁵ (Figure I-9). Due to the fact that this mechanism of delayed fluorescence was discovered in eosin solutions, it was first called E-type delayed fluorescence.

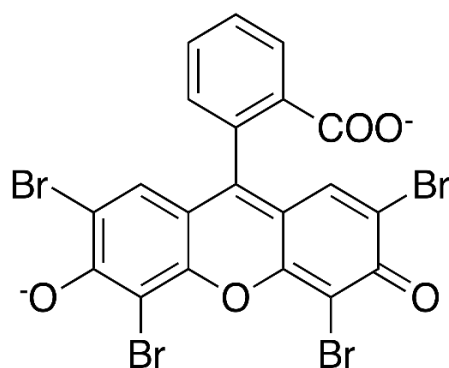


Figure I-9 : Eosin-Y, the first molecule in which TADF was reported by Parker and Hatchard in 1961.

After this, nearly twenty years were necessary before the first complex based on copper(I) and displaying TADF would be studied. Indeed, $[\text{Cu}(\text{dmp})_2]^+$ was presented in 1980 by Blaskie and McMillin³¹, closely followed by two similar copper(I) complexes in 1983 : $[\text{Cu}(\text{bcp})_2]^+$ and $[\text{Cu}(\text{tmbp})_2]^+$, presented by Kirchhoff *et al* (Figure I-10).³²

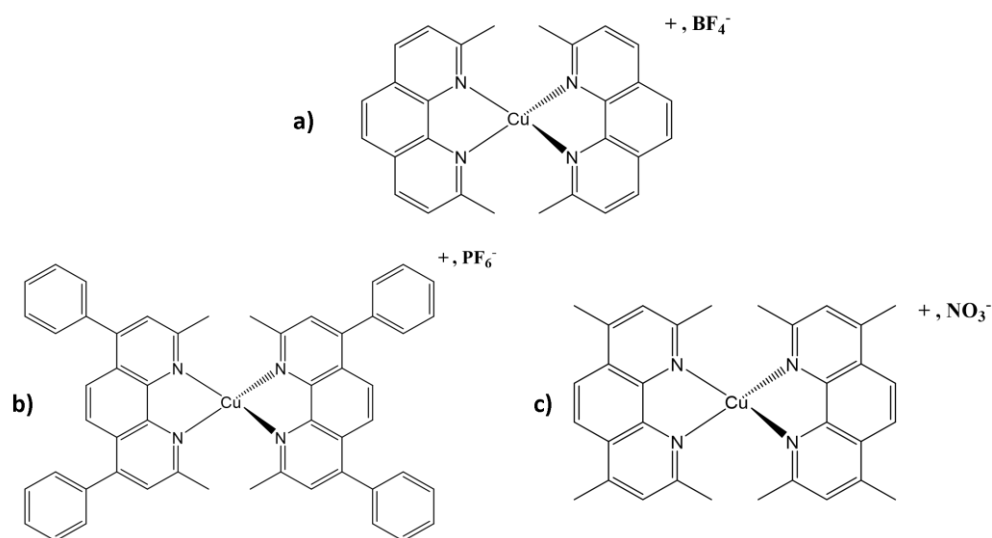


Figure I-10 : First three Cu(I) complexes reported presenting TADF behavior. a) $[\text{Cu}(\text{dmp})_2]^+$; b) $[\text{Cu}(\text{bcp})_2]^+$; c) $[\text{Cu}(\text{tmbp})_2]^+$.

In later years, inspired by their discovery a few years earlier of an highly emissive $[\text{Cu}(\text{PNP})_2]$ complex possessing a quantum yield of 68 %³³, the group of Peters and Harkins published in 2010 a $[\text{Cu}(\text{PNP-}^t\text{Bu})_2]$ complex, exhibiting TADF behavior and presenting an external quantum efficiency (EQE) of 16 % in doped OLEDs (Figure I-11),³⁴ promoting OLEDs based on Cu(I) complexes presenting TADF properties to the level of performance displayed by OLEDs based on heavy metal complexes.

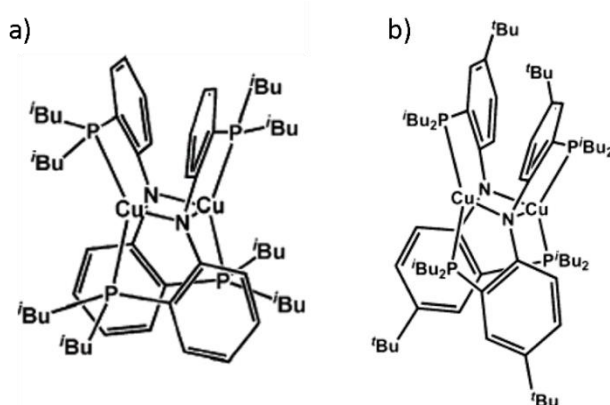


Figure I-11 : a) $[\text{Cu}(\text{PNP})_2]$, b) $[\text{Cu}(\text{PNP-}^t\text{Bu})_2]$ where PNP = bis(2-diisobutylphosphino)phenyl)amide and PNP-^tBu = bis(2-diisobutylphosphino-4-tert-butylphenyl)amide.

Nowadays, Cu(I) complexes displaying TADF behavior are designed specifically to reduce the energy gap between the lowest excited singlet and triplet states. In 2015, Volz *et al.* reported a Cu(I) complex doped OLED device achieving 23 % EQE (Figure I-12), putting it ahead of similarly doped, Ir-based emitters.³⁵

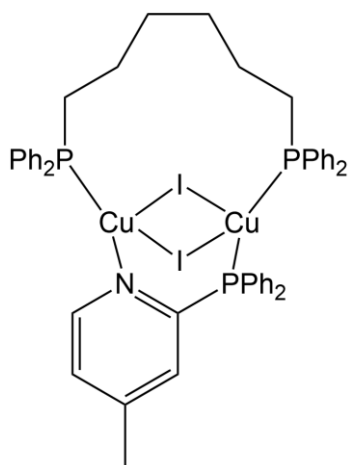


Figure I-12 : Fully bridged NHetPHOS-complex showing a high EQE in doped devices.

I-4.b Organic versus Cu(I) based TADF emitters.

As was previously established, the first reported molecule in which TADF was observed was eosin, a purely organic molecule. After this initial discovery, the study of TADF in purely organic molecules was continued with the work of Berberan-Santos *et al.* in 1996 on the delayed fluorescence of fullerene derivatives.³⁶

In 2012, Adachi *et al.* reported a highly efficient TADF material with a bright green emission in which both acceptor and donor moieties are present in one molecule.³⁷ This novel approach was conserved in following studies, and led to the development in 2015 of devices achieving up to 31 % EQE for green emission with a purely organic TADF material support (Figure I-13).³⁸

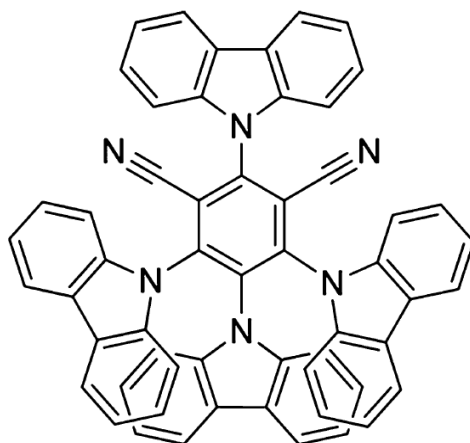


Figure I-13 : Molecular structure of 4CzIPN, a highly emissive organic green TADF emitter. Reproduced from³⁸.

Main difference regarding photophysical properties between organic and Cu(I) TADF emitters resides in the difference between decay rates of spontaneous S_1 to S_0 fluorescence and intersystem crossing from T_1 to S_1 followed by delayed fluorescence.

In purely organic materials, the intersystem crossing S_1 - T_1 transfer rate is relatively inefficient, resulting in processes occurring in the nanosecond timescale, leading to competition between spontaneous fluorescence and delayed fluorescence. In Cu(I) based emitters, the ISC process is much more effective, taking place on the picoseconds scale, leading in most cases to the absence of detection of a spontaneous fluorescence and only the delayed fluorescence or pure phosphorescence is observed.

This implies that a purely organic emitter will be more dependent on ΔE_{ST} gap. On the other hand, Cu(I) emitters benefit from relatively higher SOC and can display TADF behavior for higher values of energy gap. On the other side, Cu(I) emitters decay times are limited by S_0 to S_1 oscillator strength. Such limitations lead to different design strategies for the synthesis of TADF emitters and the control of the ΔE_{ST} gap.³⁹

In organic emitters, a distinct spacial separation need to be present between HOMO and LUMO orbitals in order to minimize the ΔE_{ST} energy gap, achieved by breaking the conjugation from acceptor and donor moities in the molecule. In Cu(I) emitters, the design strategy can be more flexible, due to the larger ΔE_{ST} at which the TADF can still be observed. However, luminescence efficiency is important, and demands particular design rules such as high steric demand of the ligand, leading to rigid structure, avoiding excited state distortions⁴⁰, or the

avoidance of certain groups leading to vibrational quenching. This kind of design rules and their application will be explored in more details in the next section of this chapter.

As a final talking point in this section, the differences between the available preparation processes for organic and Cu(I) based devices will be discussed. Two broad categories can be found concerning processing techniques used for the development of devices : vacuum processing and solution processing. The latter involves techniques such as ink-printing, and coating, while the former involve vapor deposition of the material.

Both kinds present pros and cons, which influence which of the organic or Cu(I) based emitters would be preferred. Vacuum deposition techniques necessitate high temperature stability, as well as a high volatility, limiting the molecular weight. This encourages the use of organic emitters, provided a high enough thermal stability, due to their relatively small molecular weight.

Concerning Cu(I) based emitters processing techniques, especially in the application of OLEDs, it is possible to use vapor deposition techniques, however, only small molecular weight emitters would be possible to use, due to sublimability. Some guidelines are also necessary, such as the use of chelating ligands, to prevent side products formation, or rigid structures.

Solution based techniques are faster, more economically viable and use less energy. The typical approach is to design new emitters with limited intermolecular interactions. Another recent approach is to develop polymeric TADF emitters.^{41,42,43}

Solution based processing techniques are state of the art for Cu(I) based emitters. Indeed, such emitters are typically soluble in a large variety of polar, and non-polar, solvents. However, one drawback that can possibly arise is the dissociation of the molecular structure in solution. This leads to the formation of different molecular species from the crystal structure and hinders the predictability of the process, posing a severe issue toward designing compounds with anticipated properties. Solutions to this issue are to devise structurally stable complexes, to prevent this dissociation, or to take advantage of the dissociation by using the obtained fragments in order to synthesize novel structures. To achieve such requirements, a proper molecular design is to be used, which will be described in the following section.

I-5 Synthesis strategies for designing polymetallic Cu(I) complexes

I-5.a Supramolecular chemistry, history and interest

As was previously stated, Cu(I) based emitters present a certain appeal toward diverse applications. One drawback presents in such emitters however, resides in the labile coordination sphere of the Cu(I) ion. This lability induces excited states restructuration, leading to luminescence quenching as well as hindering the use of certain processing techniques, due to easy structural reorganisation and ligand exchange. To avoid this kind of issue, it is possible to use supramolecular principles to design more interesting Cu(I) emitters.

Supramolecular chemistry finds its roots more than fifty years ago, in 1967, from a report of the complexation of metal ions by crown ethers (Figure I-14), published by Pedersen.⁴⁴

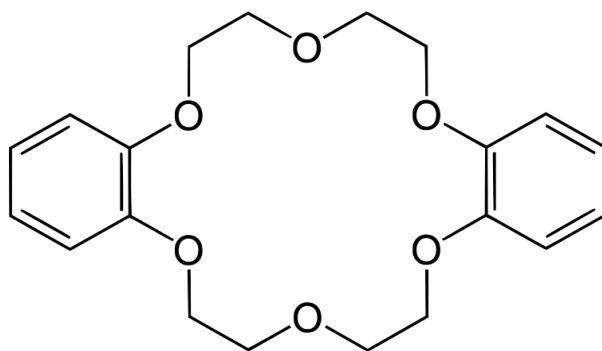


Figure I-14 : Molecular structure of dibenzo[18]crown-6, one of the crown ethers studied by Pedersen in the 1970s.

This report would lead a few years later to the development of host-guest chemistry, reported by Cram in 1974⁴⁵, and was followed by the definition of the concept of supramolecular chemistry, a term coined by Lehn, in an article published in 1978.⁴⁶ This early work would be awarded nearly twenty years later by a chemistry nobel prize given to all three of Pedersen, Cram and Lehn in 1987.

As was written by Lehn in 2017 : supramolecular chemistry can be defined as « chemistry beyond the molecule ».⁴⁷ It is based on the designing of chemical systems using molecular components that are held together by noncovalent intermolecular forces. Along the years, this kind of chemistry diversified, and attained a variety of fields of applications, from biology to physics and from polymers to solid-state engineering. One interest to supramolecular chemistry is its dynamic aspect, where it is possible to change and swap molecular components with ease until a targeted structure is obtained. This also served as a fertile soil to the development to an

adaptive kind of chemistry where components would self-assemble in order to selectively reach a certain structure, surpassing « traditional » synthetic approaches and their constraints : long synthetic procedures, low overall yield, low scalability and high cost.

1-5.b Coordination Driven Supramolecular chemistry

This behavior of components constitutes the basis for coordination driven supramolecular synthesis where the self-assembly of supramolecular molecules is achieved *via* the use of metal-ligand coordination. With this driving force in use, it is possible to produce complex discrete or infinite molecular structure, and would lead to the development of Metal-Organic Frameworks (MOFs) as well as intricate 2D and 3D discrete supramolecular assemblies. This kind of intricate structures find use in a number of applications such as catalysis, sensing, gas storage, drug delivery etc.⁴⁸ Many supramolecular assemblies presenting diverse shape such as helices, polygons, polyhedra and spheres have been developed and presented by different groups such as Lehn^{49,50}, Stang^{51,52}, Fujita^{53,54}, Newkome^{55,56}, Mirkin^{57,58,59}, Raymond^{60,61}, Nitschke^{62,63,64} and others.^{65,66,67,68}

The aim of Coordination Driven Supramolecular (CDS) chemistry is to use pre-organized coordination complexes having a precise geometry and possessing vacant coordination positions.⁶⁹ The pre-organized complexes are prepared *via* the reaction between metal ions and specific assembling ligands. Once formed, the complexes are reacted with polytopic connecting ligands in order to obtain multimetallic supramolecular assemblies. This bottom-up approach allows for control over the size and geometry of the obtained assemblies, by conducting careful selection of the nature and symmetry of the constituents.

1-5.c Use of CDS in the context of Cu(I) compounds

At first glance, Cu(I) ion is not really suitable for a use in CDS chemistry. It can accommodate highly labile and flexible linear, trigonal or tetrahedral coordination spheres. In addition, the coordination to the ligand in the case of Cu(I) is considered non-directional, with large variety in observed bond lengths and angles for a family of compounds. The aforementioned elements of Cu(I) ion in coordination chemistry render difficult to conduct successful synthesis due to the unpredictable aspect of this metallic center's coordination. In the group of Scheer, the

reaction of complexes such as pentaphosphaferrocene with Cu(I) halides led to the obtention of a plethora of supramolecular assemblies from 1D-CPs to 2D corrugated layers and even nano-sized, fullerenes like nanoclusters.⁷⁰ In 2015, the group of Scheer reported the obtention of a « Giant rugby ball » supramolecular compound, derived from pentaphosphaferrocene and CuBr₂, attaining a size of 4.6 x 3.7 nm, with a volume calculated to be 32.1 nm³, making it 62 times larger than the well-known C₆₀ fullerene molecule (Figure I-15).⁷¹

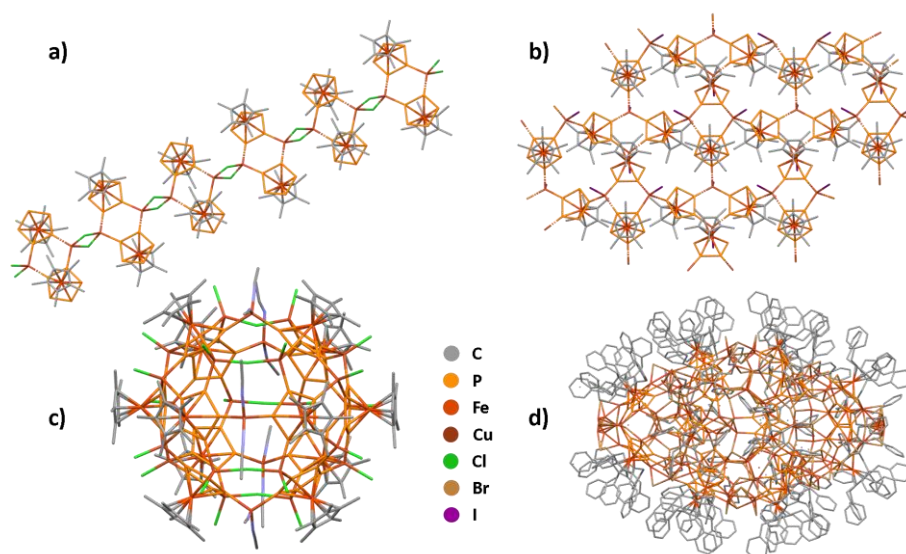


Figure I-15 : Molecular structures of some of the obtained supramolecular assemblies in the group of Scheer : a) 1D chain of $[\text{CuCl}(\text{Cp}^*\text{Fe}-(\eta^5 : \eta^1 : \eta^1\text{-P}_5))]_n$; b) 2D layer of $[\text{CuI}(\text{Cp}^*\text{Fe}(\eta^5 : \eta^1 : \eta^1\text{-P}_5))]_n$; c) Fullerene-like nanocluster $[(\text{Cp}^*\text{Fe}(\eta^5 : \eta^1 : \eta^1 : \eta^1 : \eta^1\text{-P}_5))_{12}(\text{CuCl})_{10}(\text{Cu}_2\text{Cl}_3)_5(\text{Cu}(\text{CH}_3\text{CN})_2)_5]$; d) « Giant rugby ball » $[(\text{Cp}^{\text{Bn}}\text{Fe}(\eta^5\text{-P}_5))_{24}\text{Cu}_{96}\text{Br}_{96}]$.

One proposed approach to overcome the set of limitations associated to the Cu(I) ions is to use specific ligands design, that would apply a limit to the flexibility of the coordination sphere of Cu(I) metal centers, and in the same time, impose a more pronounced directionality to the vacant coordination sites of such designed precursors.⁶⁹ This approach resembles the sets of rules established in section 5 of this chapter concerning the development of efficient Cu(I) based luminescent emitters, and more specifically TADF emitters. Indeed, this involves the development of a rigid structure to the Cu(I) emitters as to limit the excited states structural rearrangements as well as limiting non-radiative relaxation pathways to take and to help in prohibiting solution dissociation of the assemblies in the scope of solution based devices processing.

I-5.d Development of « U-shape » bimetallic Cu(I) precursors for usage in CDS chemistry

This approach was applied first in 2005, during studies conducted on 2,5-bis(2-pyridyl)phosphole ligand. Two complexes **A₁** and **A₂** were obtained displaying a unusual bridging coordination mode on dimeric units Cu(I) stabilized by N,P,N chelates (Figure I-16).⁷²

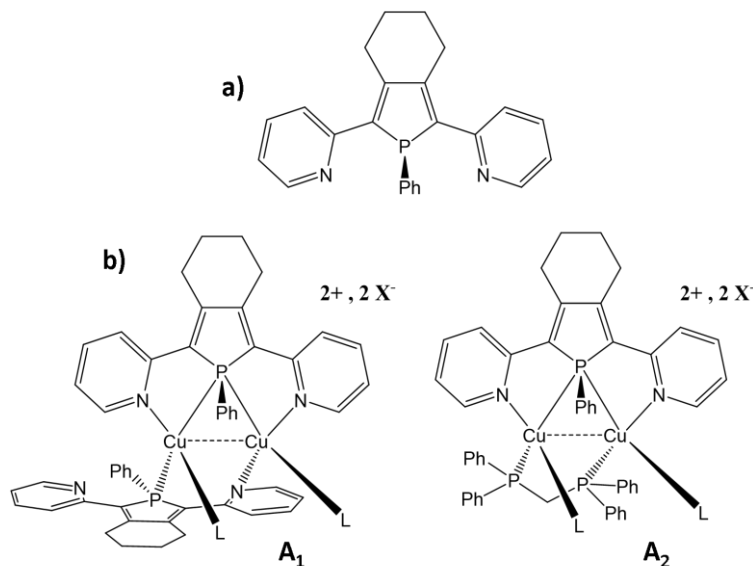


Figure I-16 : a) Molecular structure of 2,5-bis(2-pyridyl)phosphole ; b) molecular structure of obtained dimeric Cu(I) complexes. L is labile acetonitrile ligands and X are counter-anions, either PF₆⁻ or BF₄⁻.

In the above derivatives, two labile acetonitrile ligands are coordinated to the Cu(I) metallic centers, which confer to the complex a U-shape, in which moreover small intermetallic distances take place with 2.5552(8) and 2.6696(7) Å in **A₁** and **A₂** complexes respectively, which are in the commonly accepted distance range for cuprophilic interactions to occur.

These derivatives, the labile acetonitriles ligands coordinated to the Cu(I) metallic centers can be substituted by cyano-capped ditopic linkers, paving the way toward the development of a new family of tetrametallic supramolecular assemblies (Figure I-17).⁷³

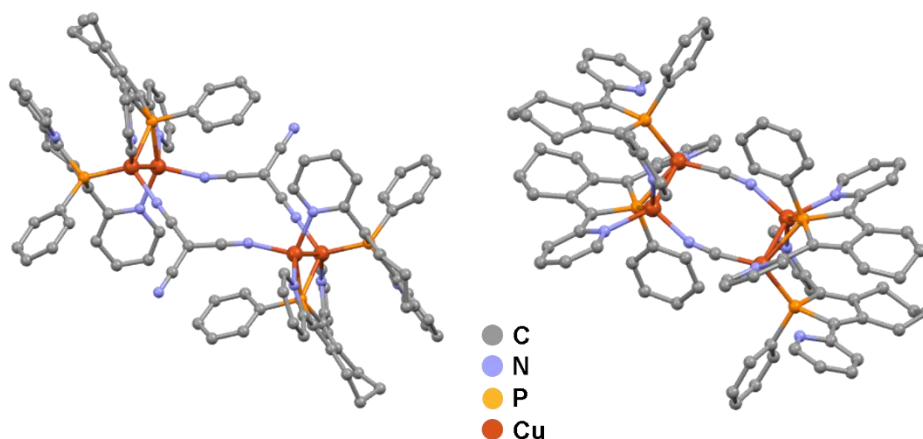


Figure I-17 : Molecular structure of two dimeric tetrametallic metallacycles obtained via single crystal X-ray diffraction (hydrogen atoms, counter-anions and solvent molecules have been omitted for clarity).⁷⁴

This initial study revealed the possibility of using this « U-shape » bimetallic precursor unit in self-assembly processes and was extended to obtain novel structures with polytopic nitrile capped organic linkers. The obtained supramolecular assemblies revealed to be further stabilized by weak intermolecular interactions as well as π - π interactions between the linkers leading to the formation of tetrametallic compact supramolecular assemblies (Figure I-18).

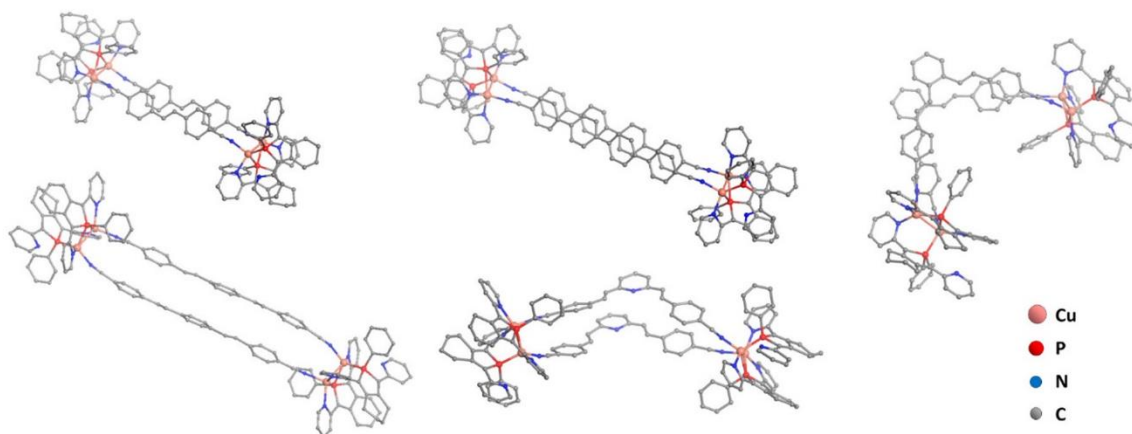


Figure I-18 : Molecular structure of tetrametallic metallacycles obtained with diverse polytopic nitrile capped linkers. Adapted from reference^{75,76}.

One issue arising from this study however, is the lack of noticeable luminescent properties in the obtained supramolecular assemblies. Indeed, the π -conjugated backbone of phosphole-based ligand used in the precursor dimeric unit provides efficient non-radiative de-excitation pathways, mostly due to the bridging coordination mode of the phosphane.

The solution to this issue was to develop a new Cu(I) based precursor, having a similar molecular architecture. The choice was made to use the ligand bis(diphenylphosphino)methane (dppm), leading to the obtention of a bimetallic unit Cu(I) precursor $[\text{Cu}_2(\mu_2\text{-dppm})_2(\text{CH}_3\text{CN})_4]^{2+}$, first described in 2003.⁷⁷ This precursor, however, does not share some of the characteristics of the earlier Cu(I) based precursor : the coordination number is higher as two acetonitrile ligands are coordinated to each Cu(I) metallic center and the intermetallic distance found in the dimeric unit is large (*ca.* 3.7 Å), far outside the accepted upper limit for cuprophilic interactions to take place. Yet, this precursor unit presents solid-state luminescent properties^{78,79}, making it interesting toward an adaptation of the previously developed CDS syntheses for the obtention of new luminescent supramolecular assemblies.

This dimeric unit was first reacted with a number of cyano-capped π -conjugated ligand, providing the structure with valuable intramolecular π - π interactions and leading to the formation of one-dimensional coordination polymers (1D-CPs) (Figure I-19).⁸⁰

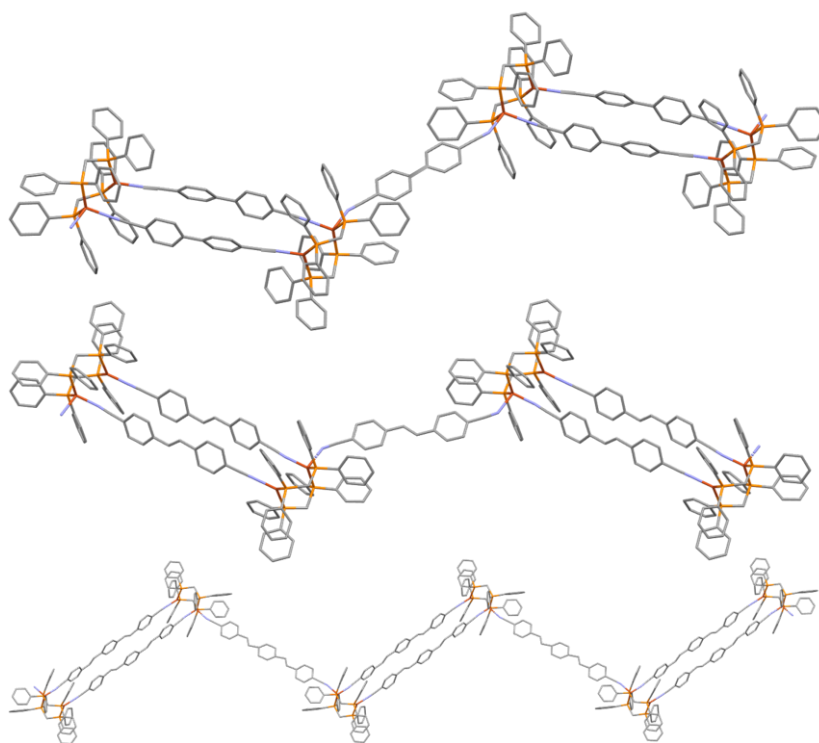


Figure I-19 : Molecular structure of some obtained 1D-CPs from the F-shape precursor $[\text{Cu}_2(\mu_2\text{-dppm})_2]^{2+}$.

In this first series of compounds, the dimeric units presents a « F-shape » geometry and the metallic centers possess either a tetrahedral or distorted trigonal planar coordination sphere. A high flexibility of the dimeric units was also noted, due to the dppm assembling ligands exhibiting « accordion-like » behavior, and still preserving the dimeric unit chemical structure.

The work presented in this PhD thesis is based on the use of this dimeric unit $[\text{Cu}_2(\mu_2\text{-dppm})_2(\text{CH}_3\text{CN})_4]^{2+}$ as a precursor in reactions taking full advantage of CDS chemistry principles, in order to design new supramolecular structures having interesting luminescent properties and stimuli responsive behavior.

References to chapter I :

1. Hong, G.; Gan, X.; Leonhardt, C.; Zhang, Z.; Seibert, J.; Busch, J. M.; Brase, S., A Brief History of OLEDs-Emitter Development and Industry Milestones. *Advanced Materials* **2021**, *33* (9), e2005630.
2. Kui, S. C. F.; Sham, I. H. T.; Cheung, C. C. C.; Ma, C.-W.; Yan, B.; Zhu, N.; Che, C.-M.; Fu, W.-F., Platinum(II) complexes with pi-conjugated, naphthyl-substituted, cyclometalated ligands (RC N N): structures and photo- and electroluminescence. *Chem. Eur. J.* **2007**, *13* (2), 417-35.
3. Yamamoto, T.; Maruyama, T.; Zhou, Z.-H.; Ito, T.; Fukuda, T.; Yoneda, Y.; Begum, F.; Ikeda, T.; Shintaro, S.; Takezoe, H.; Fukuda, A.; Kubota, K., π -Conjugated Poly(pyridine-2,5-diyl), Poly(2,2'-bipyridine-5,5'-diyl), and Their Alkyl Derivatives. Preparation, Linear Structure, Function as a Ligand to Form Their Transition Metal Complexes, Catalytic Reactions, n-Type Electrically Conducting Properties, Optical Properties, and Alignment on Substrates. *J. Am. Chem. Soc.* **1994**, *116* (11), 4832-4845.
4. Chou, P.-T.; Chi, Y.; Chung, M.-W.; Lin, C.-C., Harvesting luminescence via harnessing the photophysical properties of transition metal complexes. *Coord. Chem. Rev.* **2011**, *255* (21-22), 2653-2665.
5. Yam, V. W.-W.; Wong, K. M.-C., Luminescent metal complexes of d6, d8 and d10 transition metal centres. *Chem. Commun.* **2011**, *47* (42), 11579-11592.
6. Wilburn, D. R.; Bleiwas, D. I. *Platinum-group metals - world supply and demand*; United States Geological Survey: 2005.
7. Holleman, A. F.; Wiberg, N., *Lehrbuch der Anorganischen Chemie, 102th ed.* Walter de Gruyter: Berlin, 2007.
8. Yaroshevsky, A. A., Abundances of chemical elements in the Earth's crust. *Geochem. Int.* **2006**, *44* (1), 48-55.
9. Haynes, W. M.; Lide, D. R.; Bruno, T. J., *CRC Handbook of Chemistry and Physics*. 97 ed.; CRC Press: Boca Raton, 2016; p 2670.
10. Barbieri, A.; Accorsi, G.; Armaroli, N., Luminescent complexes beyond the platinum group: the d10 avenue. *Chem. Commun.* **2008**, (19), 2185-2193.
11. Wiedemann, E., In *Annalen der Physik*, J. A. Barth: 1888; pp 446-463.
12. Jablonski, A., Efficiency of Anti-Stokes Fluorescence in Dyes. *Nature* **1933**, *131*, 839-840.
13. Bargelletti, F.; Sandrini, D.; Maestri, M.; Balzani, V.; Zelewsky, A. v.; Chassot, L.; Jolliet, P.; Maeder, U., Temperature Dependence of the Luminescence of Cyclometalated Palladium(II), Rhodium(III), Platinum(II) and Platinum(IV) Complexes. *Inorg. Chem.* **1988**, *27* (20), 3644-3647.
14. Wong, K. M.-C.; Yam, V. W.-W., Luminescence platinum(II) terpyridyl complexes—From fundamental studies to sensory functions. *Coord. Chem. Rev.* **2007**, *251* (17-20), 2477-2488.
15. Montalti, M.; Credi, A.; Prodi, L.; Gandolfi, M. T., *Handbook of Photochemistry*. CRC Press: Boca Raton, 2006.
16. Armaroli, N.; Accorsi, G.; Cardinali, F.; Listorti, A., Photochemistry and Photophysics of Coordination Compounds: Copper. *Top. Curr. Chem.* **2007**, *280*, 69-115.
17. Armaroli, N., Photoactive mono- and polynuclear Cu(i)-phenanthrolines. A viable alternative to Ru(ii)-polypyridines? *Chemical Society Reviews* **2001**, *30* (2), 113-124.
18. Vitale, M.; Ford, P. F., Luminescent mixed ligand copper(I) clusters (CuI)_n(L)_m (L=pyridine, piperidine): thermodynamic control of molecular and supramolecular species. *Coord. Chem. Rev.* **2001**, *219-221*, 3-16.

19. Perruchas, S., Molecular copper iodide clusters: a distinguishing family of mechanochromic luminescent compounds. *Dalton Transactions* **2021**, 50 (35), 12031-12044.
20. Perruchas, S.; Tard, C.; Le Goff, X. F.; Fargues, A.; Garcia, A.; Kahlal, S.; Saillard, J.-Y.; Gacoin, T.; Boilot, J.-P., Thermochromic luminescence of copper iodide clusters: the case of phosphine ligands. *Inorg. Chem.* **2011**, 50 (21), 10682-10692.
21. Perruchas, S.; Le Goff, X. F.; Maron, S.; Maurin, I.; Guillen, F.; Garcia, A.; Gacoin, T.; Boilot, J.-P., Mechanochromic and Thermochromic Luminescence of a Copper Iodide Cluster. *J. Am. Chem. Soc.* **2010**, 132 (32), 10967-10969.
22. Benito, Q.; Le Goff, X. F.; Maron, S.; Fargues, A.; Garcia, A.; Martineau, C.; Taulelle, F.; Kahlal, S.; Gacoin, T.; Boilot, J.-P.; Perruchas, S., Polymorphic copper iodide clusters: insights into the mechanochromic luminescence properties. *J. Am. Chem. Soc.* **2014**, 136 (32), 11311-11320.
23. Benito, Q.; Maurin, I.; Poggi, M.; Martineau-Corcoss, C.; Gacoin, T.; Boilot, J.-P.; Perruchas, S., Impact of crystalline packing on the mechanochromic luminescence properties of copper based compounds: towards functional coatings. *Journal of Materials Chemistry C* **2016**, 4 (47), 11231-11237.
24. Benito, Q.; Balogh, C. M.; El Moll, H.; Gacoin, T.; Cordier, M.; Rakhmatullin, A.; Latouche, C.; Martineau-Corcoss, C.; Perruchas, S., Luminescence Vapochromism of a Dynamic Copper Iodide Mesocate. *Chem. Eur. J.* **2018**, 24 (71), 18868-18872.
25. Parker, C. A.; Hatchard, C. G., Triplet-singlet emission in fluids solutions. Phosphorescence of eosin. *Trans. Faraday Soc.* **1961**, 57, 1894-1904.
26. Brown, R. E.; Singer, L. A.; Parks, J. H., Prompt and delayed fluorescence from benzophenone. *Chem. Phys. Lett.* **1972**, 14 (2), 193-195.
27. Saltiel, J.; C., C. H.; Metts, L.; Miley, J. W.; Winterle, J.; Wrighton, M., Delayed Fluorescence and Phosphorescence of Aromatic Ketones in Solution. *J. Am. Chem. Soc.* **1970**, 92 (2), 410-411.
28. Parker, C. A.; Hatchard, C. G., TRIPLET-SINGLET EMISSION IN FLUID SOLUTION. *J. Phys. Chem.* **1962**, 66, 2506-2511.
29. Yersin, H., *Highly Efficient OLEDs: Materials Based on Thermally Activated Delayed Fluorescence*. Wiley-VCH Verlag GmbH&Co: KGaA, Germany, 2018.
30. Moussa, M. E.; Evariste, S.; Wong, H.-L.; Le Bras, L.; Roiland, C.; Le Polles, L.; Le Guennic, B.; Costuas, K.; Yam, V. W.-W.; Lescop, C., A solid state highly emissive Cu(I) metallacycle: promotion of cuprophilic interactions at the excited states. *Chem. Commun.* **2016**, 52 (76), 11370-11373.
31. Blaskie, M. W.; McMillin, D. R., Photostudies of Copper(I) Systems. Room-Temperature Emission and Quenching Studies of [Cu(dmp)₂]⁺. *Inorg. Chem.* **1980**, 19 (11), 3519-3522.
32. Kirshhoff, J. R.; Gamache Jr., R. E.; Blaskie, M. W.; Del Paggio, A. A.; Lengel, R. K.; McMillin, D. R., Temperature Dependence of Luminescence from Cu(NN)₂⁺ Systems in FLuid Solution. Evidence for the Participation of Two Excited States. *Inorg. Chem.* **1983**, 22 (17), 2380-2384.
33. Harkins, S. B.; Peters, J. C., A Highly Emissive Cu₂N₂ Diamond Core Complex Supported by a [PNP]- Ligand. *J. Am. Chem. Soc.* **2005**, 127 (7), 2030-2031.
34. Deaton, J. C.; Switalski, S. C.; Kondakov, D. Y.; Young, R. H.; Pawlik, T. D.; Giesen, D. J.; Harkins, S. B.; Miller, A. J. M.; Mickenberg, S. F.; Peters, J. C., E-Type Delayed Fluorescence of a Phosphine-Supported Cu₂(μ-NAr₂)₂ Diamond Core: Harvesting Singlet and Triplet Excitons in OLEDs. *J. Am. Chem. Soc.* **2010**, 132 (27), 9499-9508.
35. Volz, D.; Chen, Y.; Wallesch, M.; Liu, R.; Flechon, C.; Zink, D. M.; Friedrichs, J.; Flugge, H.; Steininger, R.; Gottlicher, J.; Heske, C.; Weinhardt, L.; Bräse, S.; So, F.; Baumann,

- T., Bridging the efficiency gap: fully bridged dinuclear Cu(I)-complexes for singlet harvesting in high-efficiency OLEDs. *Advanced Materials* **2015**, 27 (15), 2538-43.
36. Berberan-Santos, M. N.; Garcia, J. M. M., Unusually Strong Delayed Fluorescence of C70. *J. Am. Chem. Soc.* **1996**, 118 (39), 9391-9394.
37. Uoyama, H.; Goushi, K.; Shizu, K.; Nomura, H.; Adachi, C., Highly efficient organic light-emitting diodes from delayed fluorescence. *Nature* **2012**, 492 (7428), 234-238.
38. Lee, D. R.; Kim, B. S.; Lee, C. W.; Im, Y.; Yook, K. S.; Hwang, S.-H.; Lee, J. Y., Above 30% external quantum efficiency in green delayed fluorescent organic light-emitting diodes. *ACS Appl. Mater. Interfaces* **2015**, 7 (18), 9625-9629.
39. Bergmann, L.; Zink, D. M.; Brase, S.; Baumann, T.; Volz, D., Metal-Organic and Organic TADF-Materials: Status, Challenges and Characterization. *Top. Curr. Chem.* **2016**, 374 (3), 22.
40. Czerwieniec, R.; Kowalski, K.; Yersin, H., Highly efficient thermally activated fluorescence of a new rigid Cu(I) complex [Cu(dmp)(phanephos)]⁺. *Dalton Transactions* **2013**, 42 (27), 9826-30.
41. Lee, S. Y.; Yasuda, T.; Komiyama, H.; Lee, J.; Adachi, C., Thermally Activated Delayed Fluorescence Polymers for Efficient Solution-Processed Organic Light-Emitting Diodes. *Advanced Materials* **2016**, 28 (21), 4019-24.
42. Huang, T.; Jiang, W.; Duan, L., Recent progress in solution processable TADF materials for organic light-emitting diodes. *Journal of Materials Chemistry C* **2018**, 6 (21), 5577-5596.
43. Paisley, N., R.; Tonge, C. M.; Hudson, Z. M., Stimuli-Responsive Thermally Activated Delayed Fluorescence in Polymer Nanoparticles and Thin Films: Applications in Chemical Sensing and Imaging. *Front. Chem.* **2020**, 8, 229.
44. Pedersen, C. J., Cyclic polyethers and their complexes with metal salts. *J. Am. Chem. Soc.* **1967**, 89 (26), 7017-7036.
45. Cram, D. J.; Cram, J. M., Host-Guest Chemistry: Complexes between organic compounds simulate the substrate selectivity of enzymes. *Science* **1974**, 183 (4127), 803-809.
46. Lehn, J.-M., Cryptates: The Chemistry of Macropolycyclic Inclusion Complexes. *Acc. Chem. Res.* **1978**, 11 (2), 49-57.
47. Lehn, J.-M., Supramolecular chemistry: Where from? Where to? *Chemical Society Reviews* **2017**, 46 (9), 2378-2379.
48. Wang, W.; Wang, Y.-X.; Yang, H.-B., Supramolecular transformations within discrete coordination-driven supramolecular architectures. *Chemical Society Reviews* **2016**, 45 (9), 2656-93.
49. Lehn, J.-M.; Rigault, A.; Siegel, J.; Harrowfield, J.; Chevrier, B.; Moras, D., Spontaneous assembly of double-stranded helicates from oligobipyridine ligands and copper(I) cations: Structure of an inorganic double helix. *Proc. Natl. Acad. Sci.* **1987**, 84 (9), 2565-2569.
50. Kramer, R.; Lehn, J.-M.; Marquis-Rigault, A., Self-recognition in helicate self-assembly: spontaneous formation of helical metal complexes from mixtures of ligands and metal ions. *Proc. Natl. Acad. Sci.* **1993**, 90 (12), 5394-5398.
51. Seidel, S. R.; Stang, P. J., High-Symmetry Coordination Cages via Self-Assembly. *Acc. Chem. Res.* **2002**, 35 (11), 972-983.
52. Li, S.; Huang, J.; Zhou, F.; Cook, T. R.; Yan, X.; Ye, Y.; Zhu, B.; Zheng, B.; Stang, P. J., Self-assembly of triangular and hexagonal molecular necklaces. *J. Am. Chem. Soc.* **2014**, 136 (16), 5908-5911.
53. Yoshizawa, M.; Klosterman, J. K.; Fujita, M., Functional molecular flasks: new properties and reactions within discrete, self-assembled hosts. *Angew. Chem. Int. Ed.* **2009**, 48 (19), 3418-38.
54. Sawada, T.; Hisada, H.; Fujita, M., Mutual induced fit in a synthetic host-guest system. *J. Am. Chem. Soc.* **2014**, 136 (12), 4449-4451.

55. Wang, J.-L.; Li, X.; Lu, X.; Hsieh, I.-F.; Cao, Y.; Moorefield, C. N.; Wesdemiotis, C.; Cheng, S. Z. D.; Newkome, G. R., Stoichiometric self-assembly of shape-persistent 2D complexes: a facile route to a symmetric supramacromolecular spoked wheel. *J. Am. Chem. Soc.* **2011**, *133* (30), 11450-11453.
56. Xie, T.-Z.; Liao, S.-Y.; Guo, K.; Lu, X.; Dong, X.; Huang, M.; Moorefield, C. N.; Cheng, S. Z. D.; Liu, X.; Wesdemiotis, C.; Newkome, G. R., Construction of a highly symmetric nanosphere via a one-pot reaction of a tristerpyridine ligand with Ru(II). *J. Am. Chem. Soc.* **2014**, *136* (23), 8165-8168.
57. Holliday, B. J.; Mirkin, C. A., Strategies for the Construction of Supramolecular Compounds through Coordination Chemistry. *Angew. Chem. Int. Ed.* **2001**, *40* (11), 2022-2043.
58. Gianneschi, N. C.; Masar, M. S.; Mirkin, C. A., Development of a Coordination Chemistry-Based Approach for Functional Supramolecular Structures. *Acc. Chem. Res.* **2005**, *38* (11), 825-837.
59. Mendez-Arroyo, J.; Barroso-Flores, J.; Lifschitz, A. M.; Sarjeant, A. A.; Stern, C. L.; Mirkin, C. A., A multi-state, allosterically-regulated molecular receptor with switchable selectivity. *J. Am. Chem. Soc.* **2014**, *136* (29), 10340-10348.
60. Caulder, D. L.; Raymond, K. N., Supermolecules by Design. *Acc. Chem. Res.* **1999**, *32* (11), 975-982.
61. Zhao, C.; Sun, Q.-F.; Hart-Cooper, W. M.; DiPasquale, A. G.; Toste, F. D.; Bergman, R. G.; Raymond, K. N., Chiral amide directed assembly of a diastereo- and enantiopure supramolecular host and its application to enantioselective catalysis of neutral substrates. *J. Am. Chem. Soc.* **2013**, *135* (50), 18802-18805.
62. Nitschke, J. R., Construction, Substitution and Sorting of Metallo-organic Structures via Subcomponent Self-Assembly. *Acc. Chem. Res.* **2007**, *40* (2), 103-112.
63. Castilla, A. M.; Ramsay, W. J.; Nitschke, J. R., Stereochemistry in subcomponent self-assembly. *Acc. Chem. Res.* **2014**, *47* (7), 2063-2073.
64. Zhang, D.; Ronson, T. K.; Xu, L.; Nitschke, J. R., Transformation Network Culminating in a Heteroleptic Cd₆L₆L'₂ Twisted Trigonal Prism. *J. Am. Chem. Soc.* **2020**, *142* (20), 9152-9157.
65. Hiraoka, S.; Goda, M.; Shionoya, M., Alternate Arrangements of Two Different Metals at Chemically-Equivalent Binding Sites on a Circle. *J. Am. Chem. Soc.* **2009**, *131* (13), 4592-4593.
66. Han, M.; Engelhard, D. M.; Clever, G. H., Self-assembled coordination cages based on banana-shaped ligands. *Chemical Society Reviews* **2014**, *43* (6), 1848-1860.
67. Xu, L.; Wang, Y.-X.; Chen, L.-J.; Yang, H.-B., Construction of multiferrocenyl metallacycles and metallacages via coordination-driven self-assembly: from structure to functions. *Chemical Society Reviews* **2015**, *44* (8), 2148-2167.
68. Mukherjee, S.; Mukherjee, P. S., Template-free multicomponent coordination-driven self-assembly of Pd(II)/Pt(II) molecular cages. *Chem. Commun.* **2014**, *50* (18), 2239-2248.
69. Lescop, C., Coordination-Driven Supramolecular Synthesis Based on Bimetallic Cu(I) Precursors: Adaptive Behavior and Luminescence. *Chem. Rec.* **2021**, *21* (3), 544-557.
70. Scheer, M., The coordination chemistry of group 15 element ligand complexes-a developing area. *Dalton Transactions* **2008**, (33), 4372-4386.
71. Heindl, C.; Peresyphkina, E. V.; Virovets, A. V.; Kremer, W.; Scheer, M., Giant Rugby Ball [{Cp(Bn)Fe(eta(5)-P5)}₂₄Cu₉₆Br₉₆] Derived from Pentaphosphaferrocene and CuBr₂. *J. Am. Chem. Soc.* **2015**, *137* (34), 10938-41.
72. Leca, F.; Lescop, C.; Rodriguez-Sanz, E.; Costuas, K.; Halet, J.-F.; Reau, R., Bridging phosphanes: exotic or versatile binucleating ligands? *Angew. Chem. Int. Ed.* **2005**, *44* (28), 4362-5.

73. Lescop, C., Coordination-Driven Syntheses of Compact Supramolecular Metallacycles toward Extended Metallo-organic Stacked Supramolecular Assemblies. *Acc. Chem. Res.* **2017**, *50* (4), 885-894.
74. Vreshch, V.; Nohra, B.; Lescop, C.; Reau, R., Synthesis of small tetranuclear Cu(I) metallacycles based on bridging pseudohalogenide ions. *Inorg. Chem.* **2013**, *52* (3), 1496-503.
75. Nohra, B.; Graule, S.; Lescop, C.; Reau, R., Mimicking [2,2]Paracyclophane Topology: Molecular Clips for the Coordination-Driven Cofacial Assembly of π -Conjugated Systems. *J. Am. Chem. Soc.* **2006**, *128* (11), 3520-3521.
76. Yao, Y.; Shen, W.; Nohra, B.; Lescop, C.; Reau, R., Coordination-driven hierarchical organization of π -conjugated systems: from molecular to supramolecular π -stacked assemblies. *Chem. Eur. J.* **2010**, *16* (24), 7143-63.
77. Wu, M.-M.; Zhang, L.-Y.; Qin, Y.-H.; Chen, Z.-N., Bis[μ -bis(diphenylphosphino)methane- κ^2 P:P']bis[diacetonitrilecopper(I) bis(hexafluorophosphate)]. *Acta Cryst. E* **2003**, *59*, 195-196.
78. Liaw, B.-J.; Lobana, T. S.; Lin, Y.-W.; Wang, J.-C.; Liu, C. W., Versatility of Dithiophosphates in the Syntheses of Copper(I) Complexes with Bis(diphenylphosphino)alkanes: Abstraction of Chloride from Dichloromethane. *Inorg. Chem.* **2005**, *44* (26), 9921-9929.
79. Bergmann, L.; Braun, C.; Nieger, M.; Bräse, S., The coordination- and photochemistry of copper(i) complexes: variation of N^N ligands from imidazole to tetrazole. *Dalton Transactions* **2018**, *47* (2), 608-621.
80. Nohra, B.; Yao, Y.; Lescop, C.; Reau, R., Coordination polymers with π -stacked metalloparacyclophane motifs: F-shaped mixed-coordination dinuclear connectors. *Angew. Chem. Int. Ed.* **2007**, *46* (43), 8242-5.

Chapter II Preparation of a series of Cu(I) based 1D coordination polymers and study of their solid-state and luminescence properties

II-1 Presentation of the Cu(I) bimetallic precursor used

Considering the latest advancements in coordination driven supramolecular chemistry and the need to develop affordable new luminescent materials, I started to work on a series of new compounds based on an inexpensive Cu(I) precursor. However, before going into the details about the results presented in this thesis, it is important to get a better understanding of properties of the starting building block that will be used throughout this chapter.

This precursor was first synthesized in 2016¹ by taking full advantage of a coordination driven supramolecular approach that was developed by the Lescop group.² This compound is based on a pre-assembled bimetallic clip of $[\text{Cu}_2(\mu_2\text{-dppm})_2(\text{CH}_3\text{CN})_4](\text{PF}_6)_2$. This bimetallic molecular clip was reacted in a 1 to 1 ratio with KCN in dichloromethane, at room temperature under air. After stirring, the solution mixture appears as a colorless cloudy solution. Upon pentane vapor diffusion into the filtered solution, homogeneous crystals of this compound, which will be denominated **A**, were obtained. The obtained crystals are block shaped, transparent, colorless, air-stable and isolated with a good yield of 80%. The coordination of the cyanide ligand to the metal centers of the bimetallic clip is indicated in the infrared spectrum by the presence of a vibration band of the cyanide ion $\nu_{(\text{CN})}$ located at 2117 cm^{-1} . The crystals of **A** were of good quality for single crystal X-ray diffraction measurement and crystal structure resolution. This measurement revealed the connection of two bimetallic units of $[\text{Cu}_2(\mu_2\text{-dppm})_2]^{2+}$ by two cyanide units acting as ditopic linkers, resulting in the formation of a novel $\text{Cu}_4(\text{CN})_2$ tetrametallic metallacycle (Figure II-1).

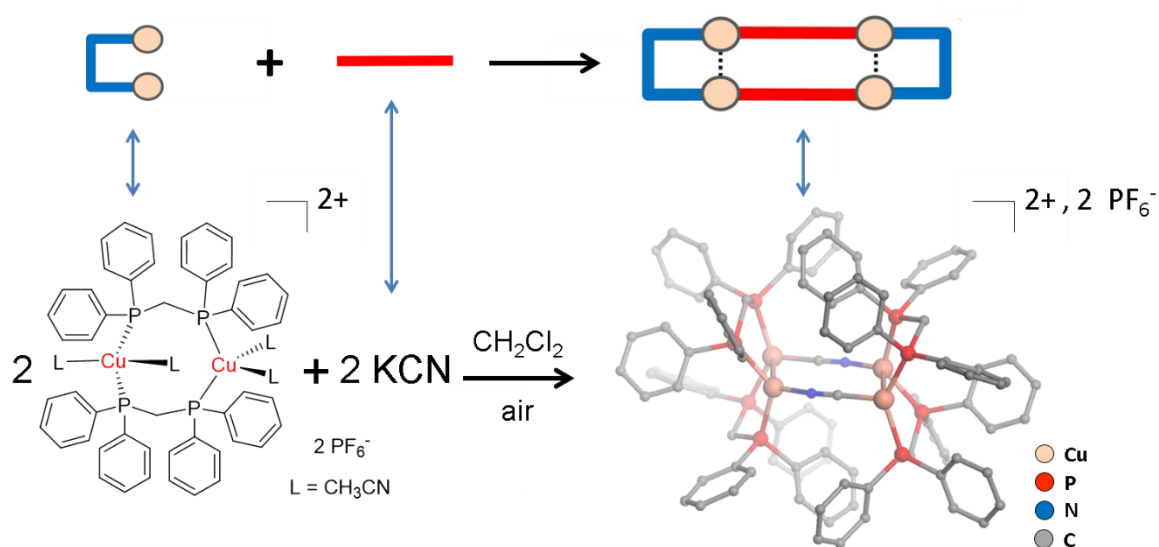


Figure II-1 : Top : Reaction scheme of the reaction between the $[\text{Cu}_2(\mu_2\text{-dppm}_2)(\text{CH}_3\text{CN})_2]^{2+}$ bimetallic unit and KCN ; Bottom : Chemical diagram of the dimeric precursor and view of the molecular structure of **A** obtained via single crystal X-ray diffraction (hydrogen atom, counter-anions PF_6^- and included solvent molecules have been omitted for clarity).

In this metallacycle **A**, the Cu(I) metal centers present a distorted trigonal planar geometry, different from the tetrahedral arrangement found in the initial $[\text{Cu}_2(\mu_2\text{-dppm})_2(\text{CH}_3\text{CN})_4](\text{PF}_6)_2$ bimetallic units. The Cu-Cu distance in the metallacycle is found to be 2.8669(6) Å which is in the reasonable range for cuprophilic interactions to take place.^{3,4,5,6} The compound **A** exhibits interesting photophysical properties which are reported in Figure II-2.

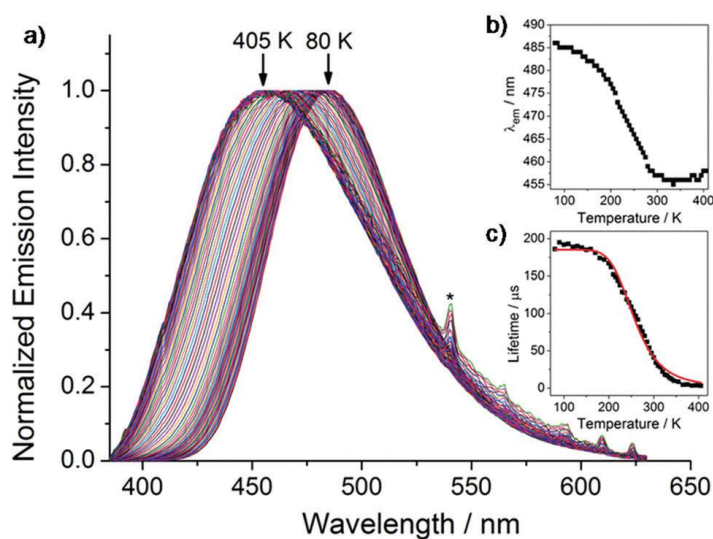


Figure II-2 : a) Normalized solid-state emission spectra of **A** depending of the temperature between 80 K and 405 K b) Plot of emission peak maximum against temperature c) Emission decay time against temperature of the long component of the bi-exponential decay time. Reproduced from¹.

A presents in the solid-state an intense eye-perceived blue emission under UV light ($\lambda_{\text{ex}} = 320$ nm) at room temperature (RT). This emission is characterized by a large and featureless band centered at 457 nm. This emission is accompanied by a bi-exponential decay time of 10 and 40 μs and an emission quantum yield in the solid-state of 72%. Upon cooling down, compound **A** presents a bathochromic shift of its emission spectrum and, at 80 K, the emission spectrum is a large band centered at 486 nm, corresponding to an eye-perceived green luminescence color ($\lambda_{\text{ex}} = 320$ nm). The emission decay times increases upon cooling, reaching 40 and 200 μs at 80 K. This particular behavior is typical of the thermochromic behavior commonly described in highly emissive Cu(I) derivatives exhibiting thermally activated delayed fluorescence (TADF). By fitting the variation of the long component of the lifetime of the excited state versus the temperature with the equation of TADF⁷ (see Equation I-1), it was possible to obtain the values of $\Delta E(S_1-T_1) = 1560 \text{ cm}^{-1}$, $\tau(S_1) = 10 \text{ ns}$ and $\tau(T_1) = 185 \mu\text{s}$.

The reactivity and the prospect of using **A** as a precursor in coordination driven supramolecular synthesis was first explored in 2018.⁸ Indeed, the coordination sphere of the Cu(I) atoms present in the metallacycle being trigonal planar distorted, it allows for the coordination of new donor ligands and thus, achieving potential new supramolecular assemblies. This prospect was investigated first with two types of donor ligand : KCN and a number of metallo-ligands $\text{K}_2[\text{M}(\text{CN})_4]$, where M = Ni, Pd or Pt. In both cases, crystals of new products were obtained and it was possible to conduct single crystal X-ray diffraction on them. This measurement revealed that the reaction between **A** and KCN led to the formation of a neutral helicoidal one-dimensional coordination polymer constituted of repeating dimeric units $[\text{Cu}_2(\mu_2\text{-dppm}_2)\text{CN}_2]$. The reaction with the metallo-ligands $\text{K}_2[\text{M}(\text{CN})_4]$ led to the obtention of a series of new metallacycles composed of four dimeric units $\text{Cu}_2(\mu_2\text{-dppm}_2)$ linked together *via* cyano ligand, surrounding a square planar $\text{M}(\text{CN})_4$ moiety resulting in the formation of a $[\text{Cu}_8\text{M}(\text{CN})_8\text{dppm}_3]^{2+}$ discrete unit (Figure II-3).

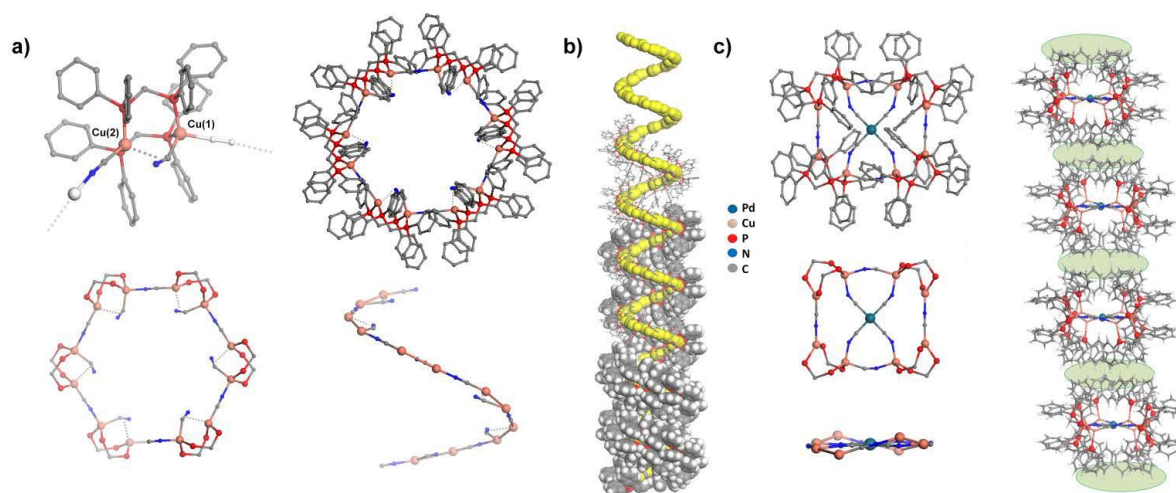


Figure II-3 : a) Different views of the molecular X-ray structure after the reaction between **A** and KCN b) view perpendicular to the c axis of the helicoidale polymer c) views of the molecular X-ray structure of the compound resulting from the reaction between **A** and $K_2[Pd(CN)_4]$. Adapted from⁸.

The photophysical properties of the obtained new assemblies were investigated and were found to be far different from the ones exhibited in the precursor **A**. The helicoidal compound presents an eye-perceived yellow luminescence at room temperature characterized by a broad, featureless emission band centered around 538 nm, typical of metal-perturbed dppm ligand-centered phosphorescence.⁹ The metallacycles based on metallo-ligands presents an eye-perceived turquoise luminescence with a variation in intensity along the series (Ni being weakly emissive, Pd moderately and Pt being highly emissive). Considering the photophysical properties of the newly obtained supramolecular assemblies, it was concluded that the TADF behavior was retained only in the metallacycles obtained *via* the reaction with $K_2[Pd(CN)_4]$ and $K_2[Pt(CN)_4]$. All in all, this proved that **A** is a very versatile precursor that renders possible the obtention of diverse supramolecular assemblies that are accompanied by interesting photophysical behaviors.

In addition, the resulting supramolecular assemblies based on **A** also exhibit stimuli responsive behavior on top of the interesting photophysical properties already displayed in the solid-state. This was highlighted in a recent study of the mechanochromic properties of the $K_2[Pd(CN)_4]$ based compound published in 2018.⁸ It was indeed found that this compound presents a shifted luminescent spectrum as well as an increased luminescent quantum yield in the solid-state upon mechanical grinding and melting.¹⁰

This further reinforces the attractiveness of the compound **A** as a precursor to produce new supramolecular assemblies presenting diverse photophysical properties as well as possible stimuli responsive behavior.

II-2 Synthesis of a series of Cu(I) one dimensional coordination polymers

With this compound **A** in hand, and the interesting properties displayed by it, either in its assembling behavior or in its photophysical properties, it was decided to further explore this compound as a precursor. The next step in this exploration was done during my PhD where I studied the reaction between this precursor **A** and a variety of pyridyl-capped ligands. The choice of this kind of ligand was done with the idea of providing the coordinatively low-saturated Cu(I) metal centers of **A** with alternative N-donor purely organic ligands. It was done so to take advantage of the trigonal planar distorted coordination sphere found in the precursor and achieve new supramolecular polymetallic assemblies thanks to the highly directional coordination mode and the size of such ligand in particular compared to the « small » anionic ligands previously reacted with **A** (Figure II-3). This study focused on the reaction between the precursor **A** and seven pyridyl-capped polytopic ligands, and the obtained compounds' structures and photophysical properties were explored in detail. The seven ligands selected are presented in the Figure II-4 and are designated as **B_n**.

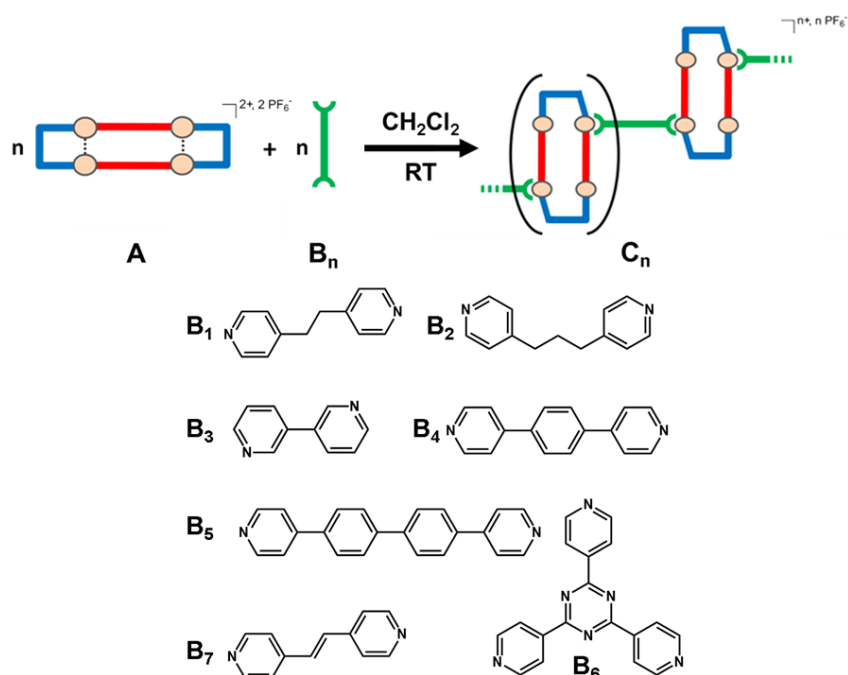


Figure II-4 : Synthesis diagram of the preparation of the derivative **C_n** and molecular structure of the pyridyl capped ligands **B_n** used in this study.

These ligands used are 3- or 4-pyridyl capped and presents various degrees of π conjugation along their backbone. Also, it is to be noted that among these ligands, all of them are ditopic in their nature, except the **B₆** ligand which presents a tritopic nature.

The reactions between **A** and **B_n** were done under room temperature. The ligands were used directly as received from chemical companies and without further purification, and it was also the case for the solvents used.

The first step of the synthesis is the dissolution of the precursor **A** in dichloromethane. Typically, 60 mg (0.028 mmol) of the precursor **A** are dissolved in 15 ml of dichloromethane in an Erlenmeyer, at room temperature, and kept under stirring for one hour. This allows for the dissolution of large part of the precursor. A solution of the ligand **B_n** is prepared in a 1 :1 ratio with **A**, dissolved in dichloromethane. This solution of the ligand **B_n** is added to the main solution and the stirring is stopped to avoid potential rapid precipitation out of solution of the forming new assemblies. Just after the addition is done, the solution retains a clear, not colored aspect and the eye-perceived blue luminescence of the solution of **A** under UV light is lost. At this point, two kind of crystallizations processes can be applied : synthesis done with the aliphatic ligands **B₁** to **B₃** are put to crystallize under pentane vapors diffusion two hours after the addition of the ligand. Once in this setup, the crystals take a few days to appear (typically between 2 and 7 for yields between 60-80 %). For the other preparation based on the more π -conjugated rigid ligands **B₄** to **B₇**, the crystallization process occurs directly after the addition of the ligands **B_n**. The solution is then set aside at room temperature and is left in the reaction flask. Crystals start to appear at the bottom of the reaction flask in a few days. For all seven syntheses, it is possible to isolate after a week homogeneous batches of yellow or white crystals of the new species **C_n**. The averaged yields of these reactions range between 50 and 80 % (Table II-1).

compound	C1	C2	C3	C4	C5	C6	C7
Reaction yield	63 %	84 %	68 %	79 %	62 %	82 %	54 %

Table II-1 : Averaged reaction yields of the compounds **C_n**.

II-3 Infrared spectroscopic characterization of the compounds **C_n**

The precursor **A** presents a band associated to the cyanide linker which is typically found to be moderately intense and measured at 2117 cm^{-1} (see Figure II-5). This $\nu_{(\text{CN})}$ stretching band is shifted to a higher value compared to the free cyano ligand (2080 cm^{-1} in aqueous solution) as

a result of the coordination to the copper atoms. This is due to the CN^- ion acting as a σ -donor toward metal centers and as a π -acceptor. This σ -donation tends to increase the frequency of the $\nu_{(\text{CN})}$ band due to electrons being removed from the 5σ , weakly antibonding, orbital. With the π -acceptor behavior, electrons enter the antibonding $2p\pi^*$, decreasing the $\nu_{(\text{CN})}$ frequency. Generally, CN^- ions are better σ -donor than π -acceptor, leading to an increase of the $\nu_{(\text{CN})}$ frequency upon coordination to metal ions compared to the free ion.¹¹

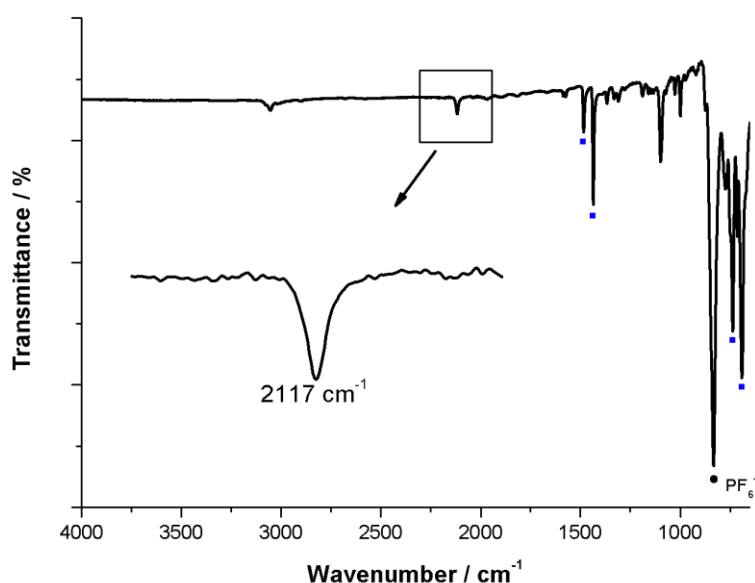


Figure II-5 : Infrared spectrum of the precursor **A** ; insert : focus on $\nu_{(\text{CN})}$ stretching vibration band. The dot marks the PF_6^- counter anion t_{1u} vibration mode band. Blue squares mark typical dppm $\delta_{(\text{C-H})}$ ligand bands.

Another noticeable absorption band present in the infrared spectrum of precursor **A** is the absorption band present at 833 cm^{-1} . This band is attributed to the t_{1u} vibration mode of the hexafluorophosphate PF_6^- counter-anion present in the compound. An harmonic pattern can be observed between 2000 and 1750 cm^{-1} and can be attributed to the $\delta_{(\text{C-H})}$ bending band of the monosubstituted aromatic rings in the dppm backbone ligands. Along with this harmonic pattern, the dppm backbone ligands display a number of absorption bands in the infrared spectrum, present at 1485 , 1435 , 737 and 691 cm^{-1} . The two medium bands present at 1485 and 1435 cm^{-1} stem from the $\delta_{(\text{C-H})}$ bending band of the aromatic ring, while the strong band at 691

cm^{-1} stems from out of plane vibration of the aromatic rings. The strong band at 737 cm^{-1} stems from the $\delta_{(\text{C-H})}$ bending band of a monosubstituted benzene ring.

The compounds C_n all present highly similar infrared spectra to that of precursor **A**. They all present the reported medium and strong bands at *ca.* 1485, 1435, 737 and 690 cm^{-1} , stemming from the presence of the dppm ligand backbone with little to no shift in the observed wavenumbers. Along with the dppm absorption band in their infrared spectra, the $\nu_{(\text{CN})}$ stretching band is also observed, albeit shifted to lower wavenumbers compared to the same band in the precursor **A**, which indicates a coordination of the pyridyl-capped linkers to the copper atoms, increasing the coordination number of the metal centers and thus lowering the frequency of the cyanide stretching band.^{11,12} The values at which the $\nu_{(\text{CN})}$ stretching band is found in the compounds C_n are reported in Table II-2.

Compound	A	C1	C2	C3	C4	C5	C6	C7
$\nu_{(\text{CN})} (\text{cm}^{-1})$	2117	2102	2095	2103	2096	2088	2102	2100

Table II-2 : Values of the $\nu_{(\text{CN})}$ vibration band found in the **A** precursor and in C_n compounds.

The t_{1u} band of the PF_6^- counter anion is also present in the infrared spectra of the compounds C_n , without noticeable changes from the precursor **A**, at 834 cm^{-1} .

All the similarities between the infrared spectra of C_n compounds and precursor **A** indicate that the reaction between the precursor **A** and the linkers B_n did not lead to a noticeable change of the structure of the tetrametallic metallacycle after the reaction.

Along with the molecular structure of the precursor **A** being preserved in the newly obtained compounds C_n , an absorption band attributed to the vibration mode of pyridyl moieties when coordinated to a metal can be observed at *ca.* 1605 cm^{-1} in the infrared spectra of all compounds except C_6 , pointing to a coordination occurring between the linkers B_n and the tetrametallic metallacycle of precursor **A** during the reactions leading to new species (Figure II-6). The absence of this absorption band in the infrared spectra of C_6 can be explained by the difference in the structure of the linker B_n used : the linker B_6 presents a triazine group in its scaffold which induced a shift of the vibration mode of the pyridyl moieties as coordinated to the metal that also overlap with the dppm ligands bands. In the case of C_6 , it is possible to identify the linker in the infrared spectrum with the presence of absorption bands of the 1,3,5-triazine pattern at *ca.* 1517 and 1375 cm^{-1} .¹³

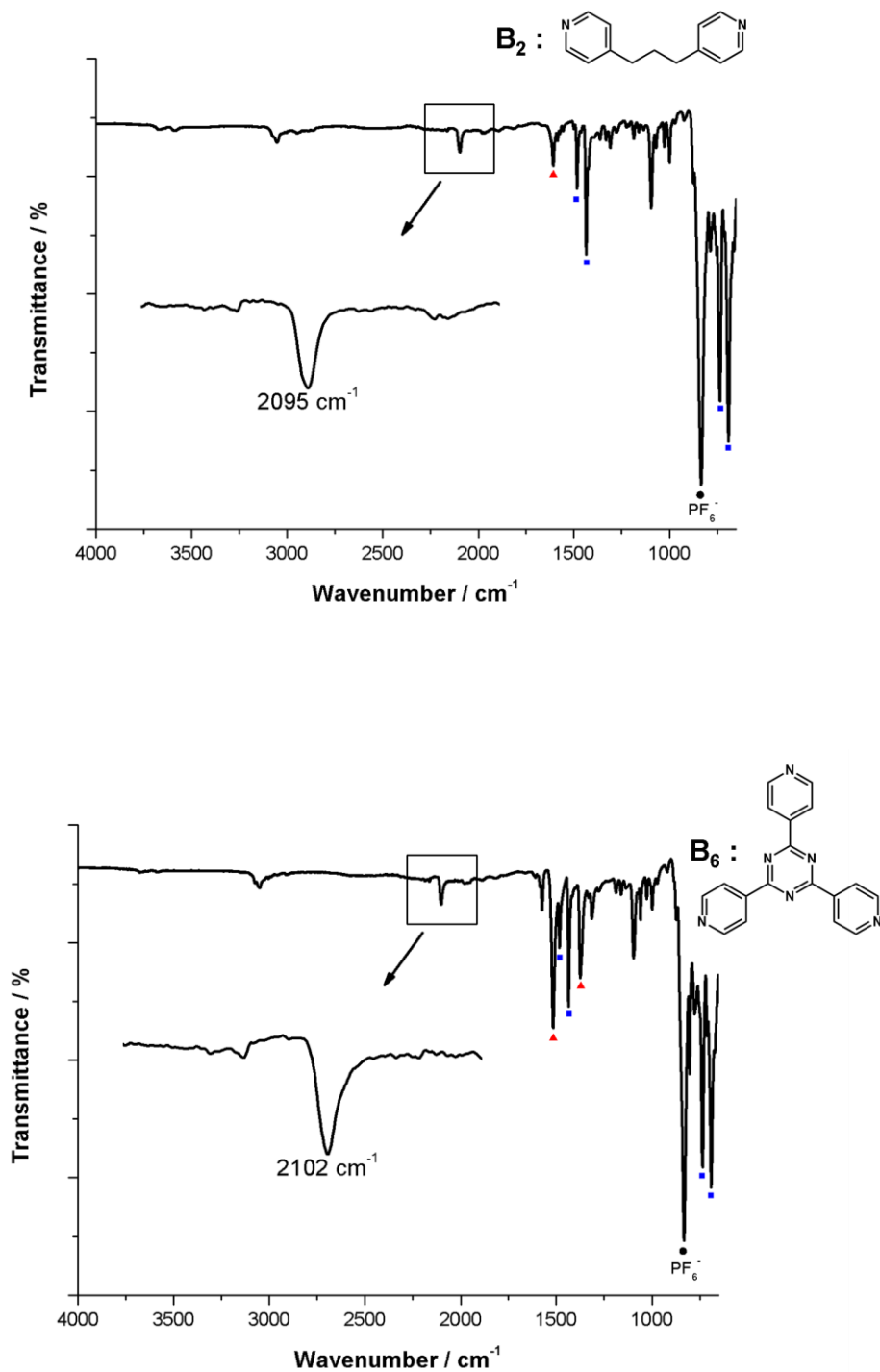


Figure II-6 : top : Infrared spectrum of compound **C₂**; bottom : Infrared spectrum of compound **C₆**. The dot marks the PF₆⁻ counter anion t_{1u} vibration mode band. Blue squares mark typical dppm $\delta_{(C-H)}$ ligand bands. Red triangles mark **B_n** ligands bands. The infrared spectra of others compounds **C_n** are available in this chapter's appendix.

II-4 Structural characterization of compounds C_n by single crystal X-ray diffraction studies

For all compounds C_n , it was possible to obtain single crystals of sufficient quality to conduct single crystal X-ray diffraction studies, whether they were obtained in the reaction flask or by pentane vapors diffusion. This measurement made it possible to determine the compounds' crystalline molecular structure (Table II-3). All compounds C_n are one-dimensional coordination polymers exhibiting an alternation between a tetrametallic metallacycle and the polytopic linkers B_n in a 1 to 1 ratio. Herein, the crystalline structure of the compound C_3 , resulting from the reaction between **A** and **B₃** will be described (Figure II-7).

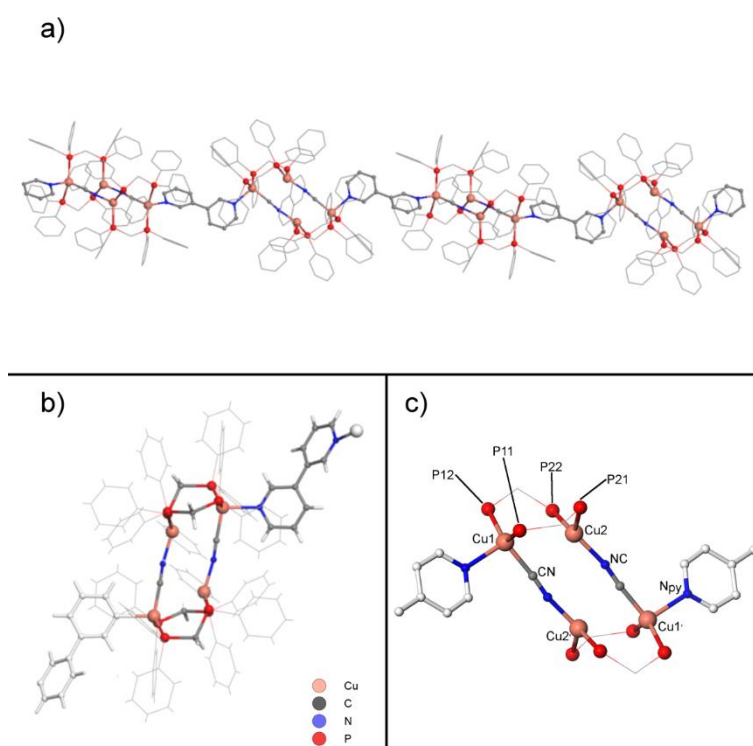


Figure II-7 : a) View of the molecular structure of the one-dimensional coordination polymer C_3 obtained via single-crystal X-ray diffraction (hydrogen atom, counter-anions PF_6^- and included solvent molecules have been omitted for clarity) b) view of the repetition unit of the polymer C_3 c) notation of the atoms of the structure for the distances and angle measurements.

C_3 consists in a one-dimensional coordination polymer crystallizing in the $C2/c$ space of the monoclinic system. The repetition unit of this polymer is composed of one bimetallic fragment $Cu_2(dppm)_2$, one cyanide ligand and the polytopic ligand **B₃**. The structure is completed by one counter-anion PF_6^- and three solvent molecules CH_2Cl_2 . The extended crystalline structure of

this compound forms a one-dimensional coordination polymer alternating between tetrametallic metallacycles $[\text{Cu}_4(\text{dppm})_4\text{CN}_2]^{2+}$ linked together by the ligand **B3**.

In this structure, two Cu(I) ions are coordinated to two phosphorus atoms of each dppm ligand that form chelates similar to the ones found in **A**, and CN^- anions are linking these bimetallic units Cu_2dppm_2 , leading to the formation of a tetrametallic metallacycle similar to the one observed in **A**. The coordination sphere of one of the two Cu(I) ion in each Cu_2dppm_2 unit is completed by a nitrogen atom from the ligand **B3** affording a tetrahedral coordination sphere while the other Cu(I) ion stays in a distorted trigonal planar coordination sphere. The bimetallic units Cu_2dppm_2 of the metallacycle are then in a peculiar situation where the Cu(I) metal centers are in two different coordination spheres : the acute metallic center (regarding the metallacycle geometry) possesses a tetrahedral coordination sphere and the obtuse metallic center possesses a distorted trigonal planar coordination sphere.

All the seven coordination polymers obtained present a similar molecular organization but it can be noted that in the particular case of **C6**, even though the ligand **B6** is tritopic in nature, only two pyridyl coordination sites are used, the third one staying free and non coordinated. This peculiar behavior account for the one-dimensional nature of the polymer **C6**. This behavior can be tentatively assigned to the steric hindrance of the ligand's environment, preventing the coordination of the third pyridyl group to occur, as well as the presence of apparent inter molecular π - π stacking interactions taking place between the polymer chains, involving the uncoordinated 4-pyridyl fragment (Figure II-8).

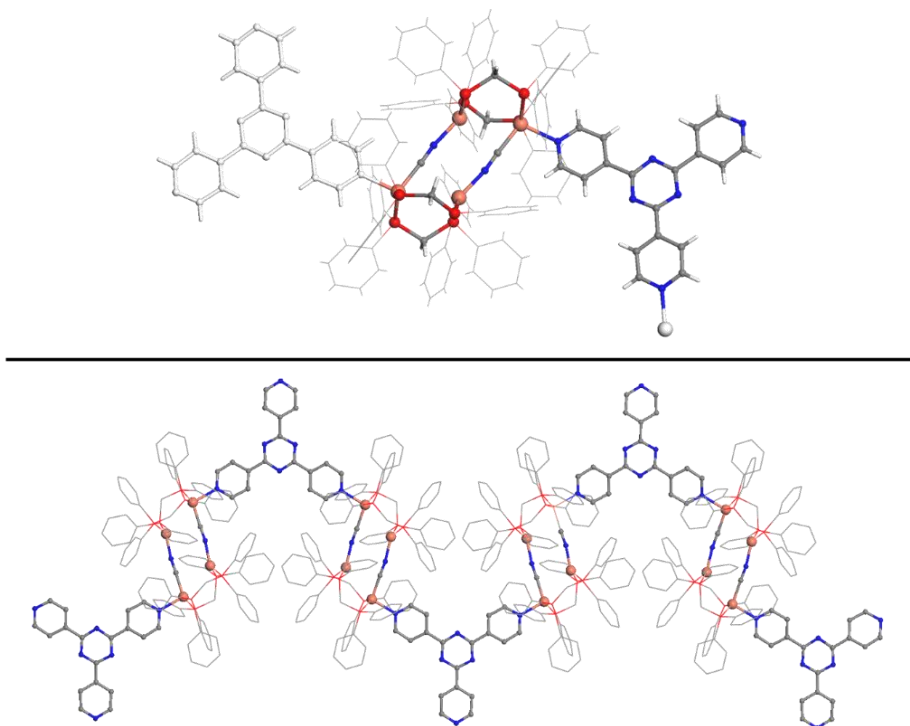


Figure II-8 : top) molecular structure of the C_6 compound's repetition unit, determined by single crystal X-ray diffraction; bottom) extended molecular structure of the 1D coordination polymer C_6 . The molecular structure of others compounds C_n are available in this chapter's appendix.

	A	C₁	C₂	C₃
Space group	P21/n	P21/n	P-1	C2/c
Cu1-Cu2 (Å)	2.8655(8)	3.127	3.208	3.276
Cu1-CN (Å)	1.956(17)	1.983	1.965(3)	1.978(3)
Cu2-NC (Å)	1.96(4)	1.973	1.987(3)	1.979(3)
Cu1'-N_{Py} (Å)	/	2.111	2.117(3)	2.181(3)
Cu1-P11 (Å)	2.2472(12)	2.304	2.2499(9)	2.2929(14)
Cu1-P12 (Å)	2.2612(12)	2.274	2.2835(10)	2.2766(12)
Cu2-P21 (Å)	2.2621(12)	2.263	2.2421(10)	2.2581(13)
Cu2-P22 (Å)	2.2590(12)	2.256	2.2548(10)	2.2591(12)
Cu1-Cu2' (Å)	5.007	5.084	5.079	5.094
Cu2-Cu1-Cu2' (°)	57.34	55.89	48.6	52.094
Cu1-Cu2-Cu1' (°)	122.66	124.11	131.4	127.96
m-m (Å)	/	13.455	12.693	9.528

	C₄	C₅	C₆	C₇
Space group	P-1	P21	C2/c	P-1
Cu1-Cu2 (Å)	3.275	3.2337	3.199	3.22
Cu1-CN (Å)	1.968(3)	1.955(3)	1.965(2)	1.9657(18)
Cu2-NC (Å)	1.965(3)	1.962(3)	1.969(2)	1.9648(17)
Cu1'-N_{Py} (Å)	2.133(2)	2.137(2)	2.1486(19)	2.1426(16)
Cu1-P11 (Å)	2.2985(10)	2.2615(8)	2.2758(8)	2.2628(7)
Cu1-P12 (Å)	2.2575(10)	2.2769(8)	2.2605(7)	2.2888(9)
Cu2-P21 (Å)	2.2575(9)	2.2553(8)	2.2657(8)	2.2611(8)
Cu2-P22 (Å)	2.2566(9)	2.2529(8)	2.2570(7)	2.2546(8)
Cu1-Cu2' (Å)	5.072	5.07	5.070	5.068
Cu2-Cu1-Cu2' (°)	54.49	49.54	57.38	54.81
Cu1-Cu2-Cu1' (°)	125.51	130.35	128.13	125.19
m-m (Å)	15.56	19.932	13.3	13.525

Table II-3 : Measurements of selected distances and angles in **A** precursor and in **C_n** compounds. « m-m » is the measured distance between the metal centers of two neighbouring metallacycles subunits (see Figure II-7 c) for notation).

Concerning the intermetallic distance of the bimetallic units, a great increase can be observed in the one-dimensional coordination polymers **C_n** compared to the precursor **A**. Indeed, while this Cu-Cu distance was found to be 2.8669(6) Å in **A** at 150 K, it ranges from 3.127 Å to 3.276 Å in the polymers **C_n** (Table II-3). This increase in the Cu-Cu distance in the bimetallic units can be attributed to the change of coordination sphere of one of the Cu(I) metallic centers from trigonal planar distorted to tetrahedral. This increase in the intermetallic distance prevents the possibility of cuprophilic interactions to take place in the newly obtained polymers as opposed to the precursor **A**. While an elongation of the inter « Cu₂dppm₂ » distances within these tetrametallic metallacycle upon coordination to the ligand is not observed, a slight « flattening » of the metallacycle seems to occur. Indeed, the distance between two opposed Cu(I) metal center (d(Cu1-Cu2')) in Table II-3) stay mostly the same, while the obtuse angle (Cu1-Cu2-Cu1') increase across the **C_n** family of compounds is in the range of 124.11° to 131.40° compared to the value of 122.66° found in **A**. Besides this, the metallacycle backbone is mostly unchanged. Finally, it can be noted that all others metric data found in derivatives **C_n** are in a classical ranges for such compounds.^{1,8} Powder X-ray diffraction have also been investigated for these compounds affording diagrams in agreement with the single crystal X-ray diffraction data assuming the homogeneity of the phase. For the sake of clarity, it was considered to be more pertinent to present and describe these diagrams in the next chapter.

II-5 Photophysical studies of the compounds C_n

In spite of all the structural differences between the linkers B_n used in this study such as the aliphatic character or the geometry and length, all obtained polymers C_n share a common and homogeneous geometry being one-dimensional coordination polymers. All the one-dimensional coordination polymers are white powders in the solid-state at room temperature, with the exception of C_6 which is a yellow polycrystalline solid. Yet they display a remarkably variety of eye-perceived emission colors of luminescence under UV light (Figure II-9).

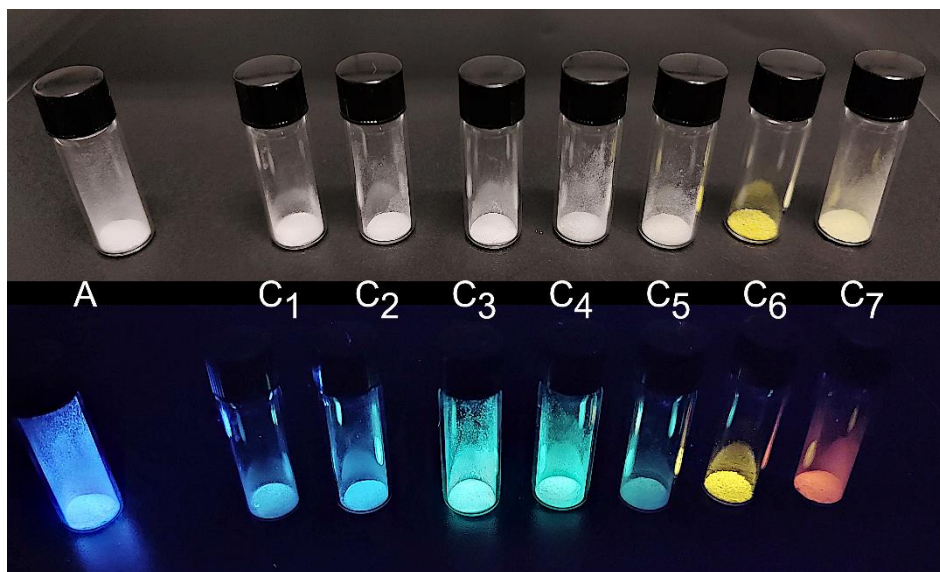


Figure II-9 : Photography under visible (top) and UV light (bottom) ($\lambda_{\text{ex}} = 365 \text{ nm}$) of all C_n polymers and precursor **A**.

II-5.a Solid-state UV-visible absorption study of the polymers C_n .

The solid-state room temperature UV-vis absorption spectrum of the polymers C_n were measured. The polymers C_n present a large and intense absorption band with maxima centered between 300 nm and 400 nm, which corresponds with the white color observed for the powders. Notably, the polymer C_6 is obtained as a yellow colored powder and this reflect in its UV-visible absorption spectra being broader than the other polymers as well as being overall red-shifted. These measured absorption spectrums can be attributed to mainly π - π^* transitions centered on the organic aromatic ligands (dppm and/or connecting B_n ligands) (Figure II-10).

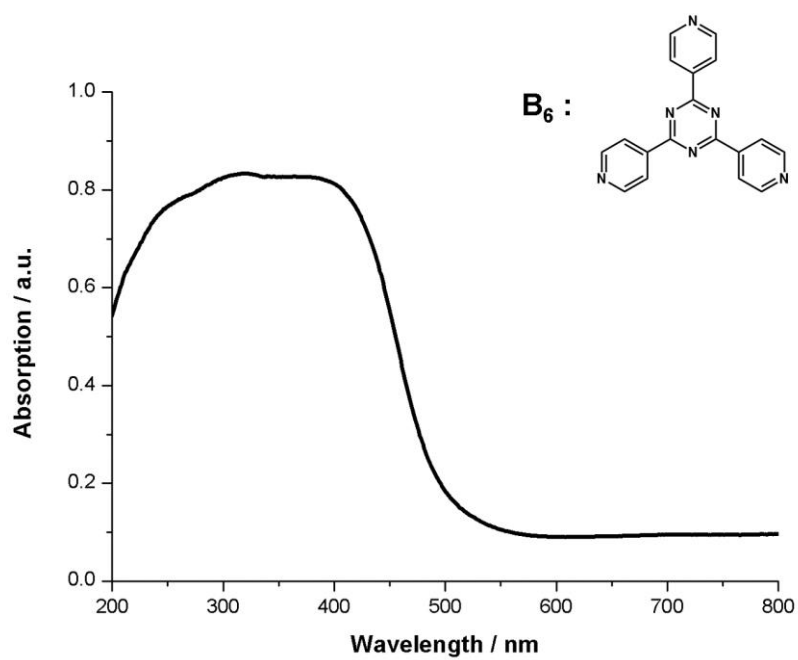
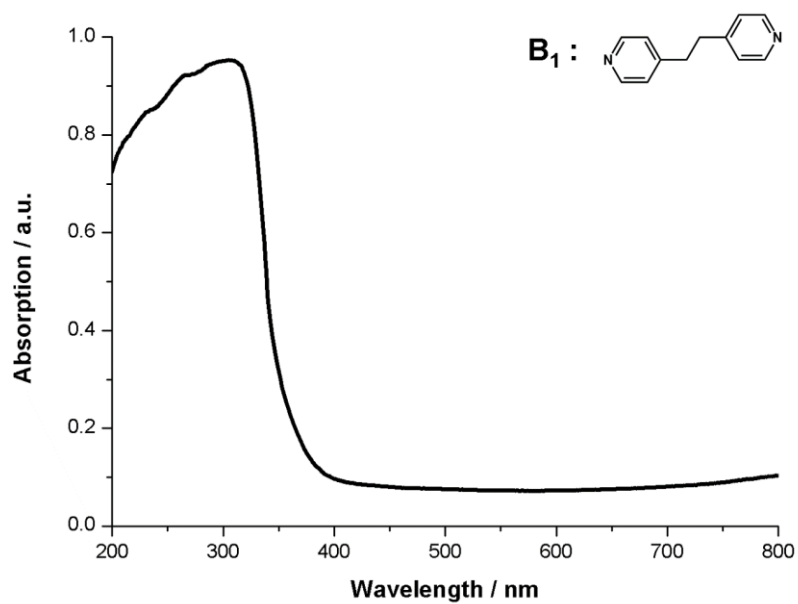


Figure II-10 : top) Solid-state UV-visible absorption spectrum of C₁; bottom) Solid-state UV-visible absorption spectrum of C₆. The other compounds' spectra are available in this chapter's appendix.

II-5.b Solid-state excitation spectra of the polymers C_n .

The solid-state room temperature excitation spectra of compounds C_n were measured and revealed the presence of two large bands with maxima located at *ca.* 325 and 370 nm across the series of polymers (Figure II-11).

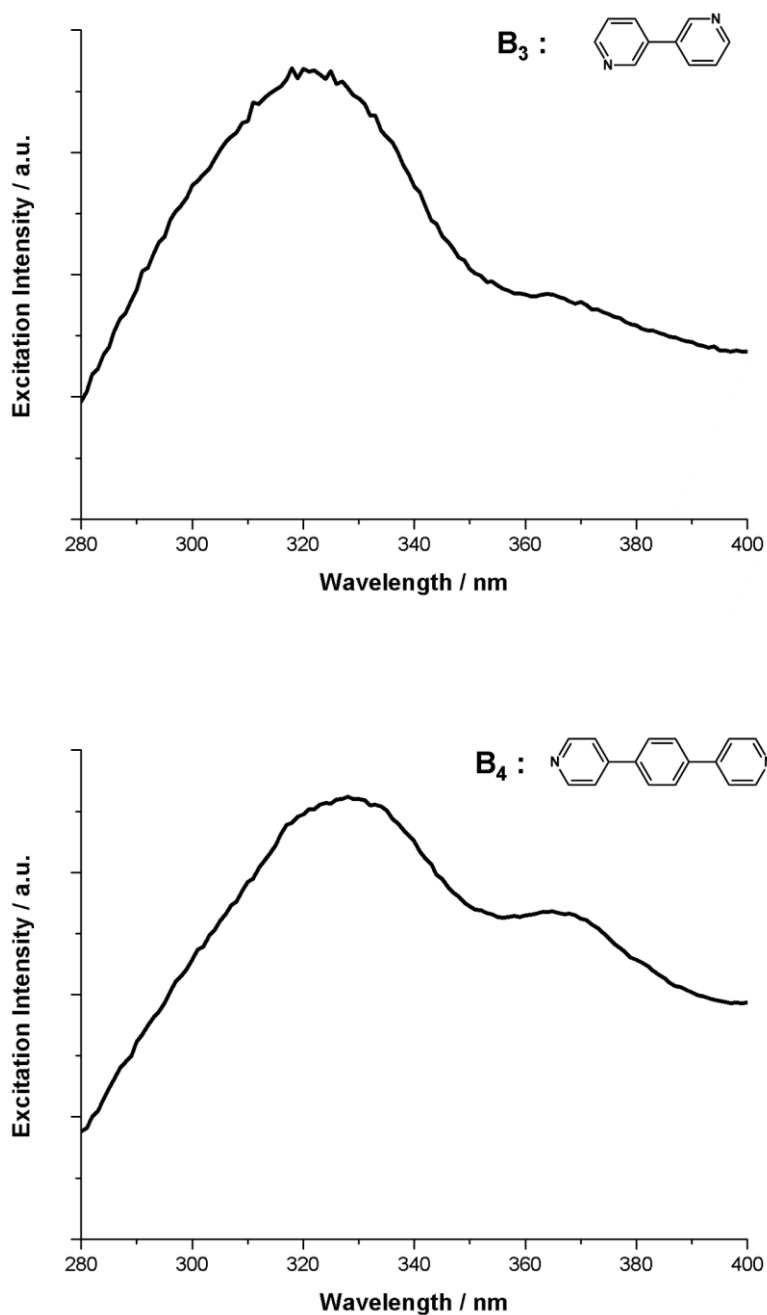


Figure II-11 : top) Solid-state room temperature excitation spectrum of C_3 , bottom) Solid-state room temperature excitation spectrum of C_4 . The other compounds' spectra are available in this chapter's appendix.

II-5.c Solid-state emission spectra of the polymers C_n .

Each one-dimensional coordination polymers C_n presents a noticeable solid-state room temperature luminescence under UV-light ($\lambda = 365$ nm) with a large variety in the intensity of the emission and of the eye-perceived colors displayed. These polymers' eye-perceived emission colors range from light blue luminescence in C_1 and C_2 to yellow-orange luminescence for C_6 and even red in the case of C_7 (Figure II-9), being markedly different from the deep blue colored luminescence displayed by the **A** metallacycle under UV-light.

In order to characterize more clearly the luminescence properties of the family of coordination polymers C_n , their RT solid-state emission spectrum were measured firstly.

The polymers C_n display large bands in their emission spectrum at room temperature, with the exception of C_5 for which emission intensity at room temperature is so weak that it was not possible to record a well resolved spectrum emerging from the background signal. The large band observed in the emission spectrum is not structured for polymers C_1 - C_3 , and C_6 , and presents an apparent vibronic substructure in the case of polymers C_4 and C_7 (Figure II-12).

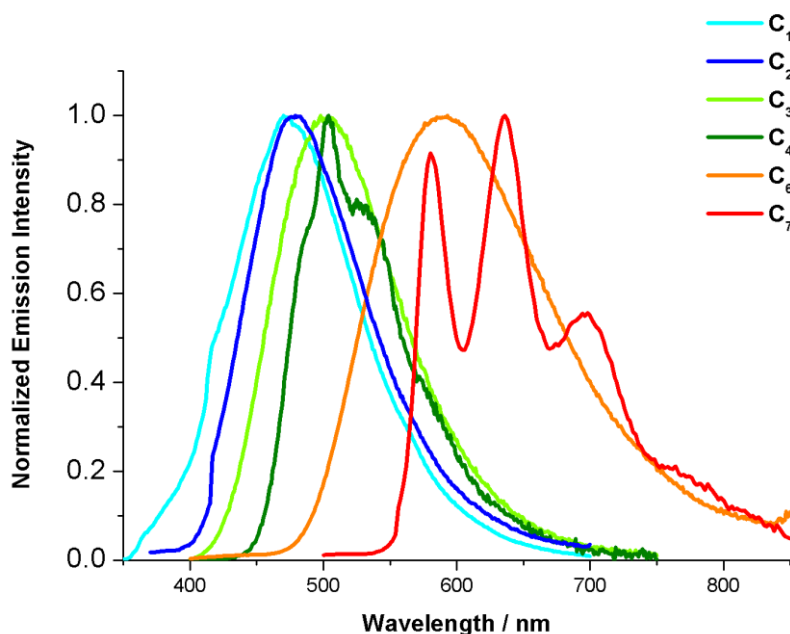


Figure II-12 : Normalized emission spectra of the 1D coordination polymers C_1 - C_4 and $C_{6,7}$ in the solid-state at room temperature ($\lambda_{\text{ex}} = 330$ nm).

The luminescence featured by this series of polymers covers a great portion of the visible part of the light spectrum, with λ_{max} (λ_{max} being the wavelength for which the maxima of emission intensity is measured in the emission spectrum) values going from 490 nm up to 636 nm (Table II-4). It can be noted that all 1D coordination polymers present at room temperature a shift to higher wavelengths in their emission spectrum compared to the emission of the tetrametallic precursor **A** ($\lambda_{\text{max}} = 457$ nm).

	λ_{em} (nm)	λ_{ex} (nm)	I_{80}/I_{RT}	Φ_{em}	τ_{obs} (μs)	k_r (s^{-1})	k_{nr} (s^{-1})
C₁	483 (475)	320	48	7	29 (185)	2.4×10^3	3.2×10^4
C₂	483 (480)	330	43	12	29 (227)	4×10^3	4×10^4
C₃	500 (510)	325	1.5	50	10 (33.9)	5.2×10^4	5.2×10^4
C₄	503, 536 ^s (475, 501, 533, 544)	325	4.5	30	4 200 (11 000)	71	1.7×10^2
C₅	500-530 (477, 510, 543 ^s)	320	114	0.01 <	688 (41 500)	14	1.4×10^3
C₆	590 (570)	335	17	20	0.5 (18.3)	4×10^5	1.6×10^6
C₇	580, 636, 700 (445, 577, 636, 700)	330	3	5	994 (2 000)	50	9.5×10^2
A	457 (486)	320	2.8	72	40 (200)	1.8×10^4	7×10^3

Table II-4 : Photophysical data for the polymers **C_n**, at 300 K and 80 K, in the solid-state. The lifetimes of **C₄**, **C₅** and **C₇** were recorded at the wavelength corresponding to the highest intensity in the emission spectrum (500, 510 and 575 nm respectively). Values at 80 K are given in parentheses. ^s designates shoulders, I_{80}/I_{RT} is the intensity at maximum of emission at 80 K divided by the intensity at maximum at 300 K. $k_r = \Phi_{\text{em}}/\tau_{\text{obs}}$, $k_{\text{nr}} = (1 - \Phi_{\text{em}})/\tau_{\text{obs}}$.

To also represent this luminescence, the calculated coordinates of the polymers **C_n** as well as the precursor **A** on the chromaticity diagram as defined by the *Comité International de l'Eclairage* (CIE) in 1931 are displayed in Figure II-13. One detail that stands out from this figure is that the polymers **C_n** resulting from the reaction with the more seemingly π -conjugated ligands **B_n** tend to display the more red shifted luminescence out of the series, as is the case for **C₆** and **C₇**.

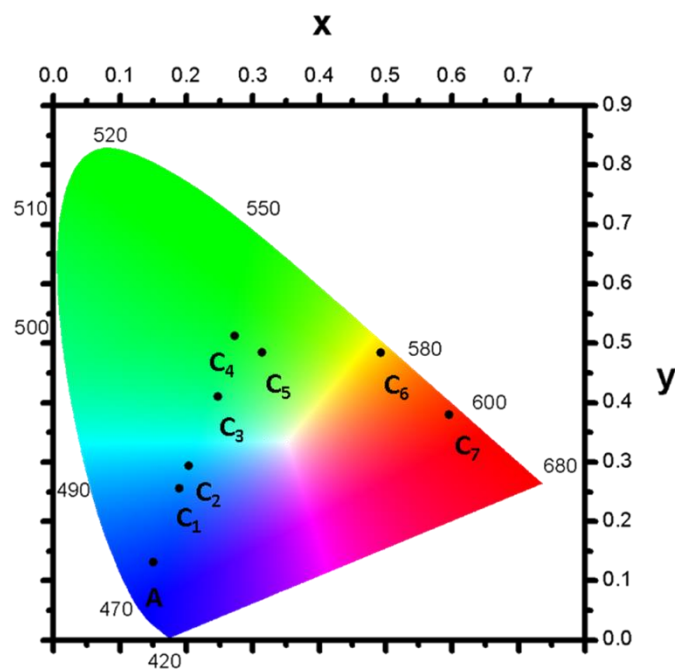


Figure II-13 : Chromaticity diagram of the 1D coordination polymers C_n in the solid-state at room temperature.

In this diagram, it is confirmed that the luminescence of the synthesized polymers covers a large part of the visible light spectrum from deep blue to red.

Measurements on the thermal variation of the luminescence properties of polymers C_n were conducted, and their emission spectrum from room temperature down to liquid nitrogen temperature were registered (Table II-4). In addition, the temperature dependence of the decay times of the excited states were also measured (Table II-4). A large variety of behaviors is therefore highlighted in this series of polymers C_n .

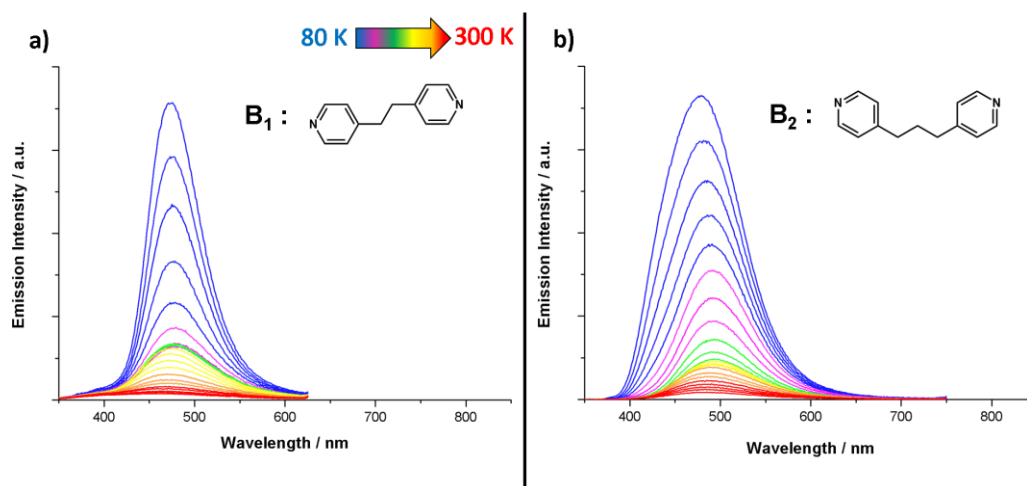


Figure II-14 : Temperature dependence of the emission spectrum of polymer C_1 (a) and C_2 (b) from 300 to 80 K.

The polymer **C**₁ displays a large increase of its intensity of emission upon cooling and this is accompanied by a small hypsochromic shift of the λ_{max} value. At 80 K its emission is characterized by a large band centered around 475 nm under a 330 nm excitation. As can be seen in Figure II-14 a), the emission at 80 K is quite narrow with a FWHM of 67 nm.

The polymer **C**₂ displays similar properties to that of derivative **C**₁ upon cooling. A large increase of the intensity of emission upon cooling can be observed, accompanied by an hypsochromic shift for the polymer **C**₂. In this case, the shift is smaller than for **C**₁ with an emission band centered around 480 nm at 80 K compared to 483 nm at RT. One difference with **C**₁ lies in the width of the emission bands, with a larger FWHM at 80 K of 104 nm (Figure II-14 b)).

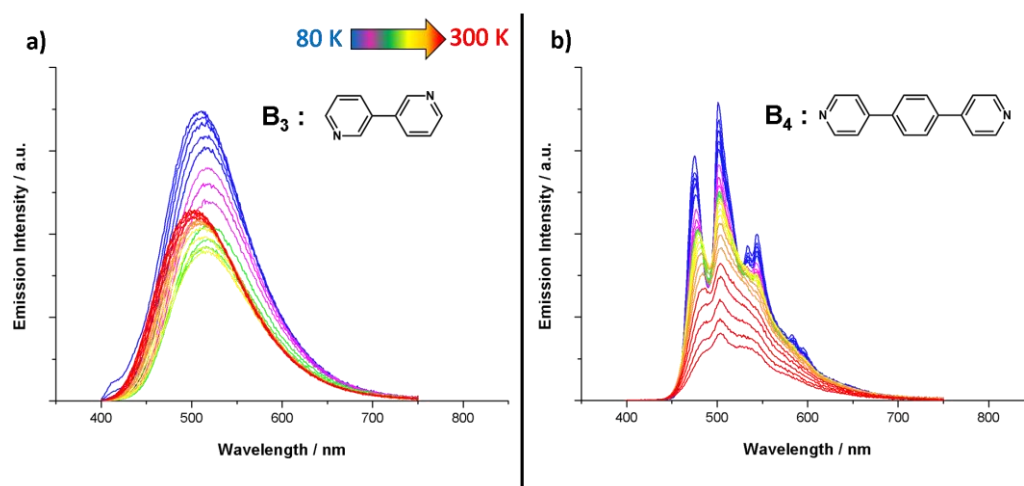


Figure II-15 : Temperature dependence of the emission spectrum of polymer **C**₃ (a) and **C**₄ (b) from 300 to 80 K.

The next polymer, **C**₃, obtained from the reaction with the **B**₃ linker presents a noticeably different behavior. An initial decrease of the emission intensity upon cooling is observed, a trend that is present down to *ca.* 200 K. At this temperature, a small plateau of intensity where a local minimum is reached can be observed. Upon further cooling of the sample down toward the temperature of liquid nitrogen, the emission intensity increases to reach its maximum at 80 K. In the case of **C**₃, a bathochromic shift is observed during all the cooling process with an emission band centered at 510 nm at 80 K. The emission band at 80 K presents a FWHM of 107 nm (Figure II-15 a)).

The temperature luminescence properties of **C**₄ present a major difference, when compared to the polymers **C**₁-**C**₃. Indeed, it displays at RT an apparent vibronic substructure in its emission

band, which is kept during the cooling process with the apparition of additional local maxima at 475, 500, 532 and 543 nm at 80 K. No particular shift in the emission can be identified during the cooling process. The vibrational structure presents energy variation averaging 1318 cm^{-1} (Figure II-15 b)).

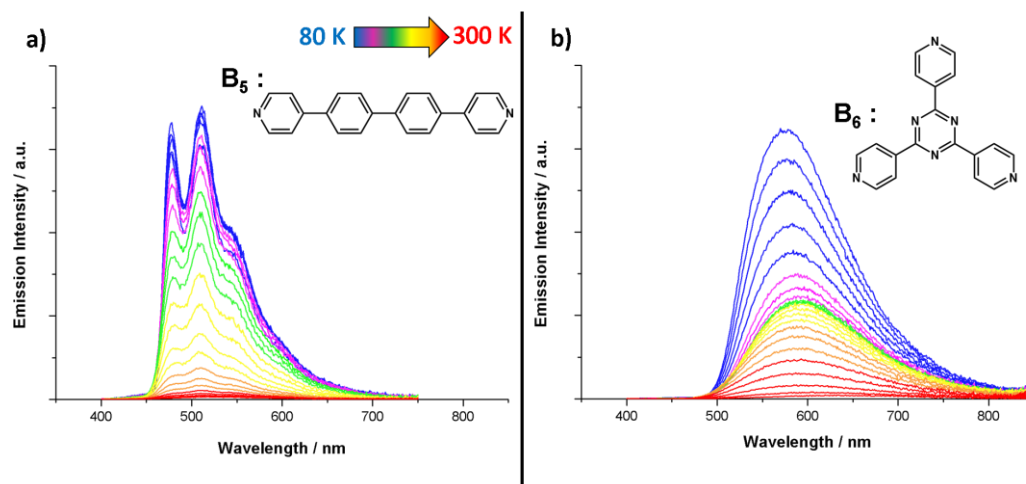


Figure II-16 : Temperature dependence of the emission spectrum of polymer **C₅** (a) and **C₆** (b) from 300 to 80 K.

The polymer **C₅** is almost not luminescent at room temperature under UV-light. A large increase of the emission intensity upon cooling, along with the apparition of a vibronic substructure in the emission band can be observed, with two maxima and a shoulder present (485, 510 and 545 nm respectively). The vibration structure found in compound **C₅** at low temperatures presents energy gaps of *ca.* 1270 cm^{-1} (Figure II-16 a)).

Polymer **C₆** presents a noticeable hypsochromic shift upon cooling, along with a large increase of the emission intensity. Once cooled to 80 K, its emission is characterized by a large band centered around 575 nm. Contrary to the precedent two polymers **C₄** and **C₅**, no vibronic substructure can be observed here. The emission band presents a FWHM of 128 nm at 80 K (Figure II-16 b)).

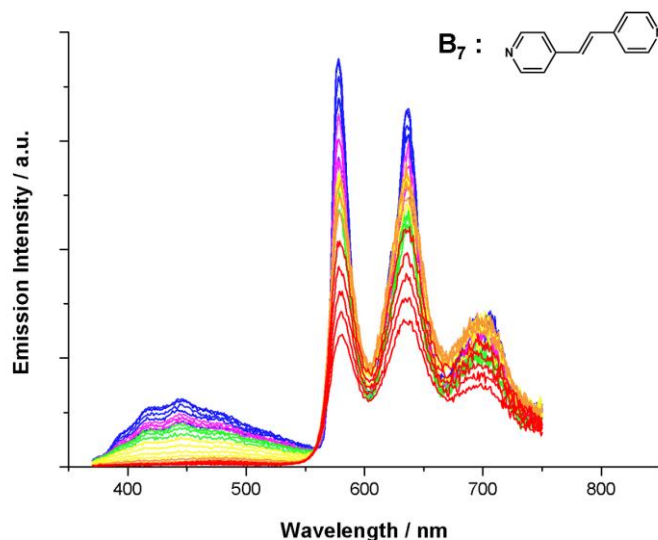


Figure II-17 : Temperature dependence of the emission spectrum of polymer **C7** from 300 to 80 K.

Finally, the last polymer presented in this study, obtained from the **B7** linker, presents a vibronic substructure in its emission band along with an increase of the emission intensity upon cooling. Upon cooling, no shift of the maximum of emission can be observed on each of the components of the vibronic substructure. The emission spectra for the more intense sub component is a band centered at 578 nm at 80 K, with the two others components presenting bands at 636 and 702 nm respectively. The energy variations found in the vibrational structure are 1529 cm^{-1} on average. One particular thing that can be noted in the case of polymer **C7** is the apparition at lower temperatures of a second emission centered around 450 nm, with much lower intensity than the main emission, and which is not visible in the RT emission spectrum (Figure II-17).

All the observed changes are reversible upon returning to room temperature, with no noticeable changes noted in the room temperature luminescence of the polymers **C_n** after the cooling process.

II-5.d Measurements of the lifetime of the excited states of the polymers C_n

The thermal evolution of the lifetime of the excited states of the compounds **C_n** in the solid-state has been studied. The lifetimes were studied from 80 to 300 K using a laser diode having an excitation wavelength of 375 nm (Table II-4). The measurement of the lifetime have been

made at the wavelength corresponding to the maximum of the emission spectrum at the given temperature.

The determined lifetimes were treated with a monoexponential decay mode, affording acceptable fit parameters with R^2 values superior than 0.9. Attempts to fit the curves using a biexponential decay led to comparable values and did not improve the quality of the fit. One can wonder, due to the complexity of these compounds, the variety in their structures and their photophysical behaviors, about the fact that all compounds present such a monoexponential decay, meaning that only one radiative relaxation pathway takes place. It is always possible to proceed with a polynomial fit which would induce an overparameterization of the data and question the relevance of such a fit. Therefore, the data presented here are thus processed with a monoexponential decay, however giving access to a value of the lifetime of the excited state that we prefer to define as an average value outlining that potentially different relaxation processes that can take place simultaneously.

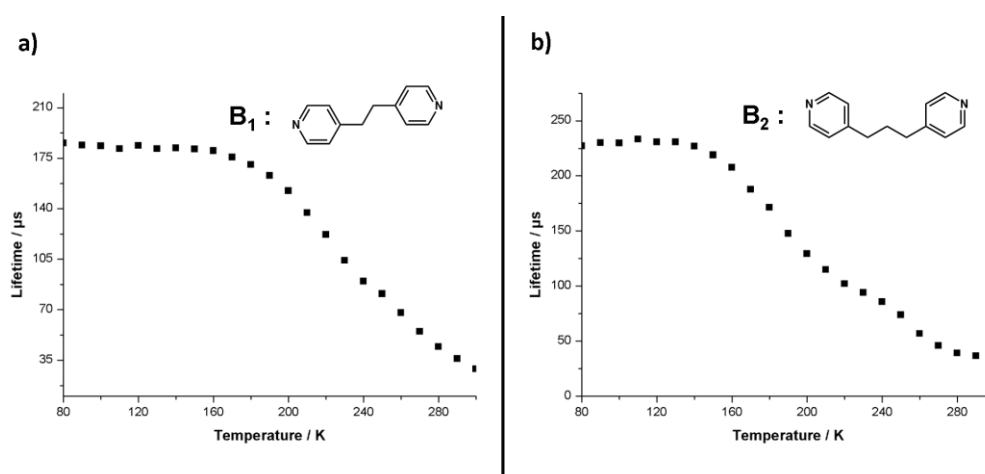


Figure II-18 : a) Variation of the lifetime depending of the temperature of C_1 from 80 to 300 K ; b) Variation of the lifetime depending of the temperature of C_2 from 80 to 300K.

In Figure II-18 a), it can be observed that the curve of the variation of the lifetime of the compound C_1 presents a plateau at low temperature with a lifetime of 185 μ s at 80 K and up to 190 K where it begins to decrease. Once at ambient temperature, the lifetime of the excited state is found to be 29 μ s.

The curve of the variation of the lifetime depending of the temperature of compound C_2 , depicted in Figure II-18 b) follows a similar trend, with a plateau at low temperature with an

excited state lifetime of 227 μs at 80 K. At 160 K, the lifetime starts to decrease. Once heated to 300 K, the lifetime of the excited state of **C**₂ was found to be 29 μs .

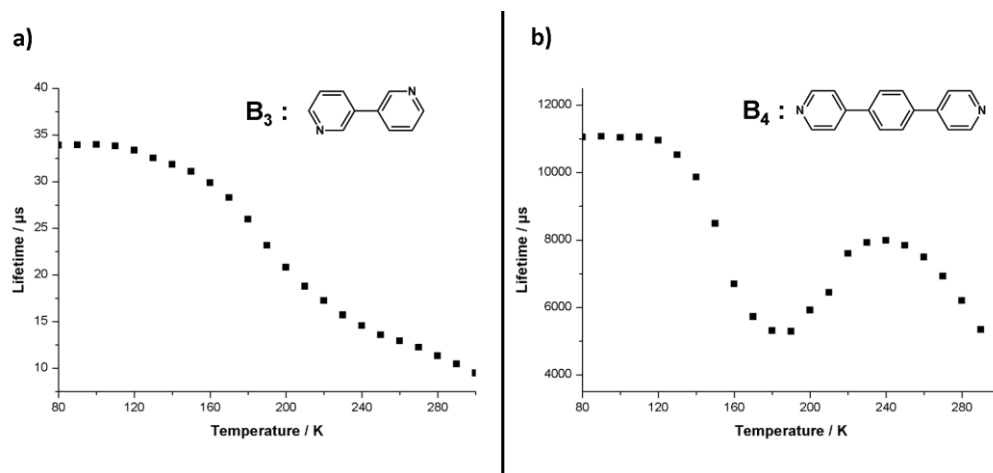


Figure II-19 : a) Variation of the lifetime depending of the temperature of **C**₃ from 80 to 300 K ; b) Variation of the lifetime depending of the temperature of **C**₄ from 80 to 300K.

In Figure II-19 a), it can be seen that the compound **C**₃ follow a similar pattern in its the temperature dependence of the lifetime of its excited states, with a plateau at low temperature, followed by a decrease at *ca.* 180 K. However, the values of the lifetime are much smaller than what was observed in **C**₁ and **C**₂, as the lifetime of **C**₃ was measured to be 34 μs at 80 K and 10 μs once heated to 300 K.

The curve of the variation of the lifetimeof the excited state of compound **C**₄, depicted in Figure II-19 b) shows an unusual aspect when compared to the previous compounds. Besides a similar small plateau observed at 80 K lasting to 120 K, the decrease in the lifetime during heating is followed by an increase leading to the formation of a local maximum at 240 K, before the lifetime decreases again. The values of the lifetime of the excited states are also much longer than what was observed for previous compounds with values of 11 ms at 80 K, 8 ms at 240 K and 4.2 ms at 300 K. Such a behavior suggests that competitive radiative relaxation processes may take place with relative predominance being dependant of the temperature.

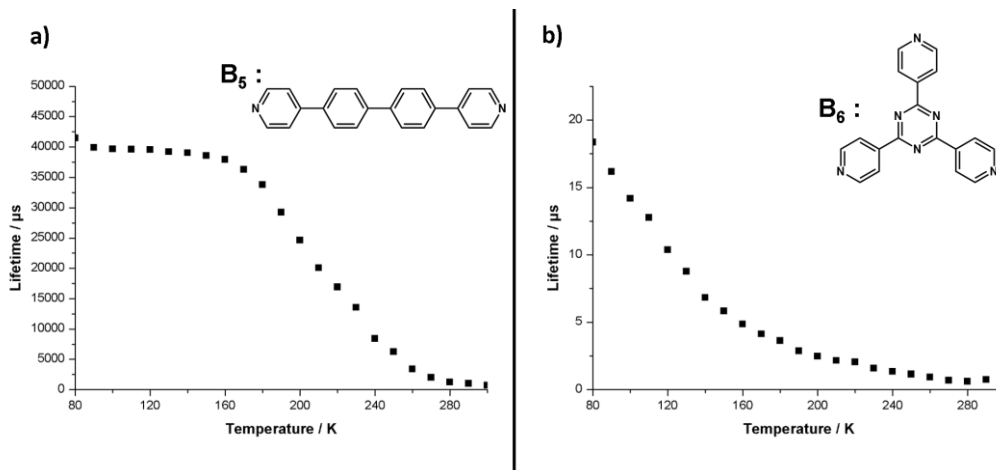


Figure II-20 : a) Variation of the lifetime depending of the temperature of C_5 from 80 to 300 K ; b) Variation of the lifetime depending of the temperature of C_6 from 80 to 300K.

The curve of the lifetime depending of the temperature of compound C_5 follows the trend of compounds C_1 - C_3 but with much longer decay times : a plateau is present at low temperature with the highest lifetime of the excited states measured for compounds C_n at 41.5 ms, and is maintained up to 170 K. Then, a decrease is observed in the lifetime values, attaining 688 μs at 300 K.

In Figure II-20 b), the curve of the variation of the lifetime depending of the temperature of compound C_6 presents a steep decrease, beginning from the lowest temperature of 80 K, with an initial lifetime measured to be 18.3 μs . The value of the lifetime of the excited states seems to attain a low value plateau starting at *ca.* 280 K. Once heated to 300 K, the value of the lifetime of the excited state is 0.5 μs .

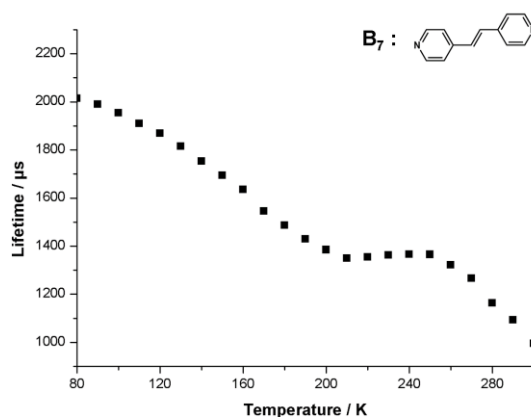


Figure II-21 : Variation of the lifetime depending of the temperature of C_7 from 80 to 300 K.

Finally, in Figure II-21, the curve of the variation of the lifetime of the excited state depending of the temperature of compounds **C7** is presented. The curve follow a downward trend starting from the low temperture and a lifetime of 2 ms. This trend in interrupted by a small lifetime plateau, reminiscent of the local maximum observed in **C4** and located at *ca.* 240 K. After this plateau, the lifetime decrease again during the heating, and attain 994 μ s at 300 K.

II-5.e Quantum yield measurements of the polymers C_n

The quantum yields of the polymers were measured, in the solid-state and at room temperature. In order to insure a greater accuracy, they have been measured three times, and the value given is obtained from the averaging of these measurements. The values are given in Table II-4.

These values of the emission quantum yield are very disperse, being 50% for the highest **C3**, and as low a 0 % for **C5**. Contrary to their color of emission which follow a gradual shift to the red emissions along the series of polymers **C_n** potentially correlated with the degree of π -conjugation in the linkers backbone, no such behavior can be observed here for the quantum yields.

II-5.f Tentative assignment of the photophysical properties of polymers C_n

The description of the thermal dependence of the solid-state emission spectra and decay time of the excited states, together with the quantum yield for all these compounds reveal some various luminescence behaviors, despite the high homogeneity of the structural architectures. Tentatively, one can distinguish roughly two groups of compounds : **C1-C2** and **C4-C5-C7**, while **C3** and **C6** present quite different behaviors. **C1** and **C2** present large emission bands that are preserved upon cooling together with a slight hypsochromic shift and thermal values of the decay times ranging from roughly 200 μ s at low temperature, to 30 μ s at room temperature. At the opposite, **C4**, **C5** and **C7** present structured emission spectra with resolution that got higher upon cooling, with virtually no shift of the emission spectrum, while the decay times of the excited states are much longer going from tens of milliseconds at low temperature to roughly one millisecond at room temperature. The radiative rate constants for these compounds have been determined, being at *ca.* 4 to $2.4 \times 10^3 \text{ s}^{-1}$ for the first family and much smaller values the second family. Values in the range of few 10^3 s^{-1} can be assigned to ³MLCT phosphorescence

properties, while the k_r values for the second series, together with the high structuration of the emission bands likely suggests metal perturbed intralinker phosphorescence properties, that can eventually be associated in case of polymer **C4** with quite high emission quantum yields due to a certain rigidification of the linker backbone in the packing.^{14,15} Considering the **C3** and **C6** derivatives, the k_r values are much higher and could be proof of the preservation of the TADF behavior of the **A** precursor within the polymers. This is supported by the sigmoidal curve that can be observed for the **C3** compound, however, for the **C6** compound the sigmoidal profile cannot be observed, eventually due to the fact that measurements at lower temperature might be necessary. One can note that it is quite remarkable that if it is eventually confirmed that the **C6** compound present a TADF behavior, it is associated with a quite high emission quantum yield in a spectral domain which corresponds to the emission of an eye-perceived yellow-orange light for which non-radiative de-excitation pathways due to vibrations have generally a great impact on the luminescence efficiencies.

II-5.g Luminance measurements of the polymers C_n

To complete the study of their photoluminescence properties, the luminance of the one-dimensional coordination polymers **C_n** were measured in the solid-state and at room temperature under irradiation with $\lambda_{\text{ex}} = 365$ nm and by varying the irradiance directed toward the sample. Luminance was first defined as the « brightness » of a sample, however, this term was deemed obsolete in 1997. In the IUPAC goldbook, luminance is now defined as « Photometric counterpart of radiance, producing the visual sensation called brightness. ».¹⁶ It consists of the luminous intensity per unit area, with the luminous intensity being the intensity weighted by the luminosity function of the human eye,¹⁷ and expressed in Cd/m². The irradiance is the measurement of the light source power per unit area and is given in W/m².¹⁸ The luminance is given for a certain irradiance to take into account the intensity of the incident light. The luminance of a compound is related to its luminescent quantum yield, with higher quantum yields leading to higher luminance. The resulting curves from this study are given in Figure II-22 and Figure II-23.

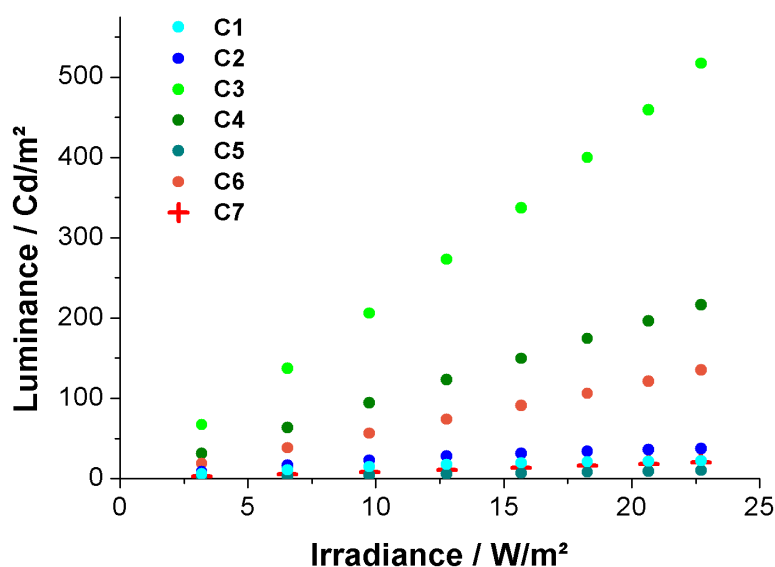


Figure II-22 : Variation of the luminance of the polymers C_n depending on the irradiance.

In Figure II-22 it can be seen that all polymers C_n present an overall linear evolution of their luminance with the variation of irradiance intensity. The luminance is found to be in the range of 1.6 Cd/m² to 47 Cd/m² under an irradiance of 3.5 W/m². One can note that the luminance range displayed by the polymers C_n is comparatively the same as their quantum yield : the polymer C_5 , presenting the lowest recorded solid-state room temperature quantum yield of the series at 0 % is also presenting the lowest luminance with a value of 1.6 Cd/m² under an irradiance of 3.5 W/m². On the other hand, polymer C_3 possesses the highest quantum yield value for the polymers C_n with 60 % and presents accordingly the highest value of luminance with 47 Cd/m² under the same irradiance.

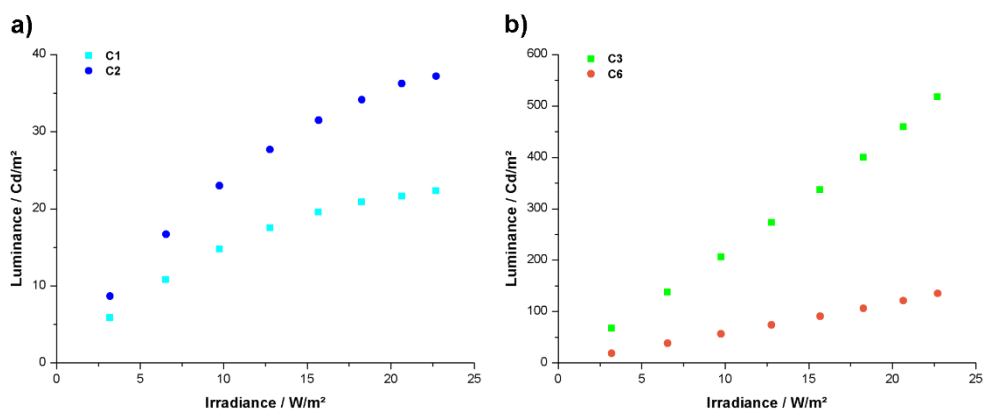


Figure II-23 : Comparison of the variation of the luminance depending on the irradiance between C_1 , C_2 , C_3 and C_6 .

The variation of the irradiance intensity was studied in order to determine if the polymers C_n would suffer from saturation effects under high intensity UV lights irradiation or if their luminescence would remain unaffected. It was found that the vast majority of polymers C_n do not suffer from saturation effects, only polymers C_1 and C_2 seem to present such effects as the curve of the luminance begins to flatten (Figure II-23) when approaching the highest available irradiance. This peculiar behavior could be tentively related to the fact that B_1 and B_2 are the two ligands used in this study that present a linear aliphatic backbone.

II-6 Thermal properties of the polymers C_n

The thermal stability of the one-dimensional coordination polymers C_n was studied by TGA-DTA analysis. The samples were first analyzed by conducting a heating from room temperature to 950 °C with a heating ramp of 5 °C/min under nitrogen flux. Once at 950 °C, this temperature was maintained for one hour with an oxygen flux being applied, in order to insure the best possible combustion of the compound. The resulting graph is presented in Figure II-24 for derivative C_6 . The complete TGA-DTA measurements for the other polymers C_n are available in this chapter's appendix.

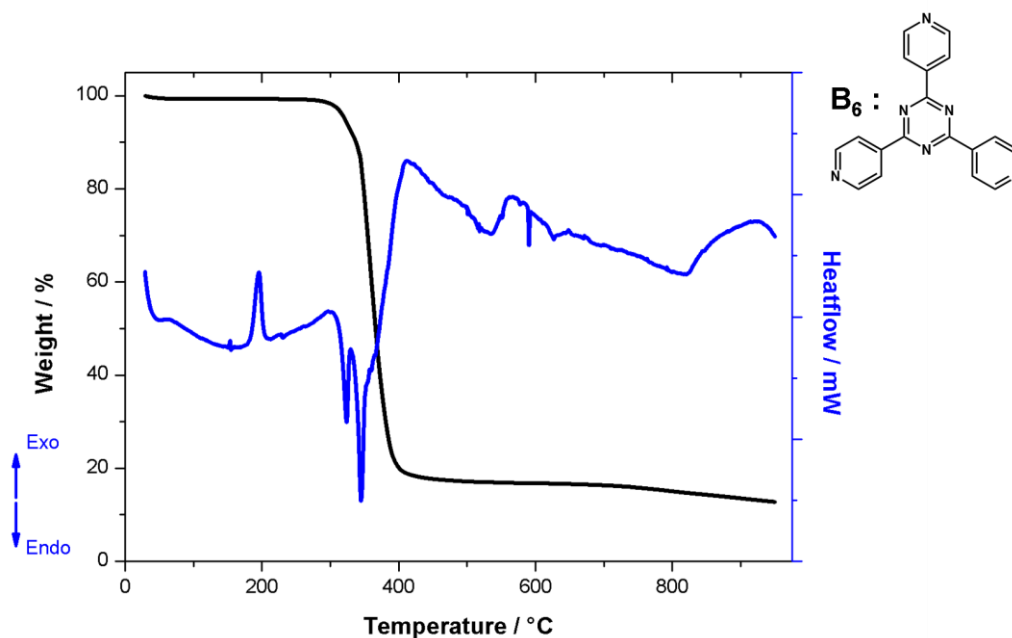


Figure II-24 : TGA-DTA analysis of C_6 compound until 950 °C.

The coordination polymers C_n are established to be thermally stable up to a temperature of *ca.* 350 °C (Table II-5) where an endothermic event occurs along with an important loss of mass corresponding to the thermal decomposition. During this decomposition for example, the coordination polymer C_1 loses *ca.* 80 % of the total starting weight. The final residue, obtained as a dark solid, is very likely composed of oxydized copper species resulting from the Cu(I) metallic centers of the tetrametallic metallacycles present in the polymers. Similar behaviors are observed for all the seven polymers C_n .

Compound	C₁	C₂	C₃	C₄	C₅	C₆	C₇
Decomposition temperature (°C)	362	352	356	345	336	344	354
Exothermic transition temperature (°C)	217	166	185	189	209	190	231

Table II-5 : Temperature of decomposition of polymers C_n .

It can be noted that at a temperature lower than the the temperature of thermal decomposition, an exothermic peak can be observed in each of these TGA-DTA analyses, not accompanied by any direct loss of weight. To investigate more precisely this exothermic event, other TGA-DTA measurements were conducted, where the coordination polymers were heated to 270°C (below the temperature of thermal decomposition) under nitrogen flow, maintained for 5 minutes at this temperature and then subsequently left to return to room temperature (Figure II-25).

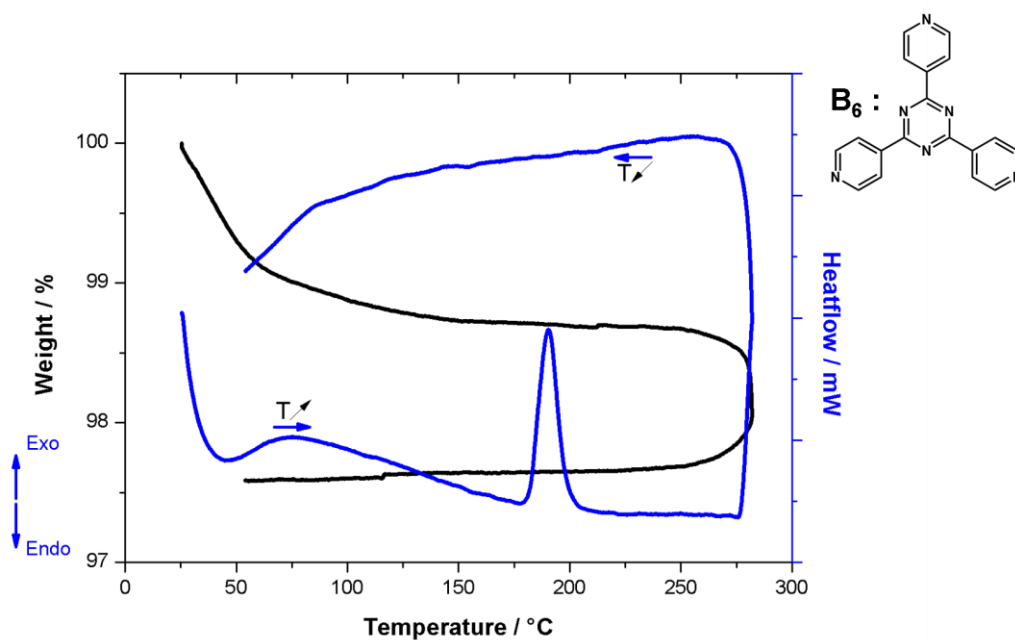


Figure II-25 : TGA-DTA analysis of compound C_6 until 270 °C and record of the return to room temperature.

In each case, some minor loss of weight can be observed at the very beginning of the measurement along with an endothermic aspect of the DTA curve. This can be attributed to the evaporation of CH_2Cl_2 solvents molecules trapped in the structure or alternatively from evaporation of adsorbed water molecules originated from moisture in the air since all collected materials can be kept under air without any damages occurring upon time. However at higher temperature, an exothermic event can be observed without any loss of weight as can be seen in the Figure II-25 related to the thermal treatment of the polymer C_6 .

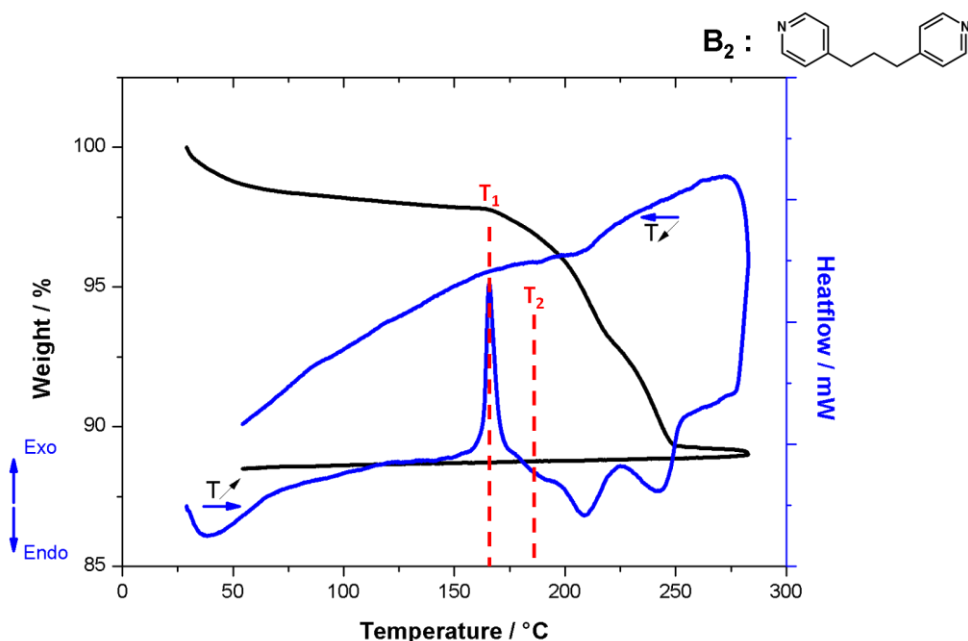


Figure II-26 : TGA-DTA analysis of compound **C₂** until 270 °C and record of the return to room temperature.

In addition, when considering the TGA-DTA measurement of derivative **C₂** (Figure II-26) conducted in the same manner, it can be seen that this exothermic event happens at a temperature T_1 slightly lower than a temperature T_2 associated with an endothermic event. This event is accompanied by a moderate loss of weight. In both cases, importantly the TGA-DTA curves recorded as the system is cooled down back to room temperature reveals that these thermic events are not reversible as there was no exo- or endothermic peak present in the DTA curve recorded upon cooling, except in the case of **C₅** where an exothermic peak can be observed, potentially attributed to state changes of the linker. Similarly, there was no change in weight upon cooling.

This behavior is exhibited across the entire series of coordination polymers **C_n** with the only noticeable difference being the temperature at which these exothermic events takes place and if it is followed by a moderate loss of weight before the decomposition temperature is reached (see in this chapter's appendix). Only the TGA-DTA curve of the compound **C₆** exhibit only the first exothermic peak.

One really intriguing aspect of this thermal behavior was that upon taking the sample out with this second TGA-DTA sequence (not heating up to the thermal decomposition) and exposing it to UV light ($\lambda = 365$ nm), all polymers **C_n** were emitting an intense, eye-perceived blue

luminescent light, clearly different from the initial varied luminescence displayed by the coordination polymers. Therefore, these irreversible thermal transitions induced a transition in the luminescence properties carried by the polymers C_n as they are returned to room temperature.

II-7 Conclusion

The straightforward, high yield preparation of a new family of one-dimensional coordination polymers was achieved by reacting the Cu(I) based tetrametallic metallacycle **A** as a precursor, with different 3- or 4- pyridyl capped ligands. The reaction is done under air along a one pot strategy and without further purification steps needed, affording polycrystalline C_n compounds.

The obtained compounds C_n are one-dimensional coordination polymers composed of the Cu(I) tetrametallic metallacycle of **A**, connected by the ligands **B_n**. This pattern is repeated, allowing for the linear propagation of the polymers regarding the metallacycle **A** structure. The coordination of the connecting pyridyl capped ligand induces a change in the coordination sphere of one of the Cu(I) metallic centers from trigonal planar distorted to tetrahedral compared to the structure of the metallacycle precursor **A**. Concomitantly, an increase of the intermetallic distance in the dimeric unit is observed prohibiting the observation of cuprophilic interactions in the newly obtained polymers.

The polymers of the C_n family are all white polycrystalline powders in the solid-state except for the polymer C_6 which is a yellow colored powder. They all present a large UV-visible absorption band, which is attributed to $\pi - \pi^*$ transition centered on the aromatic ligand. When the polymers C_n are observed under UV light irradiation ($\lambda = 365$ nm) at room temperature, they emit a luminescent light clearly different from the one observed in the precursor **A**. The eye-perceived luminescence colors emitted by the polymers C_n span the entirety of the visible light spectrum. Such solid-state luminescence is characterized by large single bands in their emission spectrum at room temperature for four polymers C_1 - C_3 , C_6 , while three of them C_4 , C_5 , C_7 present bands bearing vibronic sub-structure in their emission spectrum. The four polymers presenting a non structured emission spectrum at room temperature exhibit some thermochromic behavior of their luminescence upon cooling to liquid nitrogen temperature being either hypso- or bathochromism. In all polymers C_n , a large increase of the emission spectra intensity is observed upon cooling. This diversity in luminescence properties of the polymers is also observed in their temperature dependant lifetimes. The polymers C_1 - C_3

presents shorter lifetime in the range of few microseconds to few hundreds microseconds. The more π -conjugated ligands used result in longer lifetimes in the resulting polymer with values ranging from a few of hundreds microseconds up to tens of milliseconds. The quantum yield measured for the polymers C_n are very diverse as well, ranging from no observable emission at room temperature to emission quantum yield reaching the value of 60 %. This behavior is echoed in the measurement of the room temperature solid-state photoluminance of the polymers, where the ones exhibiting the highest quantum yields were also the ones displaying the highest luminance under high irradiance. A tentative interpretation of the photophysical properties of these polymers suggest that in some cases, the TADF regime observed in the precursor **A** is preserved (C_3) while some derivatives present pure $^3\text{MLCT}$ phosphorescence (C_1 - C_2). The coordination polymers based on the more π -conjugated linkers (C_4 - C_5 - C_7) likely have radiative relaxation processes based on a mixture of locally excited state and charge transfer, metal perturbed intralinker phosphorescence. The assignment of the radiative relaxation processes will have to be confirmed by theoretical calculations that are still undergone at the time of writing this manuscript. The case of the luminescence of the polymer C_6 remains unclear. In order to get more insights about these luminescence processes, TD-DFT calculations are currently undergone.

Finally, when conducting TGA-DTA measurements to investigate behavior of the polymers C_n an unexpected thermal transition was discovered. When heated up to *ca* 200 °C all polymers present in the solid-state an exothermic transition. Once this transition is achieved and the derivatives returned to room temperature, all polymers display a different RT solid-state luminescent behavior than initially emitting a strong, eye-perceived blue luminescence under UV light. From this point onward, the phases obtained after the thermal transition are denominated C_n' .

This unexpected change in the photophysical properties upon thermal treatment in the solid-state is studied in depth in the chapter III.

References of chapter II :

1. Moussa, M. E.; Evariste, S.; Wong, H.-L.; Le Bras, L.; Roiland, C.; Le Polles, L.; Le Guennic, B.; Costuas, K.; Yam, V. W.-W.; Lescop, C., A solid state highly emissive Cu(I) metallacycle: promotion of cuprophilic interactions at the excited states. *Chem. Commun.* **2016**, 52 (76), 11370-11373.
2. Lescop, C., Coordination-Driven Syntheses of Compact Supramolecular Metallacycles toward Extended Metallo-organic Stacked Supramolecular Assemblies. *Acc. Chem. Res.* **2017**, 50 (4), 885-894.
3. Bondi, A., van der Waals Volumes and Radii. *J. Phys. Chem.* **1964**, 68 (3), 441-451.
4. Carvajal, M. A.; Alvarez, S.; Novoa, J. J., The nature of intermolecular Cu^I...Cu^I interactions: a combined theoretical and structural database analysis. *Chem. Eur. J.* **2004**, 10 (9), 2117-2132.
5. Zhang, X.-M.; Hao, Z.-M.; Wu, H.-S., Cuprophilicity-Induced Cocrystallization of [Cu₂(4,4'-bpy)(CN)₂]_n Sheets and [Cu(SCN)]_n Chains into a 3-D Pseudopolyrotaxane. *Inorg. Chem.* **2005**, 44 (21), 7301-7303.
6. Naik, S.; Mague, J. T.; Balakrishna, M. S., Short-bite PNP ligand-supported rare tetranuclear [Cu₄I₄] clusters: structural and photoluminescence studies. *Inorg. Chem.* **2014**, 53 (7), 3864-3873.
7. Yersin, H.; Rausch, A. F.; Czerwieniec, R.; Hofbeck, T.; Fischer, T., The triplet state of organo-transition metal compounds. Triplet harvesting and singlet harvesting for efficient OLEDs. *Coord. Chem. Rev.* **2011**, 255 (21-22), 2622-2652.
8. Evariste, S.; Khalil, A. M.; Moussa, M. E.; Chan, A. K.-W.; Hong, E. Y.-H.; Wong, H.-L.; Le Guennic, B.; Calvez, G.; Costuas, K.; Yam, V. W.-W.; Lescop, C., Adaptive Coordination-Driven Supramolecular Syntheses toward New Polymetallic Cu(I) Luminescent Assemblies. *J. Am. Chem. Soc.* **2018**, 140 (39), 12521-12526.
9. Li, D.; Che, C.-M.; Wong, W.-T.; Shieh, S.-J.; Peng, S.-M., Luminescent three-coordinated dinuclear copper(I) complexes of bis(diphenylphosphino)methane: photophysical properties and crystal structure. *J. Chem. Soc., Dalton Trans.* **1993**, (4), 653-654.
10. Moutier, F.; Schiller, J.; Lecourt, C.; Khalil, A. M.; Delmas, V.; Calvez, G.; Costuas, K.; Lescop, C., Impact of Intermolecular Non-Covalent Interactions in a Cu^{II} Pd^{III} Discrete Assembly: Conformers' Geometries and Stimuli-Sensitive Luminescence Properties. *Chem. Eur. J.* **2022**, 28 (24), e202104497.
11. Nakamoto, K., *Infrared and Raman Spectra of Inorganic and Coordination Compounds. Part B: Applications in Coordination, Organometallic, and Bioinorganic Chemistry*. Wiley: Hoboken, New Jersey, 2009.
12. Fernandez-Bertran, J.; Blanco-Pascual, J.; Reguera-Ruiz, E., The CN stretch of hexacyanometallates as a sensor of ligand-outer cation interactions-I. Ferricyanides and cobalticyanides. *Spectroc. Acta A* **1990**, 46 (5), 685-689.
13. Larkin, P. J.; Makowski, M. P.; Colthup, N. B., The Form of the normal modes of s-triazine: infrared and Raman spectral analysis and ab initio force field calculations. *Spectroc. Acta A* **1999**, 55 (5), 1011-1020.
14. Czerwieniec, R.; Yersin, H., Diversity of copper(I) complexes showing thermally activated delayed fluorescence: basic photophysical analysis. *Inorg. Chem.* **2015**, 54 (9), 4322-7.
15. Zhang, Y.; Schulz, M.; Wächtler, M.; Karnahl, M.; Dietzek, B., Heteroleptic diimine–diphosphine Cu(I) complexes as an alternative towards noble-metal based photosensitizers: Design strategies, photophysical properties and perspective applications. *Coord. Chem. Rev.* **2018**, 356, 127-146.

16. McNaught, A. D.; Wilkinson, A., *IUPAC. Compendium of Chemical Terminology, 2nd ed. (the "Gold Book")*. Blackwell Scientific Publications: Oxford, 1997.
17. Rea, M. S., Lighting simply made better: Providing a full range of benefits without much fuss. *Build. Environ.* **2018**, *144*, 57-65.
18. Wong, K.-L.; Bünzli, J.-C. G.; Tanner, P. A., Quantum yield and brightness. *Journal of Luminescence* **2020**, *224*, 117256.

Chapter III Study of irreversible thermal transition occurring in the solid-state for the polymers C_n

III-1 Study of the high temperature behavior in the solid-state of the precursor A

III-1.a TGA-DTA measurements of precursor A

Before considering the photophysical properties of the newly obtained thermally transitioned compounds C_n', and to help to understand the phenomena that occurs, it is important to study first the thermal behavior of the precursor A in the solid-state, at high temperature. In a first step, a similar TGA-DTA analysis to that of the polymers C_n was conducted for the tetrametallic metallacycle A. The first measurement is a thermal analysis until 950 °C to explore a large range of temperature and highlight the thermal stability of this compound (Figure III-1).

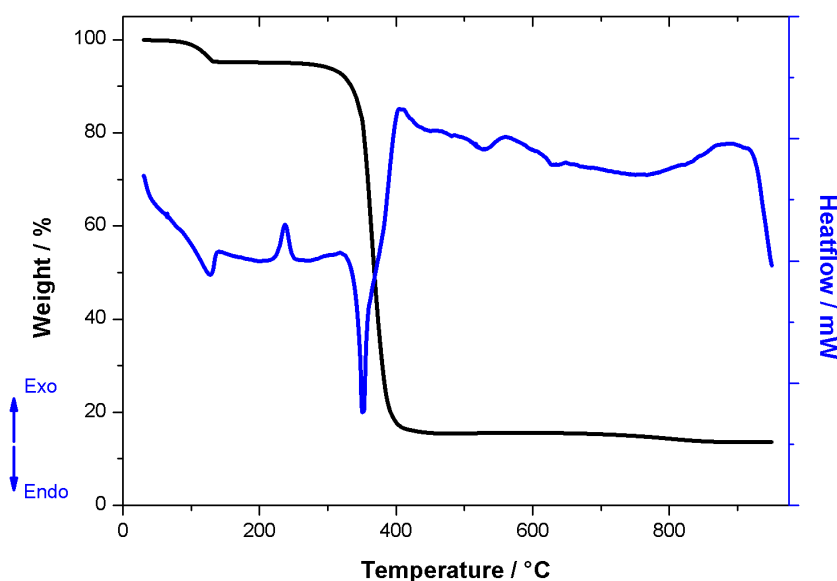


Figure III-1 : TGA-DTA analysis of the precursor A, under nitrogen flux and up to 950 °C.

A quite similar thermal behavior compared to the one generally recorded in the polymers C_n is observed with a small endothermic effect at low temperature (*ca.* 136 °C) accompanied by a small loss of weight (4 %) that can be attributed to the loss of trapped solvents molecules or/and

adsorbed water molecules. The precursor **A** is then stable until 350 °C where an endothermic peak, accompanied by a significant loss of weight of *ca.* 80 % occurs, attributed to the thermal decomposition of the tetrametallic metallacycle precursor **A**.

Interestingly, an exothermic peak not accompanied by a loss of weight is also observed at *ca.* 240 °C. Such an exothermic transition resembles the events observed in the case of the TGA-DTA analysis of the C_n polymers. In order to get more insights, another TGA-DTA analysis up to 300 °C was performed, and the study was extended to the cooling of the derivative back to RT (Figure III-2).

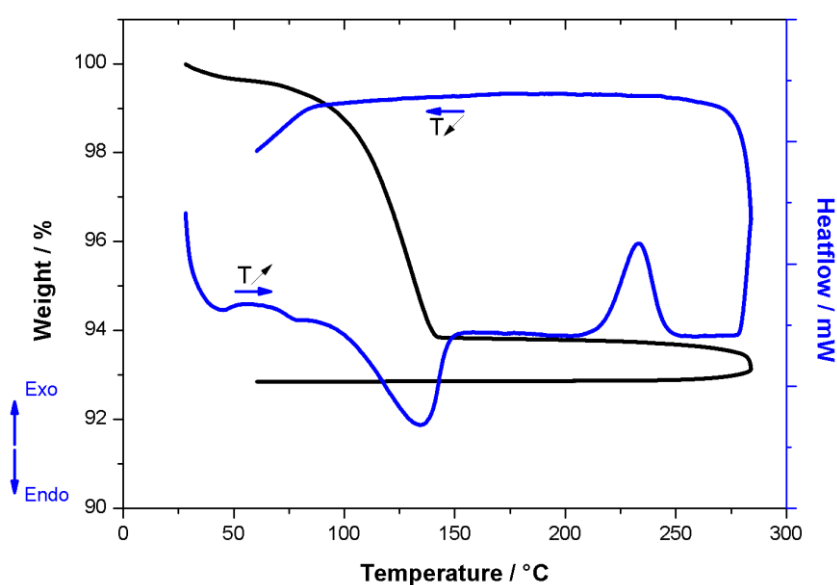


Figure III-2 : TGA-DTA analysis of the precursor **A** under nitrogen flux, up to 270 °C and back to room temperature.

In this second measurement, this exothermic peak occurring at 233 °C is clearly observed and it is confirmed that it is not accompanied by a loss of weight. No similar peak can be seen occurring during the cooling process, hinting to an irreversible transition. When the sample, after such thermal treatment was collected and exposed to UV light ($\lambda_{\text{ex}} = 365 \text{ nm}$), no emitted perceptible changes occurred regarding the RT eye-perceived solid-state luminescence properties displayed, with an eye-perceived blue light, very similar to the one displayed by the precursor **A** before the heating experiment. Concomitantly, the solid-state sample morphology (a colorless polycrystalline powder) remained similar as before the thermal treatment.

Considering this irreversible thermal transition observed for the precursor **A**, reminding of the one found in the coordination polymers **C_n**, it was decided to further study in details this transition of the precursor affording a new phase denominated **A'**.

III-1.b Infrared spectroscopy of transited phase **A'**

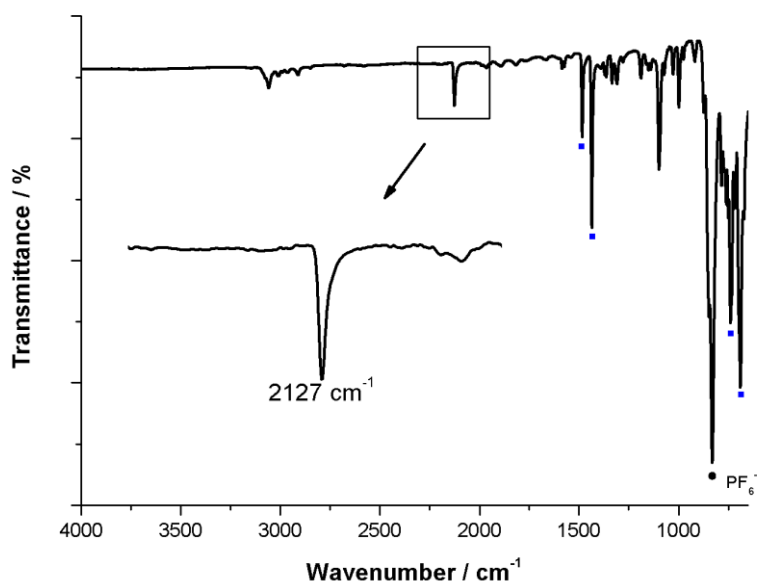


Figure III-3 : Infrared spectrum of the thermally transited phase **A'** ; insert : focus on the $\nu_{(\text{CN})}$ stretching vibration band. The dot marks the PF_6^- counter-anion t_{1u} vibration mode band. The blue squares mark dppm ligand bands.

It is apparent in the solid-state infrared spectrum of derivative **A'** (Figure III-3) that the $\nu_{(\text{CN})}$ stretching band is preserved after the heating experiment, however, shifted to a higher frequency and is found at 2127 cm^{-1} in the infrared spectrum of **A'** (Figure III-4).

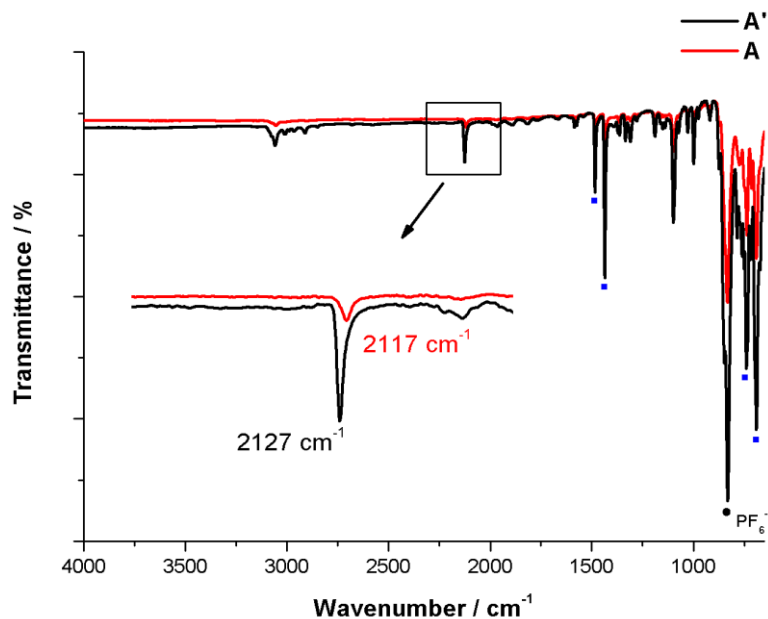


Figure III-4 : Superimposition of the infrared spectrum of **A** and **A'** ; insert : focus on the $\nu_{(\text{CN})}$ stretching vibration band. The dot marks the PF_6^- counter-anion t_{1u} vibration mode band. The blue squares mark the dppm ligand bands.

This shift in the position of the $\nu_{(\text{CN})}$ stretching band is the only noticeable change observed in the IR spectrum of **A'** when compared with **A**. Otherwise, the infrared spectrum of **A'** is highly similar to the spectrum of the initial phase **A**, with the presence of typical absorption bands of the dppm ligands backbone present at the same wavenumbers. The PF_6^- counter anion is also confirmed to be preserved in the transitioned phase **A'** with the presence of a band at 834 cm^{-1} . This observation along with the similarities between the two spectra suggests that the irreversible thermal transition in **A** is not a chemical reaction and does not change the composition of the compound. Considering the observed shifting of the $\nu_{(\text{CN})}$ stretching band to higher wavenumbers, it can be attributed to structural rearrangements taking place in the solid-state along the thermal transition and leading to small changes in the tetrametallic metallacycle structure of the compound.

III-1.c Powder X-ray diffraction of transitioned precursor **A'**

However, it was unfortunately not possible to conduct single crystal X-ray diffraction measurements on this derivative **A'** since the initial crystals of the phase **A** did not keep single

crystal integrity once removed from the crystallisation solution. Nonetheless, it is possible to assess the crystallinity of the thermally transited **A'** phase by powder X-ray diffraction analysis (Figure III-5).

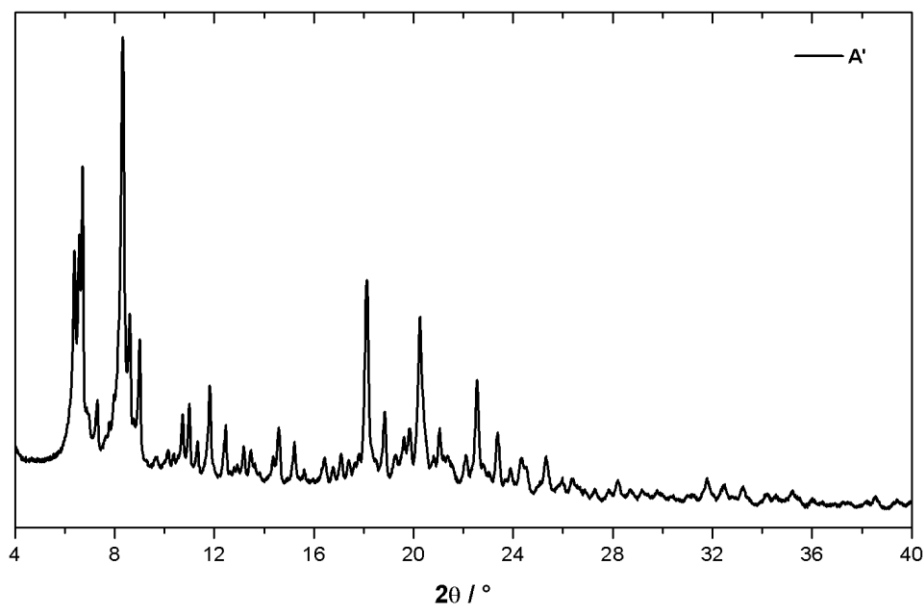


Figure III-5 : Powder X-ray diffraction diagram of thermally transited phase **A'**.

As can be seen in the powder X-ray diffraction diagram (Figure III-5), after the thermal transition occurring, the **A'** phase presents a significant crystallinity in spite of the thermal process applied. Moreover, when superimposed to the powder X-ray diffraction diagram of derivative **A** freshly synthesized, it is clear that a structural change occurred during the heating applied on **A** (Figure III-6). Nonetheless, when the transited phase of the precursor **A'** is recrystallized by dissolving it in dichloromethane and submitted to pentane vapor diffusion, colorless crystals could be recovered which have been characterized as crystals of the initial precursor **A** by single crystal X-ray diffraction measurements. This result confirms that the thermal treatment applied to the solid-state of derivative **A**, occurring as an exothermic transition located at 233 °C does not cause a chemical reaction but rather a crystal phase transition. A measurement of the variation of the powder X-ray diffraction of **A** depending on the temperature was also performed.

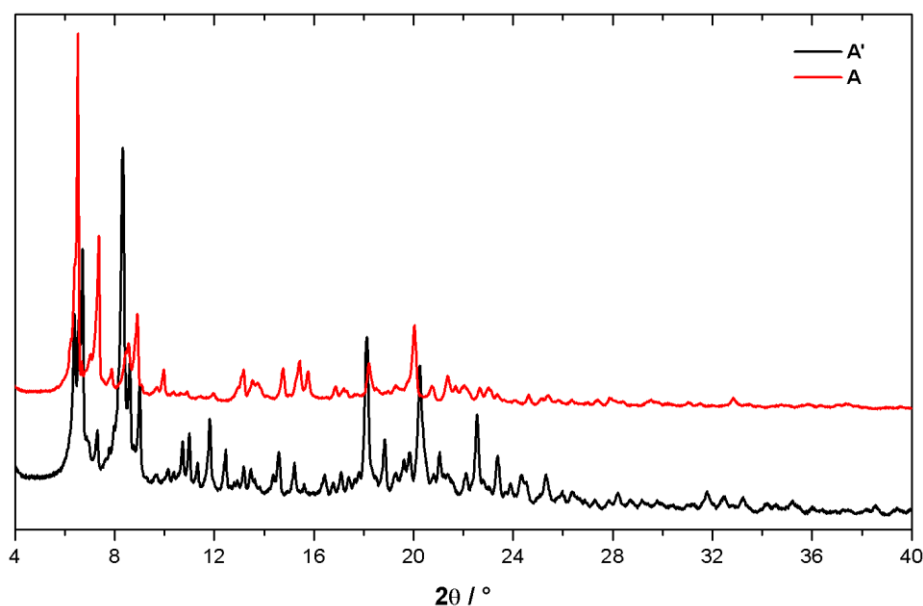


Figure III-6 : Comparison between the powder X-ray diffraction of **A** (red) and **A'** (black).

This measurement revealed that upon heating of the precursor **A**, three distinct crystalline phases could be observed. The first one is thermally stable up to 140 °C, where a second crystalline phase appears. This second phase is stable up to 210 °C. The final phase obtained is stable all the way up to 280 °C, and is conserved back to room temperature. This last phase, obtained at high temperature is identical to the crystalline phase of the thermally transitioned precursor **A'** obtained at RT (Figure III-5). The presence of multiple successive crystalline phases during the heating process leading to the irreversible thermal transition adds to the complexity of understanding the mechanism behind this transition. A direct correlation between these TD-PXRD data (under Argon) and the TGA-DTA (under Nitrogen) measurement is not straightforward since the conditions of both measurements are not strictly similar. Moreover the kinetics of the heating are not the same. Yet one can suggest that the phase transition observed at 233 °C in the TGA-DTA measurement correspond to the crystal phase transition observed at 210 °C in the TD-PXRD measurement since the phase obtained *in fine* are the same according to their PXRD diagrams. The crystal phase transition observed in the TD-PXRD diagrams at 140 °C is likely associated to another crystal phase reorganization of the RT crystal phase that is itself not strictly corresponding to the calculated diagram obtained from the single crystal structure, likely due to a crystalline phase transition after the crystals are dried and a significant

amount of included CH_2Cl_2 molecules are evaporated. However, all these crystal phases transition reflect the high flexibility of the Cu(I) based supramolecular assemblies.

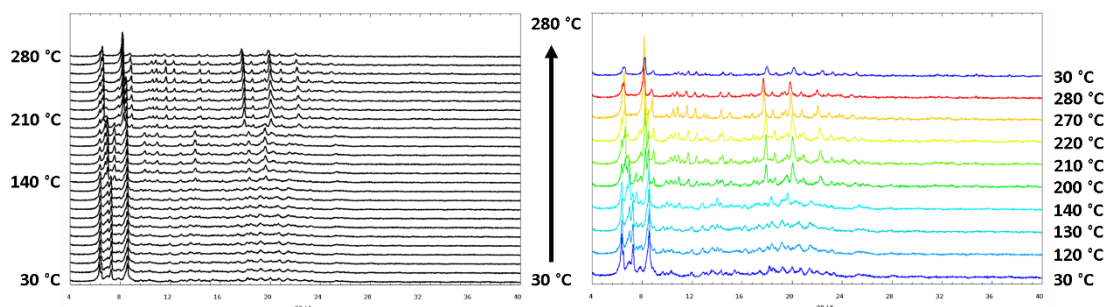


Figure III-7 : Temperature dependant powder X-ray diffraction (TD-PXRD) of precursor **A** from 30 to 280 K.

Even if the thermal transition and the subsequent structural rearrangement does not lead *a priori* to a striking change in the luminescence in **A** compared to the polymers **C_n**, mainly due to the fact that the precursor is originally blue luminescent at RT, the luminescence properties of this new phase **A'** were investigated in details.

III-1.d Luminescence properties of thermally transited precursor A'

The compound **A'** retains a crystalline white powder aspect under visible light. Its solid-state UV-visible absorption spectrum was recorded, consisting in a band centered around 300 nm, similarly to the UV-visible absorption spectrum of the precursor **A**. The RT excitation spectrum of **A'** recorded at 455 nm presents two large band situated at 325 and 375 nm, close to the values observed for the precursor **A** (310 and 360 nm) (Figure III-9).

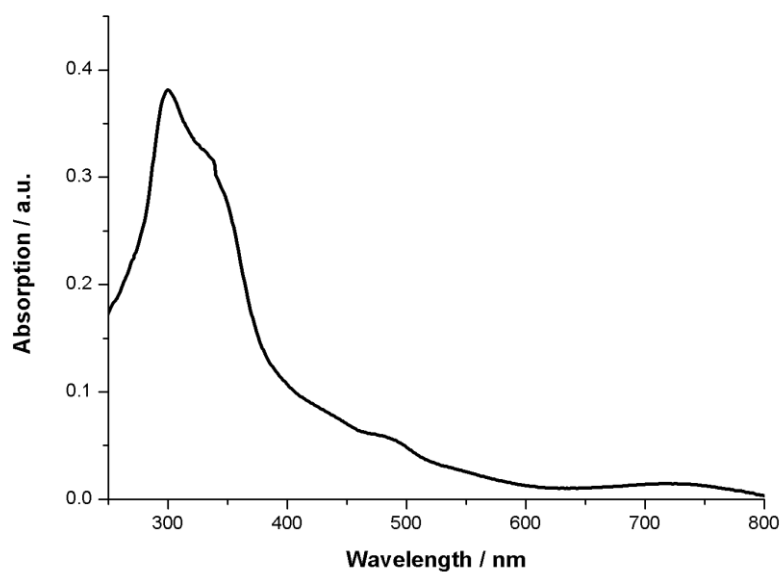


Figure III-8 : Solid-state UV-visible absorption spectrum of **A'**.

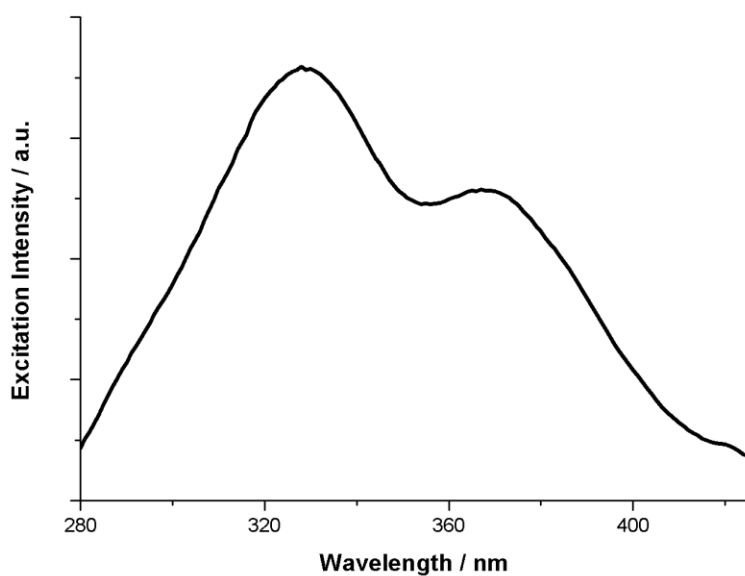


Figure III-9 : Solid-state room temperature excitation spectrum of **A'**.

Upon the irreversible thermal transition taking place, no drastic changes are occurring in the solid-state RT luminescence of **A'**. Under UV-light ($\lambda_{\text{ex}} = 365 \text{ nm}$) it stills emits an intense eye-perceived deep blue light, similar to the one displayed by the precursor **A**. This luminescence

is characterized in the solid-state at room temperature by a large band (FWHM = 70 nm) in the emission spectrum centered around 455 nm, highly similar to the RT emission spectra of **A**, (Figure III-10).

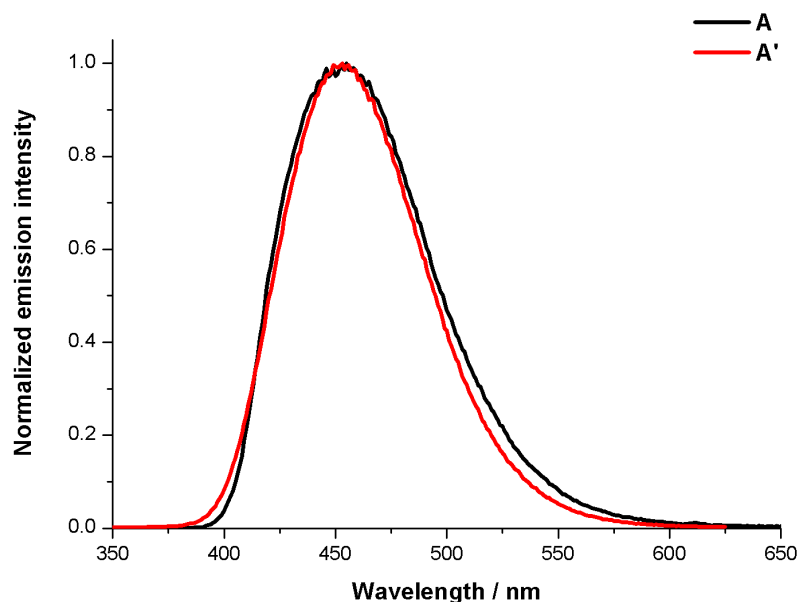


Figure III-10 : Solid-state RT normalized emission spectrum of **A** (black) and **A'** (red) ($\lambda_{\text{ex}} = 325$ nm).

The study of the thermal dependence of the emission spectrum of **A'** reveals a bathochromic shift of the large unstructured band observed at RT occurring upon cooling of the sample, a similar behavior than observed for **A**. At 80 K, the luminescence is characterized in the emission spectrum by a large band (FWHM = 77 nm) centered at *ca.* 492 nm, corresponding to the emission of an eye-perceived greenish luminescence. It can be noted that a shift of 6 nm to the higher wavelengths at 80 K is observed for the λ_{max} value when compared to **A**. Beside this shift, there is almost no difference in the thermal dependence of the emission spectrum of **A** and **A'** (Figure III-11).

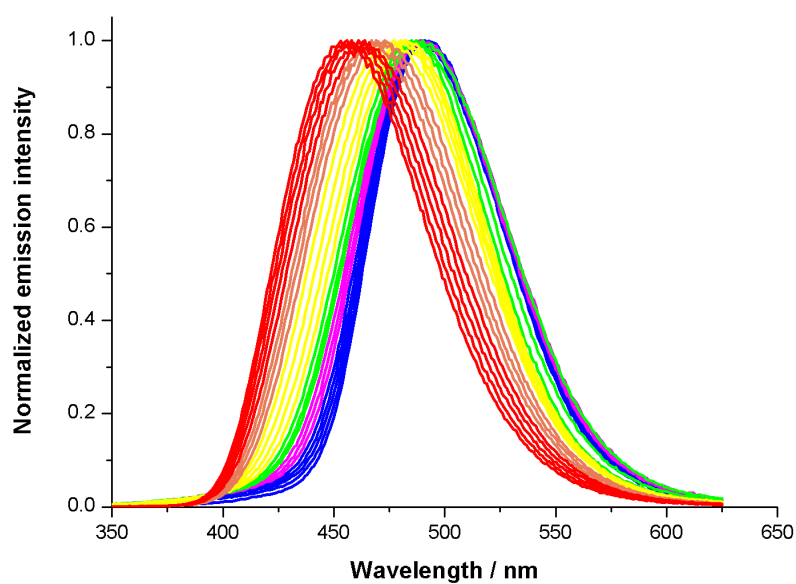


Figure III-11 : Temperature dependence of the normalized emission spectrum of thermally transitioned precursor **A'** ($\lambda_{\text{ex}} = 325$ nm).

A study of the temperature dependence of the decay times of the excited states of this new phase **A'** in the solid-state was also performed (Figure III-12). At room temperature, the lifetime consists in a monoexponential component with a decay time of 20 μs . Upon cooling, an increase of the decay time is observed and upon reaching 80 K, the lifetime value is 200 μs . It can be noted that a plateau of the lifetime values is reached at *ca.* 200 K during the cooling process and is maintained as the temperature decreases.

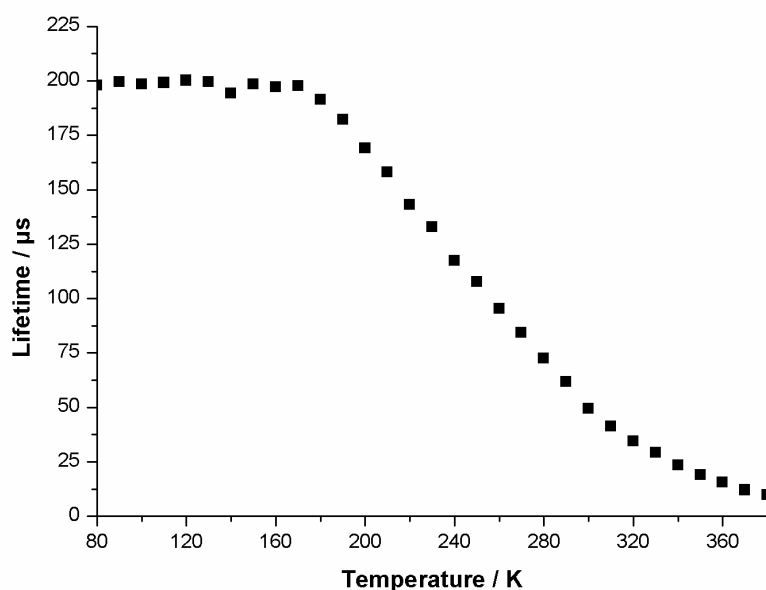


Figure III-12 : Temperature dependence of the decay time of the thermally transitioned phase **A'**.

The photoluminescence properties displayed by the thermally transitioned phase **A'**, on top of being similar to the ones displayed by the precursor **A**, are reminiscent of TADF behavior, hinting that this property of **A** is retained during the irreversible thermal transition. The curve of the thermal dependence of the decay time of the excited state has been fitted with the equation given in the introduction chapter (Equation I-1) and gives values of lifetimes of 198 μs for T_1 , 45 ns for S_1 and an energy band gap $\Delta E_{(S_1-T_1)}$ of 1281 cm^{-1} , that compare to values that are similar to the ones found for the initial precursor **A** ($\Delta E_{(S_1-T_1)} = 1560 \text{ cm}^{-1}$, $\tau(T_1) = 185 \text{ μs}$ and $\tau(S_1) = 9.9 \text{ ns}$).

The RT solid-state luminance of the phase **A'** under UV light irradiance of 3.5 W/m^2 is 59 Cd/m^2 , very close to the value of 55 Cd/m^2 measured for the solid-phase of **A** under the same irradiance.

III-1.e Thermal behavior of the transited phase A'

Finally, the thermal properties of this new phase A' were measured (Figure III-13).

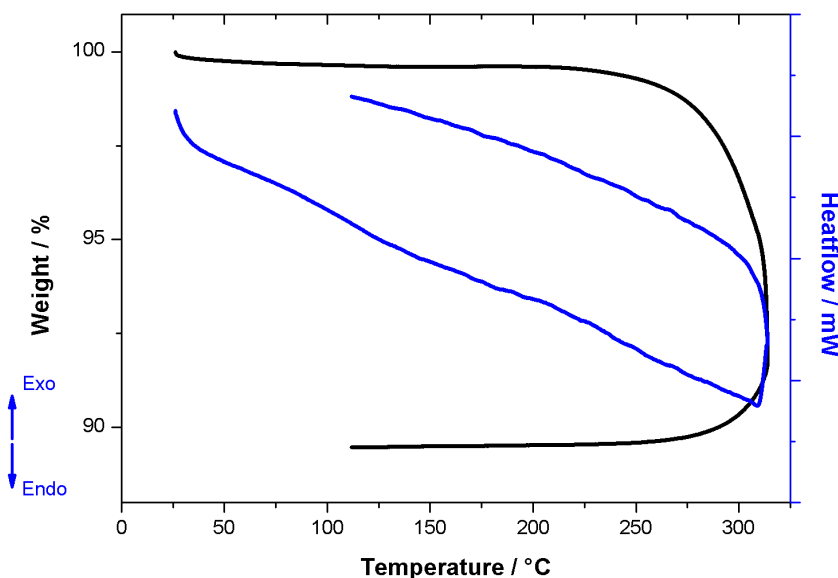


Figure III-13 : TGA-DTA analysis of thermally transited precursor A' until 300 °C and back to room temperature.

The TGA-DTA analysis of A' reveals that no further thermal events are present during the heating process up to 300 °C. The measurement was not conducted at higher temperatures due to the fact the initial compound A is thermally stable only until 350 °C. The loss of weight registered during the measurement is attributed to the beginning of a thermal decomposition of the compound when it is maintained at the maximum temperature of the measurement. During the cooling process, the presence of any thermal events was not observed.

These measurements indicate that upon this irreversible transition occurring, the precursor A undergoes a structural rearrangement in the solid-state, likely reaching a more thermodynamically crystalline stable phase in which no solvent molecules are included. Upon further heating of this new phase A', no new thermally induced structural rearrangements seem to occur hinting that this new phase is stable in these ambient condition in the solid-state.

This result, along with the previously conducted recrystallization of A from A', comforted us in the idea that A' and A are two solid-state phases of the same compound, with A being

obtained directly from synthesis and crystallization and **A'** being the result of a solid-state thermal transition of the phase **A**.

To sum up this preliminary study, upon discovering an irreversible thermal transition in the polymers **C_n**, leading to a noticeable change in their luminescence properties, a similar TGA-DTA study was performed on the precursor **A**, to possibly gather more information about this transition. An irreversible thermal transition is also found to be occurring (at 233 °C) in the precursor in the solid-state, leading to a new solid-state RT blue luminescent phase **A'**. This thermally transitioned precursor **A'** was analyzed in depth, leading to a better understanding of the thermal transition. Upon this transition the general metallacycle structure of **A** is likely preserved but a reorganization in the crystalline solid-state occurs, leading to changes in the overall geometry of the tetrametallic metallacycle structure and the luminescent properties, especially observed at low temperatures. This behavior in the solid-state reflects the high flexibility of the Cu(I) based polymetallic assemblies that can undergo phase transition in the solid-state at rather high temperature for a molecular solid without collapse of their gross molecular structure.

III-2 Effect of the transition on the polymers C_n

III-2.a Infrared measurements of the transitioned compounds C_n' .

Infrared spectroscopy measurements on the compounds C_n' have been first conducted (Figure III-14).

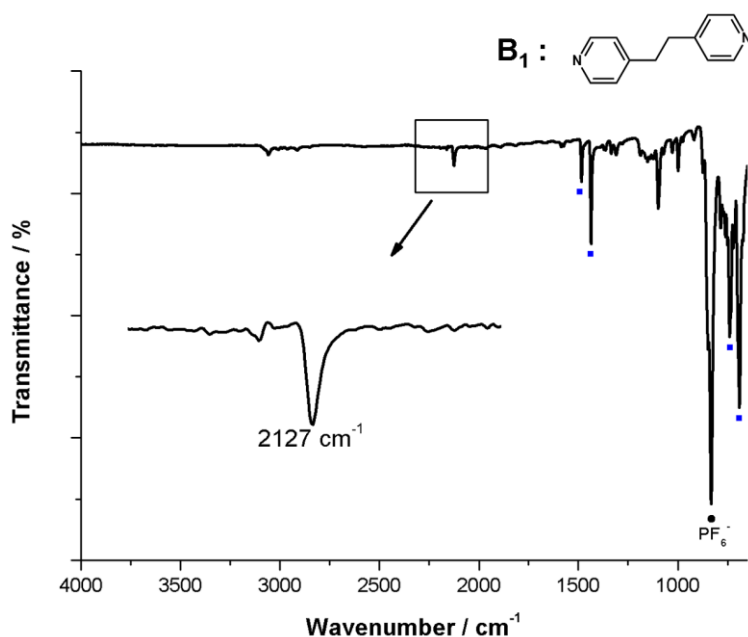


Figure III-14 : Infrared spectrum of the thermally transitioned phase C_1' ; insert : focus on the $\nu_{(CN)}$ stretching band. The dot marks the PF_6^- counter anion t_{1u} vibration mode band. Blue squares mark dppm ligand bands.

For example, in the RT solid-state infrared spectrum of the thermally transitioned phase C_1' , the $\nu_{(CN)}$ stretching band can be observed to be a moderately intense band located at 2127 cm^{-1} , shifted to higher frequencies, from 2102 cm^{-1} , in the initial polymer C_1 . This value is different from the one found in the tetrametallic metallacycle precursor **A**, however it is identical to the $\nu_{(CN)}$ stretching band found in the infrared spectrum of the thermally transitioned precursor **A'**.

When the RT solid-state infrared spectrum of C_1' is compared to the RT solid-state infrared spectrum C_1 (Figure III-15), it can be observed that they are highly similar. The most intense absorption band found in both spectra is located at 832 cm^{-1} in the infrared spectrum of C_1' and is attributed to the PF_6^- counter anion. In addition, the typical absorption bands attributed to the dppm ligand backbone are still present with no noticeable shifts in their frequencies. In the case of the infrared spectrum of C_1' , the absorption bands of the dppm ligand can be found at 1485,

1436, 739 and 690 cm^{-1} , values that are very similar to the ones found in the initial polymer C_1 infrared spectrum.

Yet, importantly, the vibration band located at *ca.* 1609 cm^{-1} in the infrared spectrum of C_1 and which is attributed to the coordination of the B_n linker to the metallic centers, is absent in the infrared spectrum of the thermally transited phase C_1' . No bands that are attributed to the linker can be observed in the infrared spectrum of the transited phase which leads to the assumption that the ligand is missing the phase C_1' after the heating process. This observation can help explain the shift of the $\nu_{(\text{CN})}$ stretching band as the coordination number of the Cu(I) metal centers would be lowered, leading to an increased frequency when compared to the initial polymer C_1 .

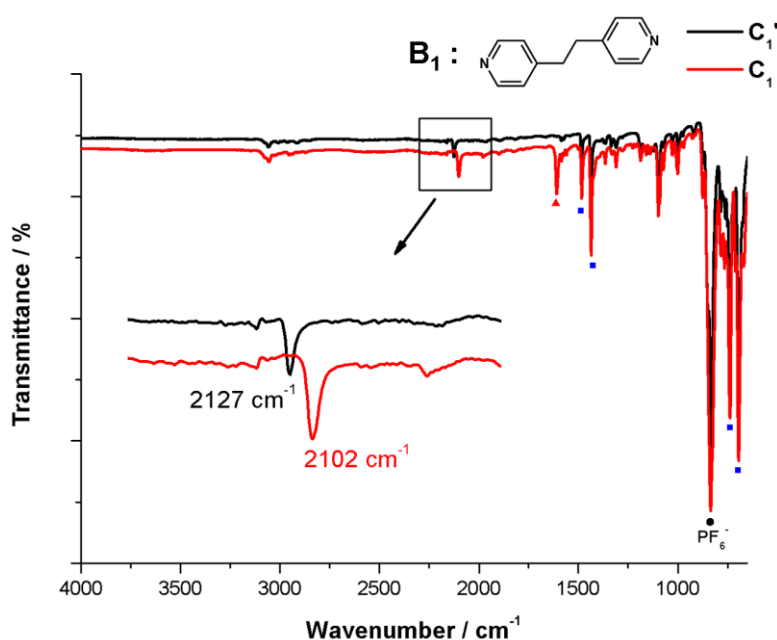


Figure III-15 : Comparison between the infrared spectrum of C_1' (black) and C_1 (red); insert : focus on the $\nu_{(\text{CN})}$ stretching band and reported values. The dot marks the PF_6^- counter anion t_{1u} vibration mode band. Blue squares mark dppm ligand bands. Red triangles mark ligand B_1 bands.

Such observation in the infrared spectrum of thermally transited phases C_n' are similar for a majority of them, from C_1' - C_4' , and C_7' . Each of the aforementioned thermally transited compounds present an infrared spectrum in which the $\nu_{(\text{CN})}$ stretching can be observed at 2127 cm^{-1} , with a similar shift to higher frequencies compared to the initial polymers C_n . They all present similar values of the absorption bands of the dppm ligand backbone, as well as the lack of the absorption band attributed to the coordinated linker at *ca.* 1610 cm^{-1} (Figure III-16).

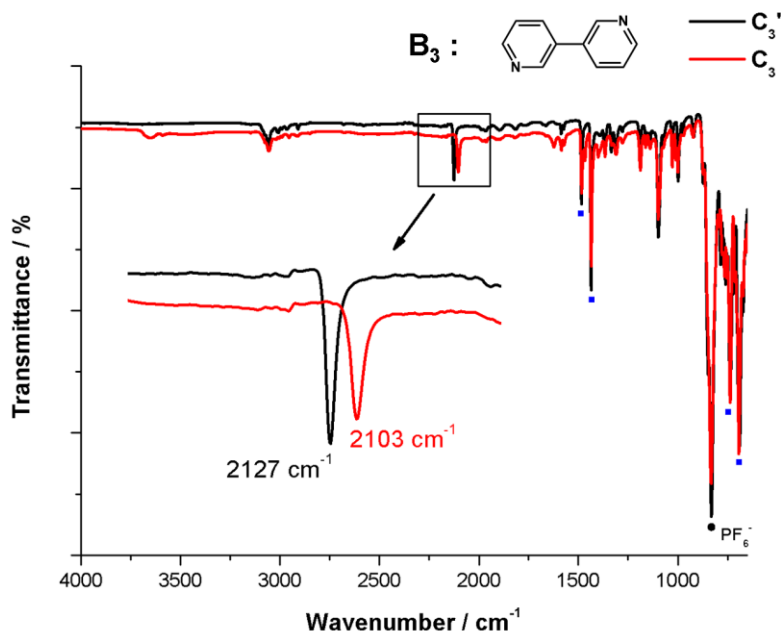


Figure III-16 : Comparison between the infrared spectrum of C_3' (black) and C_3 (red); insert : focus on the $\nu_{(CN)}$ stretching band. The dot marks the PF_6^- counter anion t_{1u} vibration mode band. Blue squares mark dppm ligand bands. Red triangles mark ligand B_3 bands.

This similarity between the infrared spectra before and after the thermal transition for compounds C_1' - C_4' and C_7' indicate that all polymers follow the same behavior upon heating where a decoordination of the linker B_n from the tetrametallic metallacycle subunit seems to take place, as suggested by the observed shift of the cyanide stretching band. Moreover the connecting ligands seems also to be removed from the solid-state samples since there are no more band typical of these ligands that are observed in the solid phases at the end of the thermal process.

Concerning the remaining two transitioned phases, C_5' and C_6' , both follow a similar other trend, with a clear shift toward higher frequencies for the stretching band of the cyanide ligand (Figure III-17).

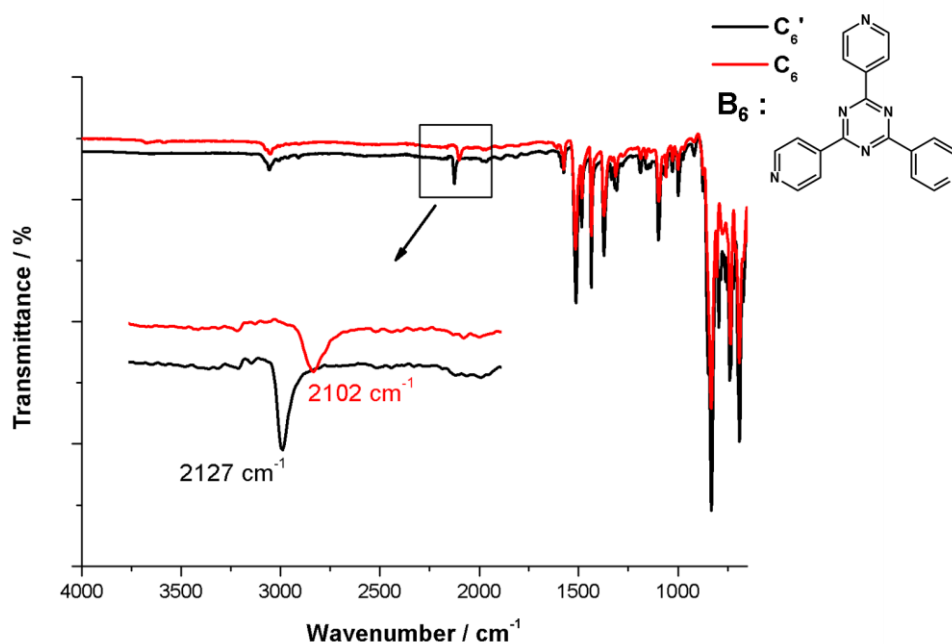


Figure III-17 : Comparison between the infrared spectrum of C_6' (black) and C_6 (red); insert : focus on the $\nu_{(CN)}$ stretching band. The dot marks the PF_6^- counter anion t_{1u} vibration mode band. Blue squares mark dppm ligand bands. Red triangles mark ligands bands B_6 .

Both transited phases C_5' and C_6' present a $\nu_{(CN)}$ stretching band located at 2127 cm^{-1} , similar to the transited precursor A' and also to the other transited C_n' compounds. Both display similar bands of their dppm ligand backbones, and a similar PF_6^- counter anion t_{1u} vibration band. One main difference however lies in their infrared spectra compared to the other transited phases : a band located at *ca.* $1600\text{--}1575\text{ cm}^{-1}$ attributed to the corresponding non coordinated linkers B_5 and B_6 can be found in their infrared spectra, suggesting that the linker is still present in the compounds.

The infrared measurements conducted on the thermally transited phases C_n' point toward a decoordination of the linker B_n from the metallic centers of the tetrametallic metallacycle subunit as the exothermic event observed in the TGA-DTA analysis occurs. The linkers seems to be missing in the transited compounds except in the case of C_5' and C_6' . It seems that upon this decoordination occurring, the molecular solid undergoes a structural rearrangement in a strictly identical manner across the entire series of compounds C_n' as in the phase A' (obtained after thermal treatment of A) witnessed by an identical value of the $\nu_{(CN)}$ stretching band located at 2127 cm^{-1} for all thermally transited compounds A' and C_n' .

To better understand the loss of the linker **B_n** observed in the transitioned phases **C₁₋₄'** and **C₇'**, heating experiments in a sublimation apparatus were conducted. After the thermal process was performed, colorless residue were observed on the cold part of the sublimation device and collected for NMR analysis that revealed that the linker molecules **B₁-B₄** were condensed, confirming the hypothesis of their sublimation along the thermal process. In the case of **C₇** polymer the decoordination temperature is the highest of the series and it is likely that the linker **B₇** decomposes at this temperature, leading to the sublimation of a mixture of unidentified degradation species.

This experiment confirmed the observed loss of the linker in the solid-state during the heating process for the **C₁-C₄** and **C₇** polymers, due to their sublimation once their decoordination in the solid-state occurs.

III-2.b Hypothesis of the nature of the thermal transition

The study of the thermally transitioned compounds **C_n'** so far indicates that as the thermal transition happens, all compounds undergo an irreversible and non destructive change in the solid-state. This crystalline change is further supported by the recorded infrared spectrum of the transitioned compounds with in particular, a change of the $\nu_{(\text{CN})}$ stretching band energy of the cyanide ligand. Despite the different values for this stretching band obtained prior to the transition, all transitioned compounds display this band at 2127 cm^{-1} , a value that is similar to the one recorded for the transitioned precursor **A'**. Furthermore, for all transitioned compounds, with the exception of **C₅'** and **C₆'**, the ligands bands previously identified are missing from the infrared spectrum.

To probe further in this mechanism, an experiment was conducted where these transitioned compounds **C₁'-C₄'** and **C₇'** were dissolved in CH_2Cl_2 , and the resulting solution left to crystallize under pentane vapor diffusion. The crystals obtained were characterized by single crystal X-ray diffraction as being identical to crystals of the precursor **A**, a result that is similar to the outcome obtained as the same recrystallization procedure was conducted on the thermally transitioned precursor **A'**.

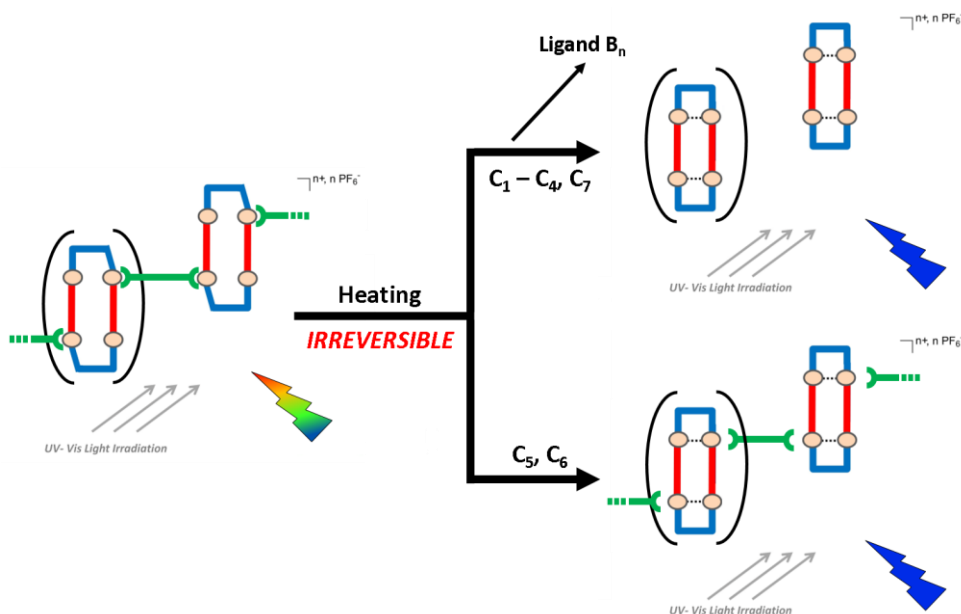


Figure III-18 : Hypothesis concerning the mechanism behind the thermal transition observed in compounds C_n' .

Upon the thermal transition occurring in the initial polymers C_n , a decoordination of the linker B_n from the tetrametallic metallacycle likely occurs. The linker B_n , once decoordinated from the metallacycle is, in most cases, sublimates at these temperatures. Concomitantly, the sample undergoes a structural rearrangement, reaching an identical structure across all transited compounds C_n' and the transited precursor A' .

This hypothesis applies for the transited precursor A' and all transited compounds C_n' , with the exception of C_5' and C_6' . Indeed, the infrared measurements of these two compounds show that the ligand is still present after the thermal transition occurs since they apparently do not sublimate. This can be correlated with their relatively high molecular weights. In any case, regarding such assumption, the photophysical properties of the transited phases should be markedly different of those of the initial one-dimensional coordination polymers C_n .

III-2.c Photophysical properties of the thermally transited C_n' compounds

Indeed, as reported at the end of the previous chapter, this irreversible thermal transition was first detected due to the fact that the luminescence of the solid-state samples changed after the thermal process, leading for all transited compounds to emit under UV-light an intense, eye-perceived blue luminescence. In addition, upon the irreversible thermal transition occurring,

most of the samples of phases C_n' returned to room temperature retain the aspect of a white polycrystalline powder. Only two exceptions are found in the series : After this thermal transition, C_5' present the aspect of a pale red powder different from white powder observed before transition and C_6' becomes a light orange red powder contrasting from the yellow powder observed for C_6 .

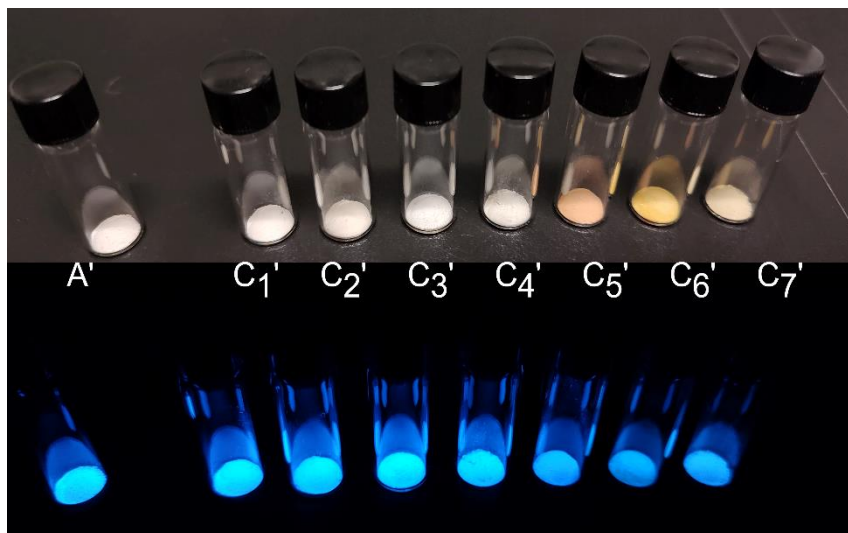


Figure III-19 : Photography of the thermally transited phases C_n' as well as the thermally transited precursor A' under visible (top) and UV light ($\lambda_{\text{ex}} = 365 \text{ nm}$) (bottom).

Therefore the photophysical properties of the transited phases C_n' were studied in order to better characterize this transition (Figure III-19).

III-2.c.i Solid-state UV-visible absorption spectra

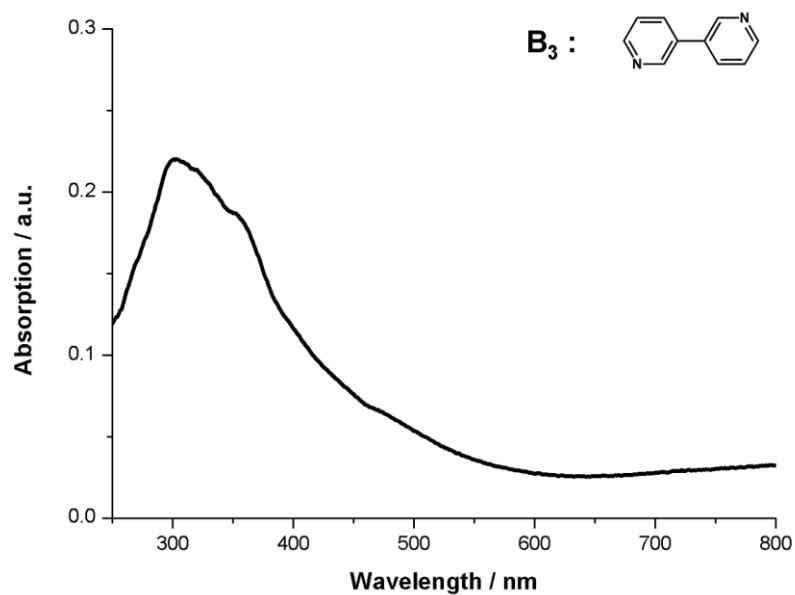


Figure III-20 : UV-visible absorption spectrum of compound C₃'.

In the UV-visible absorption spectrum of transited compound C₃', presented in Figure III-20, a large band starting at *ca.* 400 nm is observed with a maximum at *ca.* 320 nm. This band is reminiscent of the band presents in the absorption spectrum of the transited precursor A', associated with π - π^* transitions centered on the organic aromatic ligands.

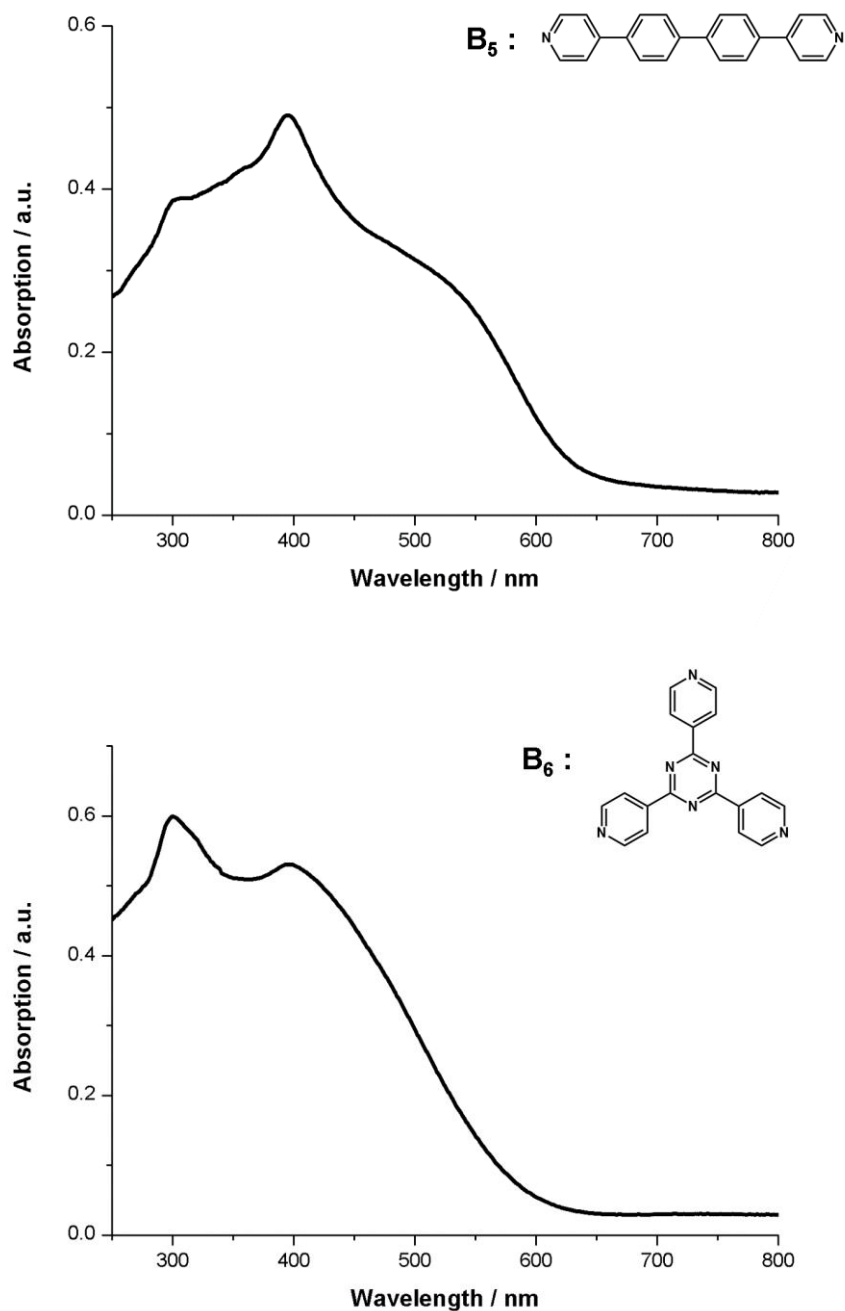


Figure III-21 : top) Uv-visible absorption spectrum of C_5' ; bottom) UV-visible absorption spectrum of C_6' .

The absorption spectra of transitioned compounds C_5' and C_6' , presented in Figure III-21, show a similar large band with a maximum located at *ca.* 320 nm, but the absorption band extends to wavelengths up to 600 and 550 nm respectively before it vanishes, which can be related to the coloration of the powder observed after the transition for both compounds and is likely connected with the presence of the uncoordinated linkers B_5 and B_6 in these molecular solids.

III-2.c.ii Luminescent properties of transited compounds C_n'

In the solid-state at room temperature under UV-visible excitation, all the thermally transited C_n' compounds present an eye-perceived colored blue luminescence, characterized by a large, featureless band in their emission spectrum, centered at 454 nm and presenting a FWHM of 74 nm (Figure III-22).

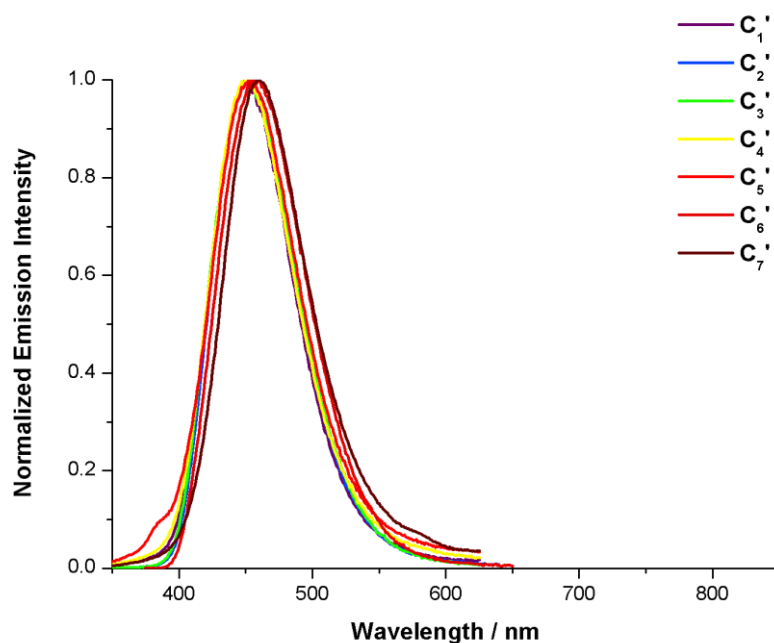


Figure III-22 : Normalized emission spectra of transited compounds C_n' ($\lambda_{ex} = 325$ nm).

The temperature dependence of the emission of the transited phases C_n' revealed that they all present a very similar behavior : Upon cooling, a large, gradual increase of their emission intensity can be observed along with a bathochromic shift of the emission maximum. At 80 K, their emissions are characterized by large featureless bands centered at *ca.* 494 nm, with a FWHM of 64 nm (Figure III-23).

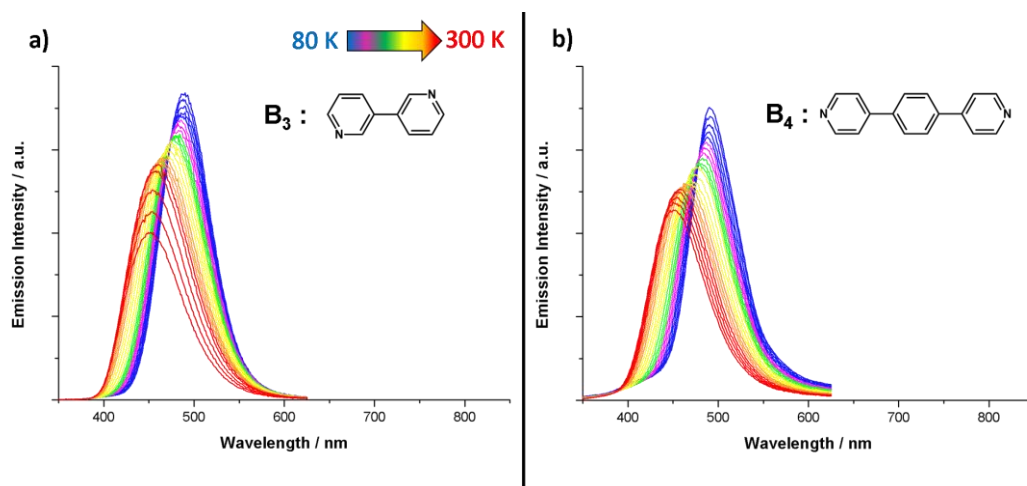


Figure III-23 : Temperature dependence of the emission spectrum of transited phases C_3' (a) and C_4' (b) from 300 to 80 K.

Importantly, such temperature dependant behavior of the emission spectra is very similar to the behavior found in the transited precursor A' , with the same bathochromic shift upon cooling.

	λ_{em} (nm)	λ_{ex} (nm)	I_{80}/I_{RT}	Φ_{em}	τ_{obs} (μs)	k_r (s^{-1})	k_{nr} (s^{-1})
C_1'	450 (491)	325	1.7	70	44 (262)	1.6×10^4	7×10^3
C_2'	452 (493)	325	1.6	72	56 (264)	1.3×10^4	5×10^3
C_3'	451 (489)	325	1.8	85	44 (263)	1.9×10^4	3×10^3
C_4'	450 (490)	325	1.5	63	53 (268)	1.2×10^4	7×10^3
C_5'	452 (492)	325	1.3	66	43 (251)	1.5×10^4	8×10^3
C_6'	457 (498)	325	1.7	67	35 (259)	1.9×10^4	9×10^3
C_7'	459 (496)	325	1.8	65	40 (255)	1.6×10^4	9×10^3

Table III-1 : Photophysical data ($\lambda_{ex} = 325$ nm) for the transited C_n' compounds, at 300 K and 80 K, in the solid-state. Values at 80 K are given in parentheses. I_{80}/I_{RT} is the intensity at maximum of emission at 80 K divided y the intensity at maximum at 300 K. $k_r = \Phi_{em}/\tau_{obs}$, $k_{nr} = (1-\Phi_{em})/\tau_{obs}$.

III-2.c.iii Lifetime measurements of the transited compounds C_n'

The lifetime of the excited states of the transited compounds C_n' have all been measured depending of the temperature from 80 to 300 K, under an irradiation of 375 nm. At RT, the transited compounds display a lifetime in the range of 35-55 μ s. Upon gradual cooling the transited compounds to liquid nitrogen temperature of 80 K, the lifetime of the excited states of compounds C_n' follow a steady, gradual increase to attain a lifetime values in the range of 250-265 μ s (Figure III-24).

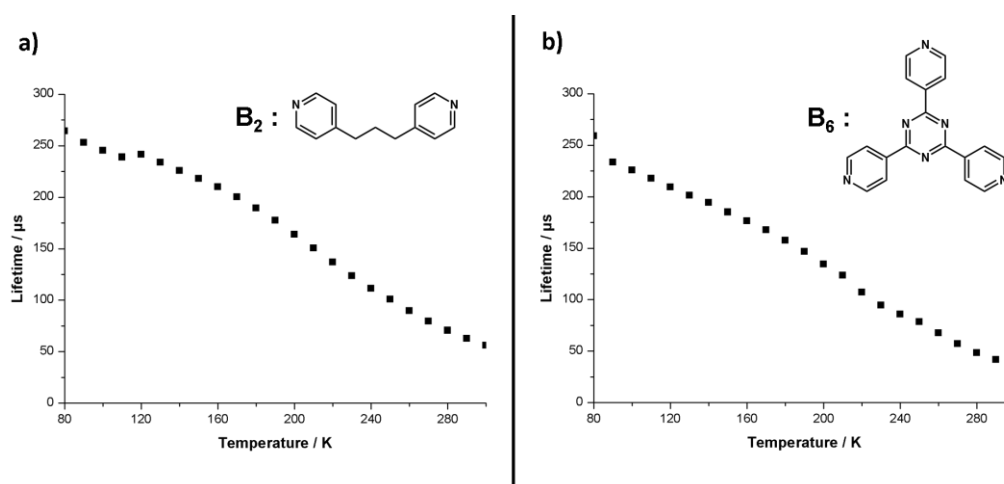


Figure III-24 : Variation of the lifetime of the excited state depending of the temperature of transited phases C_2' (a) and C_6' (b) from 300 K to 80 K.

III-2.c.iv Quantum yields and luminance of the transited compounds C_n'

Along the very noticeable change in the photophysical properties of the transited compounds C_n' compared to the coordination polymers C_n , a change in the intensity of the RT luminescence of the solid-state samples is clearly noted, comparing the intensity of the light emitted before and after the exothermic transition was realized. Indeed, after the thermal transition, the compounds are emitting a light that seems more intense than initially.

To characterize this change in intensity, the quantum yield in the solid-state at room temperature of the compounds C_n' was measured. The obtained values revealed a large increase in the RT luminescent quantum yield compared to the emission quantum yield observed in the initial polymers C_n , displaying an average emission quantum yield of 69 % across the series. The increase of emission quantum yield is particularly impressive in the case of C_5' , being a striking

difference when compared to the initial polymer **C₅** which is basically non emissive in the solid-state under UV light excitation at room temperature.

To complete the photophysical study of the transited compounds **C_n'**, their luminance under UV light irradiance ($\lambda_{\text{ex}} = 365 \text{ nm}$) was evaluated. This measurement revealed a change in the luminance across the series when the thermal transition occurred, leading to higher luminance values (Table III-2).

Compound	A' (A)	C ₁ ' (C ₁)	C ₂ ' (C ₂)	C ₃ ' (C ₃)	C ₄ ' (C ₄)	C ₅ ' (C ₅)	C ₆ ' (C ₆)	C ₇ ' (C ₇)
Luminance (Cd/m ²)	59 (49)	54 (6)	54 (9)	56 (67)	49 (31)	16 (1)	10 (19)	24 (3)

Table III-2 : Values of luminance for thermally transited phases **C_n'** and thermally transited precursor **A'** under an irradiance of 3.5 W/m². The values of precursor **A** and initial polymers **C_n** are given in parenthesis.

In the Table III-2, it can be noted that the transited compounds **C₁'-C₄'** have very similar values of luminance, which is also close to the luminance of the thermally transited phase **A'**. The three others compounds **C₅'**, **C₆'** and **C₇'** display noticeably lower values of their luminance with each being in the range of 10 to 20 Cd/m² under an irradiance of 3.5 W/m². In the case of **C₅'** and **C₆'**, this can be correlated to the presence of the uncoordinated linkers in the solid-state. The reason for why the value of luminance of **C₇'** is also lower is still unclear.

III-2.d Powder X-ray diffraction of transited phases **C_n'**

The thermally transited phases **C_n'** were studied by PXRD and TD-PXRD studies.

As is the case for the initial polymers once taken out of solution and **A'**, it is unfortunately not possible to conduct single crystal X-ray diffraction study on the transited compounds **C_n'**. However, it is possible to assess their crystallinity by performing powder X-ray diffraction, revealing that transited **C_n'** compounds are crystalline after the thermal exothermic transition occurs. The powder X-ray diffraction diagram of the phase **C₃'** is present in Figure III-25.

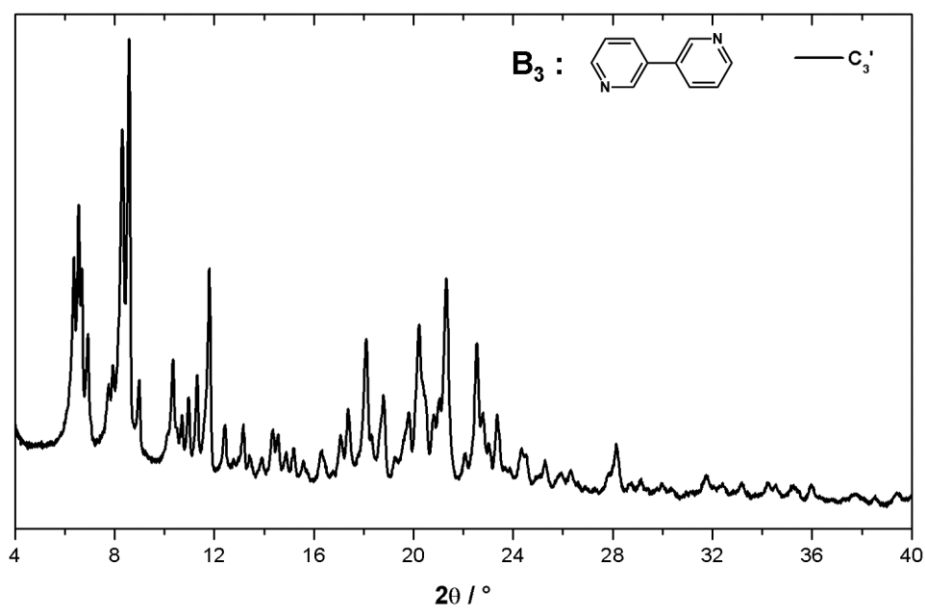


Figure III-25 : Powder X-ray diffraction diagram of compound C_3' .

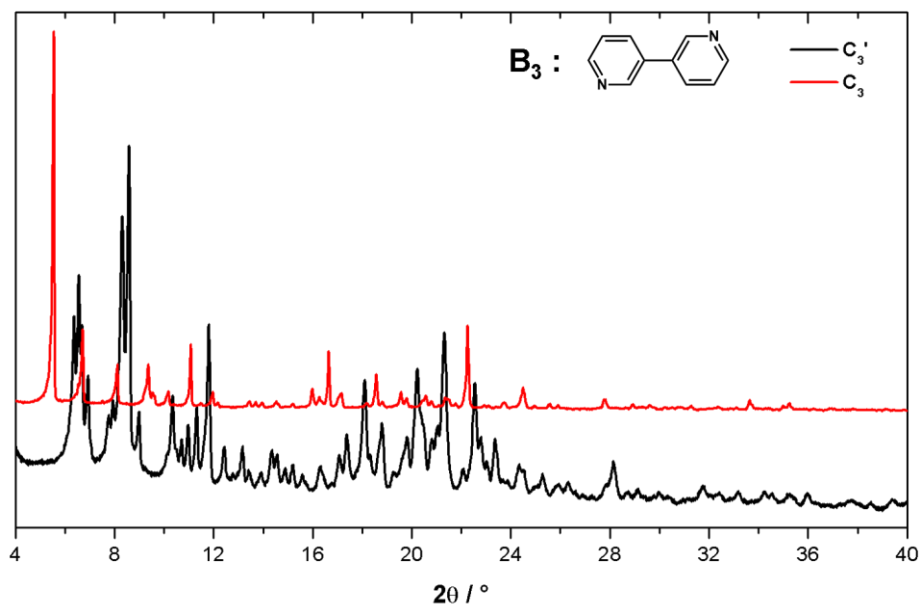


Figure III-26 : Comparison between the powder X-ray diffraction diagram of C_3 (red) and C_3' (black).

It can be noticed here in the overlaid diagrams of C_3 and C_3' that a crystalline phase transition occurred during the heating process, leading to a different crystalline structure than in the initial

compound. A similar phenomenon is displayed in the other transitioned phases C_n' (Figure III-26 and in this chapter's appendix).

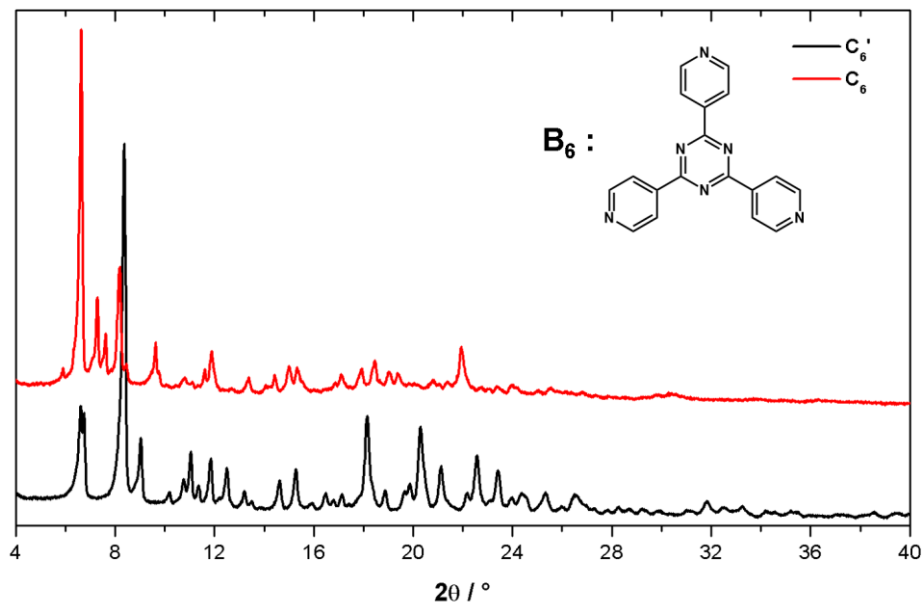


Figure III-27 : Comparison between the powder X-ray diffraction diagram of C_6 (red) and C_6' (black).

In Figure III-27 the superposition of the PXRD diagrams of C_6' and C_6 reveals a similar behavior with a new crystalline phase obtained after the thermal transition occurs. To further analyze the change in these crystalline structure Temperature Dependant X-Ray Diffraction (TD-PXRD) on compounds C_2 , C_3 and C_6 have been conducted, where the compounds were heated from room temperature to 280 °C, under nitrogen atmosphere.

Multiple crystalline phases are observed during the heating process, with three phases being observed for C_2 , from RT to 130 °C, from 140 to 170 °C, and a final phase stable up to 270 °C. A similar observation is possible for the TD-PXRD measurement of the polymer C_3 with four distinct phases present, from RT to 120 °C, a crystalline phase lasting from 130 to 140 °C, a third phase from 160 to 230 °C and finally, a final crystalline phase stable to 270 °C (Figure III-28, Figure III-29).

For the measurement conducted on C_6 , three phases are observed, one from RT to 130 °C, and the other from 160 °C up to 280 °C. An intermediate crystalline phase is observed between 140 and 160 °C (Figure III-30).

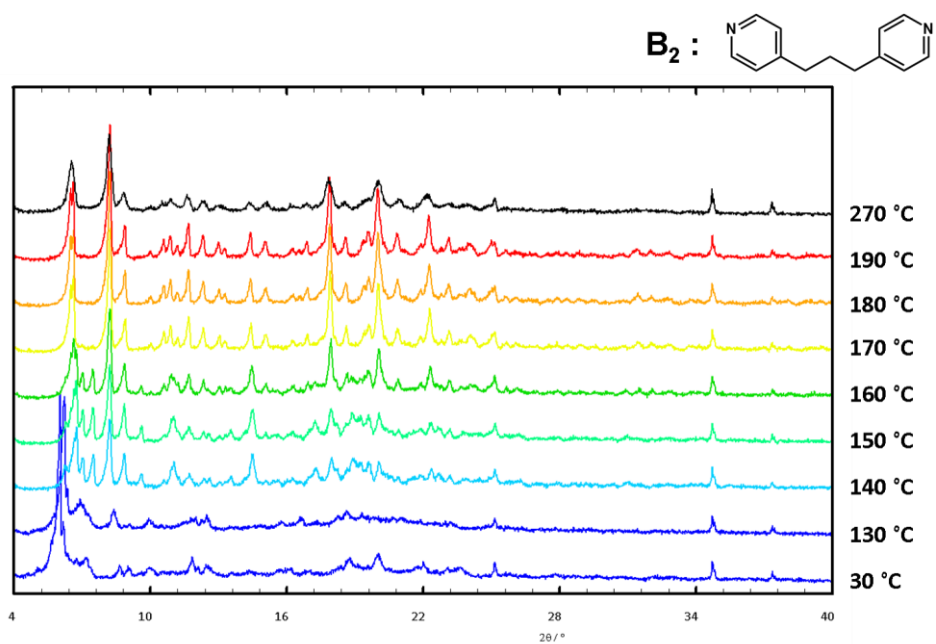


Figure III-28 : TD-PXR D measurement of polymer C₂, from 30 to 280 °C. Selected temperatures are displayed.

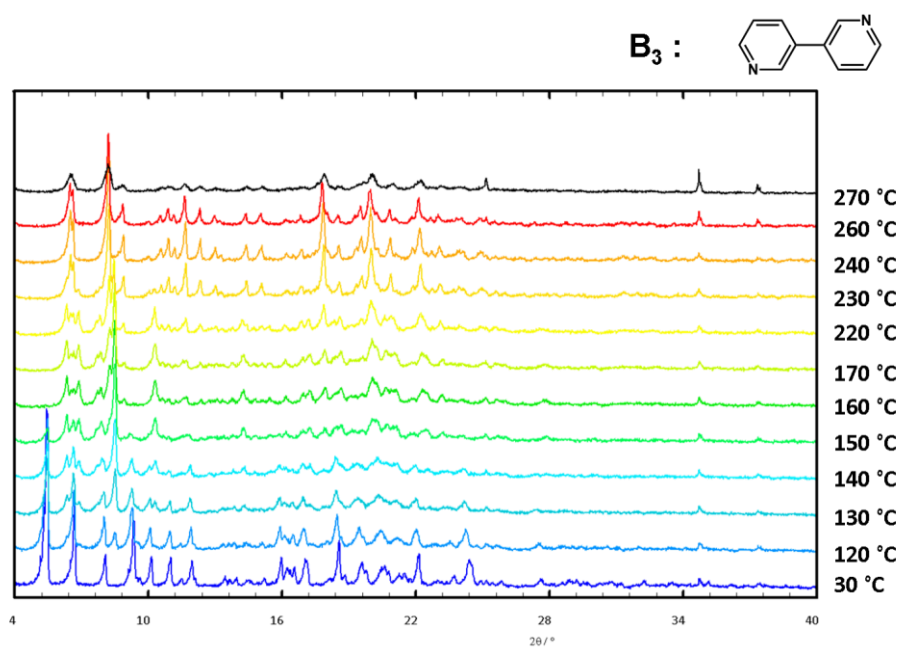


Figure III-29 : TD-PXR D measurement of polymer C₃, from 30 to 280 °C. Selected temperatures are displayed.

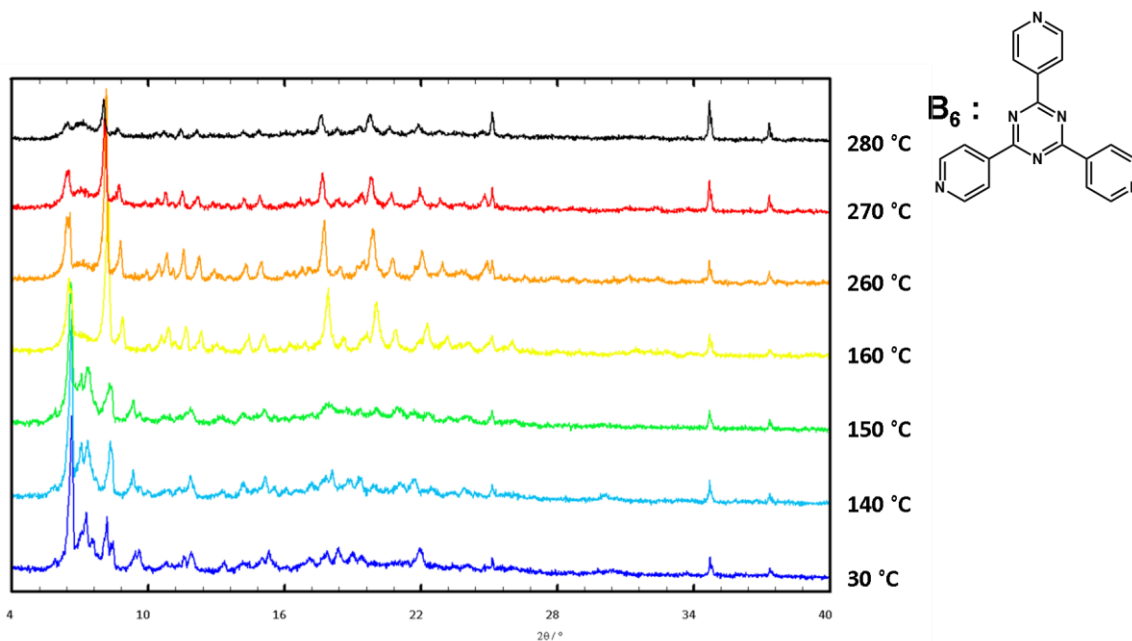


Figure III-30 : TD-PXRD measurement of polymer C_6 , from 30 to 280 °C. Selected temperatures are displayed.

This set of measurement confirm the homogeneity of the transited phases when the linker is sublimated along the thermal process after its decoordination. The obtained stable, high temperature crystalline phases from TD-PXRD measurements are identical when comparing A' , C_2' , C_3' and C_6' . It reveals that the irreversible thermal transition leads to a gradual change of the crystalline phase, in which several steps occur. Here again, the direct correlation of the TD-PXRD data and the TGA-DTA curves recorded for derivatives C_2 , C_3 and C_6 is not possible since the two measurements are conducted in different conditions. Yet, it seems coherent to assign the different phases transitions to rearrangements occurring in the crystal packing as the molecules are reorganized as a consequence of the included solvent evaporation, the connected ligands are decoordinated and finally eventually sublimated in the solid-state.

III-2.e Thermal properties of the transited phase C_n'

Similar TGA-DTA analysis to the one that led to the discovery of the irreversible thermal transition, were performed on the transited phases C_n' in order to highlight the presence or not of further transitions (Figure III-31, Figure III-32).

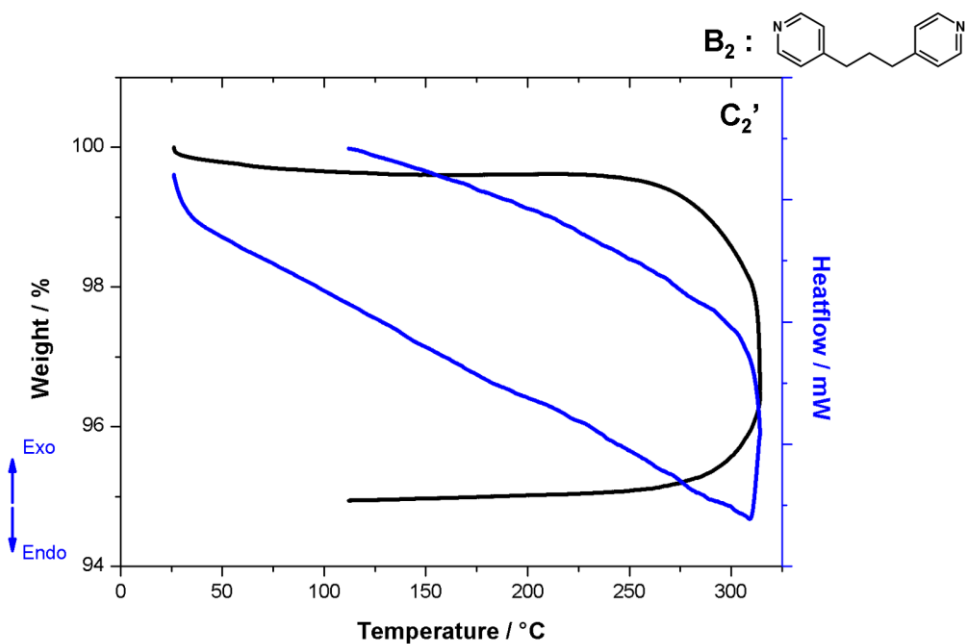


Figure III-31 : TGA-DTA analysis of thermally transitioned phase C₂'.

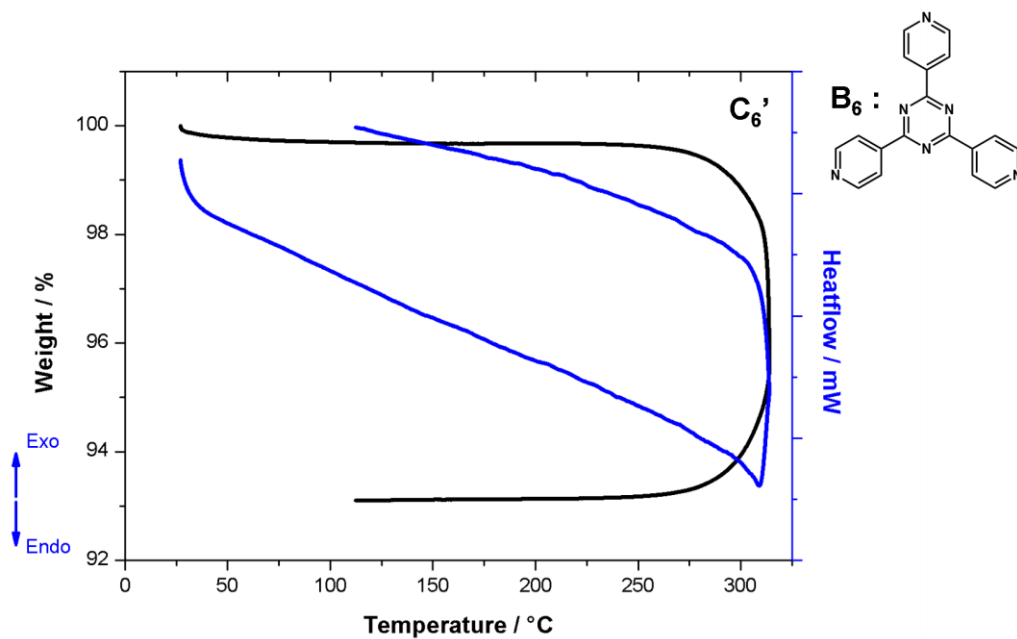


Figure III-32 : TGA-DTA analysis of thermally transitioned phase C₆'.

It can be observed that no events take place in the heating part of the experiment, up to 270 °C, and no noticeable events are seen occurring during the return to room temperature. This behavior is found across the entirety of the series of transitioned species C_n' with the series of TGA-DTA analysis provided in this chapter's appendix. Therefore, these measurements reveal that once

the solid-state thermal transition affording the phase C_n' is realized, the materials are irreversibly changed to these new C_n' phases that are now thermally stable.

III-3 Recovering the initial luminescence post thermal transition

Considering the hypothesis formulated in section III-2.b (Figure III-18), the transitioned phase C_6' should present in the solid-state a stoichiometric ratio of tetrametallic metallacycle and uncoordinated linker B_6 prearranged at the molecular level in an adequate manner to allow potentially the reformation of the 1D coordination polymer C_6 .

With this in mind, the thermally transitioned phase C_6' was exposed to few drops or vapors of dichloromethane. After this exposure, a pale yellow powder is recovered instantaneously which is hereafter denominated $C_6'_{DCM}$. This new phase $C_6'_{DCM}$ was studied in detail to determine whether or not it was indeed similar to the original polymer C_6 . The solid-state infrared spectroscopy of the $C_6'_{DCM}$ phase was firstly conducted.

III-3.a Solid-state infrared spectroscopy measurements on the $C_6'_{DCM}$ phase

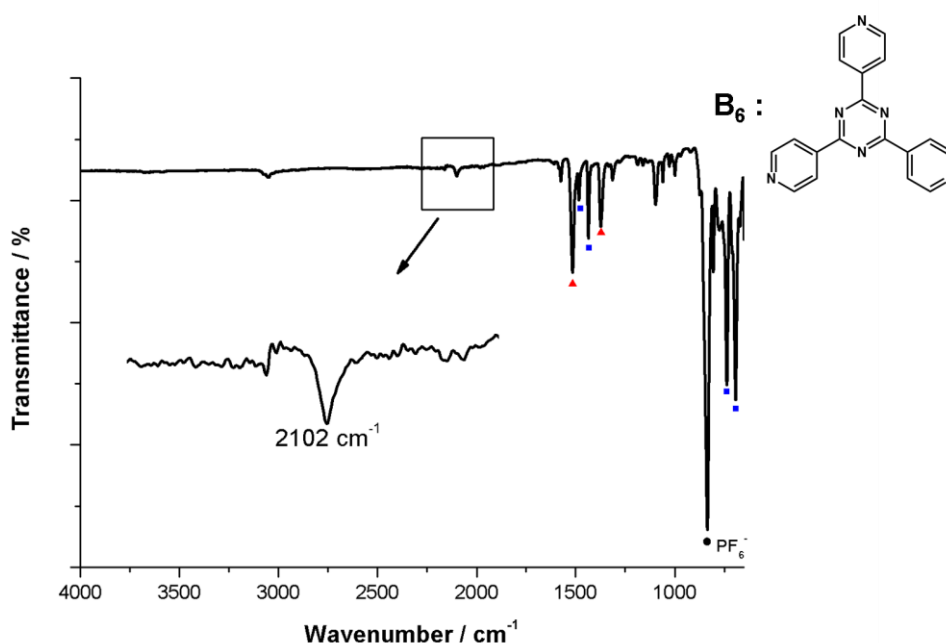


Figure III-33 : Infrared spectrum of the treated compound $C_6'_{DCM}$; insert : focus on the region of the $\nu_{(CN)}$ stretching band and report of the observed value of this band. The dot marks the PF_6^- counter anion t_{1u} vibration mode band. Blue squares mark dppm ligand bands. Red triangles mark B_6 ligand bands.

It revealed that the phase $C_6'DCM$ (Figure III-33) presents clear similarities with the initial polymer C_6 (Figure III-34). The PF_6^- counter anion presents a t_{1u} vibration located at 835 cm^{-1} in the infrared spectrum and the bands attributed to the dppm ligand backbone can still be observed at 1483, 1436, 737 and 692 cm^{-1} , values that are highly similar to the ones found across the series of polymers C_n or transited phases C_n' . The bands specific to the B_6 linker, attributed to the 1,3,5-triazine core are present in the infrared spectrum, located at 1516 and 1374 cm^{-1} , similar to the observed values in the initial polymer C_6 and its transited phase C_6' . Lastly, the $\nu_{(CN)}$ stretching band of the cyanide ligand is observed in the infrared spectrum at 2102 cm^{-1} , a value identical to the one observed for the initial polymer C_6 and clearly different of the value of 2127 cm^{-1} found in the transited phase C_6' .

The presence of the bands attributed to the dppm ligand backbone and the cyanide ligand in the infrared spectrum indicates that the tetrametallic metallacycle subunit is still present in the phase $C_6'DCM$. Bands attributed to the linker B_6 are also observed indicating that the linker is conserved in the compound. Finally, the $\nu_{(CN)}$ stretching band of the cyanide linker is shifted to lower frequencies in the infrared spectrum of $C_6'DCM$, which indicates that the Cu(I) centers possess a higher coordination number. This suggests therefore that the linker is likely re-coordinated to the copper atoms and the initial polymer C_6 is regenerated. This $\nu_{(CN)}$ stretching band in $C_6'DCM$ is also observed to be located at the exact same frequency as in the infrared spectrum of C_6 , 2102 cm^{-1} , indicating that the geometry of the two phases are likely highly similar.

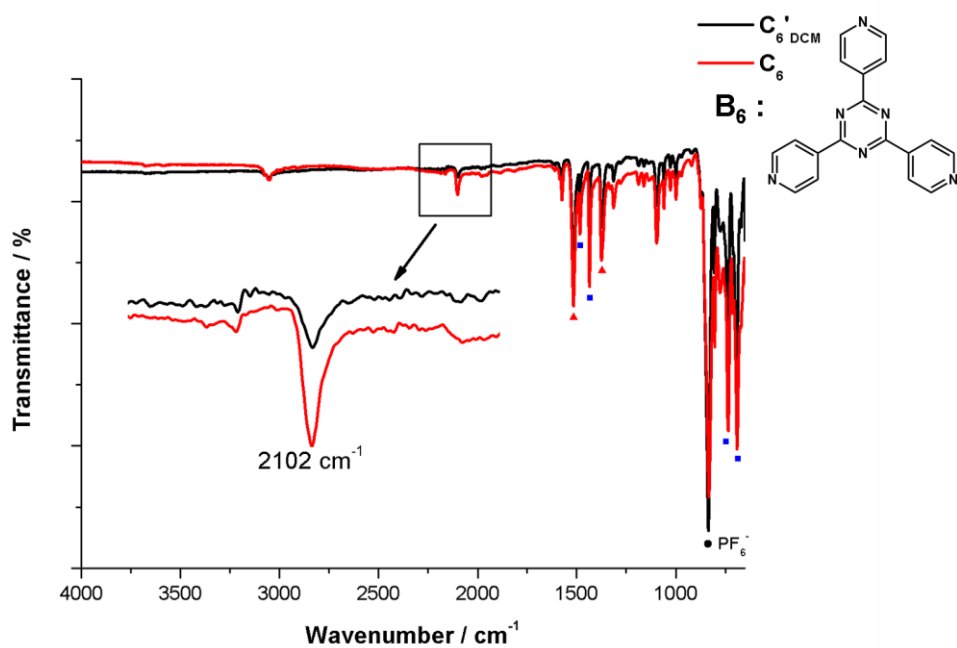


Figure III-34 : Comparison between the infrared spectrum of $\text{C}_6'\text{DCM}$ (black) and C_6 (red) ; insert : focus on the $\nu_{(\text{CN})}$ stretching band and reported wavenumber value. The dot marks the PF_6^- counter anion t_{1u} vibration mode band. Blue squares mark dppm ligand bands. Red triangles mark bands assigned to the coordinated B_6 ligand.

III-3.b Powder X-ray diffraction on the regenerated phase $\text{C}_6'\text{DCM}$

In order to get more insight on the molecular structure of the phase $\text{C}_6'\text{DCM}$, powder X-ray diffraction measurements were conducted (Figure III-35).

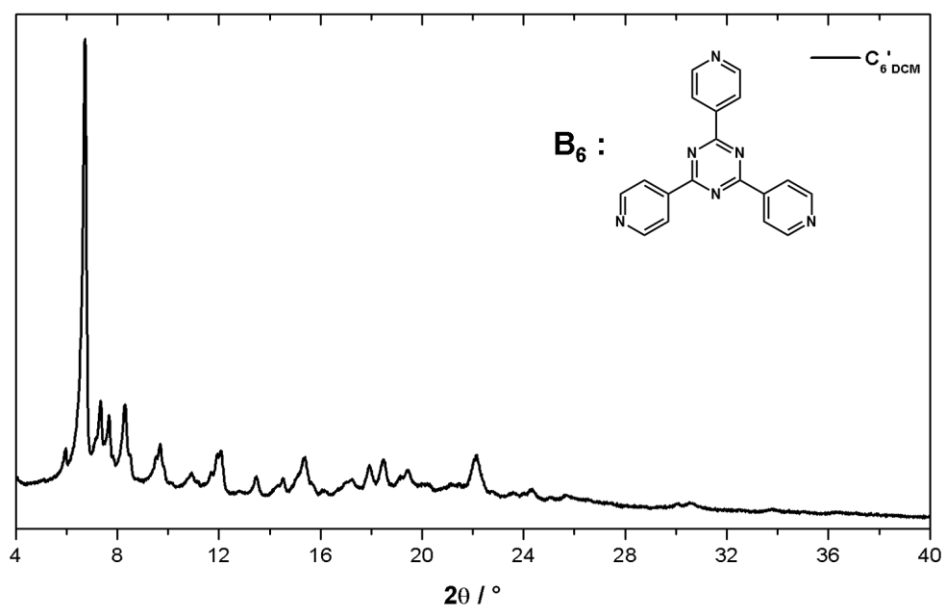


Figure III-35 : Powder X-ray diffraction diagram of treated compound $C_6'DCM$.

In these powder X-ray diffraction diagram of $C_6'DCM$, it can be observed that the treated powder remains polycrystalline. A slight amorphisation can be observed, attributed to the subsequent heating and chemical treatments the compound was subjected to. Yet the diagram is highly similar to the one obtained from the initial 1D coordination polymer C_6 , suggesting a similar crystal packing and hinting toward a recovery of the initial molecular structure (Figure III-36).

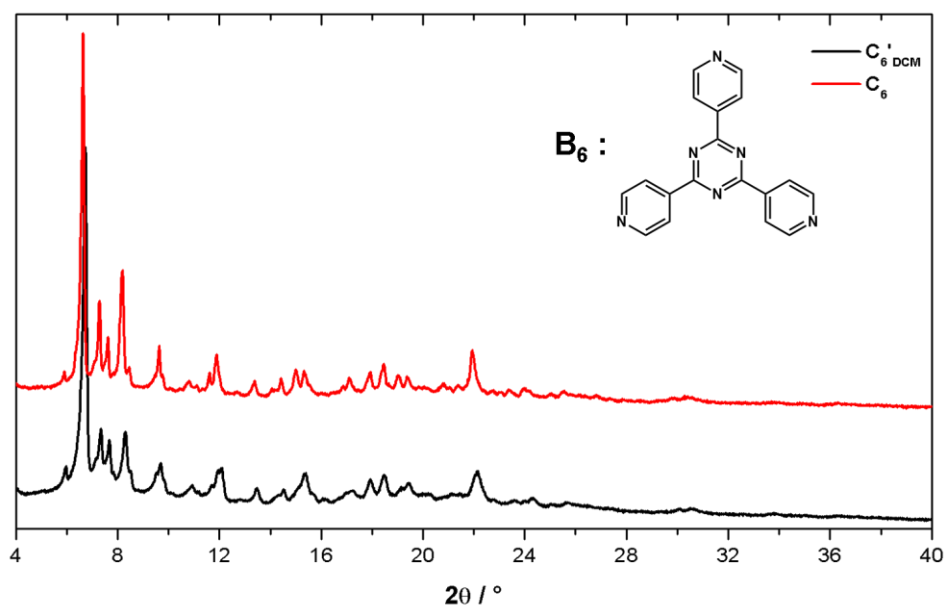


Figure III-36 : Comparison between the powder X-ray diffraction of $C_6'DCM$ (black) and the initial polymer C_6 (red).

More importantly, the photophysical properties of the phase $C_6'DCM$ are altered regarding these of the transited phase C_6' .

III-3.c Photophysical properties of the regenerated polymer $C_6'DCM$

Indeed, compound $C_6'DCM$ is a pale yellow polycrystalline powder that presents under UV-light ($\lambda_{ex} = 365$ nm) the emission of an eye-perceived yellow-orange luminescence, very reminiscent of the luminescence of the initial polymer C_6 (Figure III-37) The regeneration of this yellow-orange luminescence occurs instantaneously as the vapor of CH_2Cl_2 are exposed to the phase C_6' .

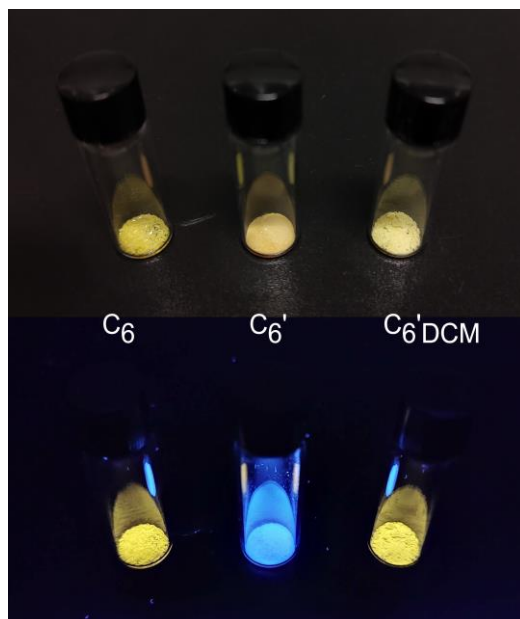


Figure III-37 : Photography of the initial polymer C_6 , the thermally transitioned phase C_6' and the regenerated phase C_6' DCM under visible (top) and UV light ($\lambda_{\text{ex}} = 365 \text{ nm}$) (bottom).

III-3.c.i Solid-state UV-visible absorption spectrum

To characterize the photophysical properties of this new phase C_6' DCM, UV-visible absorption spectroscopy measurement was conducted (Figure III-38).

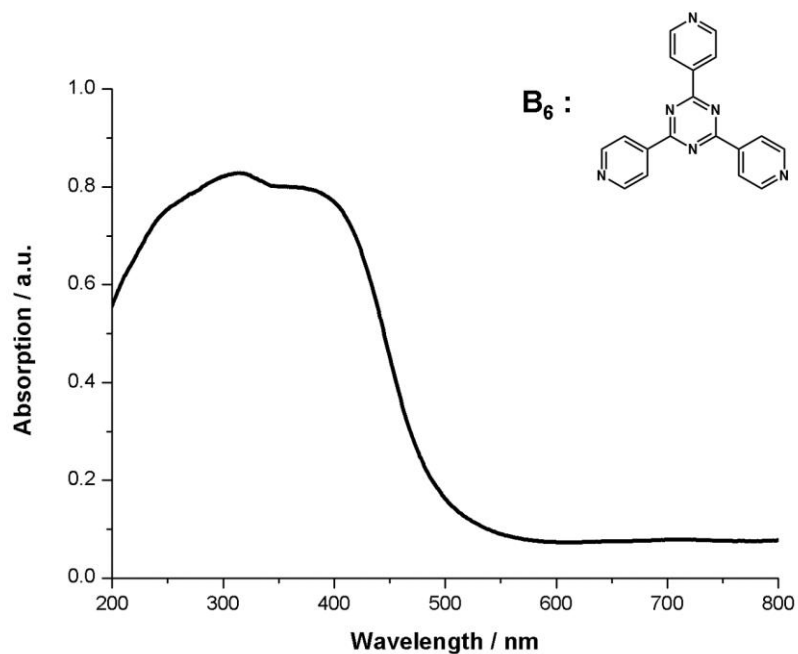


Figure III-38 : Solid-state UV-visible absorption spectrum of C_6' DCM.

It can be observed that the absorption spectrum of the treated phase is a large band centered at *ca.* 300 nm. Therefore, when comparing the absorption spectra of both the initial polymer C_6 and the treated phase C_6' _{DCM}, a high similarity can be observed (Figure III-39). The comparison of both these absorption spectra to the absorption spectrum of the transitioned phase C_6' reveals the absence of exacerbated maximas of absorption at *ca.* 300 and 400 nm and absorption bands that are blue shifted, starting at *ca.* 500 nm.

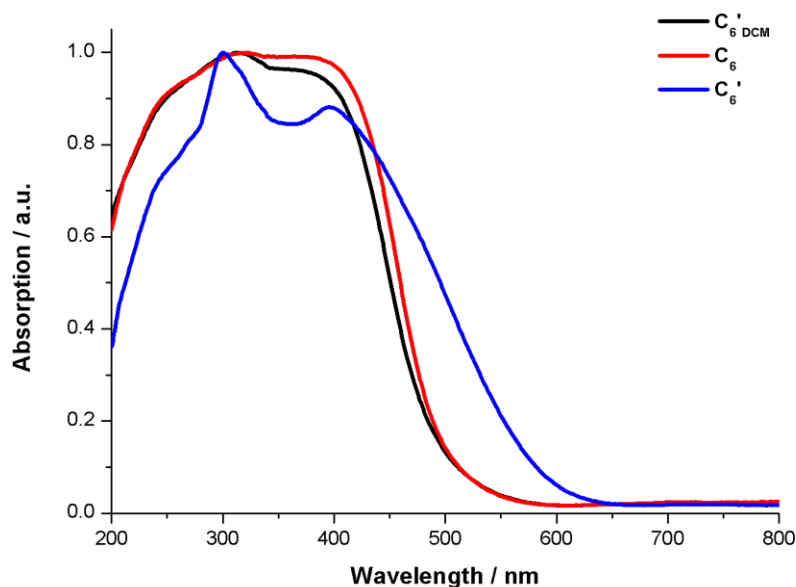


Figure III-39 : Comparison between the normalized solid-state UV-visible absorption spectra of C_6' _{DCM} (black), C_6 (red) and C_6' (blue).

III-3.c.ii Luminescence properties of the C_6' _{DCM} phase

The photophysical properties of C_6' _{DCM} have been studied in detail and compared in particular with the luminescent properties of the initial polymer C_6 . Its RT emission spectrum presents a large featureless band centered around 585 nm with a FWHM of 154 nm, similar to the emission of the initial C_6 polymer. During the measurement of the temperature dependence of the emission of C_6' _{DCM}, an increase of the emission intensity upon cooling was observed, similar to the behavior of C_6 . However, unlike the hypsochromic behavior observed for C_6 , no clear shift in the emission maximum was observed when cooling the sample, and at 80 K, the emission was still characterized by a large featureless band centered at *ca.* 585 nm, with a FWHM of 141 nm (Figure III-40).

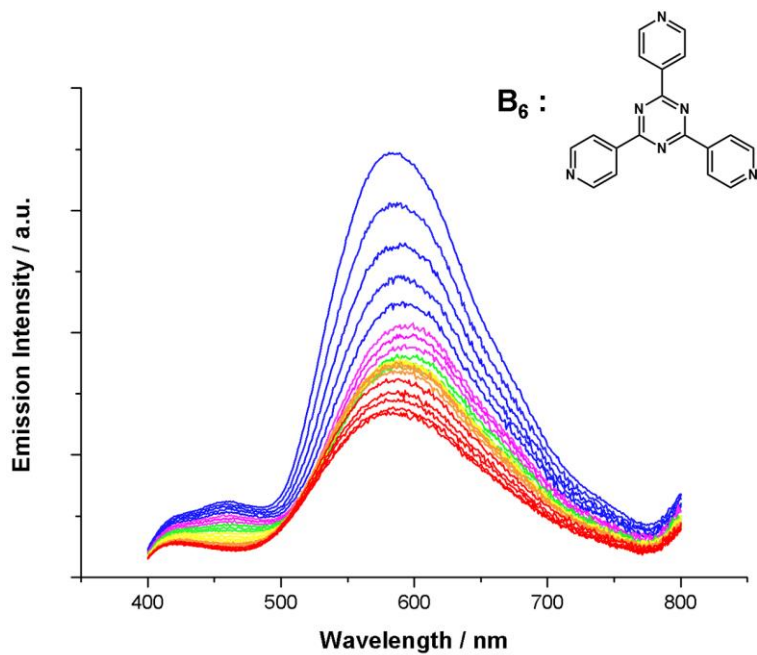


Figure III-40 : Temperature dependence of the emission spectrum of the C₆'DCM phase from 300 K to 80 K.

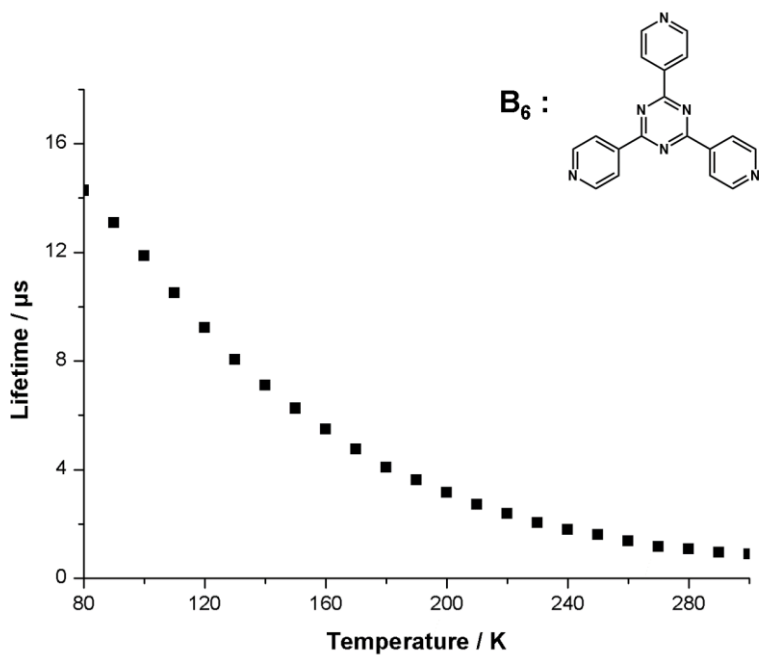


Figure III-41 : Variation of the lifetime depending on the temperature of compound C₆'DCM from 300 K to 80 K.

The temperature variation of the lifetime of the excited state of the C₆'DCM from 300 K to 80 K was measured (Figure III-41). The lifetime of the excited state at RT in the solid-state of C₆'DCM is measured to be 0.8 μs. A gradual increase of the lifetime of the excited state is observed upon

cooling, leading to a measured lifetime of 14 μs at 80 K. These measured values, and the behavior upon cooling with an observed gradual increase, are highly similar to the behavior displayed by the initial polymer C_6 ($\tau_{(300\text{ K})} = 18.3\ \mu\text{s}$, $\tau_{(80\text{ K})} = 0.5\ \mu\text{s}$, Figure II-20).

The RT solid-state quantum yield, is measured to be 15 % in the phase $\text{C}_6'\text{DCM}$, comparable to the emission quantum yield in the same conditions for the initial polymer C_6 .

In the same vein, the solid-state luminance of the treated phase $\text{C}_6'\text{DCM}$ is found to be 16 Cd/m^2 under an irradiance of 3.5 W/m^2 . This is highly similar to the luminance of the initial polymer C_6 under the same irradiance. During the measurement of the evolution of the luminance depending of the irradiance, a similar behavior was observed between both compounds C_6 and $\text{C}_6'\text{DCM}$, with a linear increase of the luminance (Figure III-42).

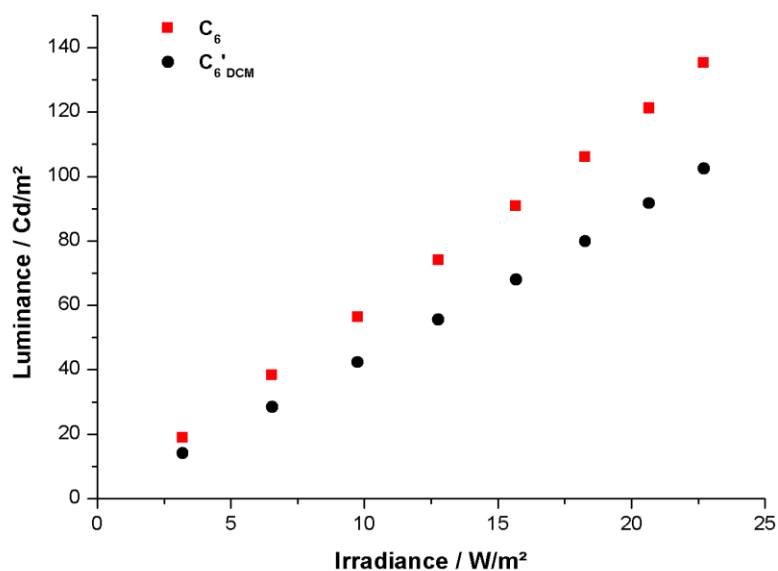


Figure III-42 : Variation of the luminance of phases C_6 and $\text{C}_6'\text{DCM}$ depending on the irradiance.

These measurements reveal a clear analogy between the photophysics of the phases C_6 and $\text{C}_6'\text{DCM}$ suggesting that the regenerated phase $\text{C}_6'\text{DCM}$ presents a very similar molecular architecture and electronic structure than its original phase C_6 .

III-3.c.iii Thermal behavior of the C₆'_{DCM} phase

Lastly, TGA-DTA analysis on the treated phase C₆'_{DCM} was conducted to assess the recyclability of the transition/regeneration process. Indeed, if the treated phase is similar to the initial polymer, then the irreversible thermal transition should be observed upon heating in the solid-state, characterized by an exothermic peak observed in the TGA-DTA measurement. The same thermal treatment was therefore applied to C₆'_{DCM}, with a heating to 270 °C followed by a return to room temperature. (Figure III-43).

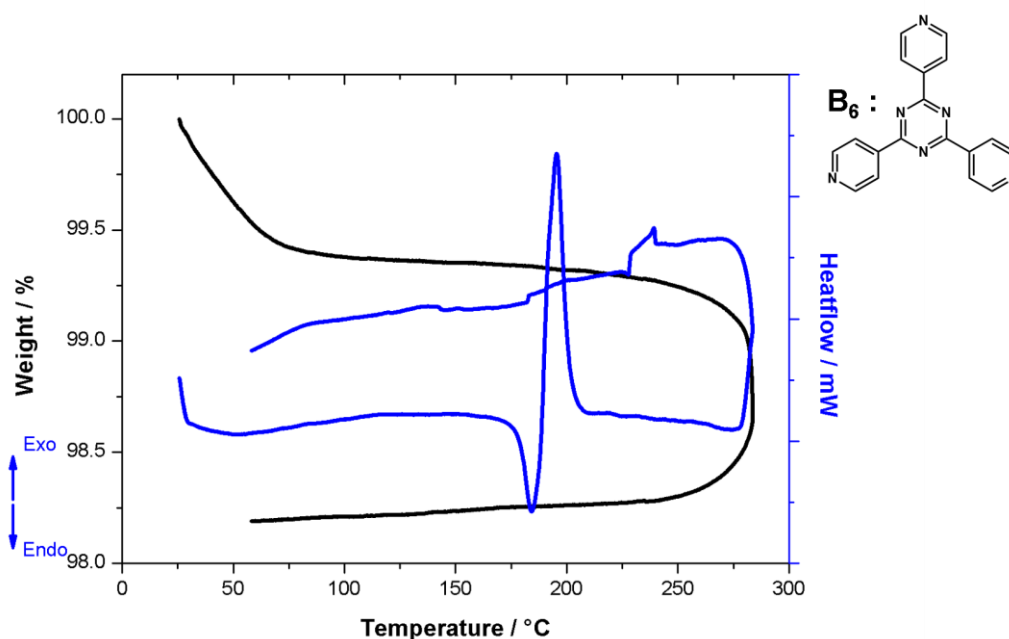


Figure III-43 : TGA-DTA analysis of C₆'_{DCM} under a nitrogen flux, up to 270 °C and with the record of the return to room temperature.

Indeed, a similar exothermic peak can be observed in the TGA-DTA analysis of C₆'_{DCM}, present at 195 °C, and not accompanied by a loss of mass. This thermal behavior is very reminiscent of the thermal response of the initial polymer C₆, occurring at 190 °C. During the return to room temperature, no thermal events can be observed, which indicates an irreversible thermal transition.

After this TGA-DTA measurement, the sample under UV-light ($\lambda_{\text{ex}} = 365 \text{ nm}$) emits an intense eye-perceived blue luminescence, markedly different to the light orange emission displayed after treatment by dichloromethane, and similar to the blue luminescence of the thermally transitioned compound C₆'.

This observation support the idea that this process is circular and that it is possible to alternate between light orange luminescent initial and regenerated phases and irreversible thermally transited blue luminescent phases. This process doesn't seem to induce noticeable changes in the properties of both phases, with the exception of a moderate structural amorphisation due to the heating process and the dichlorometane regenerating treatment.

III-4 Conclusion on the irreversible thermal transition of the polymers C_n

A drastic change in the luminescent properties of the one-dimensional coordination polymers C_n can be observed with the naked eyes as they are heated in the solid-state and returned to RT, occurring along an irreversible thermal transition. Powder X-ray diffraction and infrared spectrum analysis let to conclude that all transited compounds C_n' display a similar structural rearrangement, highly analogous to the structural rearrangement found in the transited precursor A' . This is especially observed in the infrared spectrum where the $\nu_{(CN)}$ vibration band of the cyanide fragment, present in the tetrametallic metallacycle backbone, is observed at the exact same value of 2127 cm^{-1} across the entirety of transited compounds.

The analysis of the photophysical properties of the thermally transited phases C_n' revealed also clear similarities with the transited precursor A' . The eye-perceived blue luminescence displayed at room temperature is characterized for all of them by a large band in the emission spectrum centered at 454 nm, similar to both the transited phase A' and precursor A . Upon cooling to the temperature of liquid nitrogen, a bathochromic shift is observed, and at 80 K the emission is characterized by a large band centered around 495 nm. This value is found across the series of transited C_n' compounds and is similar to the value measured for A' transited precursor. The decay times also present a clear difference in the transited phases compared with the coordination polymers C_n , with similar values across the serie of *ca.* 40 μs at RT, with a steady increase upon cooling to reaching *ca.* 250 μs at 80 K. Similarly, the photophysical properties are characterized by an increase in the emission quantum yield in the solid-state at room temperature across all transited phases C_n' . This change in the emission quantum yield is finally reflected in luminance measurements with clearly increased values under similar irradiance compared to the initial polymers C_n .

Therefore with this study, an original process is highlighted, revealing that these Cu(I) 1D-CPs C_n present the unique ability of drastically changing their luminescence properties due to an exothermic phase transition in the solid-state at a temperature significantly above the room

temperature. This might be due to the supramolecular architecture of these 1D-CPs alternating tetrametallic metallacycles building blocks and polytopic linkers. The high flexibility of the Cu(I) coordination sphere is certainly a key factor to allow such process in which, moreover, the high variety of photophysical properties of Cu(I) based derivatives confer to this transition attractive luminescence behavior. This gives access to a new class of multifunctional luminescent materials that can potentially probe the thermal history of their environment.¹

An in depth study of the phase **C₆'** revealed that it is constituted of an intimate mixture of the uncoordinated linker **B₆** and the tetrametallic metallacycle and it was showed that it is possible to « regenerate » the initial polymer **C₆**, along with its initial orange luminescence from the irreversible thermally transitioned phase **C₆'** by exposure to a minimal amount of drops of dichloromethane. It can be noted that it is also possible to obtain a seemingly similar regenerative process from exposure to vapors of the same solvent, with a similar return to a yellow colored polycrystalline powder emitting an eye-perceived orange luminescence.

The regenerated phase **C₆'_{DCM}** was also characterized by infrared spectrum and powder X-ray diffraction. It was found that this regenerated phase presents mostly a similar molecular structure to that of the initial 1D coordination polymer **C₆**. The photoluminescence properties of the treated phase were studied and revealed very close, with some minutes differences, luminescence properties when compared to the one displayed by the **C₆** compound, with similar luminescence at room temperature as well as similar behavior upon cooling to 80 K. The measurements of the emission quantum yield in the solid-state at room temperature and the luminance revealed values in close range to the one displayed by the initial polymer **C₆**. Finally, the study of the thermal behavior of the regenerated phase revealed the presence of a similar exothermic irreversible transition in the regenerated phase to that of the initial polymer. This result is particularly interesting since it reveals the possibility of recyclability of the process, where the compound **C₆** can undergo an irreversible thermal transition to become the blue luminescent phase **C₆'**, with the possibility of a regeneration of the initial phase from exposure to minimal amount of solvent (Figure III-44).

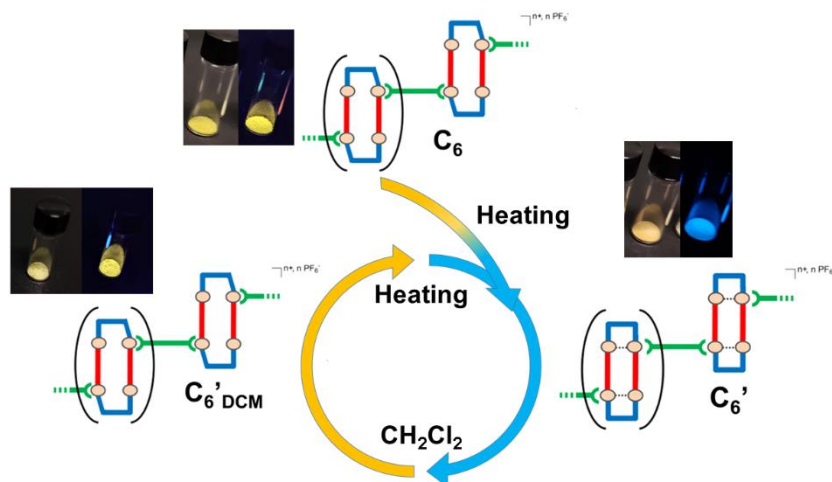


Figure III-44 : Diagram of the circular process behind the thermal transition found in C_6 .

Notably, a similar process should also take place with the phase C_5' but preliminary experiments have displayed unclear results, suggesting that the initial phase C_5 is not regenerated in the $C_5'_{DCM}$ phase but rather another new phase presenting significantly different photophysical properties. This requests further experiments to be conducted in order to succeed rationalize the phenomenon observed.

References of chapter III :

1. Lescop, C. POLYMER DE COORDINATION D'UN PRECURSEUR A BASE D'IONS CU(I). EP3820929A1, 2020.

Chapter IV Toward the obtention of alternative self-assembled luminescent Cu(I) multimetallic species

It has been possible to obtain a number of one-dimensional Cu(I) based coordination polymers that display photophysical properties in the solid-state with diverse radiative relaxation processes and luminescent colors of emission spanning the entirety of the visible spectrum from the precursor **A**.

Moreover, these coordination polymers exhibit an intriguing irreversible thermal transition. Indeed, once the polymers were heated in the solid-state up to *ca.* 200 °C and allowed to cool down to room temperature, an irreversible change to the luminescent properties is observed. The change of the luminescent specific color of emission of the polymers to an eye-perceived blue emission of the precursor **A** occurs during this irreversible thermal transition.

This thermal transition and the change in observed luminescent properties in the obtained phases open the way toward application as luminescent markers targeting temperature sensitive applications. However, a restriction to a use of these derivatives in all day life applications is present in the core of the polymers with the presence of the cyanide linker within the tetrametallic metallacycles subunits.

Cyanide is a compound found in nature, produced by a number of plants species as a mean of antifeeding strategy. It is also present in prussian blue, an historical blue pigment, with a $[\text{Fe}_4^{\text{III}}(\text{Fe}^{\text{II}}(\text{CN})_6)_3]$ composition.¹ It is an important ditopic linker, used in a number of different coordination compounds.^{2,3,4,5,6}

However, cyanide is also a poison and a great source of pollution in air as well as in water. Its use in the gold and silver mining industry as a way to separate the metal from the raw rocks exposes workers to large amounts of cyanide⁷ and it has led to disastrous industrial spills that destroyed entire rivers' fish population. It can also be found in more common applications in the gases emitted by the exhaust of cars, contributing to the worsening of air quality in metropolitan areas.⁸

Finally, its presence in manufactured objects can lead to the release of highly hazardous hydrogen cyanide gas in the event of a fire. All the dangerous aspects of cyanide, whether be it

ecologically or toward health, lead to it being phased out of most concrete applications and industrial processes.

Our interest in this part was to study the feasibility of obtaining a new series of luminescent 1D coordination compounds that would exhibit a similar irreversible thermal transition impacting the luminescence properties similarly to that of the coordination polymers previously studied, but without the presence of cyanide fragment at their core.

The first attempt undertaken for this prospect was to study the reactivity of the bimetallic core $[\text{Cu}_2(\mu_2\text{-dppm})_2]^{2+}$ itself with ditopic linkers other than cyanide. The idea was to keep using pyridyl-terminated organic ligands such as the linkers \mathbf{B}_n already presented earlier in this PhD thesis. In this context, a serendipity result was obtained with the use of the 3,3'-bipyridine \mathbf{B}_3 linker, due to the propensity of the 3-pyridyl site to form discrete supramolecular assemblies.^{9,10,11,12}

IV-1 Synthesis and structural characterization of the metallacycles \mathbf{D}_x ¹³

The first experiment conducted in this context was to react directly the $[\text{Cu}_2(\mu_2\text{-dppm})_2]^{2+}$ precursor to the linker \mathbf{B}_3 targeting the synthesis of a 1D coordination polymer. The pre-assembled Cu(I) precursor was first prepared in solution by dissolving stoichiometric amount of $[\text{Cu}(\text{CH}_3\text{CN})_4] \text{PF}_6$ and bis(diphenylphosphino)methane (dppm) under stirring at room temperature, under air, in dichloromethane. After one hour, time given to allow the $[\text{Cu}_2(\mu_2\text{-dppm})_2]^{2+}$ precursor to be formed *in-situ*, the linker \mathbf{B}_3 was added, dissolved in dichloromethane (Figure IV-1).

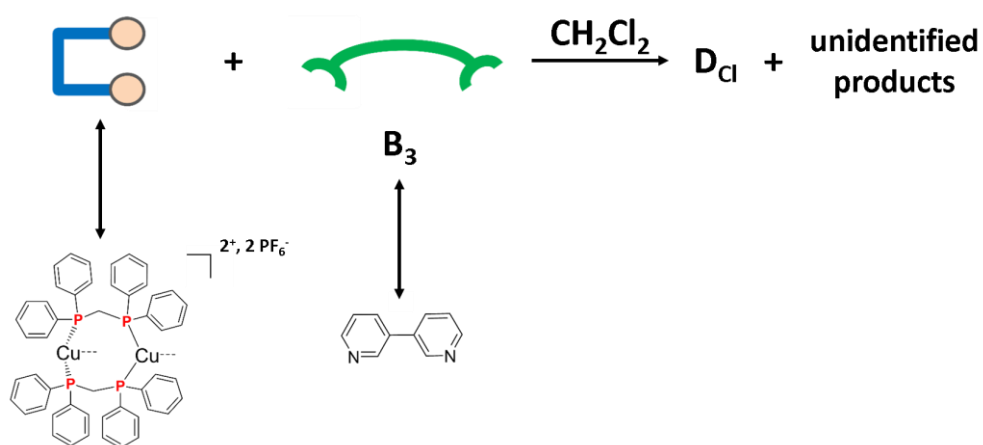


Figure IV-1 : Synthesis diagram of the reaction between the $[\text{Cu}_2(\mu_2\text{-dppm})_2]^{2+}$ dimeric unit, 3,3' bipyridine \mathbf{B}_3 linker.

A colorless clear solution was obtained, which was then put to crystallize by slow pentane vapor diffusion. After few days, several kind of polycrystalline species were present in the solution, displaying under UV light excitation ($\lambda_{\text{ex}} = 365 \text{ nm}$) various eye-perceived colors of emission, ranging from light blue to yellow.

From this batch, it was not possible to determine the crystal structure of any of the species formed, due to poor quality of the crystals and it was also not possible to manually separate the different species due to rapid collapse of the crystals into polycrystalline powder once taken out of the solution.

However, a few weeks after this initial set of polycrystalline species appeared, few crystals of another species, bearing eye-perceived light blue luminescent under UV light ($\lambda_{\text{ex}} = 365 \text{ nm}$), began forming in the crystallisation experiment. Single crystal X-ray diffraction experiment were able to be conducted on this new compound, denominated **D_{Cl}**. This measurement revealed that **D_{Cl}** crystallizes in the triclinic P-1 space group, with an asymmetric unit which contains half of the discrete supramolecular assembly **D_{Cl}**, one hexafluorophosphate PF_6^- counter anion and five dichloromethane solvent molecules. The structure of **D_{Cl}** compound (Figure IV-2) consists of a centrosymmetric tetrametallic metallacycle formed by two dimeric units $[\text{Cu}_2(\mu_2\text{-dppm})_2(\mu_2\text{-Cl})]^+$ that are linked together *via* the coordination to two linkers **B₃**. The two Cu(I) ions of each dimeric units share a similar $\text{P}_2\text{Cl}_1\text{N}_1$ tetrahedral distorted coordination sphere. The intermetallic distance found in the dimeric units is quite large at $d(\text{Cu-Cu}) = 3.179(7) \text{ \AA}$, clearly above the upper limit commonly accepted for cuprophilic interactions to take place (Figure IV-2).^{14,15}

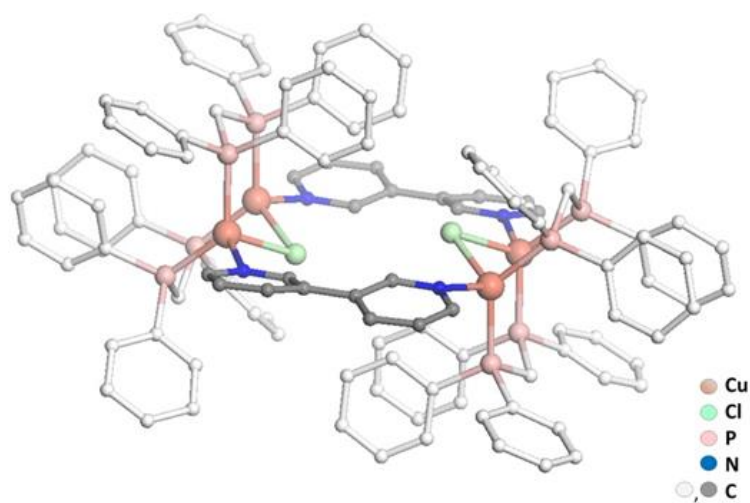


Figure IV-2 : Molecular structure of **D_{Cl}** obtained via single-crystal X-ray diffraction (hydrogen atoms, counter-anion PF_6^- and included solvent molecules have been omitted for clarity).

The two binding μ_2 -chloro ligands are located within the ring defined by the copper atoms of the metallacycle, directed toward the center but outside of the mean plane by 0.753 Å. The distance between the two chlorine atoms is 4.55 Å. The 3,3' bipyridine linkers **B**₃ are coordinated in a cisoid and symmetrical manner to the dimeric units, with similar Cu-Cu-N angles as well as identical Cu-N bond lengths (Table IV-1). The Cu-N bond length is observed in **D**_{Cl} to be 2.121(3) Å, a value close to the similar Cu-N bond length value of 2.181(3) Å observed in polymer **C**₃, and higher than the Cu-N bond length of 2.034(3) Å found in a previously reported 2D network of Cu₂I₂ units linked by **B**₃.^{16,17} The torsion angle between the 6-membered rings of **B**₃ is found to be 17.1°, much smaller than the value of 42.1° for the polymer **C**₃ or 43.5° found in the reported Cu₂I₂ 2D network. This small torsion angle highlights the steric constraints that are applied to the linker **B**₃ due to its coordination within the tetrametallic metallacycle unit of **D**_{Cl}.

The bridging μ_2 -chloro ligand's origin is hypothesized to come from abstraction of the dichloromethane CH₂Cl₂ solvent used during the reaction, with similar examples having been previously reported.^{18,19,20,21,22} Due to the long time required for the obtention of crystals of **D**_{Cl} it seems that equilibria between several species occur in solution. With this in mind, it seems possible to introduce on purpose a μ_2 -chloro ligand on the initial dimeric unit [Cu₂(μ_2 -dppm)₂]²⁺, leading to the formation of μ_2 -Cl bridged dimeric units, and paving the way toward a more selective self-association reaction with linker **B**₃.

To assess this theory, a new synthesis was tried, where a CH₂Cl₂ solution of two equivalents of dppm ligand, one equivalent of [Cu(CH₃CN)₄]PF₆ and one equivalent of CuCl was prepared and left upon stirring at room temperature, under air for one hour. This afforded a clear, colorless solution to which was added one equivalent of linker **B**₃ dissolved in CH₂Cl₂, leading to the obtention of slightly yellow clear solution. This solution was left under stirring at room temperature overnight and was then left to crystallize under air at room temperature under slow pentane vapor diffusion. After few days, a batch of homogeneous crystals formed from the solution and were confirmed to be crystals of **D**_{Cl} from single crystal X-ray diffraction experiments. This batch of crystals were filtered off from the solution and after drying under air, afforded a homogeneous sample of block-shaped colorless polycrystalline solid **D**_{Cl} with a yield of 66 %.

This confirmed the hypothesis that the presence of chloride anions with the CuCl reagent in the crude solution enables the formation *in-situ* of the dimeric unit [Cu₂(μ_2 -dppm)₂(μ_2 -Cl)]⁺, acting as a precursor in the reaction with linker **B**₃. This in turn, permits to avoid the slow unselective

process encountered during the initial reaction, with the slow formation of competing species, followed by the late formation of the **D_{Cl}** metallacycle in a very low yield. This new reaction procedure enables the obtention of the **D_{Cl}** compound directly and selectively in high yield.

Additionally, this approach may allow for the use of other halogens in place of the μ_2 -chloro bridging ligand. Similar syntheses were therefore conducted, replacing the CuCl reagent by CuBr and CuI. Following the same crystallization conditions, these reactions led to the formation of homogeneous batch of colorless crystals, denominated respectively **D_{Br}** and **D_I**. The obtained crystals were of suitable quality to conduct single crystal X-ray diffraction experiments, revealing that **D_{Br}** and **D_I** are isostructural to **D_{Cl}**, where two bimetallic units $[\text{Cu}_2(\mu_2\text{-dppm})_2(\mu_2\text{-X})]^+$ are linked together in a tetrametallic metallacycle *via* two linkers **B₃** (Figure IV-3).

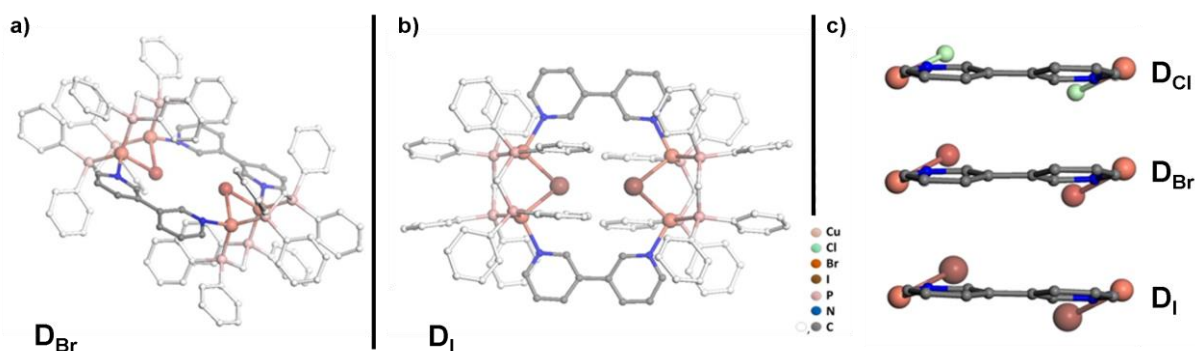


Figure IV-3 : a) Sideway view of the molecular structure of **D_{Br}** ; b) Top view of the molecular structure of **D_I** ; c) Side view of the three obtained metallacycles **D_x**.

The change of halide atom used during the reaction led to an increase of the intermetallic distance inside the dimeric units of the obtained assemblies, following the increase of atomic radius of the halide atom : **D_{Cl}** : 3.179(7) Å < **D_{Br}** : 3.261(8) Å < **D_I** : 3.362(7) Å. Concerning the rest of the metallacycle, the other values observed in the tetrametallic metallacycles **D_x** are highly similar, with a conservation of the μ_2 -symmetry of the bridging coordination halide atom, as well as its deviation from the mean plane of the metallacycle being in the same range across the series. The length of the Cu-N coordination bond to the linker **B₃** as well as the Cu-Cu-N angle are also found to be of similar values when compared to the initial compound **D_{Cl}**. The only metric showing a significant evolution is the torsion angle between the rings of the **B₃** linker, displaying a flattening of the linker across the series, from 17.1° in the initially obtained **D_{Cl}**, to 15.9° in **D_{Br}**, and to 9.8° in **D_I**, leading to a significant planarity of the linker (Table IV-1).

Distances	D _{Cl}	D _{Br}	D _I
Cu-Cu (Å)	3.180(4)	3.261(5)	3.362(5)
Cu-N (Å)	2.121(3)	2.109(4)	2.119(6)
	2.121(3)	2.121(5)	2.124(5)
Cu-X (Å)	2.4034(12)	2.5218(11)	2.6646(11)
	2.4048(11)	2.5211(10)	2.6636(12)
Cu-P (Å)	2.2687(10)	2.2682(15)	2.2474(17)
	2.2569(10)	2.2567(14)	2.2576(16)
	2.2604(11)	2.2595(16)	2.2549(19)
	2.2527(11)	2.2546(16)	2.2539(19)
Cu-Cu-N (°)	150.25(3)	150.76(5)	151.51(5)
	150.37(4)	150.27(6)	151.15(5)
Cu-X-Cu (°)	82.80(3)	80.58(2)	78.24(3)

Table IV-1 : Measurements of selected distances and angles in **D_x** metallacycles.

Interestingly, the nature of the halide atoms used in the reaction seems to have influenced mainly on the intermetallic Cu(I) distances, as well as the conformation of the two **B₃** linkers, with the other parts of the molecular structure being highly similar.

The tetrametallic metallacycles **D_x** were also characterized by infrared spectroscopy. Their infrared spectra are highly similar, with the strongest band, located at 832 cm⁻¹, being attributed to the t_{1u} band of the hexafluorophosphate PF₆⁻ counter anion present in the structure and bands attributed to the dppm ligand backbone, at 1484, 1434, 737 and 690 cm⁻¹. The IR measurement conducted afforded infrared spectra that are actually similar to the one observed from the compounds **C₃**, except for the absence of bands around 2000~2200 cm⁻¹, that indicates the presence of CN linker in the **C_n** structure. Moreover, contrary to the polymer **C₃**, bands associated to the coordination of the linker **B₃** are not present in the infrared spectra of compounds **D_x**, being very likely overlapped with the dppm ligand's bands (Figure IV-4 and Figure IV-5).

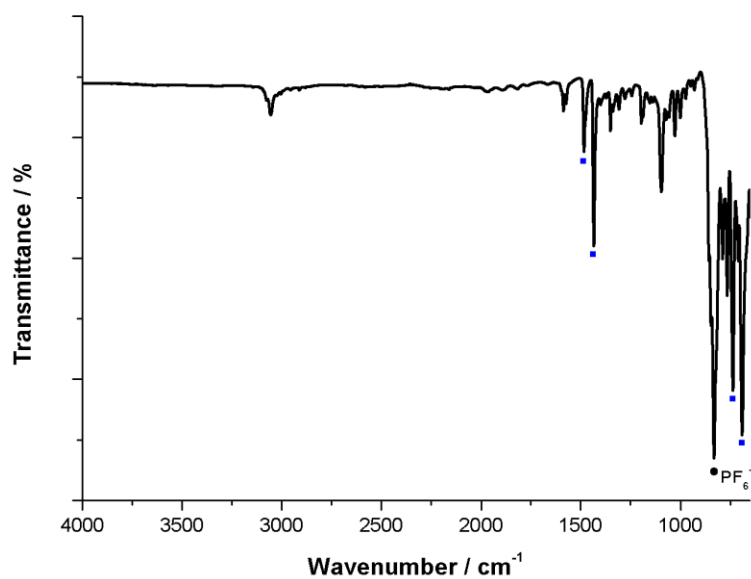


Figure IV-4 : Infrared spectrum of the D_{Cl} metallacycle. The black dot marks the PF_6^- counter anion t_{1u} vibration mode. Blue squares mark dppm ligand bands. The other individual infrared spectra are available in this chapter's appendix.

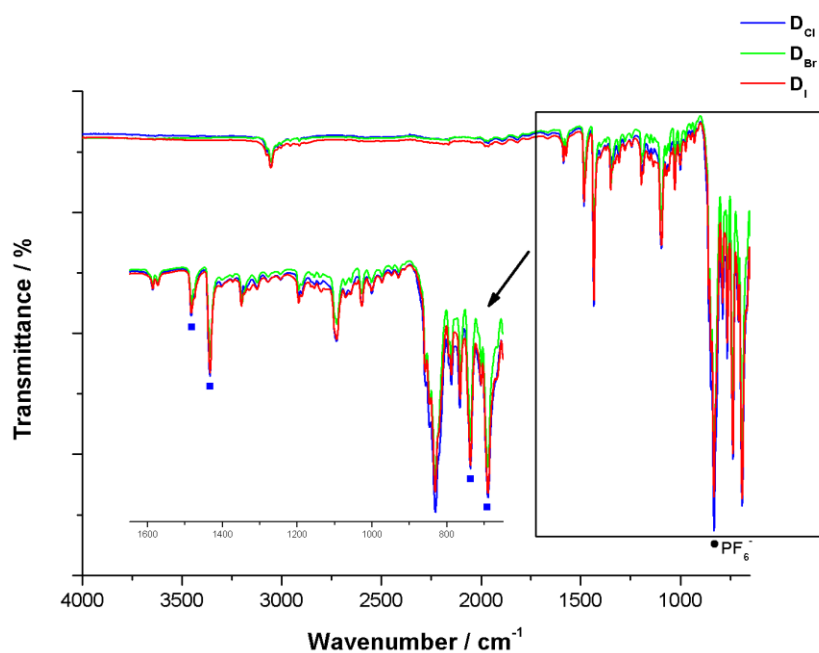


Figure IV-5 : Infrared spectra of the D_x metallacycles, superimposed. The black dot marks the PF_6^- counter-anion t_{1u} vibration mode. Blue squares mark dppm ligand bands.

IV-2 Photophysical measurements of the tetrametallic metallacycles D_x ¹³

IV-2.a Solid-state UV-visible absorption spectrum

The metallacycles D_x (where $X = \text{Cl}, \text{Br}$ or I) are white powders under visible light and emit under UV light irradiation ($\lambda_{\text{ex}} = 365 \text{ nm}$), in the solid-state, at RT, an intense eye-perceived blue-cyan luminescence (Figure IV-6).

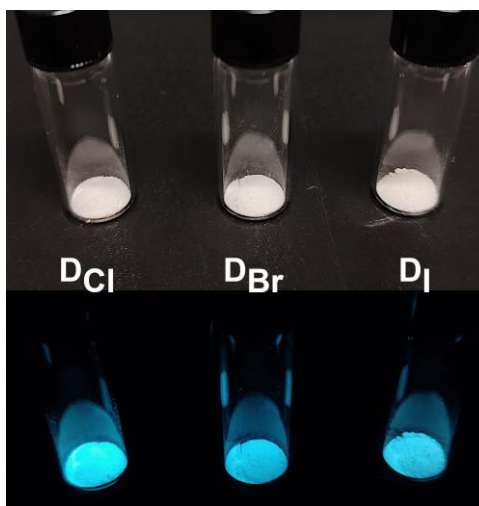


Figure IV-6 : Photography of the tetrametallic metallacycles D_x under visible (top) and UV light ($\lambda_{\text{ex}} = 365 \text{ nm}$) (bottom).

The solid-state RT absorption spectra of the D_x supramolecular assemblies display a broad absorption band in the UV region, with a maximum centered at *ca.* 300 nm (Figure IV-7, absorption spectra of D_{Br} and D_{I} can be found in this chapter's appendix). Such absorption spectra are typical of π - π^* type transition centered on the aromatic rings of the dppm backbone ligand as well as on the B_3 linkers.

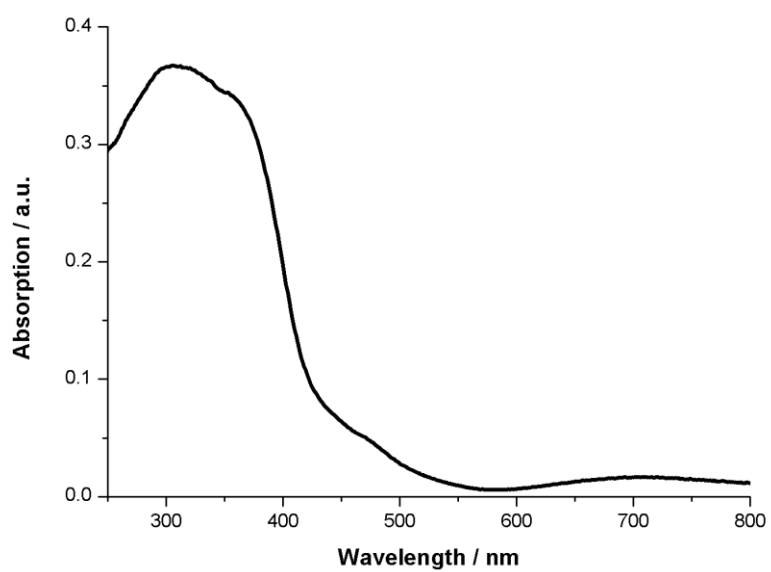


Figure IV-7 : Solid-state RT absorption spectrum of the **D_{Cl}** metallacycle.

IV-2.b Solid-state luminescence of the metallacycles D_x

Two maxima located at *ca.* 325 nm and *ca.* 370 nm can be observed in the solid-state room temperature excitation spectrum of the tetrametallic metallacycles compounds **D_x** (Figure IV-8).

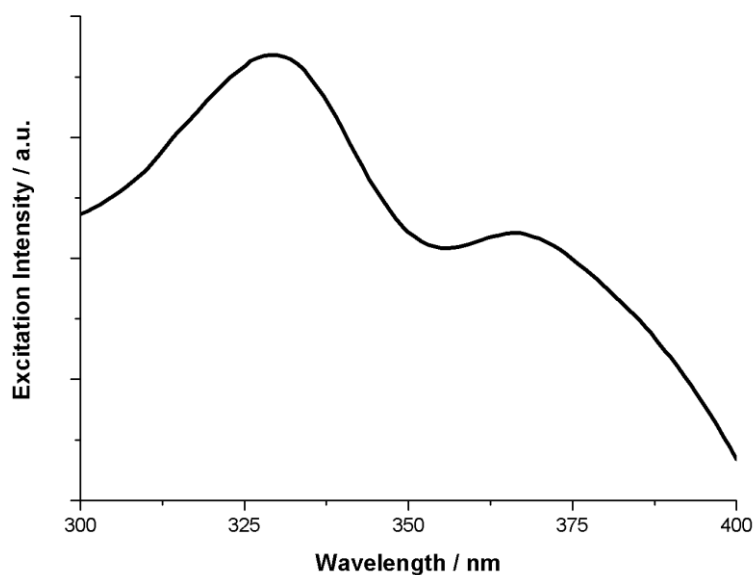


Figure IV-8 : Solid-state room temperature excitation spectrum of the **D_{Cl}** metallacycle.

The emission spectra of **D_{Cl}**, **D_{Br}** and **D_I** are characterized in the solid-state at room temperature by broad featureless bands centered around 475, 476 and 464 nm respectively, with large FWHM values of 105, 116 and 100 nm across the series. Their room temperature, solid-state excited state lifetimes are 74, 119 and 70 μ s respectively, which are accompanied by RT solid-state emission quantum yields (EQYs) values of 80, 60 and 54 %, respectively for **D_{Cl}**, **D_{Br}** and **D_I**. The values of RT solid-state EQY found for the **D_x** are quite high for compounds exhibiting such long lifetimes of several tenths of microseconds. This kind of excited state lifetime values indicates a triplet origin for the luminescence. Another point worth mentioning is the fact that the EQY of the obtained metallacycles follow a downward trend with the increase of the atomic number of the bridging μ_2 -halide ligand, going against the general behavior observed in Cu(I)-halide derivatives with more efficient radiative relaxation processes due to the heavy-atom effect.

To gain a better understanding of the photophysical processes observed in the **D_x** tetrametallic metallacycles, a study of their temperature dependant response of their photophysical properties, from 300 to 80 K was conducted.

During the cooling process, a net increase of the intensity of emission from **D_{Cl}** can be observed, along with a progressive red-shift of the large band. This behavior is completed by a gradual structuration of the emission band, leading to the apparition at 80 K of a vibronic substructure

centered at 432 and 484 nm. The highest intensity is attained at 484 nm. This emission band is completed by the presence of three shoulders located at 452, 465 and 502 nm (Figure IV-9).

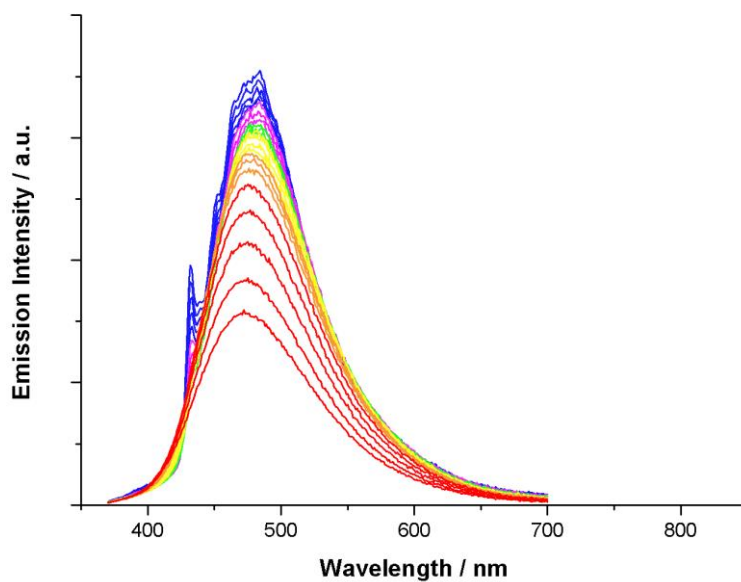


Figure IV-9 : Temperature dependence of the solid-state emission spectra of the **DCl** metallacycle, from 80 to 300 K, upon excitation of 325 nm.

In the temperature variation of the lifetime of the excited state of **DCl**, a continuous increase of the decay time is observed during the cooling process, leading to an excited state lifetime of 4.3 ms at 80 K (Figure IV-10).

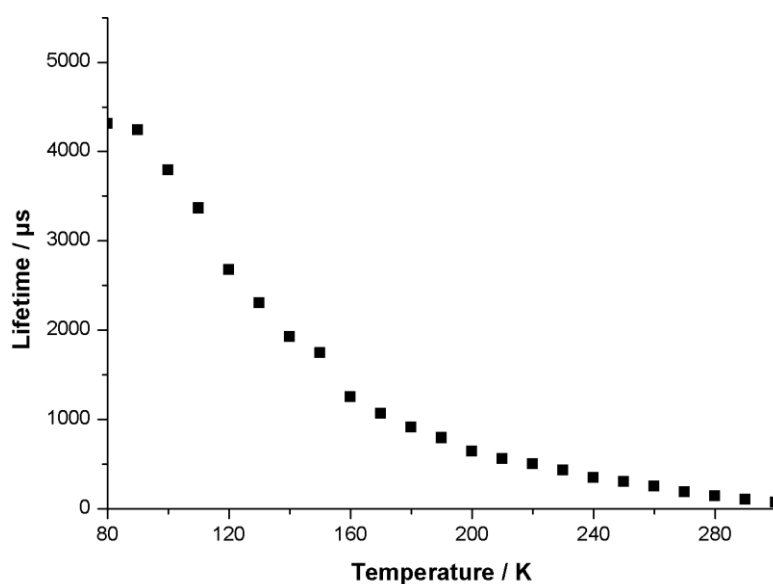


Figure IV-10 : Plot of the emission decay lifetime of the **D_{Cl}** metallacycle against temperature, from 80 to 300 K.

This behavior of the photophysical properties upon cooling observed in **D_{Cl}**, with an increase of the intensity and gradual structuration of the emission band, along with an important increase of the excited state lifetime upon reaching 80 K is also observed in the other two metallacycles **D_{Br}** and **D_I** (Figure IV-11, Figure IV-12 and Table IV-2).

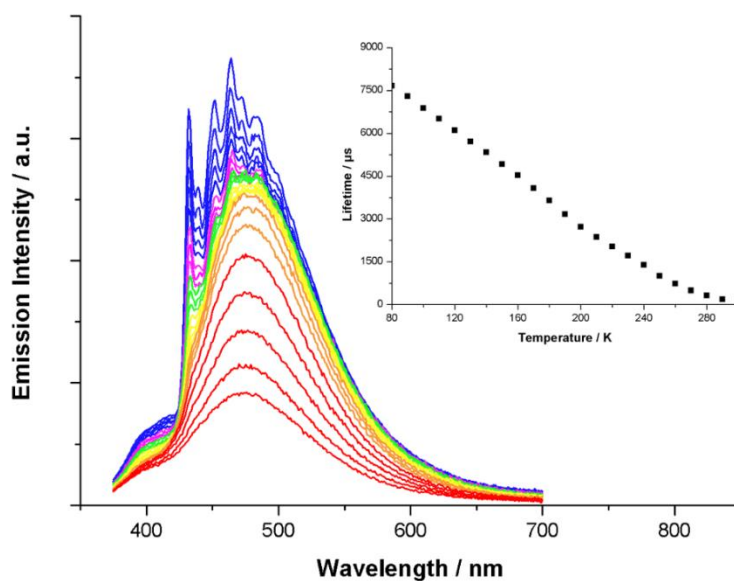


Figure IV-11 : Temperature dependence of the solid-state emission spectra of **D_{Br}** from 80 to 300 K, upon excitation at 325 nm. Inset : plot of the emission decay lifetime against temperature, from 80 to 300 K.

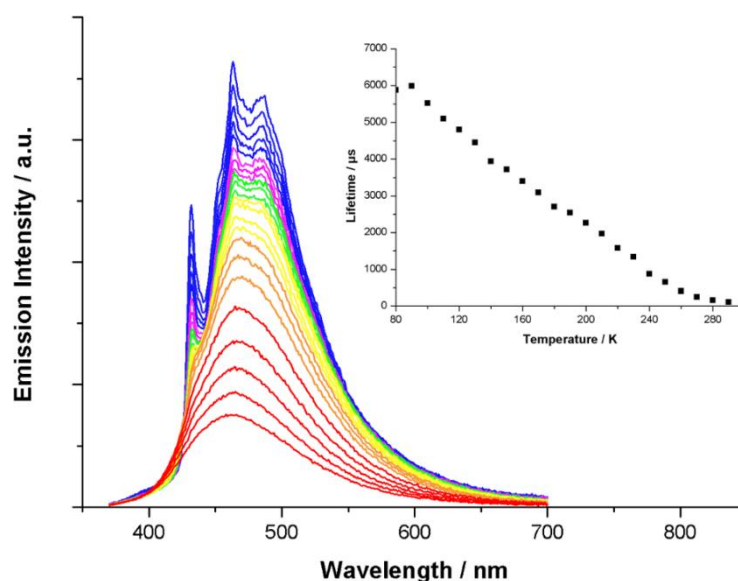


Figure IV-12 : Temperature dependence of the solid-state emission spectra of **D₁** from 80 to 300 K, upon excitation at 325 nm. Insert : plot of the emission decay lifetime against temperature, from 80 to 300 K.

	λ_{em} (nm)	I_{80}/I_{RT}	Φ_{em}	τ_{obs} (μs)	k_r (s^{-1})	k_{nr} (s^{-1})
D_{Cl}	475 (432, 452 ^s , 465 ^s , 484, 502 ^s)	2.3	80	74 (4315)	1.1×10^4	2.7×10^3
D_{Br}	476 (432, 452, 464, 484 ^s , 500 ^s)	4	60	119 (7660)	5.0×10^3	3.4×10^3
D_I	464 (432, 452 ^s , 462, 486, 505 ^s)	4.8	54	70 (5881)	7.7×10^3	6.6×10^3

Table IV-2 : photophysical data ($\lambda_{ex} = 325$ nm) for the **D_x** metallacycles, at 300 K and 80 K, in the solid-state. Values at 80 K are given in parentheses. s designates shoulders, I_{80}/I_{RT} is the intensity at maximum of emission at 80 K divided by the intensity at maximum of emission at 300 K. $k_r = \Phi_{em}/\tau_{obs}$, $k_{nr} = (1-\Phi_{em})/\tau_{obs}$.

It can be noted that a large, weak additional emission band appears during the cooling process at *ca.* 200 K in the emission spectrum of the **D_{Br}** compound between 375 and 425 nm. This emission band is accompanied by a fast decay time of the excited state of 3.5 ns, typical of purely organic fluorescence and therefore is associated with ligand centered residual luminescence. This is confirmed by photophysical measurements conducted on the linker **B₃**, revealing an emission characterized by a large unstructured band centered around 455 nm, accompanied by a decay time of the excited state of 4.5 ns at 80 K.

The values of the recorded emission lifetimes clearly indicate a triplet origin of the luminescence arising from these Cu(I) metallacycles and, together with the general thermal variation of the profiles of the emission spectra, preclude to suggest a TADF process to explain

the overall temperature-dependent data collected for the photophysical properties of these three metallacycles, in spite of the high RT EQY measured.

Regarding specifically the RT photophysical behaviors for this series of metallacycles, the k_r radiative rate constant values are in agreement with a $^3\text{MLCT}$ phosphorescence in which the high temperature large emission bands can be assigned to radiative processes involving likely electronic densities located on the 3,3'-bipyridine ligands **B3**. Yet, the large enhancement of the decay times of the excited states as the temperature decreases, together with the vibronic structuration that appears in the low temperature emission band, suggest at low temperature a $^3\pi\text{-}\pi^*$ phosphorescence centered on the connecting ligands **B3**. Such vibronic structuration is indeed not observed in the thermal variation of related TADF luminescent polymetallic supramolecular assemblies based on the $[\text{Cu}_2(\mu_2\text{-dppm})_2]$ moiety and cyano-based connecting inorganic ligands,^{23,24,25} in which radiative processes mostly rely on transitions from the highest occupied molecular orbitals (HOMOs), being metal-cyano antibonding, to low unoccupied molecular orbitals including the LUMO that presents a mixed metal and ligand character involving the four metal centers of the metallacycle and the dppm ligands. Conversely, in a 1D-coordination polymer based on related $[\text{Cu}_2(\mu_2\text{-dppm})_2(\mu_2\text{-OH}_2)]^{2+}$ dicationic fragments connected by 1,4-dicyanobenzene connecting ditopic ligands,²⁶ a similar progressive structuration of the emission band is observed upon temperature cooling. In the case of this 1D-coordination polymer, the low temperature photophysical properties were assigned to 1,4-dicyanobenzene ligand-centered $^3\pi\text{-}\pi^*$ phosphorescence which supports the activation of such radiative processes in the low temperature luminescence properties of derivatives **DCl**, **DBr** and **DI**. Considering these observations, it is likely that purely ligand-centered $^3\pi\text{-}\pi^*$ phosphorescence occurs at low temperature and tends to vanish at higher temperatures due to a thermally activated interconversion between $^3\pi\text{-}\pi^*$ and $^3\text{MLCT}$ states.^{27,28,29}

Interestingly, it is worth noting that only a minor contribution of the orbital lying on the semi-bridging aqua ligand $\mu_2\text{-OH}_2$ was observed in the electronic excitation process in the previously reported 1D-coordination polymer based on the $[\text{Cu}_2(\mu_2\text{-dppm})_2(\mu_2\text{-OH}_2)]^{2+}$ dicationic unit and the 1,4-dicyanobenzene connecting ditopic ligand.²⁶ Regarding the similarities in the local molecular structures of the Cu(I) dimer in this coordination polymer and the metallacycles reported herein ($[\text{Cu}_2(\mu_2\text{-dppm})_2(\mu_2\text{-OH}_2)]^{2+}$ fragments versus $[\text{Cu}_2(\mu_2\text{-dppm})_2(\mu_2\text{-X}_2)]^+$ moieties, X = Cl, Br, I), a similar electronic structure could explain the relatively low and unusual impact of the variation of the μ_2 -bridging halide atom on the photophysical properties of the metallacycles **DCl**, **DBr** and **DI**. Unfortunately, the computational cost of the full TD-DFT

geometry optimizations of the excited states of the large assemblies **D_{Cl}**, **D_{Br}** and **D_I** studied here, that would allow getting deep insights of the photophysical mechanisms, revealed to be too prohibitive to be conducted along this study. In this context, it is not straightforward to account the origin of the high solid-state RT EQY exhibited by these metallacyclic triplet luminophores. It was previously observed that the overall multicyclic networks built in such Cu(I)-based CDS assemblies clearly induce structural constraints that significantly hamper highly detrimental non-radiative relaxation pathways and structural re-organisation in the excited states. The RT values of the k_{nr} non-radiative rate constants in this series of metallacycles reveals that non-radiative decays are quite small and more effectively suppressed in the case of the lighter bridging halides. This may be related to backbones bearing shorter intermetallic distances. Indeed, in the one hand, this might be responsible of overall lower degrees of conformational flexibilities allowed in the solid-state in more compact and rigid assemblies. In the other hand, shorter intermetallic distances associated with lighter bridging halides also induce higher spin-orbit coupling constants²³ which impact the electronic processes, facilitating radiative de-excitation pathways. This is supported by the higher k_r radiative rate constant values obtained for the μ_2 -Cl bridged derivative **D_{Cl}** (Table IV-2). Therefore, varying the nature of the bridging halides in this family of metallacycles leads to a dual effect, favoring the lighter halide regarding both radiative and non-radiative processes for the exaltation of the solid-state luminescence properties.

Finally, the pronounced planarity observed in the solid-state for the 3,3'-bipyridine ligands **B₃** in **D_{Cl}**, **D_{Br}** and **D_I** reveals that the coordination of these ditopic ligands on the $[\text{Cu}_2(\mu_2\text{-dppm})_2(\mu_2\text{-X})]^+$ units locks their conformation within these self-assembled metallacycles in an arrangement that promotes an efficient overlap of the π -orbitals along the ligands **B₃** quasi-planar backbone. This induces a stabilization of the molecular orbitals located on these 3,3'-bipyridine ligands in **D_{Cl}**, **D_{Br}** and **D_I** and supports the assumption that ³MLCT and ³ILCT phosphorescence radiative relaxation processes occur in these metallacycles being based on molecular orbitals lying at least partially on these connecting ligands **B₃**. Very likely, such conformational constrains applied on the coordinated ligands **B₃** in derivatives **D_{Cl}**, **D_{Br}** and **D_I** contribute to the differences observed between the photophysics of these metallacycles and those of the previously reported luminescent Cu(I) coordination polymer bearing the 3,3'-bipyridine ligands in a twisted conformation.^{16,17} Indeed, in this latter case, it was concluded that the recorded emission could be attributed to the delayed fluorescence from the ¹(M+X)LCT excited state at RT and changed to simple phosphorescence from the same triplet

excited state at 77 K, suggesting radiative relaxation processes involving a larger contribution of molecular orbitals centred on the inorganic part of this derivative.^{16,17}

Therefore, by forcing upon self-assembly processes the 3,3'-bipyridine scaffolds to be almost planar (Figure IV-3c), the radiative relaxations pathways in derivatives **D_{Cl}**, **D_{Br}** and **D_I** are significantly altered compared to the luminescent Cu(I) coordination polymer bearing the 3,3'-bipyridine ligand **B₃** reported previously. This clearly demonstrate, in such Cu(I)-based supramolecular assemblies, the great dependence of the photophysical properties to the molecular engineering applied.

The tetrametallic metallacycles **D_x** are discrete supramolecular assemblies, and thus did not fulfill the original goal of this chapter of obtaining 1D coordination polymers. However, the molecular structure of these derivatives and the exhibited luminescence behaviors proved to be attractive and the study of the thermal stabilities of the metallacycles **D_x** were investigated.

IV-3 Thermal stability study of the **D_x tetrametallic metallacycles**

The thermal stabilities of the tetrametallic metallacycles **D_x** were studied by conducting TGA-DTA measurements. During the measurement, the samples were heated up to 950 °C with a heating ramp of 5 °C/min, under a constant nitrogen atmosphere.

This measurement revealed that the metallacycle **D_{Cl}** is thermally stable up to *ca.* 250 °C where a loss of mass of *ca.* 7 % is occurring along an endothermic event at 265 °C. This loss of mass may be attributed to the decoordination of the **B₃** ligand from the tetrametallic metallacycles, and its subsequent sublimation. This endothermic event is directly followed by another endothermic event occurring at *ca.* 300 °C and accompanied by the loss of 80 % of the total mass of the sample. This large loss of mass can be attributed to the thermal decomposition of the compound leading to the isolation of a black residue, likely composed of inorganic materials. No notable events are occurring at higher temperatures (Figure IV-13).

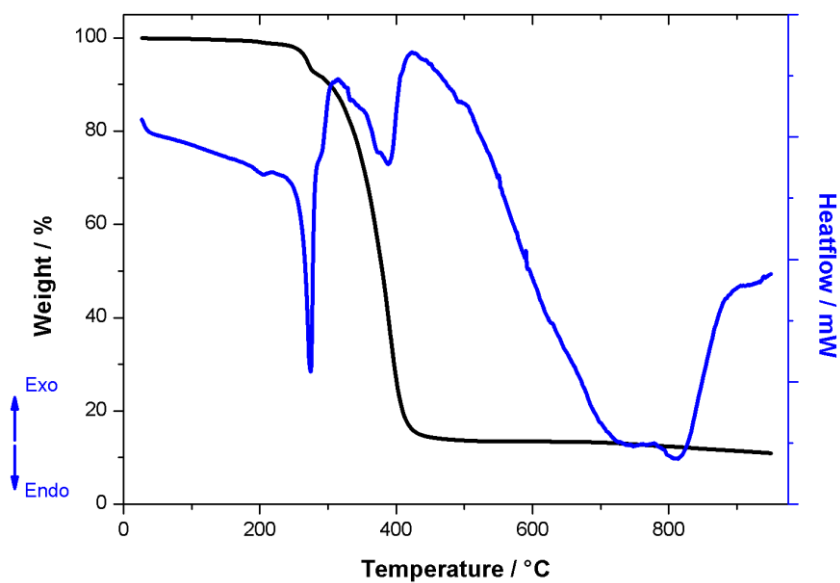


Figure IV-13 : TGA-DTA analysis of \mathbf{D}_{Cl} metallacycle until 950 °C.

This thermal behavior from \mathbf{D}_{Cl} is also observed with the other tetrametallic metallacycles \mathbf{D}_{Br} and \mathbf{D}_I when subjected to a similar heating experiment. A similar initial loss of mass amounting to *ca.* 10 % of the total mass is observed along an endothermic event occurring at 260 °C. This initial event is directly followed by a second endothermic event accompanied by the loss of 80 % of the total mass of the sample (Figure IV-14).

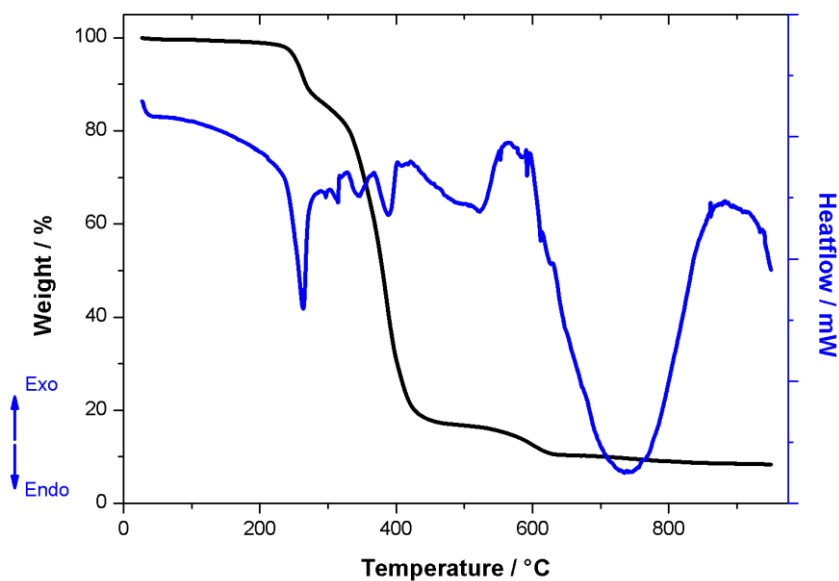
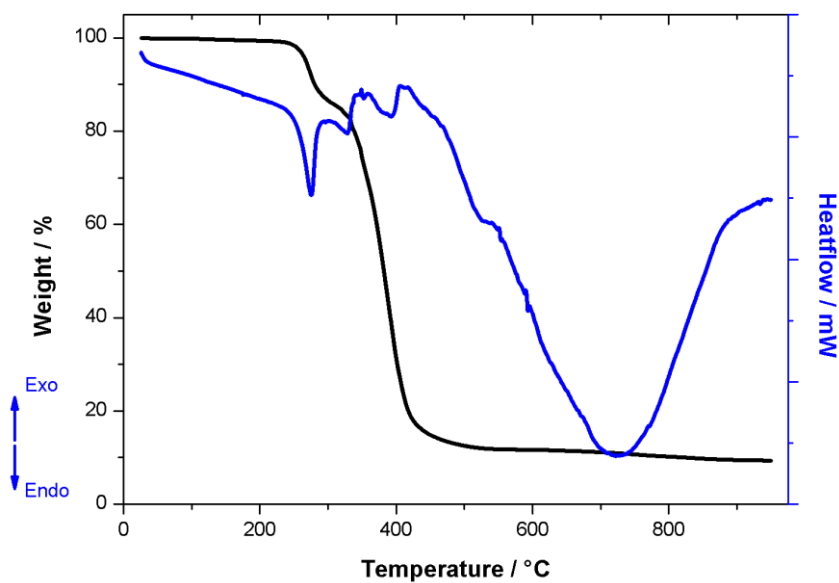


Figure IV-14 : top) TGA-DTA analysis of D_{Br} until 950 °C ; bottom) TGA-DTA analysis of D_f until 950 °C.

It can be observed in the thermal behavior of the tetrametallic metallacycles D_x that no thermal events are found to be occurring before the sublimation of the B_3 linker, hinting at the absence of a thermal transition similar to the one discovered in the studied series of 1D coordination polymers C_n . This is quite not surprising and confirm the importance of the formation of a 1D network to allow the observation of the thermal transition observed in the polymers C_n .

IV-4 Conclusion

In the search toward new supramolecular assemblies displaying a similar irreversible thermal transition to that of 1D coordination polymers C_n , it was possible to obtain a new series of tetrametallic metallacycles D_x .

The incorporation of CuX in the initial reaction mixture leads to the *in-situ* formation of dimeric units $[Cu_2(\mu_2\text{-dppm})_2(\mu_2\text{-X})]^+$ that provides a rigid and directed environment toward the coordination of the B_3 linker.

This novel series of supramolecular assemblies presents an emission in the solid-state at room temperature characterized by an intense, eye-perceived blue-cyan luminescence that was characterized as originating from $^3\text{MLCT}$ phosphorescence centered on the linker and switching to $^3\text{ILCT}$ phosphorescence centered on the linker at low temperature. The planarity of the linker B_3 backbone, associated with the presence of μ_2 -bridging halides atoms allow for high RT EQY to be observed in these derivatives. The thermal stability of the D_x tetrametallic metallacycles revealed that the compounds are stable up to 250 °C where the decoordination and subsequent sublimation of the linker start to occur. The thermal decomposition of the compounds begins at *ca.* 300 °C leading to a complete decomposition of the tetrametallic metallacycles. This measurement revealed that no irreversible thermal transition akin to the one discovered in the 1D coordination polymers C_n is present in this series of metallacycles.

To summarize, the tetrametallic metallacycles D_x required the use of an original synthetic strategy to be obtained selectively and rapidly, and presented photoluminescent properties with high solid-state room temperature quantum yields. However, they do not display an irreversible thermal transition of their photophysical properties reinforcing the idea that a one-dimensional architecture is necessary. In order to gain access to this irreversible thermal transition without the use of cyanide ligand, the use of a different assembling and connecting ligand backbone and the search for a molecular structure different from a Cu(I) tetrametallic metallacycle might be an option to study.

With this in mind, promising results have been obtained by using the tridentate ligand bis(diphenylphosphinomethyl)phenylphosphine (dpmp) allowing the identification of a Cu(I) trimetallic building block $[Cu_3(\mu_2\text{-X})_2(\mu_3\text{-dpmp})_2]^+$ (with X = Cl, Br or I), that can be reacted with a variety of polytopic linkers. For examples with X = Br and the linker B_6 , a 1D coordination polymer have been characterized (Figure IV-15).

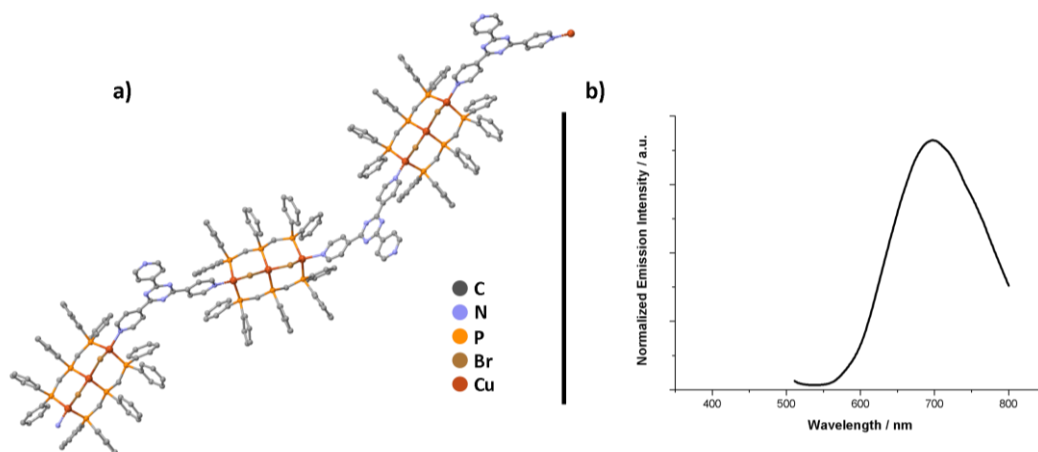


Figure IV-15 : a) View of the molecular structure of the 1D coordination polymer obtained *via* single crystal X-ray diffraction (hydrogen atoms, counter-anions PF_6^- and included solvent molecules have been omitted for clarity). b) Normalized emission spectrum of the $[\text{Cu}_3(\mu_2\text{-X})_2(\mu_3\text{-dpmp})_2]^+$ based 1D coordination polymer in the solid-state at RT ($\lambda_{\text{ex}} = 415 \text{ nm}$).

This 1D coordination polymer is luminescent in the solid-state, emitting an eye-perceived deep red light under UV-visible excitation. Preliminary results has shown that upon heating in the solid-state, this 1D polymer undergoes an irreversible change in its luminescence properties (from deep red to a yellow eye-perceived luminescence) (Figure IV-16), suggesting that the properties of the 1D coordination polymers C_n can be also observed in other 1D coordination polymer assemblies highlighting the generality of this original property.

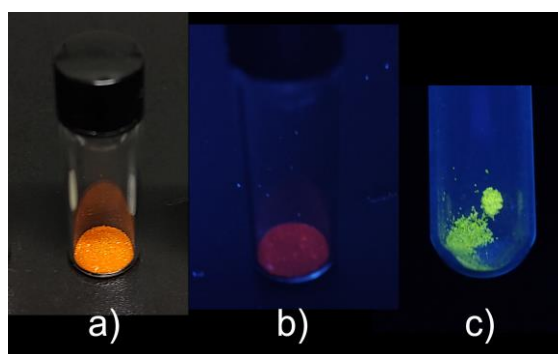


Figure IV-16 : Photographs of the 1D coordination polymer a) as obtained, under visible light ; b) as obtained, under UV light ($\lambda_{\text{ex}} = 365 \text{ nm}$) ; c) After heating, under UV light ($\lambda_{\text{ex}} = 365 \text{ nm}$).

References of chapter IV :

1. Woodward, J., Praeparatio Caeruli Prussiacy Ex Germania Missa ad Johannem Woodward, M.D. Prof. Med. Gresh. R. S. S. *Philos. Trans. R. Soc. London* **1724**, *33*, 15-17.
2. Corain, B., The coordination chemistry of hydrogen cyanide, cyanogen and cyanogen halides. *Coord. Chem. Rev.* **1982**, *47* (1-2), 165-200.
3. Efremova, O. A.; Mironov, Y. V.; Fedorov, V. E., Design of Cyano-Bridged Coordination Polymers Based on Tetrahedral Rhenium Cluster Cyanide Complexes and 3d Transition Metals. *Eur. J. Inorg. Chem.* **2006**, *2006* (13), 2533-2549.
4. Newton, G. N.; Nihei, M.; Oshio, H., Cyanide-Bridged Molecular Squares – The Building Units of Prussian Blue. *Eur. J. Inorg. Chem.* **2011**, *2011* (20), 3031-3042.
5. Nie, P.; Shen, L.; Luo, H.; Li, H.; Xu, G.; Zhang, X., Synthesis of nanostructured materials by using metal-cyanide coordination polymers and their lithium storage properties. *Nanoscale* **2013**, *5* (22), 11087-93.
6. Cui, J.-W.; An, W.-J.; Van Hecke, K.; Cui, G.-H., Two copper(i) cyanide coordination polymers modified by semi-rigid bis(benzimidazole) ligands: syntheses, crystal structures, and electrochemical and photocatalytic properties. *Dalton Transactions* **2016**, *45* (43), 17474-17484.
7. Knoblauch, A. M.; Farnham, A.; Ouoba, J.; Zanetti, J.; Müller, S.; Jean-Richard, V.; Utzinger, J.; Wehrli, B.; Brugger, F.; Diabougoua, S.; Winkler, M. S., Potential health effects of cyanide use in artisanal and small-scale gold mining in Burkina Faso. *J. Clean. Prod.* **2020**, *252*, 119689.
8. Baum, M. M.; Moss, J. A.; Pastel, S. H.; Poskrebyshev, G. A., Hydrogen Cyanide Exhaust Emissions from In-Use Motor Vehicles. *Environ. Sci. Technol.* **2007**, *41* (3), 857-862.
9. Zhu, R.; Regeni, I.; Holstein, J. J.; Dittrich, B.; Simon, M.; Prevost, S.; Gradzielski, M.; Clever, G. H., Catenation and Aggregation of Multi-Cavity Coordination Cages. *Angew. Chem. Int. Ed.* **2018**, *57* (41), 13652-13656.
10. Li, R.-J.; Tessarolo, J.; Lee, H.; Clever, G. H., Multi-stimuli Control over Assembly and Guest Binding in Metallo-supramolecular Hosts Based on Dithienylethene Photoswitches. *J. Am. Chem. Soc.* **2021**, *143* (10), 3865-3873.
11. Regeni, I.; Chen, B.; Frank, M.; Baksi, A.; Holstein, J. J.; Clever, G. H., Coal-Tar Dye-based Coordination Cages and Helicates. *Angew. Chem. Int. Ed.* **2020**, *60* (11), 5673-5678.
12. Pullen, S.; Clever, G. H., Mixed-Ligand Metal-Organic Frameworks and Heteroleptic Coordination Cages as Multifunctional Scaffolds-A Comparison. *Acc. Chem. Res.* **2018**, *51* (12), 3052-3064.
13. Moutier, F.; Schiller, J.; Calvez, G.; Lescop, C., Self-assembled luminescent Cu(i) tetranuclear metallacycles based on 3,3'-bipyridine ligands. *Org. Chem. Front.* **2021**, *8* (12), 2893-2902.
14. Naik, S.; Mague, J. T.; Balakrishna, M. S., Short-bite PNP ligand-supported rare tetranuclear [Cu₄I₄] clusters: structural and photoluminescence studies. *Inorg. Chem.* **2014**, *53* (7), 3864-3873.
15. Harisomayajula, N. V. S.; Makovetskyi, S.; Tsai, Y.-C., Cuprophilic Interactions in and between Molecular Entities. *Chemistry* **2019**, *25* (38), 8936-8954.
16. Liu, W.; Fang, Y.; Wei, G. Z.; Teat, S. J.; Xiong, K.; Hu, Z.; Lustig, W. P.; Li, J., A Family of Highly Efficient CuI-Based Lighting Phosphors Prepared by a Systematic, Bottom-up Synthetic Approach. *J. Am. Chem. Soc.* **2015**, *137* (29), 9400-9408.
17. Kobayashi, A.; Fujii, M.; Shigeta, Y.; Yoshida, M.; Kato, M., Quantitative Solvent-Free Thermal Synthesis of Luminescent Cu(I) Coordination Polymers. *Inorg. Chem.* **2019**, *58* (7), 4456-4464.

18. Rodriguez-Sanz, E.; Lescop, C.; Réau, R., A Cu(I) cluster bearing a bridging phosphane ligand. *Comptes Rendus Chimie* **2010**, *13* (8-9), 980-984.
19. Liu, C. W.; Liaw, B. J.; Liou, L. S.; Wang, J. C., A 2D honeycomb-shaped network based on a starburst cluster: $[\text{Ag}_4(\mu_3\text{-Cl})(\text{PPh}_2(\text{CH}_2)_2\text{PPh}_2)_{1.5}\{\text{S}_2\text{P}(\text{OR})_2\}_3](\text{R} = \text{Et}, \text{Pr}^i)$. *Chem. Commun.* **2005**, (15), 1983-5.
20. Liaw, B.-J.; Lobana, T. S.; Lin, Y.-W.; Wang, J.-C.; Liu, C. W., Versatility of Dithiophosphates in the Syntheses of Copper(I) Complexes with Bis(diphenylphosphino)alkanes: Abstraction of Chloride from Dichloromethane. *Inorg. Chem.* **2005**, *44* (26), 9921-9929.
21. Anson, C. E.; Ponikiewski, L.; Rothenberger, A., Halide Abstraction from Organic Solvents in Reactions of a Copper(I) Alkoxide: Synthesis and Crystal Structures of $[\text{Cu}_5(\text{dppm})(\text{dppm-})_2(\text{OtBu})\text{Cl}_2]$ and $[\text{Cu}_3(\text{dppm})_3\text{Br}_2][\text{CuBr}_2]$. *Z. anorg. allg. Chem.* **2006**, *632* (15), 2402-2404.
22. Doyle, K. J.; Tran, H.; Baldoni-Olivencia, M.; Karabulut, M.; Hoggard, P. E., Photocatalytic Degradation of Dichloromethane by Chlorocuprate(II) Ions. *Inorg. Chem.* **2008**, *47* (15), 7029-7034.
23. Moussa, M. E.; Evariste, S.; Wong, H.-L.; Le Bras, L.; Roiland, C.; Le Polles, L.; Le Guennic, B.; Costuas, K.; Yam, V. W.-W.; Lescop, C., A solid state highly emissive Cu(I) metallacycle: promotion of cuprophilic interactions at the excited states. *Chem. Commun.* **2016**, *52* (76), 11370-11373.
24. Evariste, S.; Khalil, A. M.; Moussa, M. E.; Chan, A. K.-W.; Hong, E. Y.-H.; Wong, H.-L.; Le Guennic, B.; Calvez, G.; Costuas, K.; Yam, V. W.-W.; Lescop, C., Adaptive Coordination-Driven Supramolecular Syntheses toward New Polymetallic Cu(I) Luminescent Assemblies. *J. Am. Chem. Soc.* **2018**, *140* (39), 12521-12526.
25. El Sayed Moussa, M.; Khalil, A. M.; Evariste, S.; Wong, H.-L.; Delmas, V.; Le Guennic, B.; Calvez, G.; Costuas, K.; Yam, V. W.-W.; Lescop, C., Intramolecular rearrangements guided by adaptive coordination-driven reactions toward highly luminescent polynuclear Cu(i) assemblies. *Inorg. Chem. Front.* **2020**, *7* (6), 1334-1344.
26. Evariste, S.; Khalil, A. M.; Kerneis, S.; Xu, C.; Calvez, G.; Costuas, K.; Lescop, C., Luminescent vapochromic single crystal to single crystal transition in one-dimensional coordination polymer featuring the first Cu(I) dimer bridged by an aqua ligand. *Inorg. Chem. Front.* **2020**, *7* (18), 3402-3411.
27. Zhang, Y.; Schulz, M.; Wächtler, M.; Karnahl, M.; Dietzek, B., Heteroleptic diimine–diphosphine Cu(I) complexes as an alternative towards noble-metal based photosensitizers: Design strategies, photophysical properties and perspective applications. *Coord. Chem. Rev.* **2018**, *356*, 127-146.
28. Casadonte, D. J.; McMillin, D. R., Hindered internal conversion in rigid media. Thermally nonequilibrated 3IL and 3CT emissions from $[\text{Cu}(5\text{-X-phen})(\text{PPh}_3)_2]^+$ and $[\text{Cu}(4,7\text{-X}_2\text{-pehn})(\text{PPh}_3)_2]^+$ systems in a glass at 77 K. *J. Am. Chem. Soc.* **1987**, *109* (2), 331-337.
29. Parker, W. L.; Crosby, G. A., Assignment of the charge-transfer excited states of bis(N-heterocyclic) complexes of copper(I). *J. Phys. Chem.* **1989**, *93* (15), 5692-5696.

General conclusion

This thesis reports the study of the photophysical properties of Cu(I) based complexes obtained using the $[\text{Cu}_2(\mu_2\text{-dppm})_2(\text{CH}_3\text{CN})_4]^{2+}$ bimetallic unit. The photophysical properties of such complexes were studied, taking advantage of the electronic configuration of the Cu(I) ion and the rigidity provided to the structure by the chelating polydentate phosphine based backbone ligand. In this thesis, new luminescent supramolecular assemblies were obtained and their photophysical and thermal properties were studied in detail.

In chapter II, a number of 1D coordination polymers were obtained after reaction between a tetrametallic metallacycle precursor **A** and different polytopic 3- and 4-pyridyl capped linkers. The seven coordination polymers **C_n** obtained possess a similar molecular structure presenting an alternation of the tetrametallic metallacycle and the linker coordinated to one of the Cu(I) ions of the bimetallic units. A change of geometry of the tetrametallic metallacycle is noted in infrared spectroscopy measurements characterized by a shift of the cyanide $\nu_{(\text{CN})}$ stretching band. Despite the similarities in the molecular structure of the 1D coordination polymers **C_n**, they display very diverse luminescence properties with the emission in the solid-state at room temperature of eye-perceived luminescent colors spanning the entirety of the visible spectrum, from light blue in **C₁** to red in **C₇**. The photophysical properties were studied with the measurement of the variation of the emission spectrum and the decay times of the excited states depending on the temperature. These measurements revealed diverse radiative relaxation processes displayed by the polymers with the compounds **C₁** and **C₂** presenting $^3\text{MLCT}$ phosphorescence properties. The polymers **C₄**, **C₅** and **C₇** present, with low k_r values and high structured bands in their emission spectra, seemingly metal perturbed intralinker phosphorescence properties. Finally, the polymers **C₃** and **C₆** likely present a conservation of the TADF behavior of the precursor **A**. The thermal properties of the polymers **C_n** were studied, revealing the presence, in their DTA curves, of an exothermic peak associated, or not, with a loss of weight. This exothermic peak is accompanied by a drastic change of the luminescence properties observed in the polymers after heating, with the emission at room temperature of an eye-perceived intense blue color of emission, highlighting an irreversible phase transition.

This irreversible thermal transition observed in the 1D coordination polymers **C_n** was studied in depth in chapter III, along with the photophysical properties of the heated phases,

denominated C_n' . A thermal transition was also observed in the precursor **A** leading to the obtention of the transitioned phase **A'** presenting slightly modified photophysical properties but conserving the TADF behavior of the initial precursor.

This irreversible thermal transition was characterized in the solid-state by infrared spectroscopy with a systematic shift of the cyanide $\nu_{(CN)}$ stretching band to 2127 cm^{-1} , along with the disappearance of the bands assigned to the linkers B_n , in the phases C_1' - C_4' and C_7' . The disappearance of the linker was confirmed by heating experiments conducted in a sublimation apparatus. The photophysical properties of the phases C_n' are similar in the entirety of the series with an observed behavior upon cooling in their emission spectrum and their decay times of the excited states similar to the transitioned phase **A'**: a bathochromic shift of the emission spectrum with an increase of the decay times of the excited states to $200\text{ }\mu\text{s}$ at 80 K from $40\text{ }\mu\text{s}$ at RT. This could indicate a TADF behavior displayed by the heated phases C_n' which would coincide with the increase of their solid-state RT emission quantum yield compared to those of the initial polymers C_n . A study of the PXRD diagrams of the phases C_n' reveals a crystal phase transition occurring in the structure during the irreversible thermal transition and TD-PXRD measurements conducted on polymers C_2 , C_3 and C_6 showed that this structural rearrangement is gradual, with different intermediate phases appearing which can be attributed to the different steps of the transition: desolvation, decoordination, sublimation of the linker. Finally, TGA-DTA measurements conducted on the phases C_n' revealed that no further thermal processes are present after the irreversible thermal transition occurs, showing that the heated compounds C_n' are thermally stable phases.

In the second part of chapter III, the phase C_6' was studied in more depth as it was observed that the linker B_6 is not sublimated during the thermal transition, leading to the heated phase being an intimate mixture of the tetrametallic metallacycle and the linker. It was possible, after exposing C_6' to few drops or vapors of the reaction solvent (CH_2Cl_2), to obtain a new phase denominated $C_6'_{\text{DCM}}$ presenting under UV light the emission of an eye-perceived orange luminescence, highly reminiscent of the emission of polymer C_6 . The study of the infrared spectroscopy spectrum, PXRD diagram and photophysical properties of this regenerated phase revealed highly similar behaviors when compared to the polymer C_6 , leading to the conclusion that $C_6'_{\text{DCM}}$ and C_6 are almost identical. The study of the thermal properties of $C_6'_{\text{DCM}}$ revealed the conservation of the irreversible thermal transition leading to the emission of an eye-perceived blue luminescence, showing that a circular process based on irreversible thermal transition in the solid-state and regeneration by exposure to the reaction solvent is possible for

polymer **C**₆. The irreversible thermal transition observed in the polymers **C**_n allows these compounds to be attractive toward potential applications reporting of the thermal history of temperature sensitive tools and machine parts for example.

In chapter IV, The possibility of obtaining other luminescent Cu(I) based multimetallic species without relying on the presence of a cyanide fragment was explored. The reaction of the [Cu₂(μ₂-dppm)₂]⁺ bimetallic unit with the ditopic linker 3,3'-bipyridine **B**₃ led to the obtention of a series of Cu(I) based tetrametallic metallacycles bridged by halide ions, denominated **D**_x where X can be Cl, Br or I. The photophysical properties of these tetrametallic metallacycles were studied in details, revealing a ligand centered triplet luminophore behavior with high RT emission quantum yields being displayed. It was noted that the structural parameters and the photophysical properties in the solid-state of these tetrametallic metallacycles are comparable, regardless of the bridging halide ions. Lastly, the thermal stability of these metallacycles **D**_x was investigated by conducting TGA-TDA experiments. These measurements revealed that no exothermic peaks are present in the TDA curves of the metallacycles **D**_x and that they do not display the irreversible thermal transition that was observed in the polymers **C**_n.

To conclude, this work studied the obtention of a series of 1D coordination polymers from the reaction between a Cu(I) based tetrametallic metallacycle precursor and polytopic linkers, displaying in the solid-state varied photophysical properties. The presence on an unexpected and original thermal transition in the solid-state of these polymers was discovered and the subsequent change of their luminescence was studied. The search to reproduce this thermal property without the use of cyanide led to the obtention of a novel series of Cu(I) based tetrametallic metallacycles displaying attractive ligand centered photophysical properties, however not displaying the thermal transition property. This study highlights the stimuli sensitive behavior of Cu(I) based coordination polymers, with further studies of polymers displaying the discovered novel thermal transition being currently under way.

Appendix

I-General Appendix :

For all reported syntheses, procedures were performed under air, in a simple flask. Commercially available solvents and reagents were used as received, without further purification. $[\text{Cu}(\text{CH}_3\text{CN})_4]\text{PF}_6$, CuBr , 1,2-di(4-pyridyl)ethane (**B1**), and 1,2-di(4-pyridyl)ethylene (**B7**) were obtained from Sigma-Aldrich. 1,1'-bis(diphenylphosphino)methane (dppm) and CuCl were obtained from Acros Organics. 1,3-di(4-pyridyl)propane (**B2**), 3,3'-bipyridyl (**B3**), 1,4-di(4-pyridyl)benzene (**B4**) and 4,4'-di(4-pyridyl)biphenyl (**B5**) were obtained from TCI Chemicals. CuI was obtained from STREM Chemicals. 2,4,6-tri(4-pyridyl)-1,3,5-triazine (**B6**) was obtained from AmBeed. 1,6-dicyanohexane (**B8**) was obtained from Alfa Aesar. Bis(diphenylphosphinomethyl)phenylphosphine (dpmp) was synthesized in the Universität Regensburg, Regensburg, Germany, in the group of Pr. Dr. Manfred Scheer according to literature procedures with minor alterations¹. The purity of the ligand was verified by ^1H and ^{31}P NMR measurements.

FT-IR measurements were performed on a Perkin-Elmer Frontier spectrometer using UATR (Universal Attenuated Total Reflectance) accessory. Spectra have been recorded between 650 and 4000 cm^{-1} on pure samples.

UV-visible solid-state absorption measurements have been recorded on a Perkin-Elmer Lambda 650 spectrometer using a 60 mm integrating sphere. Spectra have been recorded between 800 and 200 nm on the powder samples spread and smoothed under a 15 mm diameter uncoated fused silica window from Edmund Optics, in a lab-made sample holder.

Steady-state emission spectra and luminescence quantum yield measurements were recorded on a Horiba Jobin-Yvon (HJY) Fluorolog-3 (FL3-2iHR550) fluorescence spectrofluorometer equipped with an IR R928P PMT / HJY FL-1073 detector and with an integrating sphere. Low temperature measurements were performed by using an OptistatCF (Oxford Inst.) in the range of 77 K to 300 K. High temperature measurements were made by using a Newport 350B thermoelectric temperature controller in the range of 223 K to 423 K. Excited-state lifetimes in the range of 80 K to 300 K were measured with a delta hub (TCSPC : Time-Correlated-Single-Photon-Counting) + delta diode system allowing to measure excited state lifetimes between 500 ps and 10 μs and with a pulsed xenon source (FL-1035) allowing to measure excited state lifetimes longer than 10 μs . Solid samples were placed in a quartz sample holder inside the

integrating sphere and the cryostat and maintained at the desired temperature until equilibrium was reached before recording the spectrum.

Thermal analysis have been performed using a Perkin-Elmer Pyris Diamond TG/DTA, between 25 °C and 950 °C with a 5 °C.min⁻¹ heating ramp in platinum crucibles under N₂ atmosphere, and between 25 °C and 350 °C with a 5 °C.min⁻¹ heating ramp in aluminum crucibles under N₂ atmosphere.

Luminance intensities in Cd.m⁻² were measured with a Konica Minolta LS-150 luminance meter on the powder samples spread and smoothed under an 20 mm diameter uncoated fused silica window from Edmund Optics, in a lab-made sample holder. The source was a CUN66B1B 365 nm UV diode from Roithner Lasertechnik on a lab-made mount powered by a programmable bench power supply E36104B from Keysight Technologies. The intensity of the UV irradiance at the exact sample location was measured in W.m⁻² with a VilberLourmat VLX-3W radiometer with a CX-365 sensor.

Powder X-ray diffraction diagrams have been collected using a Panalytical X'Pert Pro diffractometer with an X'celerator detector. The typical recording conditions were 45 kV, 40 mA for Cu K α ($\lambda = 1.542 \text{ \AA}$), the diagrams were recorded in θ/θ mode in 60 minutes between 4° and 75° with a step size of 0.0132° and a scan time of 0.6 s. Temperature dependant powder X-ray diffraction measurements were performed by fitting a HTK1200 Anton-Paar oven, under controlled atmosphere. TD-PXRD were performed by collecting a diffraction diagram every 10 °C with a heating ramp of 20 °C.min⁻¹ between each measurement. TD-PXRD diagrams were performed in 5 minutes between 4° and 50° with a step size of 0.0132° and a scan time of 0.09s.

Sublimation experiments were conducted in a Büchi Glass Oven B580 equipped with a Drying tube sublimation insert. The transition of the luminescence was followed under UV light produced by a handheld Consort dual wavelength UV Lamp capable of 254/365 nm emission. After the transition occurred, the sublimation insert was washed with dichloromethane that was then collected in a beaker. After the dichloromethane was entirely evaporated, the residue left inside the beaker was cleaned with CDCl₃ that was subsequently analysed by NMR spectroscopy.

Solution NMR spectra were measured in CD₂Cl₂ or CDCl₃ on a Bruker 300 MHz AvI spectrometer using 5 mm standard NMR tubes. All ³¹P and ¹H NMR spectra were recorded with decoupling from either ³¹P or ¹H nuclei during acquisition at a Larmor frequency of 300.13

MHz for ^1H NMR and 121.50 MHz for ^{31}P NMR. Chemical shifts are reported relative to tetramethylsilane (TMS) for ^1H NMR and 85 wt.% H_3PO_4 for ^{31}P NMR.

II-Appendix to chapter II :

II-1 Synthesis of A precursor and polymers C_n

II-1.a Synthesis of precursor A :

The synthesis of precursor **A** presented herein is similar to the published procedure with minor alterations.²

A dichloromethane solution (30 ml) of [Cu(CH₃CN)₄].PF₆ (0.180 g, 0.48 mmol) and 1,1-bis(diphenylphosphino)methane (dppm) (0.1845g, 0.48 mmol) was prepared and stirred for one hour at room temperature. A methanol solution (5 ml) of KCN (0.0156 g, 0.24 mmol) was added to the crude solution and the stirring was maintained overnight, along the appearance of few amount of a white precipitate. This crude solution was then filtered over cotton and was left upon n-pentane vapor diffusion to afford after a week colorless crystals of **A**. The final product was taken out of the solution by filtration over a paper filter and after drying is obtained as a white polycrystalline powder with a yield of 76 % (0.1952 g, 0.09 mmol). This air-stable powder emits under UV excitation ($\lambda_{\text{ex}} = 365 \text{ nm}$) an eye-perceived deep blue luminescence.

II-1.b Synthesis of polymers C_n :

All synthesis were performed in the same manner for the whole of the family of 1D coordination polymers C_n. The main differences in the preparation of each individual polymer are the way crystalline samples are best obtained, and slight changes in the stoichiometry.

Synthesis of polymer C₁ :

A dichloromethane solution (15 ml) of **A** (0.060 g, 0.028 mmol) was prepared and stirred for one hour. A dichloromethane solution (5 ml) of 1,2-di(4-pyridyl)ethane (**B₁** linker) (0.0052 g, 0.028 mmol) was added to the crude solution. The stirring was stopped and the solution was left at room temperature for few hours. The solution was then filtered over cotton and was left upon n-pentane vapor diffusion to afford after a week small colorless crystals of **C₁**. The final product was taken out of the solution by filtration over a paper filter and after drying is obtained

as a white polycrystalline powder with a yield of 65 % (0.042 g, 0.018 mmol). This air-stable powder emits under UV excitation ($\lambda_{\text{ex}} = 365 \text{ nm}$) an eye-perceived light blue luminescence.

Synthesis of polymer C₂ :

A dichloromethane solution (15 ml) of **A** (0.060 g, 0.028 mmol) was prepared and stirred for one hour. A dichloromethane solution (5 ml) of 1,3-di(4-pyridyl)propane (**B₂** linker) (0.0056 g, 0.028 mmol) was added to the crude solution. The stirring was stopped and the solution was left at room temperature for few hours. The solution was then filtered over cotton and was left upon n-pentane vapor diffusion to afford after a week small, colorless crystals of **C₂**. The final product was taken out of the solution by filtration over a paper filter and after drying is obtained as a pure white polycrystalline powder with a yield of 82 % (0.054 g, 0.023 mmol). This air-stable powder emits under UV excitation ($\lambda_{\text{ex}} = 365 \text{ nm}$) an eye-perceived blue luminescence.

Synthesis of polymer C₃ :

A dichloromethane solution (15 ml) of **A** (0.060 g, 0.028 mmol) was prepared and stirred for one hour. A dichloromethane solution (5 ml) of 3,3'-bipyridyl (**B₃** linker) (0.0066 g, 0.042 mmol) was added to the crude solution. The stirring was stopped and the solution was left at room temperature for few hours. The solution was then filtered over cotton and was left upon n-pentane vapor diffusion to afford after a week small, colorless crystals of **C₃**. The final product was taken out of the solution by filtration over a paper filter and after drying is obtained as a pure white polycrystalline powder with a yield of 78 % (0.0502 g, 0.022 mmol). This air-stable powder emits under UV excitation ($\lambda_{\text{ex}} = 365 \text{ nm}$) an eye-perceived light green luminescence.

Synthesis of polymer C₄ :

A dichloromethane solution (15 ml) of **A** (0.060 g, 0.028 mmol) was prepared and stirred for one hour. A dichloromethane solution (5 ml) of 1,4-di(4-pyridyl)benzene (**B₄** linker) (0.0065 g, 0.028 mmol) was added to the crude solution. The stirring was stopped and the solution was left at room temperature. After a week, small colorless crystals of **C₄** were formed at the bottom of the reaction flask. The final product was taken out of the solution by filtration over a paper

filter and after drying is obtained as a pure white polycrystalline powder obtained with a yield of 81 % (0.0539 g, 0.023 mmol). This air-stable powder emits under UV excitation ($\lambda_{\text{ex}} = 365$ nm) an eye-perceived green luminescence.

Synthesis of polymer C₅ :

A dichloromethane solution (20 ml) of **A** (0.080 g, 0.038 mmol) was prepared and stirred for one hour. A dichloromethane solution (10 ml) of 4,4'-di(4-pyridyl)biphenyl (**B₅** linker) (0.0116 g, 0.038 mmol) was added to the crude solution. The stirring was stopped and the solution was left at room temperature. After a week, small colorless crystals of **C₅** were formed at the bottom of the reaction flask. The final product was taken out of the solution by filtration over a paper filter and after drying is obtained as a pure white polycrystalline powder with a yield of 77 % (0.0706 g, 0.029 mmol). This air-stable powder emits under UV excitation ($\lambda_{\text{ex}} = 365$ nm) an eye-perceived weak green luminescence.

Synthesis of polymer C₆ :

A dichloromethane solution (15 ml) of **A** (0.060 g, 0.028 mmol) was prepared and stirred for one hour. A dichloromethane solution (5 ml) of 2,4,6-tri(4-pyridyl)-1,3,5-triazine (**B₆** linker) (0.0088 g, 0.028 mmol) was added to the crude solution. The stirring was stopped and the solution was left at room temperature. After a week, yellow crystals of **C₆** were formed at the bottom of the reaction flask. The final product was taken out of the solution by filtration over a paper filter and after drying is obtained as a pure yellow polycrystalline powder with a yield of 90 % (0.0617 g, 0.025 mmol). This air-stable powder emits under UV excitation ($\lambda_{\text{ex}} = 365$ nm) an eye-perceived orange-red luminescence.

Synthesis of polymer C₇ :

A dichloromethane solution (20 ml) of **A** (0.080 g, 0.038 mmol) was prepared and stirred for one hour. A dichloromethane solution (10 ml) of 1,2-di(4-pyridyl)ethylene (**B₇** linker) (0.0102 g, 0.058 mmol) was added to the crude solution. The stirring was stopped and the solution was left at room temperature. After a week, small yellow crystals of **C₇** were formed at the bottom of the reaction flask. The final product was taken out of the solution by filtration over a paper

filter and after drying is obtained as a pure pale yellow polycrystalline powder with a yield of 57 % (0.0491 g, 0.021 mmol). This air-stable powder emits under UV excitation ($\lambda_{\text{ex}} = 365 \text{ nm}$) an eye-perceived deep red luminescence.

II-2 Infrared spectroscopy study

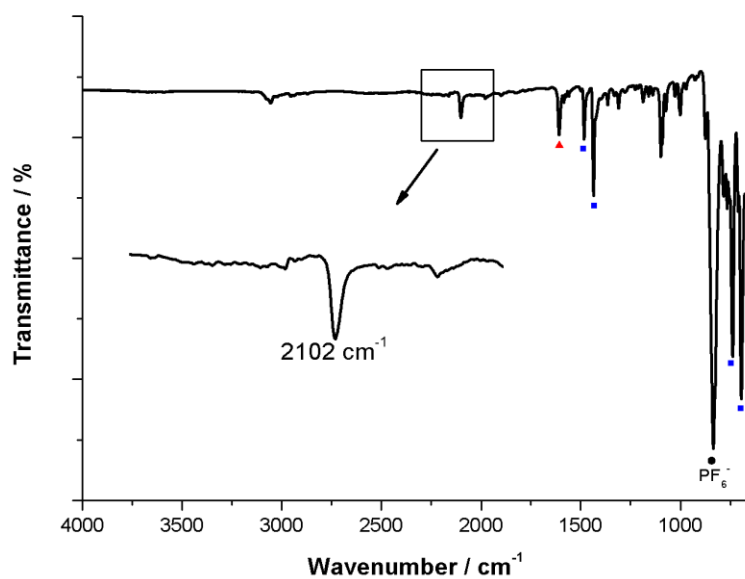


Figure SII.1 : Infrared spectrum of compound C1. The dot marks the PF₆⁻ counter anion t_{1u} vibration mode band. Blue squares mark typical dppm δ_(C-H) ligand bands. Red triangles mark B₁ ligands bands.

IR (cm⁻¹) :695 (vs), 738 (vs), 766 (s), 785 (s), 835 (vs), 971 (vw), 1001 (w), 1027 (w), 1098 (m), 1188 (w), 1227 (vw), 1279 (vw), 1311 (w), 1365 (w), 1436 (s), 1483 (m), 1574 (vw), 1586 (w), 1610 (m), 2102 (m), 3056 (w).

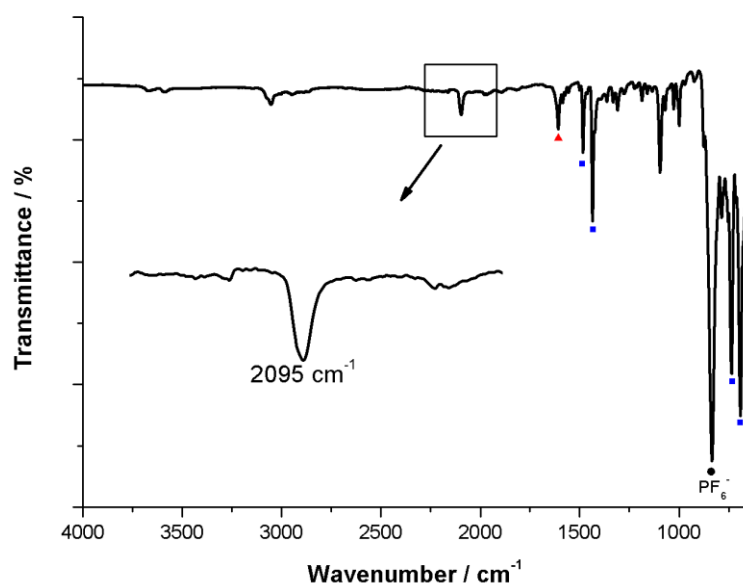


Figure SII.2 : Infrared spectrum of compound **C**₂. The dot marks the PF₆⁻ counter anion t_{1u} vibration mode band. Blue squares mark typical dppm δ_(C-H) ligand bands. Red triangles mark **B**₂ ligands bands.

IR (cm⁻¹) :691 (vs), 736 (vs), 754 (s), 786 (s), 834 (vs), 971 (vw), 1000 (w), 1027 (w), 1095 (m), 1187 (w), 1224 (vw), 1277 (vw), 1310 (w), 1364 (w), 1435 (s), 1483 (m), 1574 (vw), 1586 (w), 1608 (m), 2095 (m), 3054 (w).

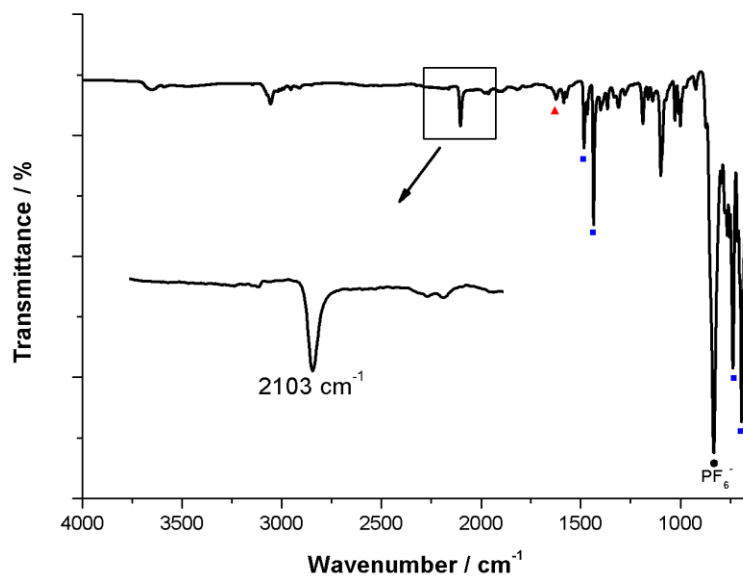


Figure SII.3 : Infrared spectrum of compound **C**₃. The dot marks the PF₆⁻ counter anion t_{1u} vibration mode band. Blue squares mark typical dppm δ_(C-H) ligand bands. Red triangles mark **B**₃ ligands bands.

IR (cm⁻¹) :693 (vs), 737 (vs), 755 (s), 833 (vs), 973 (vw), 1001 (w), 1028 (w), 1099 (m), 1190 (w), 1278 (vw), 1311 (w), 1367 (w), 1436 (s), 1484 (m), 1572 (vw), 1586 (w), 1624 (m), 2103 (m), 3057 (w).

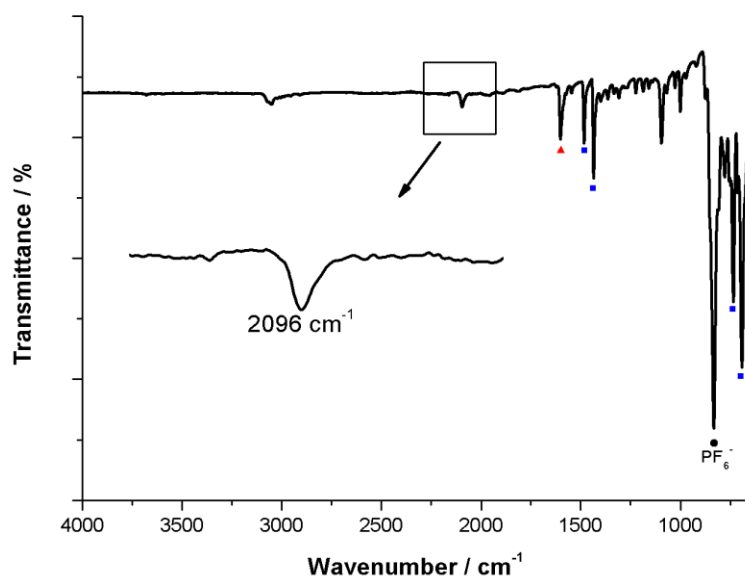


Figure SII.4 : Infrared spectrum of compound **C4**. The dot marks the PF_6^- counter anion t_{1u} vibration mode band. Blue squares mark typical dppm $\delta_{(\text{C-H})}$ ligand bands. Red triangles mark **B₄** ligands bands.

IR (cm^{-1}) : 691 (vs), 735 (vs), 756 (s), 778 (s), 833 (vs), 972 (vw), 1001 (w), 1027 (w), 1095 (m), 1187 (w), 1224 (vw), 1309 (w), 1334 (vw), 1365 (w), 1400 (vw), 1435 (s), 1484 (m), 1547 (vw), 1574 (vw), 1602 (m), 2096 (m), 3051 (w).

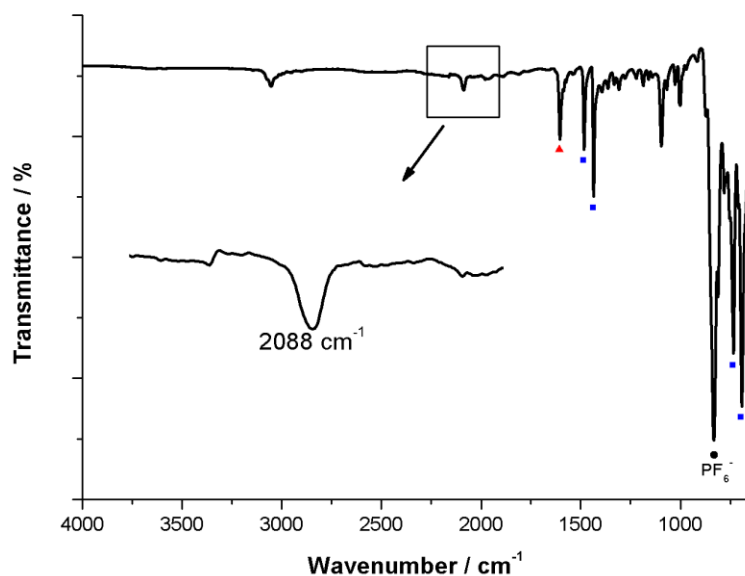


Figure SII.5 : Infrared spectrum of compound **Cs**. The dot marks the PF_6^- counter anion t_{1u} vibration mode band. Blue squares mark typical dppm $\delta_{(\text{C-H})}$ ligand bands. Red triangles mark **B₅** ligands bands.

IR (cm^{-1}) : 691 (vs), 734 (vs), 753 (s), 782 (s), 832 (vs), 971 (vw), 1001 (w), 1027 (w), 1069 (w), 1097 (m), 1161 (vw), 1187 (w), 1221 (vw), 1278 (vw), 1309 (w), 1333 (vw), 1364 (w), 1395 (vw), 1435 (s), 1483 (m), 1547 (vw), 1574 (vw), 1586 (w), 1605 (m), 2088 (m), 3055 (w).

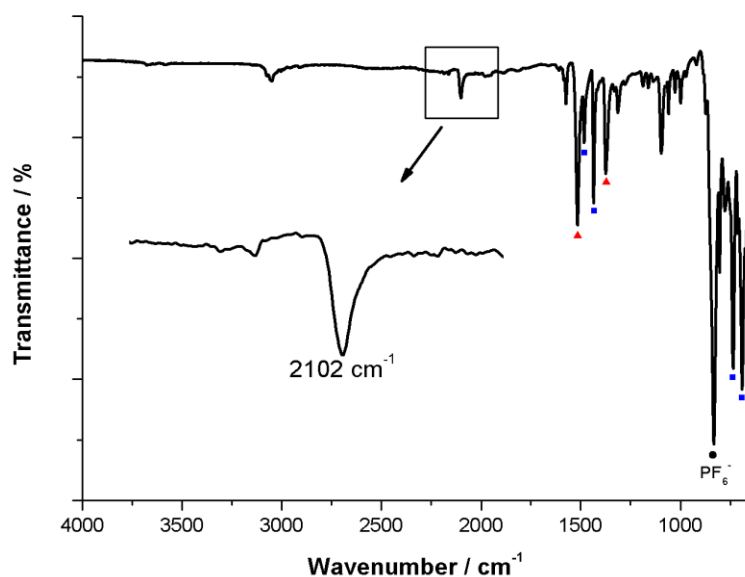


Figure SII.6 : Infrared spectrum of compound **C6**. The dot marks the PF_6^- counter anion t_{1u} vibration mode band. Blue squares mark typical dppm $\delta_{(\text{C-H})}$ ligand bands. Red triangles mark **B6** ligands bands.

IR (cm^{-1}) : 690 (vs), 736 (vs), 777 (s), 832 (vs), 972 (vw), 999 (w), 1027 (w), 1060 (w), 1096 (m), 1188 (w), 1278 (vw), 1315 (w), 1331 (vw), 1364 (w), 1375 (s), 1436 (s), 1482 (m), 1517 (s), 1575 (m), 1586 (w), 2102 (m), 3050 (w).

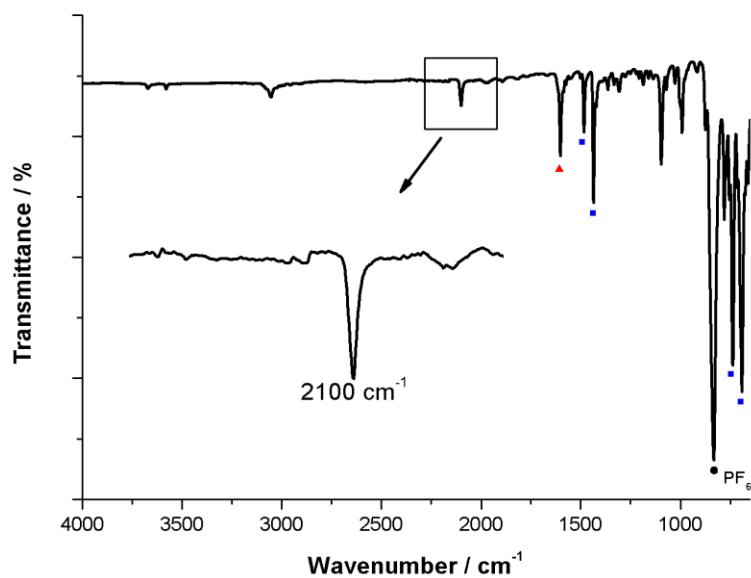


Figure SII.7 : Infrared spectrum of compound **C7**. The dot marks the PF_6^- counter anion t_{1u} vibration mode band. Blue squares mark typical dppm $\delta_{(\text{C-H})}$ ligand bands. Red triangles mark **B7** ligands bands.

IR (cm^{-1}) : 691 (vs), 738 (vs), 755 (s), 781 (s), 833 (vs), 992 (w), 1027 (w), 1071 (w), 1096 (m), 1187 (w), 1277 (vw), 1308 (w), 1333 (vw), 1364 (w), 1375 (s), 1436 (s), 1484 (m), 1501 (vw), 1575 (vw), 1586 (vw), 1603 (m), 2100 (m), 3055 (w).

II-3 X-ray crystallographic study

Single crystal data collection for polymers C_n were performed at 150 K with a D8 Venture Bruker AXS (Centre de Diffractométrie, Université de Rennes 1, France) with Mo- $K\alpha$ radiation ($\lambda = 0.71073 \text{ \AA}$). Reflections were indexed, Lorentz-polarization corrected and integrated by the *DENZO* program of the KappaCCD software package. The data merging process was performed using the SCALEPACK program.³ Structure determinations were performed by direct methods with the solving program SIR97,⁴ that revealed all the non-hydrogen atoms. SHELXL program⁵ was used to refine the structures by full-matrix least-squares based on F^2 . All non-hydrogen atoms were refined with anisotropic displacement parameters.

The measured single crystals were always coated in Fomblin oil, mounted at low temperature on the diffractometer goniometer as quickly as possible. The X-ray data collections were performed at low temperature. In all the derivatives studied, the included dichloromethane solvent molecules were found to be highly disordered and a correct modelling of the disorder of these solvent molecules was not always possible leading to rather high anisotropic displacement parameters for some of their atoms. A « squeeze » treatment^{6,7} was therefore conducted to remove the scattering contribution of these molecules which cannot be correctly modelled.

II-3.1 Molecular structure of C_n compounds

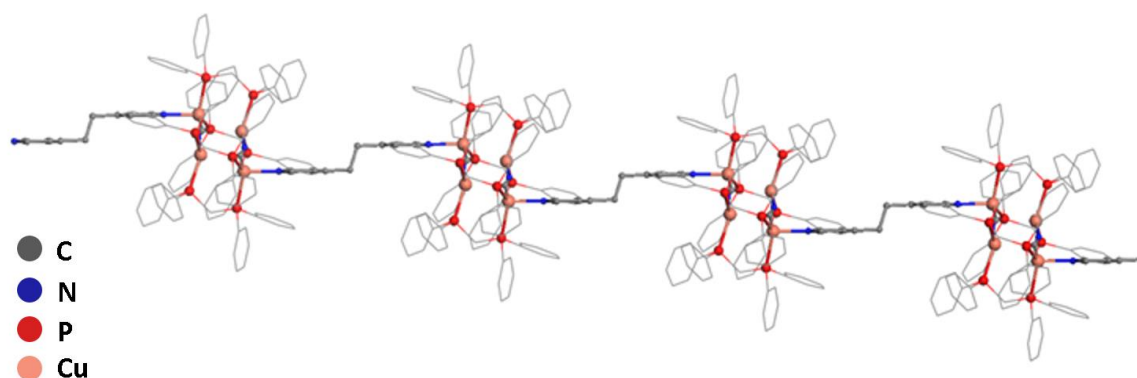


Figure SII.8 : View of the molecular structure of the one-dimensional coordination polymer C_1 obtained via single-crystal X-ray diffraction (hydrogen atoms, counter-anions PF_6^- and included solvent molecules have been omitted for clarity). Only one of the orientation of the cyano ligands over the two orientations possible are shown.

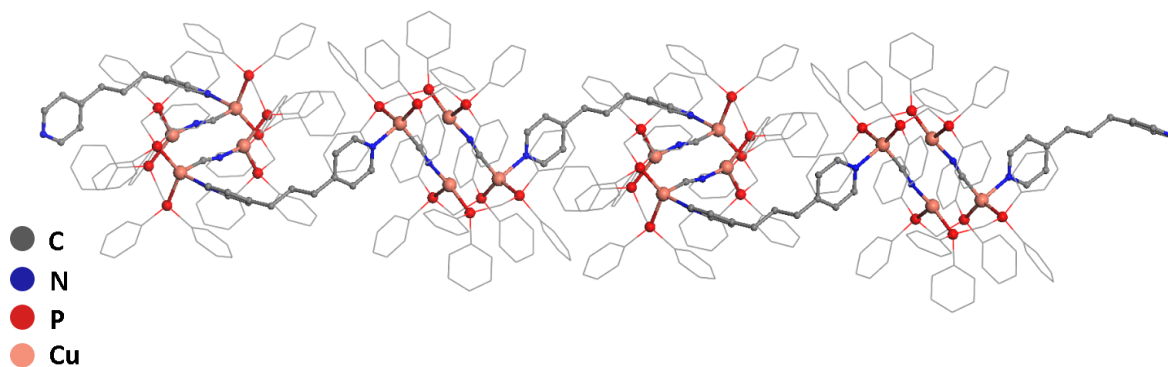


Figure SII.9 : View of the molecular structure of the one-dimensional coordination polymer **C₂** obtained via single-crystal X-ray diffraction (hydrogen atoms, counter-anions PF_6^- and included solvent molecules have been omitted for clarity). Only one of the orientation of the cyano ligands over the two orientations possible are shown.

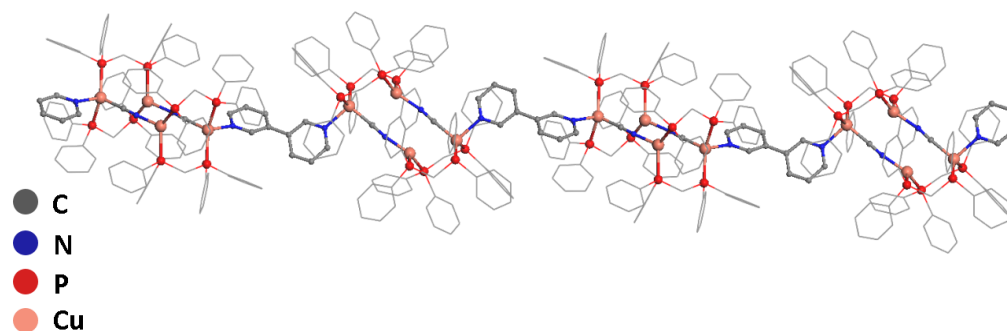


Figure SII.10 : View of the molecular structure of the one-dimensional coordination polymer **C₃** obtained via single-crystal X-ray diffraction (hydrogen atoms, counter-anions PF_6^- and included solvent molecules have been omitted for clarity). Only one of the orientation of the cyano ligands over the two orientations possible are shown.

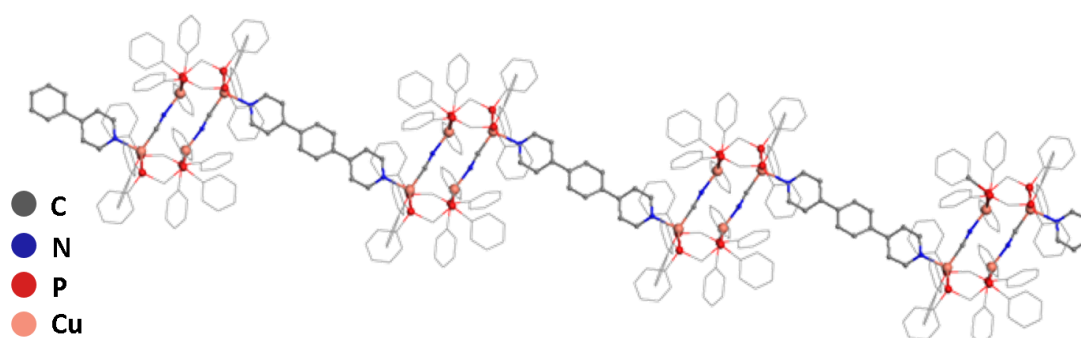


Figure SII.11 : View of the molecular structure of the one-dimensional coordination polymer **C₄** obtained via single-crystal X-ray diffraction (hydrogen atoms, counter-anions PF_6^- and included solvent molecules have been omitted for clarity). Only one of the orientation of the cyano ligands over the two orientations possible are shown.

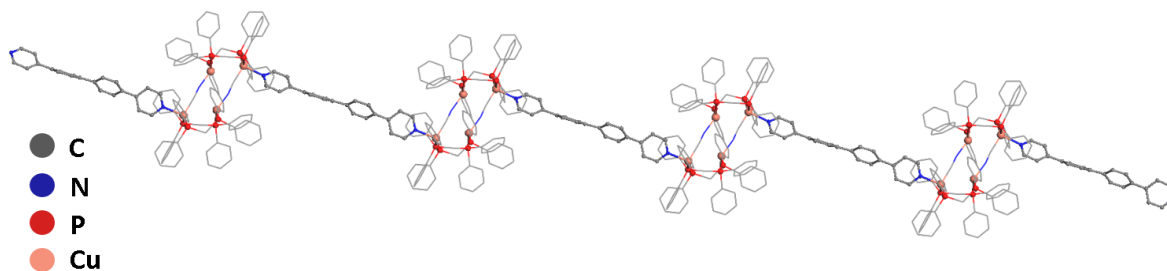


Figure SII.12 : View of the molecular structure of the one-dimensional coordination polymer **C₅** obtained via single-crystal X-ray diffraction (hydrogen atoms, counter-anions PF_6^- and included solvent molecules have been omitted for clarity). Only one of the orientation of the cyano ligands over the two orientations possible are shown.

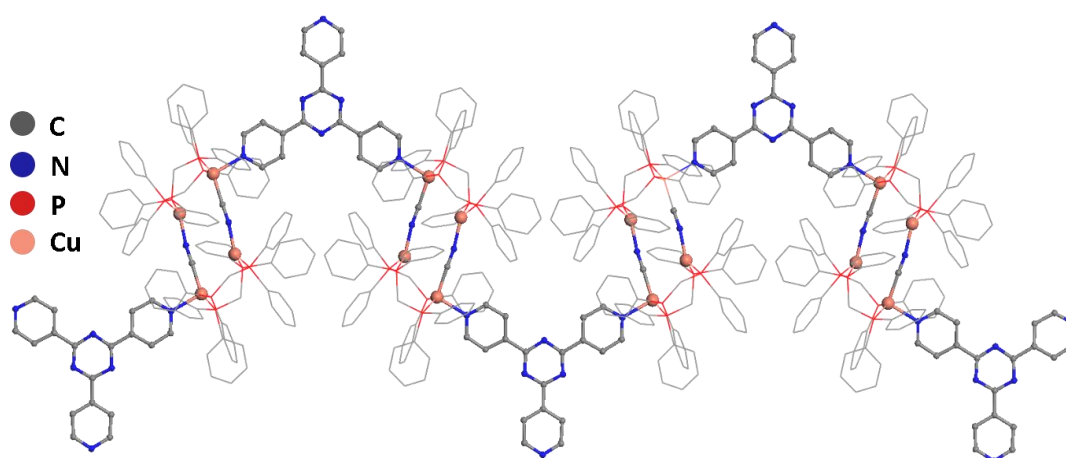


Figure SII.13 : View of the molecular structure of the one-dimensional coordination polymer **C₆** obtained via single-crystal X-ray diffraction (hydrogen atoms, counter-anions PF_6^- and included solvent molecules have been omitted for clarity). Only one of the orientation of the cyano ligands over the two orientations possible are shown.

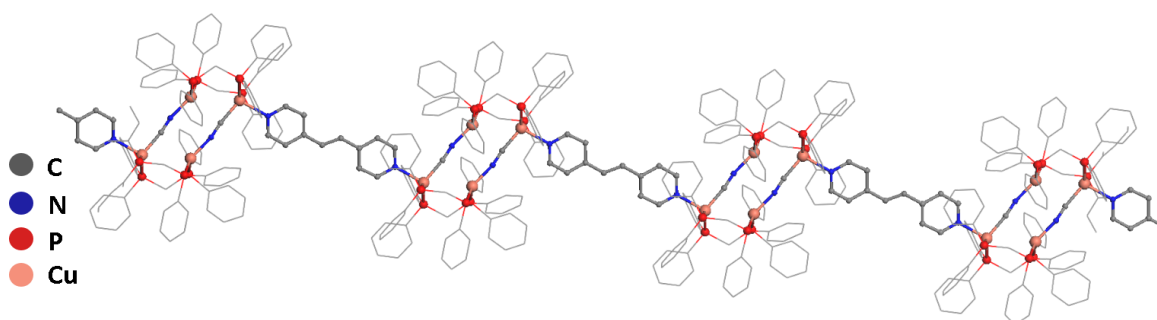


Figure SII.14 : View of the molecular structure of the one-dimensional coordination polymer **C₇** obtained via single-crystal X-ray diffraction (hydrogen atoms, counter-anions PF_6^- and included solvent molecules have been omitted for clarity). Only one of the orientation of the cyano ligands over the two orientations possible are shown.

II-3.2 Crystallographic tables of the polymers C_n:

	C ₁ *	C ₂	C ₃	C ₄
Molecular formula	C ₁₁₄ H ₁₀₀ Cu ₄ F ₁₂ N ₄ P ₁₀ (C ₁₂₂ H ₁₀₈ Cl ₁₆ Cu ₄ F ₁₂ N ₄ P ₁₀)	C ₁₁₅ H ₁₀₂ Cu ₄ F ₁₂ N ₄ P ₁₀ (C ₁₂₀ H ₁₀₂ Cl ₁₀ Cu ₄ F ₁₂ N ₄ P ₁₀)	C ₅₆ H ₄₈ Cu ₂ F ₆ N ₂ P ₅ (C ₁₁₅ H ₁₀₀ Cl ₆ Cu ₄ F ₁₂ N ₄ P ₁₀)	C ₅₉ H ₅₀ Cu ₂ F ₆ N ₂ P ₅ (C ₆₂ H ₅₅ Cl ₅ Cu ₂ F ₆ N ₂ P ₅)
CCDC number	/	/	/	/
Molecular weight	2317.84 (2989.18)	2331.87 (2746.42)	1144.89 (2542.55)	1182.94 (1400.25)
a (Å)	15.9341(7)	18.690(2)	34.355(6)	13.131(2)
b (Å)	23.7640(9)	19.489(2)	18.703(4)	14.318(5)
c (Å)	16.7961(7)	19.737(2)	18.816(4)	18.268(2)
α (°)	90	78.743(3)	90	105.585(4)
β (°)	96.028(4)	62.797(4)	110.418(5)	98.707(4)
γ (°)	90	76.283(3)	90	103.710(4)
V (Å³)	6324.8(5)	6180.2(11)	11331(4)	3128.0(7)
Z	2	2	8	2
Dc (g.cm⁻³)	1.217 (1.570)	1.253 (1.476)	1.342 (1.490)	1.256 (1.487)
Crystal system	Monoclinic	Triclinic	Monoclinic	Triclinic
Space group	P21/n	P-1	C2/c	P-1
Temperature (K)	150(2)	150(2)	150(2)	150(2)
Wavelength Mo-Kα (Å)	0.71069	0.71069	0.71069	0.71069
Crystal size (mm)	0.26 * 0.12 * 0.09	0.3 * 0.11 * 0.10	0.20 * 0.16 * 0.06	0.11 * 0.09 * 0.08
μ (mm⁻¹)	0.850 (1.196)	0.871 (1.096)	0.948 (1.093)	0.861 (1.080)
F(000)	2372 (3028)	2388 (2788)	4680 (5176)	1210 (1424)
θ limit (°)	3.42 – 32.36	2.16 – 27.52	2.14 – 27.73	2.18 – 27.59
Index ranges hkl	-23 < h < 23 -32 < k < 32 -25 < l < 25	-24 < h < 24 -25 < k < 24 -25 < l < 25	-44 < h < 44 -23 < h < 17 -24 < l < 24	-17 < h < 17 -18 < k < 18 -23 < l < 23
Reflections collected	48181	143965	62203	67298
Independent reflections	20063	28422	11822	14401
Reflection [I>2σ(I)]	12676 (13316)	18482 (18019)	8385 (8221)	11724 (11740)
Data/restraints/parameters	20013 / 0 / 649 (20063 / 0 / 766)	28422 / 0 / 1310 (28422 / 0 / 1517)	11822 / 0 / 635 (11822 / 0 / 680)	14401 / 0 / 668 (14401 / 0 / 758)
Goodness of fit on F²	0.970 (1.033)	0.946 (1.012)	1.095 (1.074)	1.080 (1.047)
Final R indices [I>2σ(I)]	R ₁ = 0.0629 (0.0843) wR ₂ = 0.1461 (0.1970)	R ₁ = 0.0523 (0.0660) wR ₂ = 0.1136 (0.1606)	R ₁ = 0.0682 (0.0697) wR ₂ = 0.1701 (0.1666)	R ₁ = 0.0523 (0.0583) wR ₂ = 0.1511 (0.1596)
R indices (all data)	R ₁ = 0.1028 (0.1294) wR ₂ = 0.1628 (0.2245)	R ₁ = 0.0899 (0.1199) wR ₂ = 0.1270 (0.1934)	R ₁ = 0.0961 (0.1065) wR ₂ = 0.1828 (0.1872)	R ₁ = 0.0628 (0.0733) wR ₂ = 0.1606 (0.1721)
Largest diff peak and hole (e Å⁻³)	0.961 and -0.671 (1.749 and -1.404)	0.501 and -0.713 (1.701 and -1.694)	1.051 and -1.605 (1.468 and -1.594)	1.784 and -0.920 (1.852 and -1.347)

* : measurement conducted at Universität Regensburg, Germany.

Table SII.1 : Crystallographic data of compounds C₁-C₄. Data presented are after squeeze treatment. Data before squeeze treatment are given in brackets.

	C₅	C₆	C₇
Molecular formula	C ₁₂₄ H ₁₀₃ Cu ₄ F ₁₂ N ₄ P ₁₀ (C ₁₃₂ H ₁₁₈ Cl ₁₆ Cu ₄ F ₁₂ N ₄ P ₁₀)	C ₁₂₀ H ₁₀₀ Cu ₄ F ₁₂ N ₈ P ₁₀ (C ₆₃ H ₅₄ Cl ₆ Cu ₂ F ₆ N ₄ P ₅)	C ₅₇ H ₄₉ Cu ₂ F ₆ N ₂ P ₅ (C ₅₉ H ₅₃ Cl ₄ Cu ₂ F ₆ N ₂ P ₅)
CCDC number	/	/	/
Molecular weight	2440.96 (3119.36)	2445.94 (1475.73)	1157.91 (1327.76)
a (Å)	14.0761(12)	23.594(1)	13.003(2)
b (Å)	25.029(3)	30.804(2)	14.326(2)
c (Å)	19.674(2)	18.242(2)	18.407(2)
α (°)	90	90	67.527(4)
β (°)	91.509(4)	97.462(2)	71.071(4)
γ (°)	90	90	77.265(4)
V (Å³)	6928.9(12)	13145.8(18)	2978.8(7)
Z	2	4	2
Dc (g.cm⁻³)	1.169 (1.495)	1.236 (1.491)	1.291 (1.480)
Crystal system	Monoclinic	Monoclinic	Triclinic
Space group	P21	C2/c	P-1
Temperature (K)	150(2)	150(2)	150(2)
Wavelength Mo-Kα (Å)	0.71069	0.71069	0.71069
Crystal size (mm)	0.2 * 0.13 * 0.11	0.17 * 0.15 * 0.11	0.2 * 0.16 * 0.11
μ (mm⁻¹)	0.780 (1.096)	0.823 (1.072)	0.903 (1.086)
F(000)	2496 (3168)	5000 (5992)	1184 (1352)
θ limit (°)	2.07 – 30.57	2.17 – 27.53	2.15 – 27.56
Index ranges hkl	-20 < h < 16 -35 < k < 35 -28 < l < 28	-30 < h < 30 -40 < k < 40 -23 < l < 23	-16 < h < 16 -18 < k < 18 -23 < l < 23
Reflections collected	206897	156767	51085
Independent reflections	41941	15112	13714
Reflection [I>2σ(I)]	30390 (29970)	12312 (11529)	12123 (12075)
Data/restraints/parameters	41941 / 1 / 1388 (41941 / 1 / 1604)	15112 / 0 / 696 (15112 / 0 / 787)	13714 / 0 / 651 (13714 / 0 / 727)
Goodness of fit on F²	1.001 (1.015)	1.020 (1.044)	1.101 (1.089)
Final R indices [I>2σ(I)]	R ₁ = 0.0547 (0.0709) wR ₂ = 0.1089 (0.1643)	R ₁ = 0.0427 (0.0429) wR ₂ = 0.0914 (0.0997)	R ₁ = 0.0352 (0.0360) wR ₂ = 0.0993 (0.0951)
R indices (all data)	R ₁ = 0.0847 (0.1145) wR ₂ = 0.1167 (0.1865)	R ₁ = 0.0588 (0.0668) wR ₂ = 0.0972 (0.1145)	R ₁ = 0.0392 (0.0425) wR ₂ = 0.1017 (0.1028)
Largest diff peak and hole (e Å⁻³)	0.897 and -0.657 (3.017 and -1.340)	0.377 and -0.341 (1.438 and -1.144)	0.622 and -0.554 (1.050 and -1.191)

Table SII.2 : Crystallographic data of compounds C₅-C₇. Data presented are after squeeze treatment. Data before squeeze treatment are given in brackets.

II-4 Photophysical study of C_n polymers

II-4.1 Solid-state UV-vis absorption

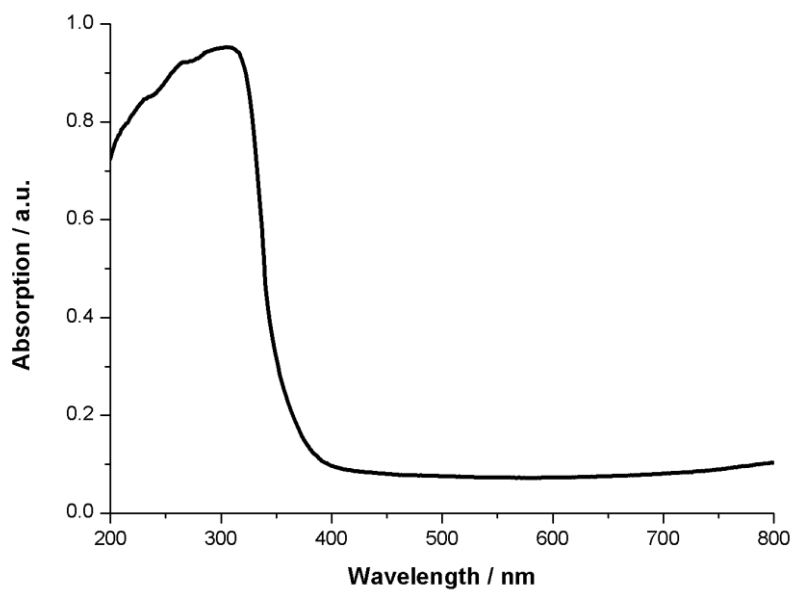


Figure SII.15 : Solid-state UV-visible absorption spectrum of C_1 .

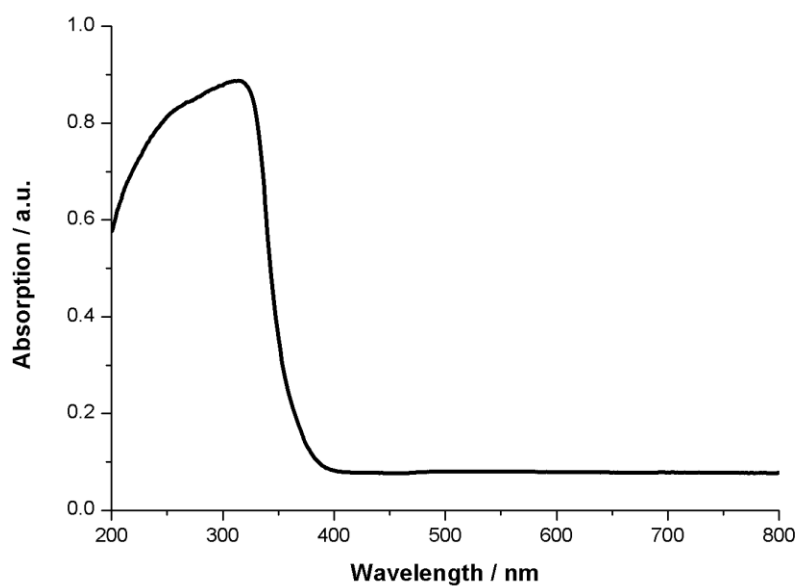


Figure SII.16 : Solid-state UV-visible absorption spectrum of C_2 .

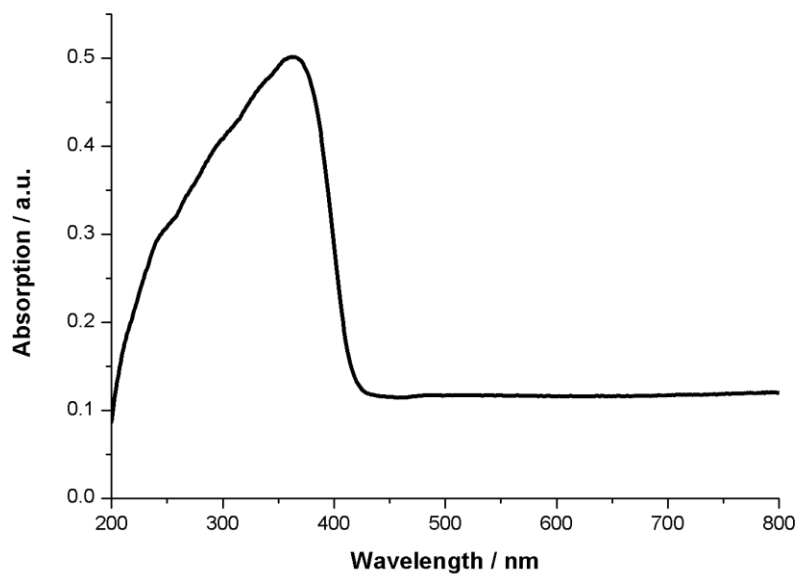


Figure SII.17 : Solid-state UV-visible absorption spectrum of **C₃**.

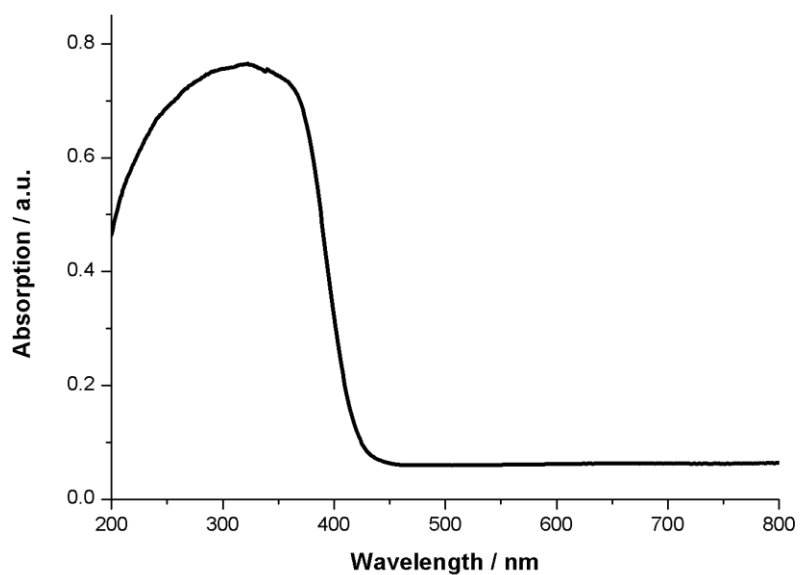


Figure SII.18 : Solid-state UV-visible absorption spectrum of **C₄**.

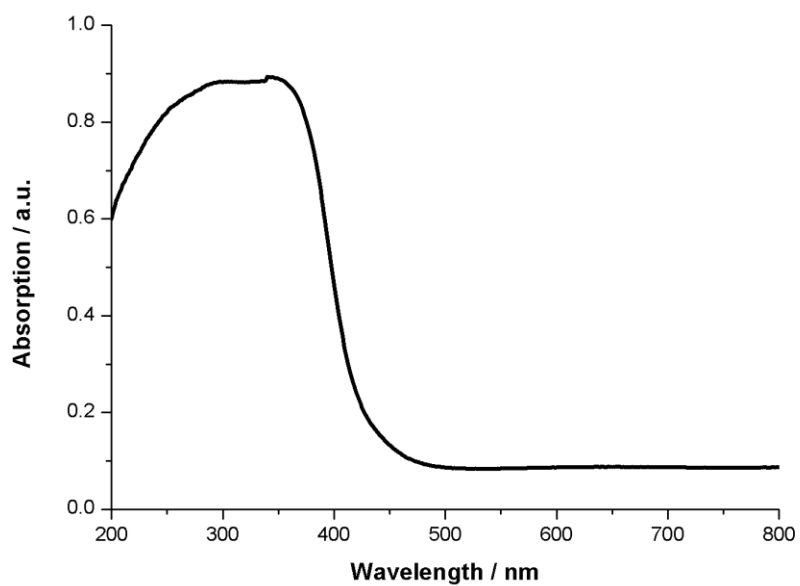


Figure SII.19 : Solid-state UV-visible absorption spectrum of C₅.

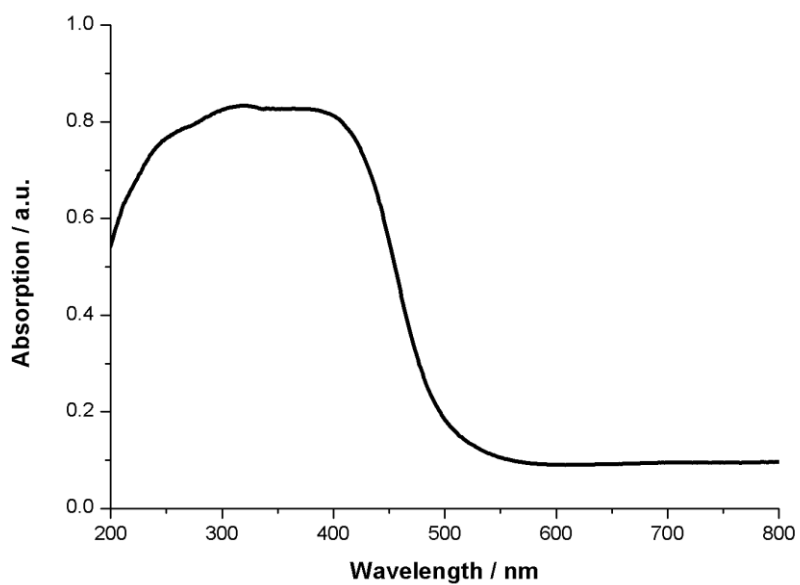


Figure SII.20 : Solid-state UV-visible absorption spectrum of C₆.

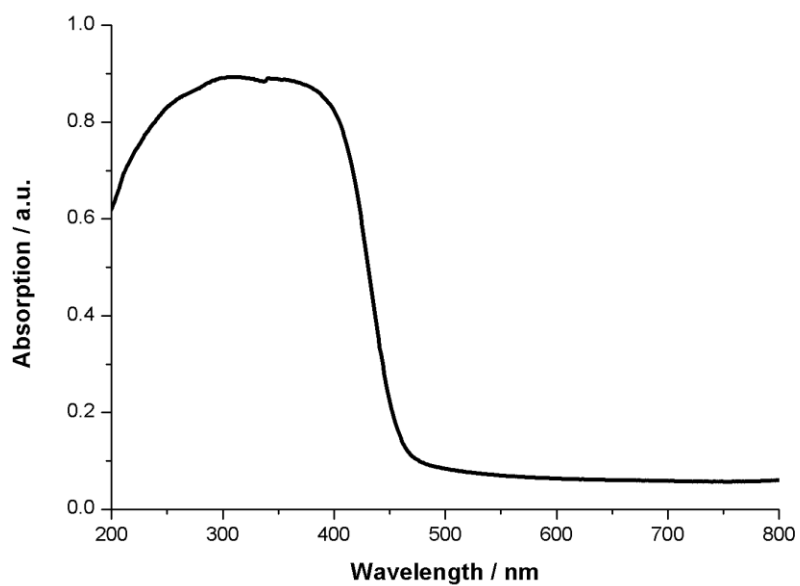


Figure SII.21 : Solid-state UV-visible absorption spectrum of **C7**.

II-4.2 Solid-state excitation spectra

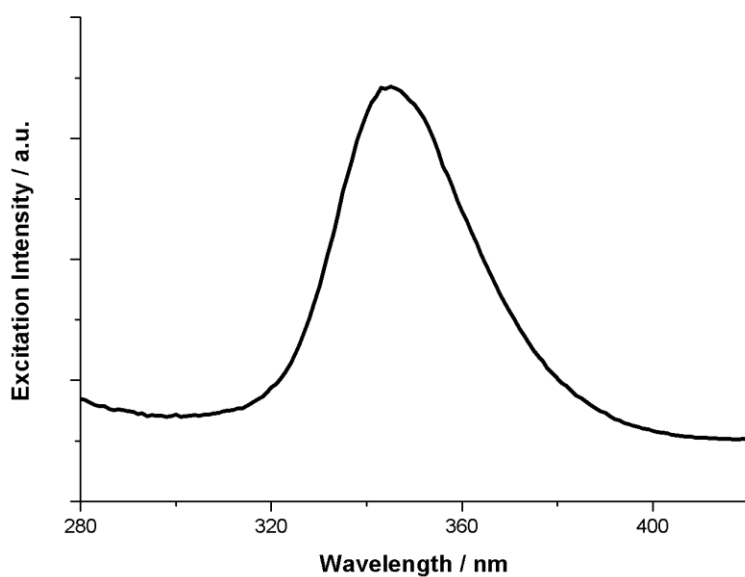


Figure SII.22 : Solid-state room temperature excitation spectrum of **C1**.

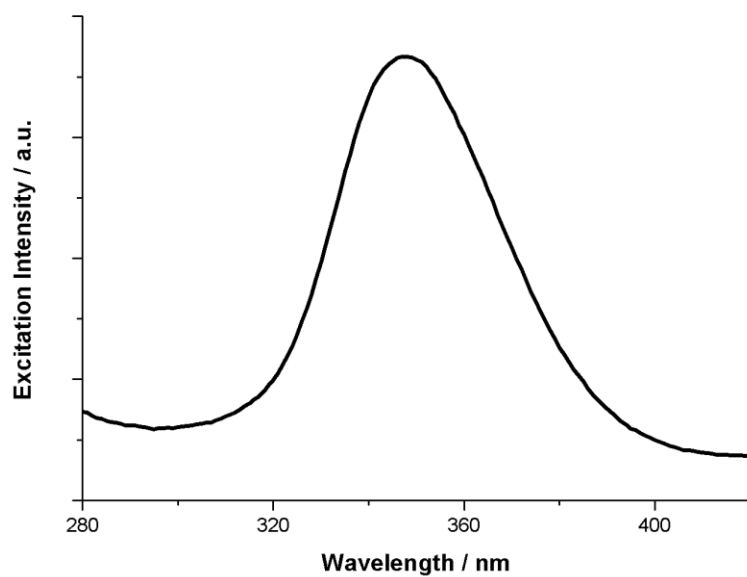


Figure SII.23 : Solid-state room temperature excitation spectrum of C₂.

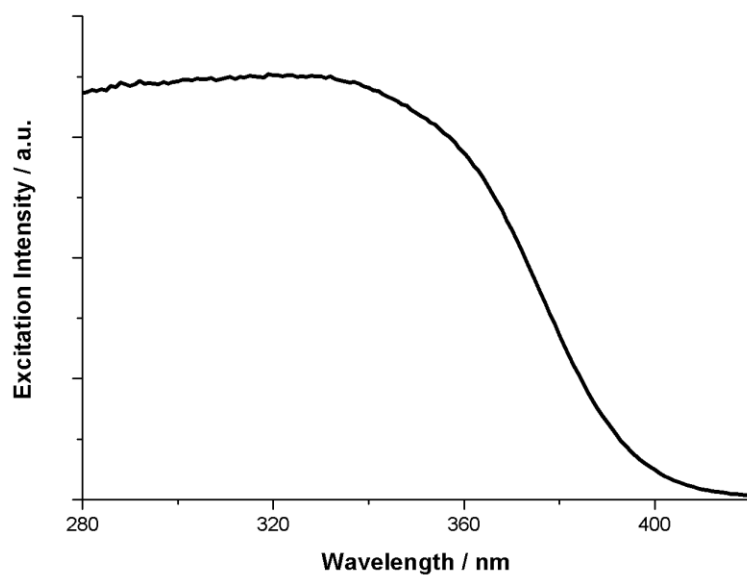


Figure SII.24 : Solid-state room temperature excitation spectrum of C₃.

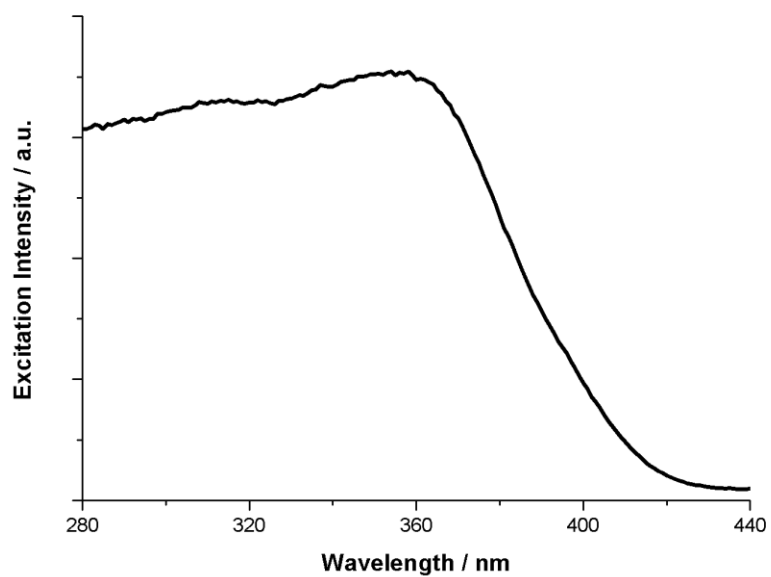


Figure SII.25 : Solid-state room temperature excitation spectrum of C4.

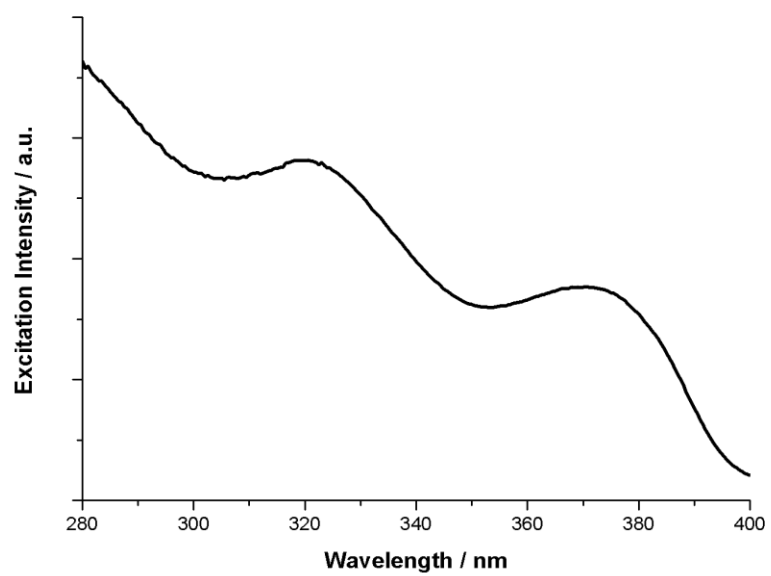


Figure SII.26 : Solid-state excitation spectrum of C5 measured at 80 K.

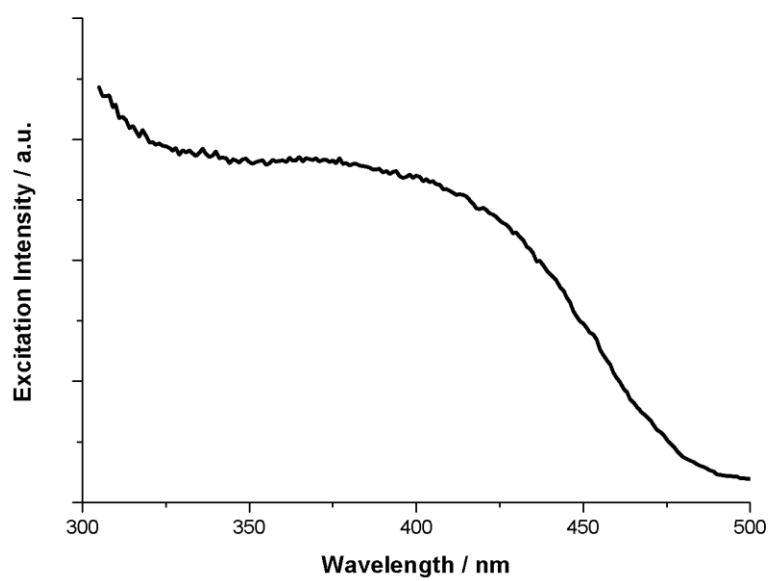


Figure SII.27 : Solid-state room temperature excitation spectrum of **C6**.

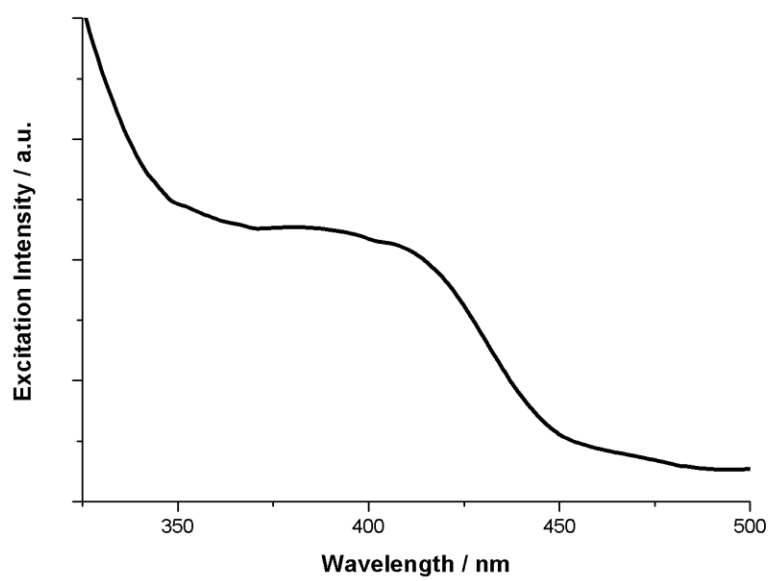


Figure SII.28 : Solid-state room temperature excitation spectrum of **C7**.

II-4.3 Solid-state temperature dependant emission spectra

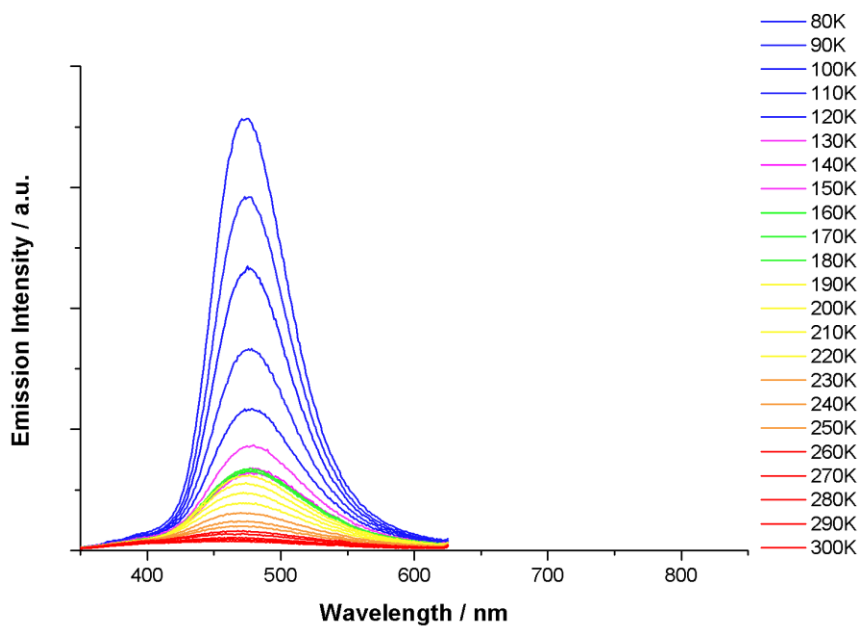


Figure SII.29 : Temperature dependence of the emission spectrum of the polymer C₁ from 80 K to 300 K.

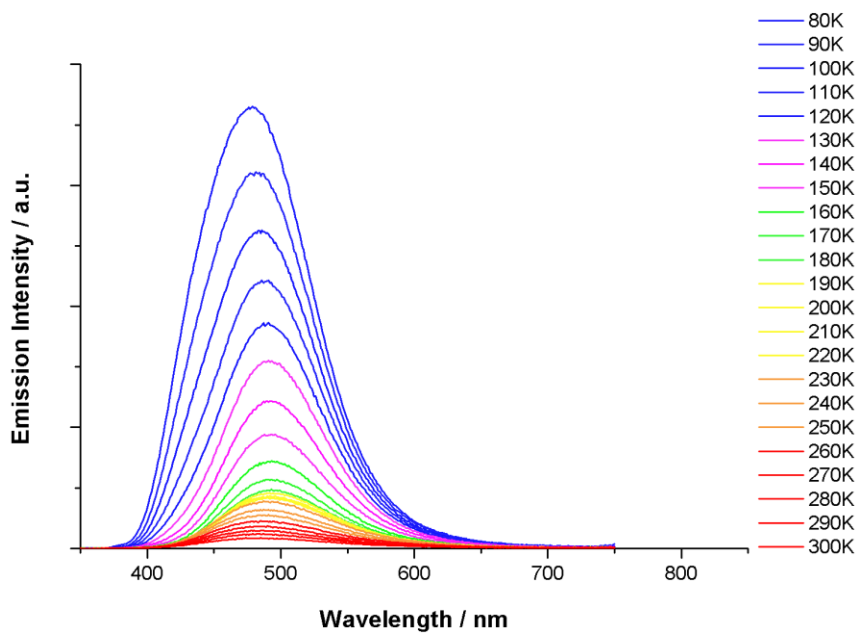


Figure SII.30 : Temperature dependence of the emission spectrum of the polymer C₂ from 80 K to 300 K.

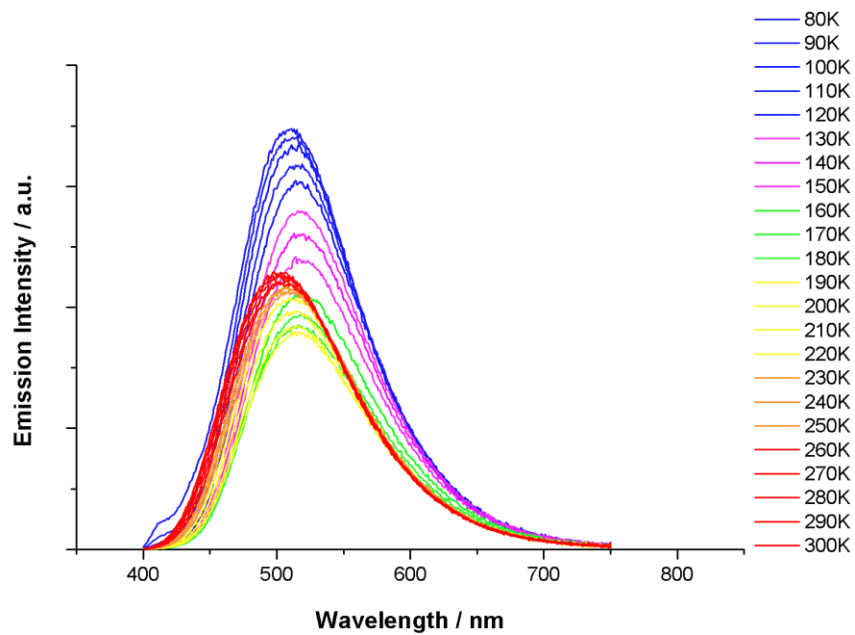


Figure SII.31 : Temperature dependence of the emission spectrum of the polymer C₃ from 80 K to 300 K.

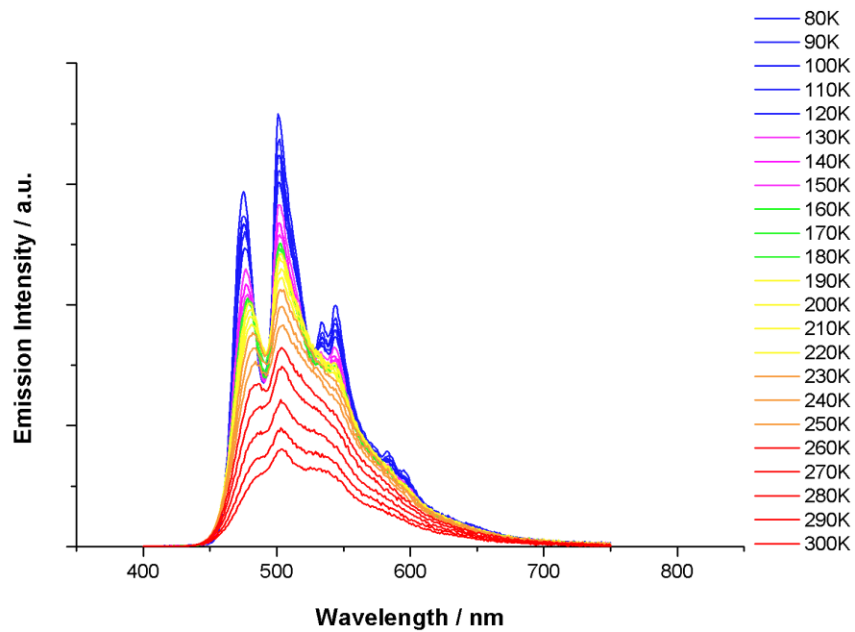


Figure SII.32 : Temperature dependence of the emission spectrum of the polymer C₄ from 80 K to 300 K.

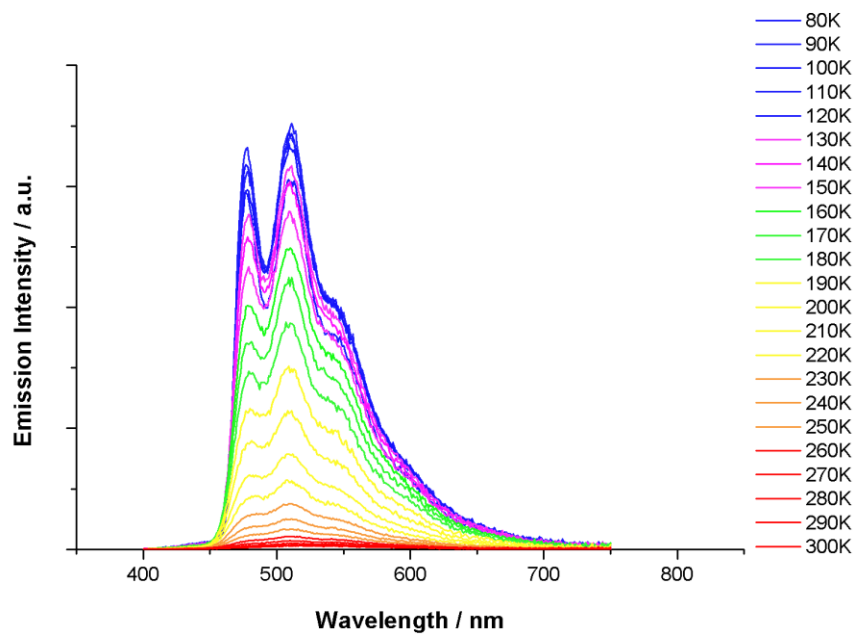


Figure SII.33 : Temperature dependence of the emission spectrum of the polymer C₅ from 80 K to 300 K.

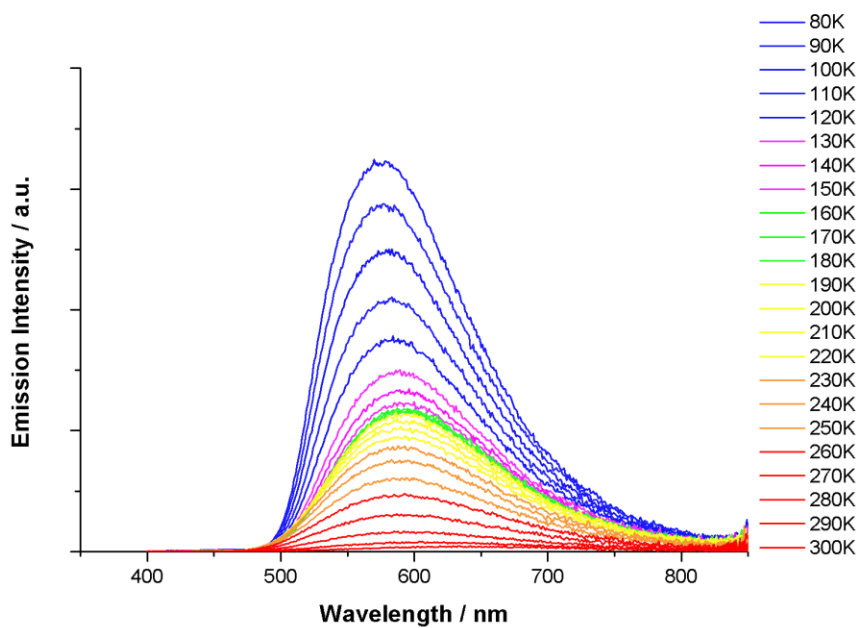


Figure SII.34 : Temperature dependence of the emission spectrum of the polymer C₆ from 80 K to 300 K.

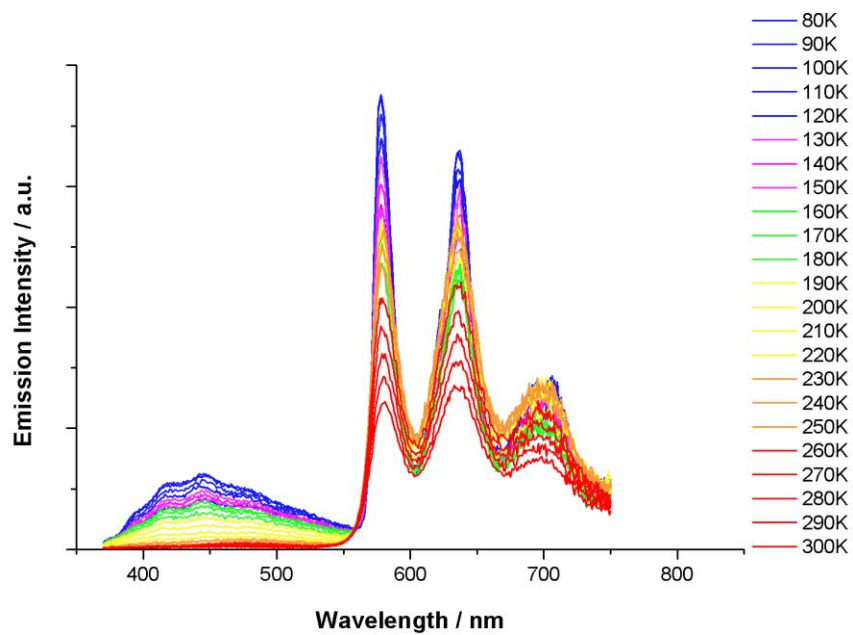


Figure SII.35 : Temperature dependence of the emission spectrum of the polymer C_7 from 80 K to 300 K.

II-4.4 Solid-state temperature dependant excited states lifetimes

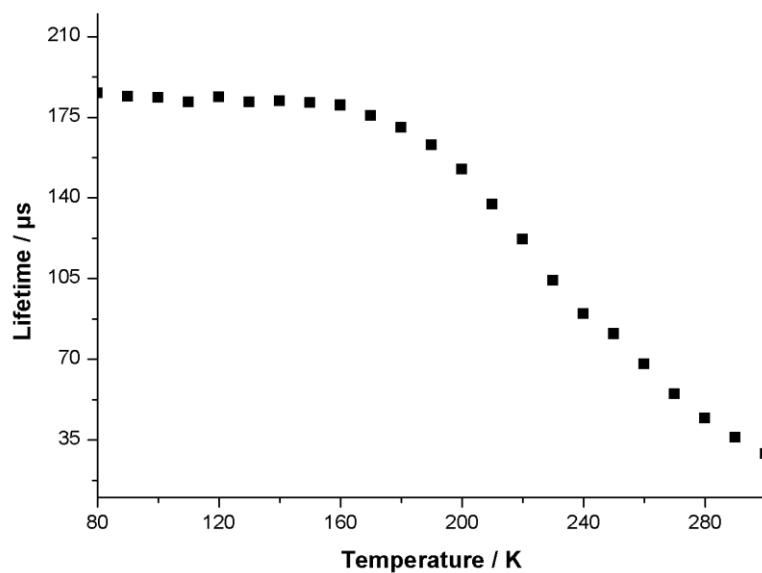


Figure SII.36 : Variation of the lifetime depending on the temperature of C_1 from 80 to 300 K

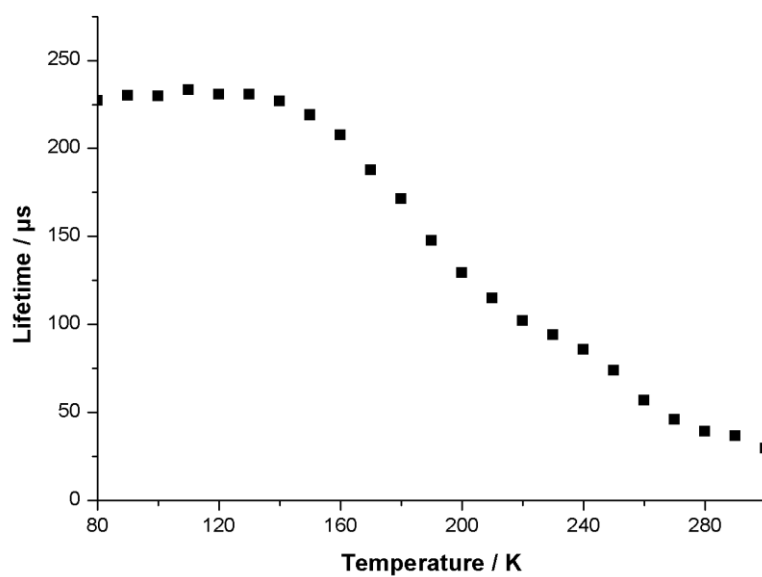


Figure SII.37 : Variation of the lifetime depending on the temperature of C_2 from 80 to 300 K

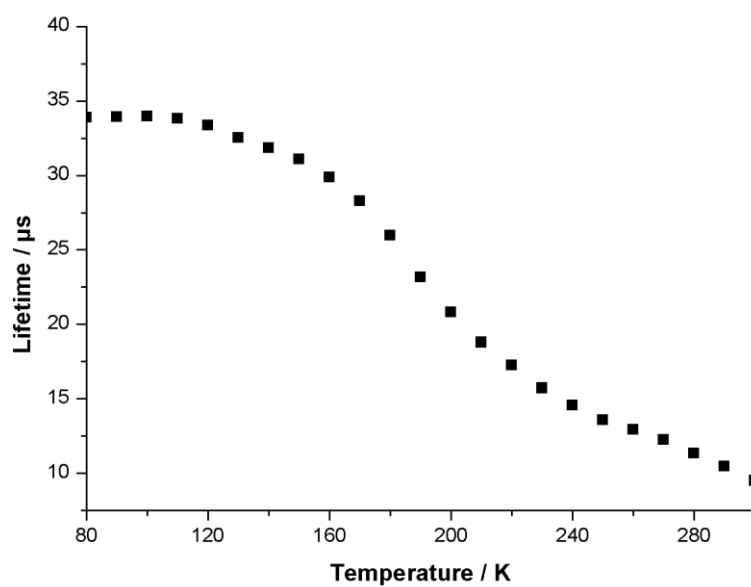


Figure SII.38 : Variation of the lifetime depending on the temperature of C_3 from 80 to 300 K

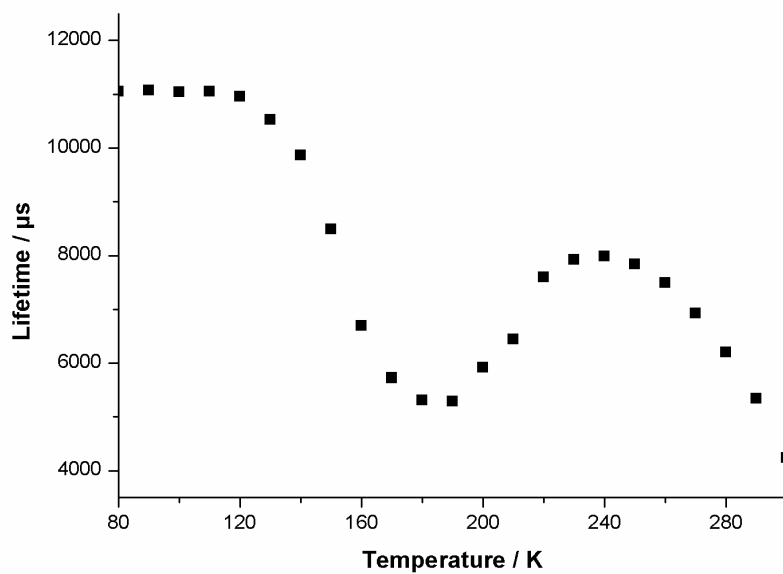


Figure SII.39 : Variation of the lifetime depending on the temperature of C_4 from 80 to 300 K

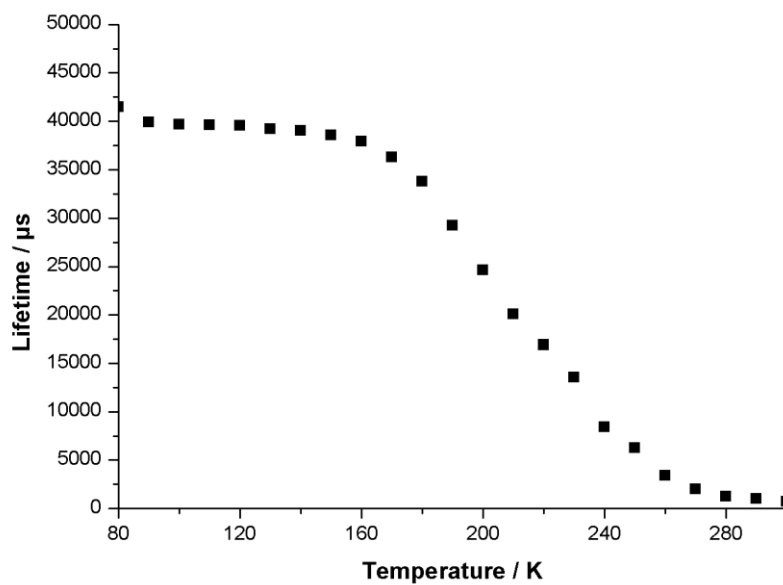


Figure SII.40 : Variation of the lifetime depending on the temperature of C_5 from 80 to 300 K

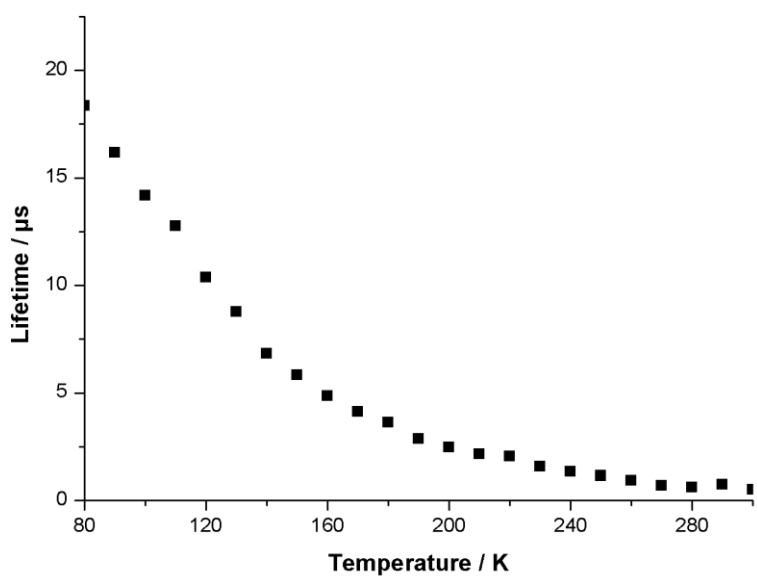


Figure SII.41 : Variation of the lifetime depending on the temperature of C₆ from 80 to 300 K

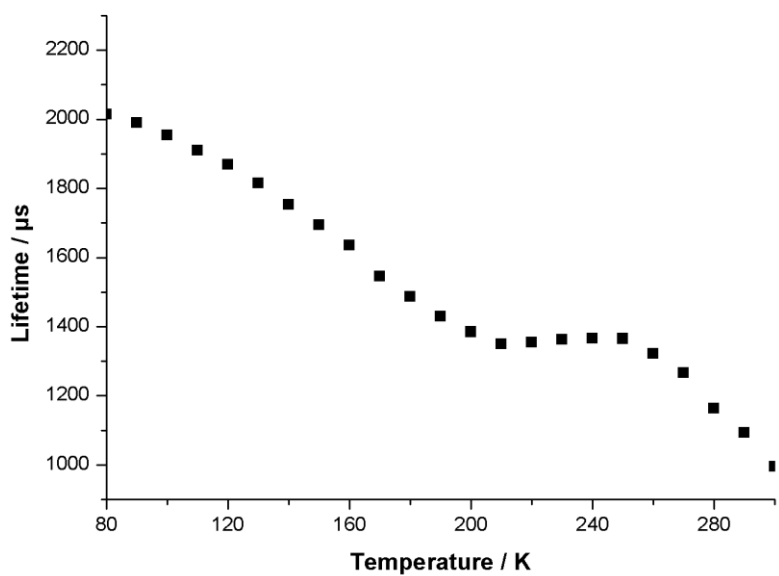


Figure SII.42 : Variation of the lifetime depending on the temperature of C₇ from 80 to 300 K

II-4.5 Solid-state variation of the luminance depending of the irradiance

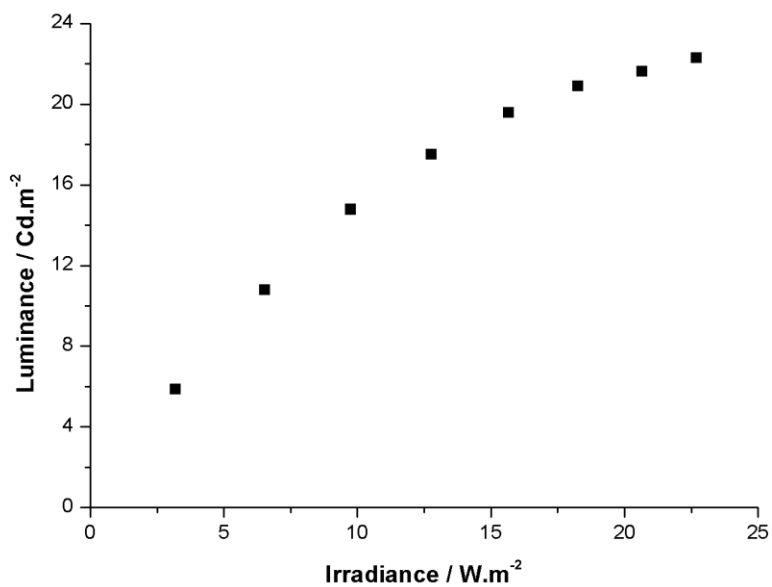


Figure SII.43 : Variation of the luminance of polymer C₁ depending on the irradiance.

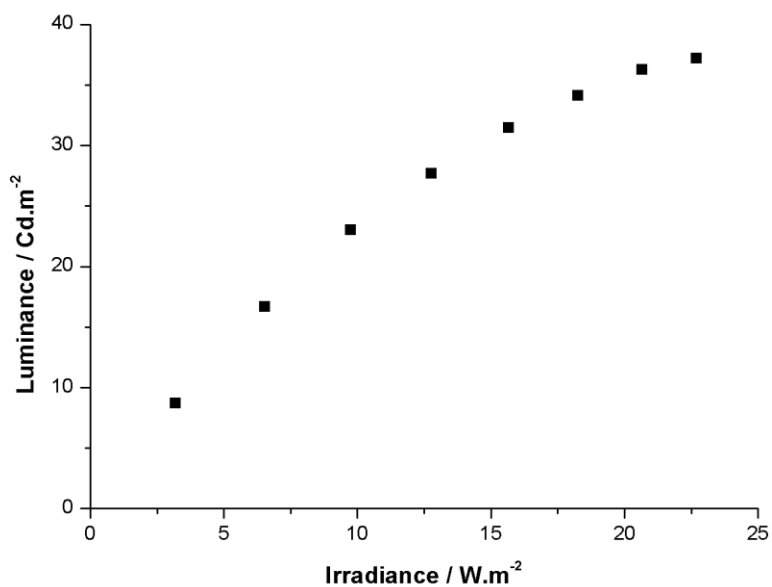


Figure SII.44 : Variation of the luminance of polymer C₂ depending on the irradiance.

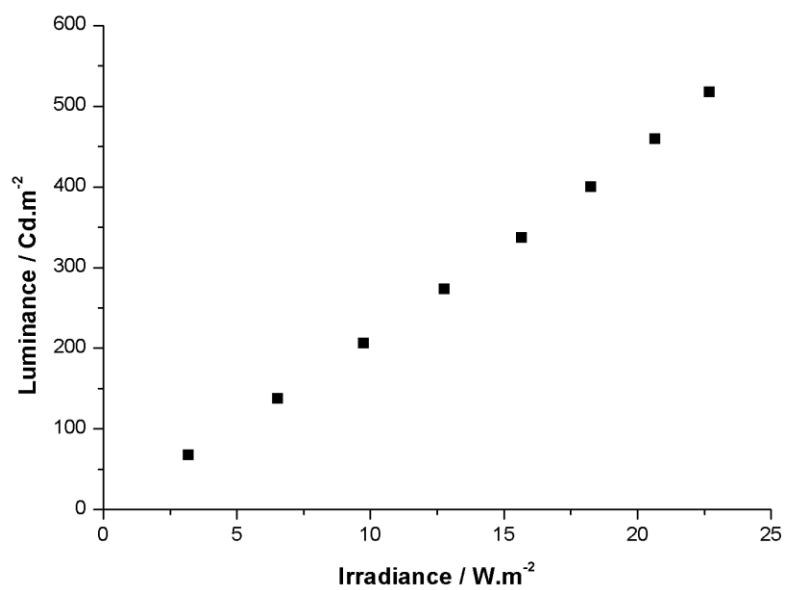


Figure SII.45 : Variation of the luminance of polymer C₃ depending on the irradiance.

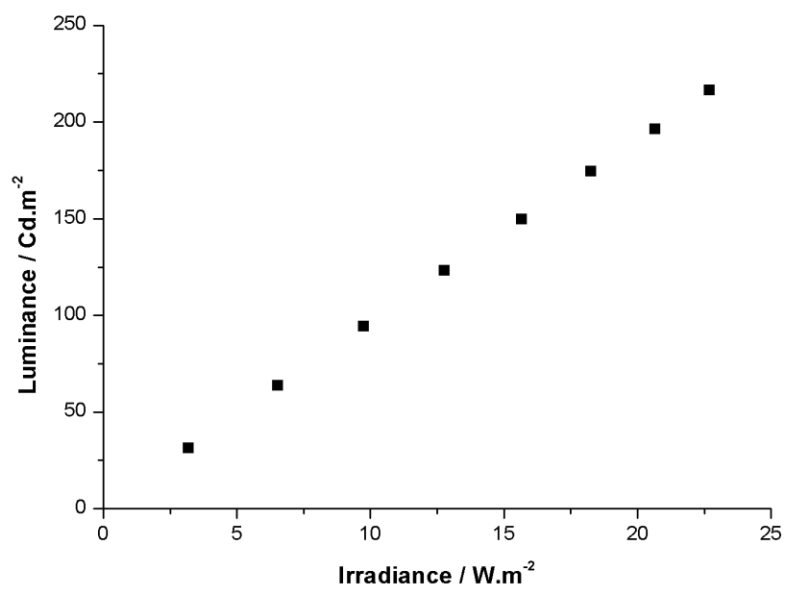


Figure SII.46 : Variation of the luminance of polymer C₄ depending on the irradiance.

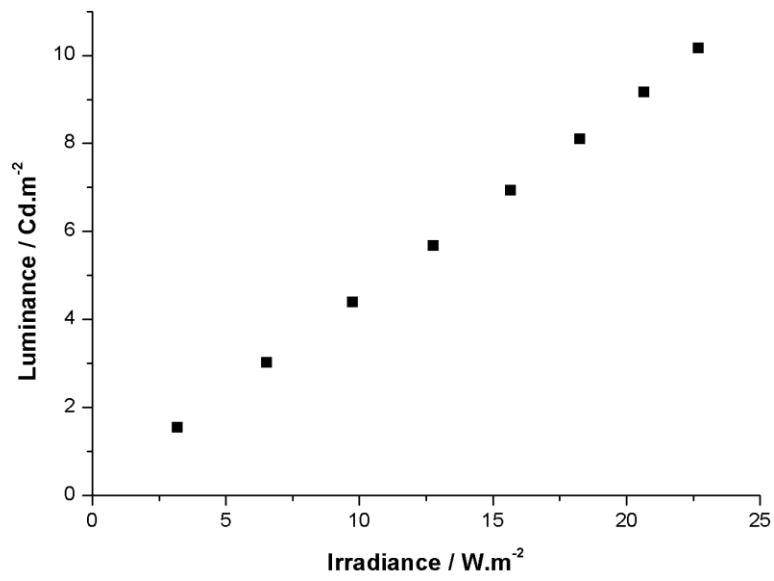


Figure SII.47 : Variation of the luminance of polymer C₅ depending on the irradiance.

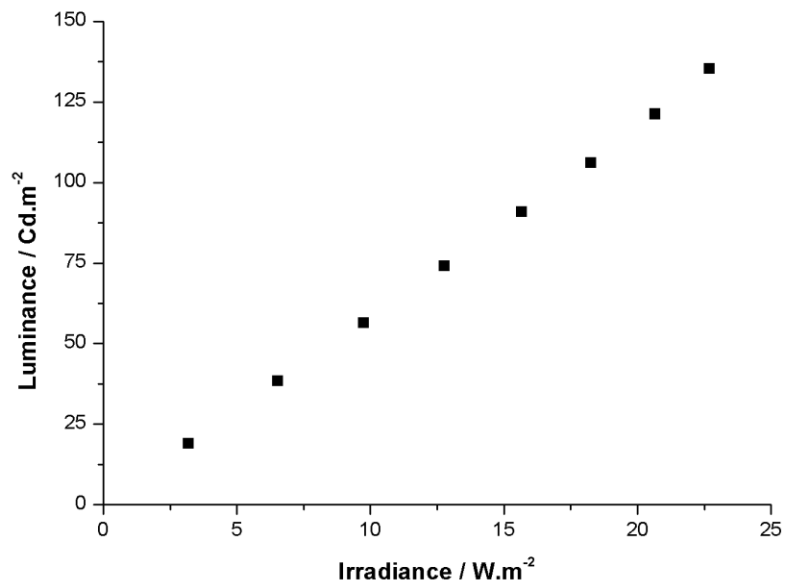


Figure SII.48 : Variation of the luminance of polymer C₆ depending on the irradiance.

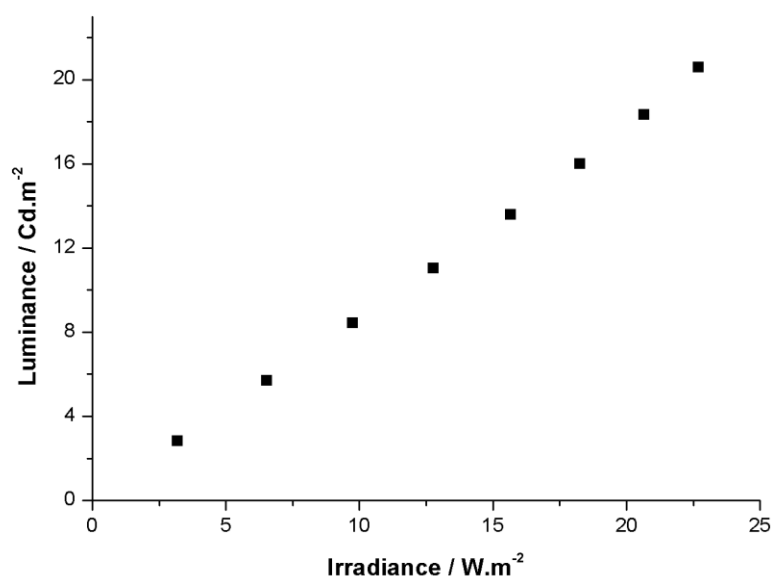


Figure SII.49 : Variation of the luminance of polymer **C₇** depending on the irradiance.

II-5 TGA-DTA measurements

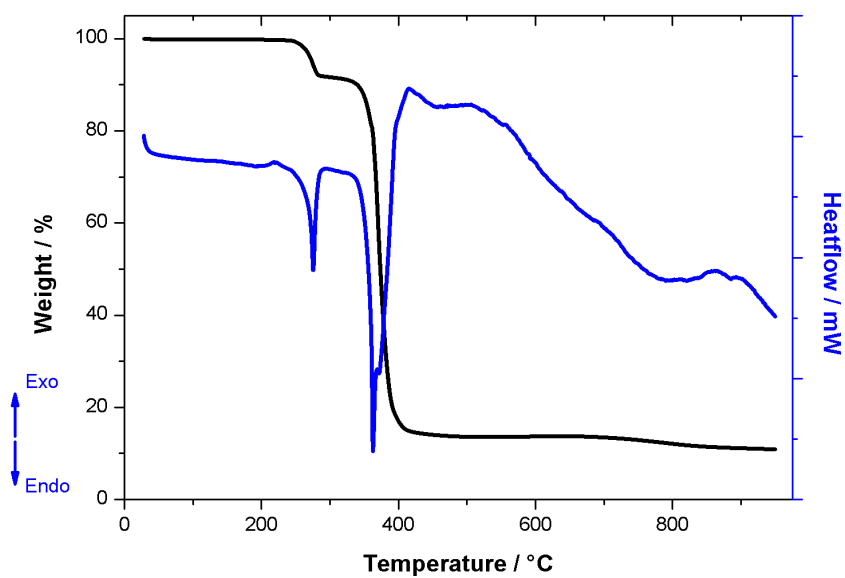


Figure SII.50 : TGA-DTA analysis of **C₁** compound until 950 °C.

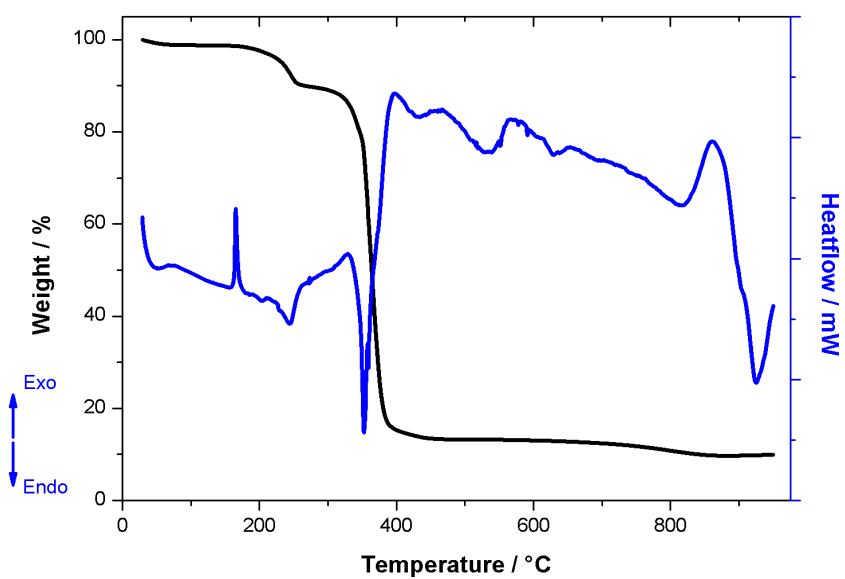


Figure SII.51 : TGA-DTA analysis of C_2 compound until 950 °C.

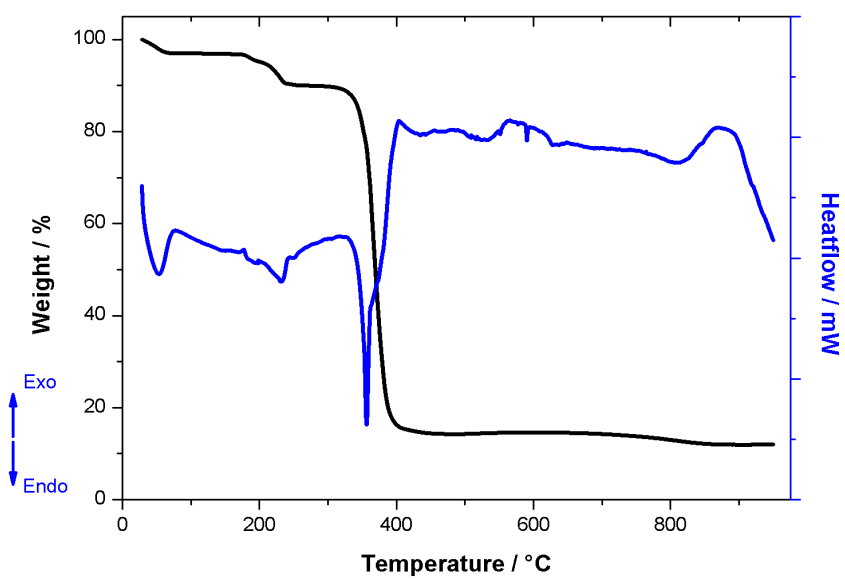


Figure SII.52 : TGA-DTA analysis of C_3 compound until 950 °C.

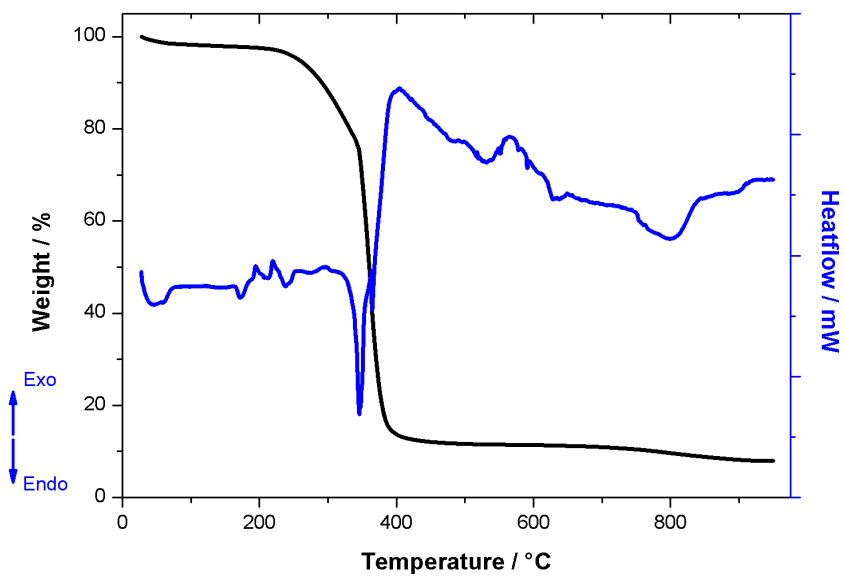


Figure SII.53 : TGA-DTA analysis of C_4 compound until 950 °C.

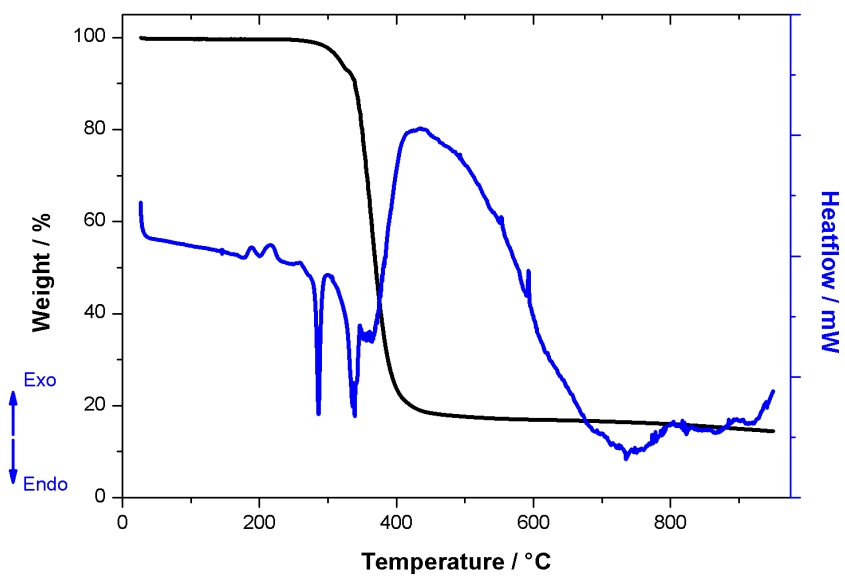


Figure SII.54 : TGA-DTA analysis of C_5 compound until 950 °C.

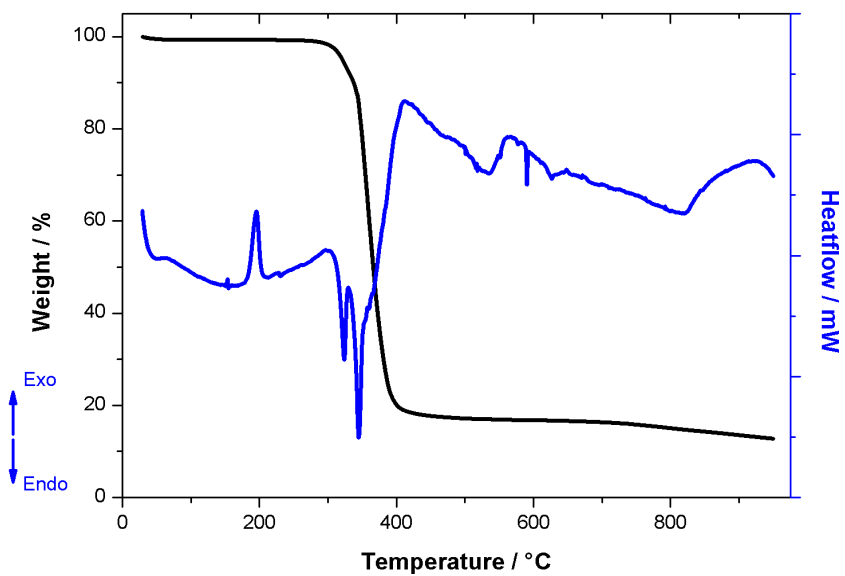


Figure SII.55 : TGA-DTA analysis of C_6 compound until 950 °C.

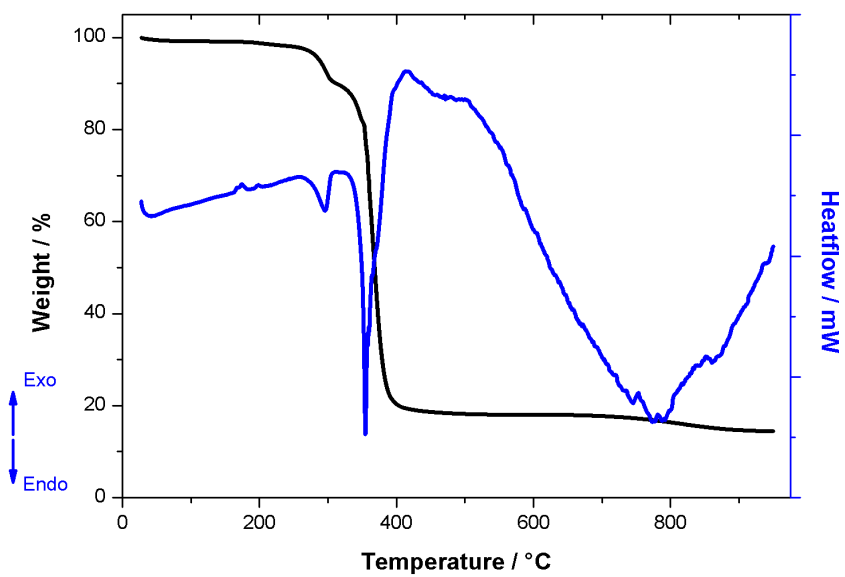


Figure SII.56 : TGA-DTA analysis of C_7 compound until 950 °C.

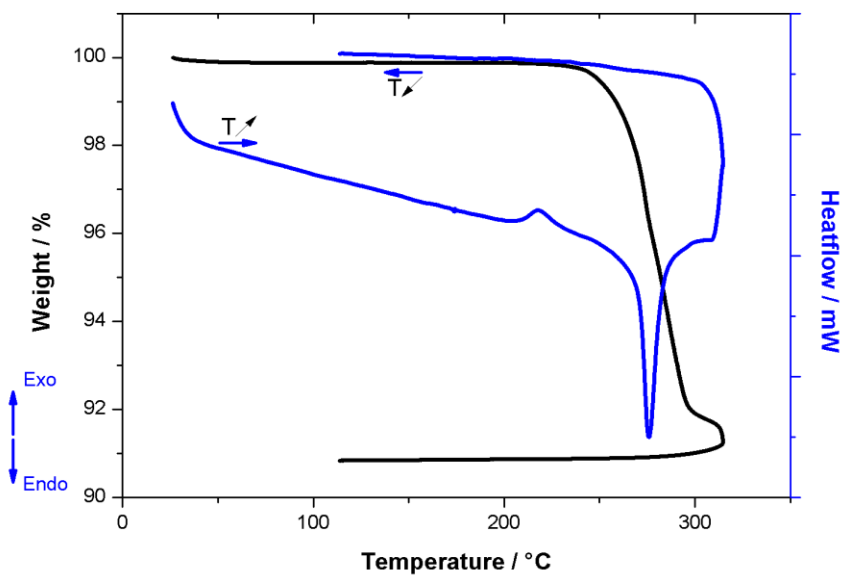


Figure SII.57 : TGA-DTA analysis of compound C₁ until 300 °C and record of the return to room temperature.

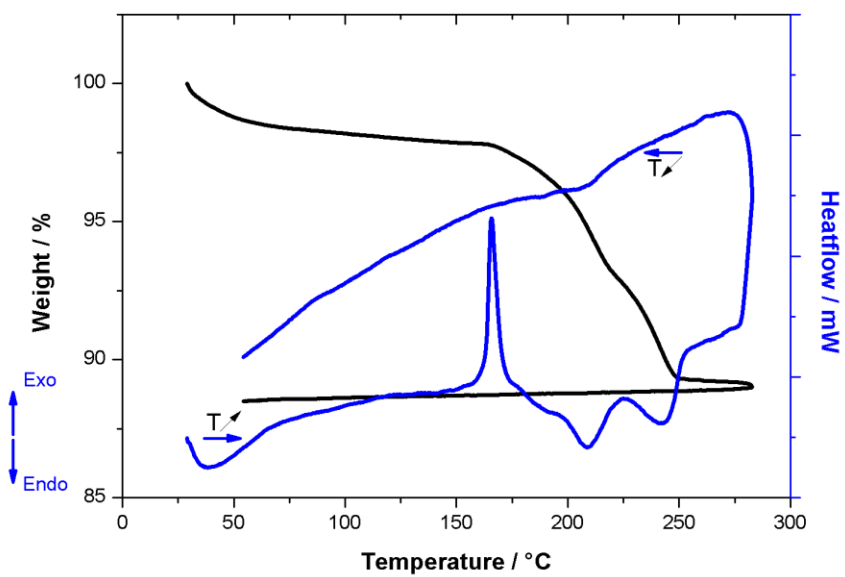


Figure SII.58 : TGA-DTA analysis of compound C₂ until 300 °C and record of the return to room temperature.

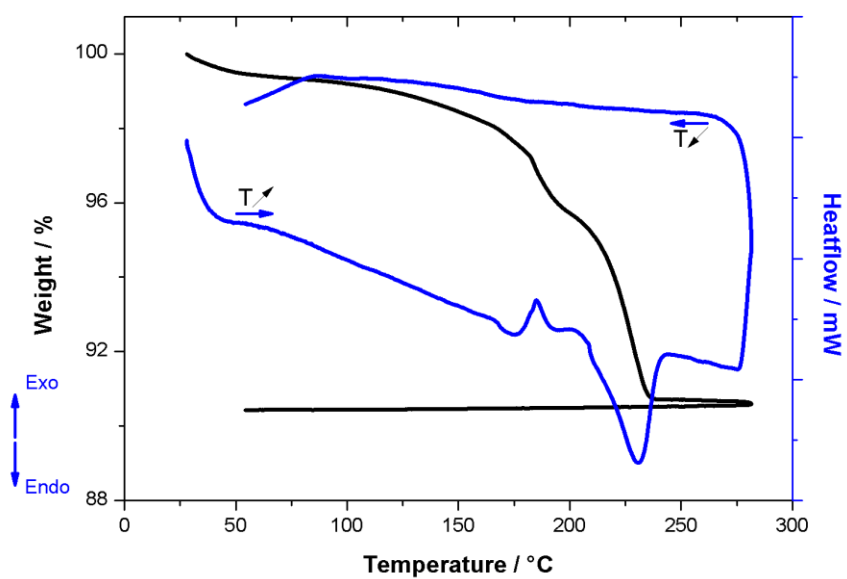


Figure SII.59 : TGA-DTA analysis of compound C₃ until 300 °C and record of the return to room temperature.

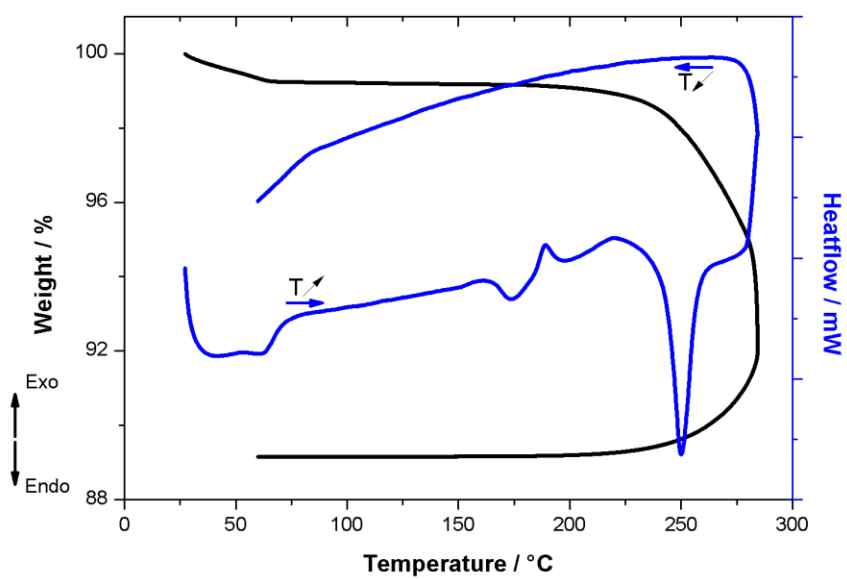


Figure SII.60 : TGA-DTA analysis of compound C₄ until 300 °C and record of the return to room temperature.

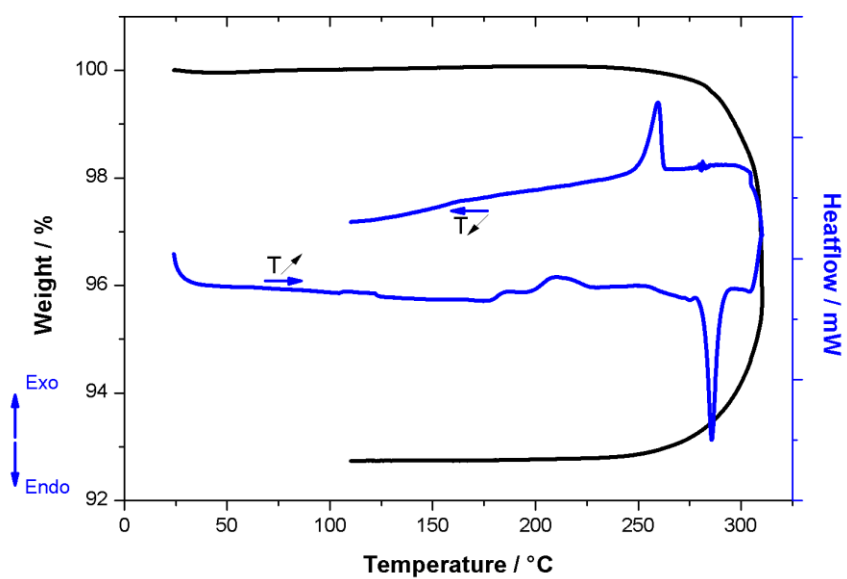


Figure SII.61 : TGA-DTA analysis of compound C₅ until 300 °C and record of the return to room temperature.

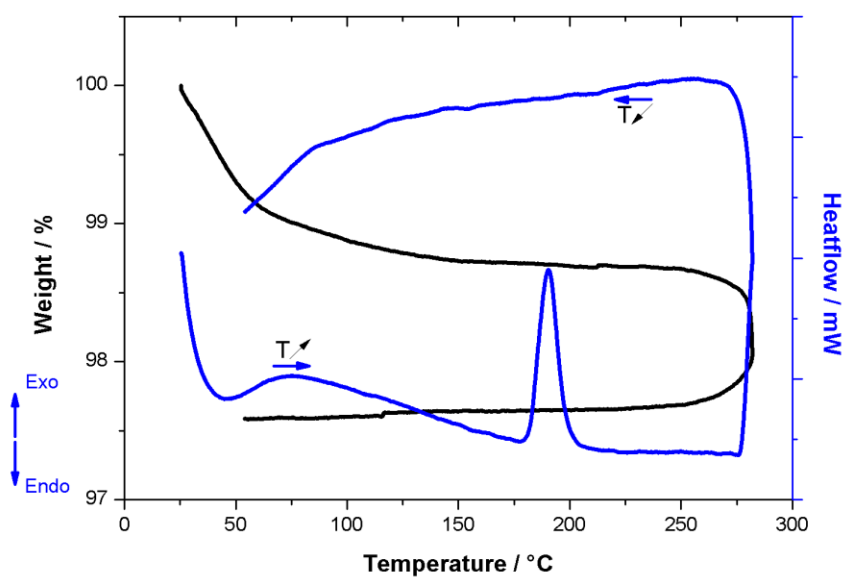


Figure SII.62 : TGA-DTA analysis of compound C₆ until 300 °C and record of the return to room temperature.

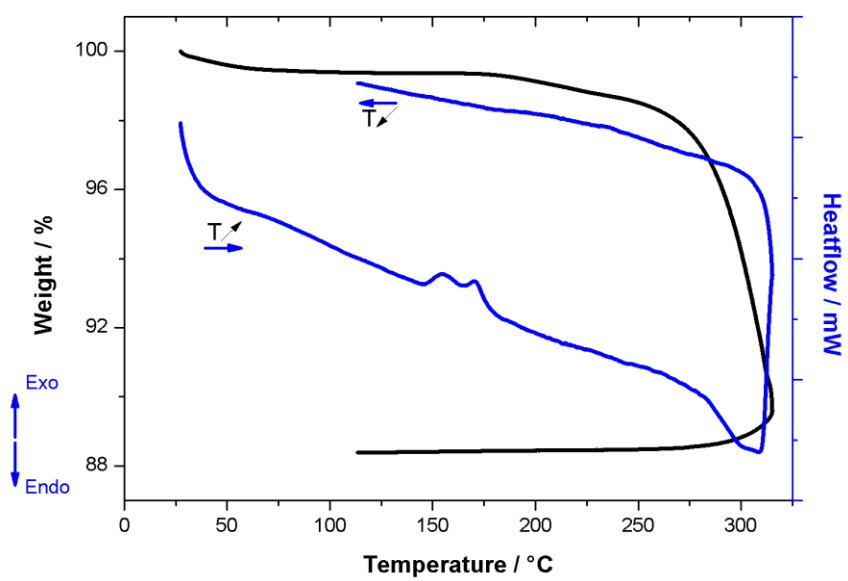


Figure SII.63 : TGA-DTA analysis of compound C₇ until 300 °C and record of the return to room temperature.

III-Appendix to chapter III :

III-1 Experimental conditions to obtain the transited phases phase A' and C_n'

The thermal transitions in the solid-state of precursor **A** to its transited phase **A'** and polymers **C_n** to their transited phases **C_n'** were performed on a heating plate. The crystalline powder of the initial phase is deposited and flattened on a glass plate then deposited on the heating plate. The evolution of the transition is followed by conducting the heating process under a UV lamp ($\lambda_{\text{ex}} = 365 \text{ nm}$). At high temperature, the luminescence displayed by the initial phase is faint, however, it is still possible to follow the transition with the naked eye. Once five minutes passed under heating at a temperature superior to the temperature of transition of the polymer, and once the transition can be observed, characterized for the heated phase by the emission of an eye-perceived blue colored light, the sample is taken out of heating and allowed to cool down to room temperature. This experiment is repeated once to allow a complete transition of the entirety of the processed sample. Concerning the the transition of the precursor **A**, the change in luminescence upon the thermal transition occurring is not perceptible by the naked eye, and the sample is simply maintained at 250 °C for the duration of the transition.

III-2 Infrared spectroscopy study of phases C_n '

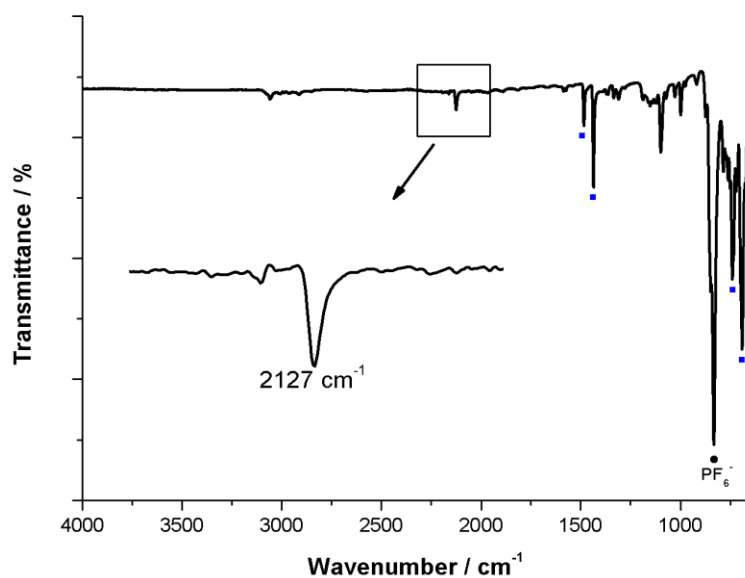


Figure SIII.1 : Infrared spectrum of compound C_1' . The dot marks the PF_6^- counter anion t_{1u} vibration mode band. Blue squares mark typical dppm $\delta_{(C-H)}$ ligand bands.

IR (cm^{-1}) : 690 (vs), 739 (vs), 762 (s), 785 (s), 832 (vs), 975 (vw), 999 (w), 1027 (w), 1072 (w), 1099 (m), 1188 (vw), 1310 (w), 1335 (vw), 1364 (vw), 1436 (s), 1484 (m), 1575 (vw), 1587 (vw), 2127 (m), 3059 (w).

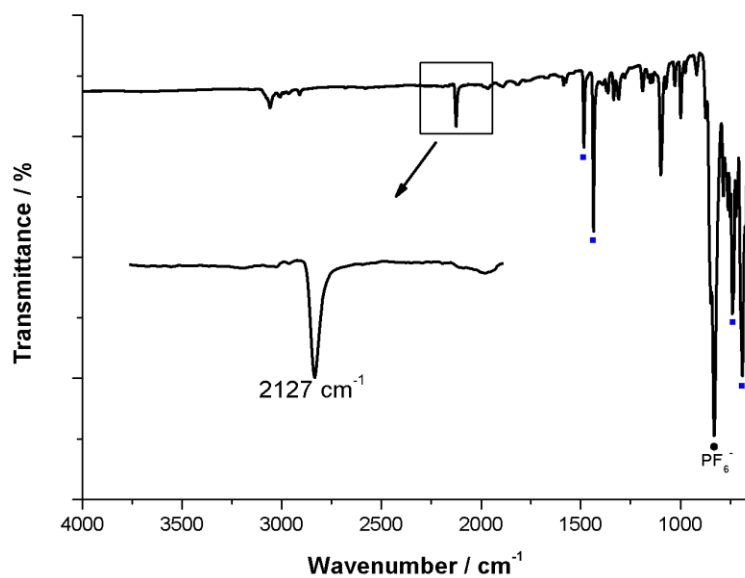


Figure SIII.2 : Infrared spectrum of compound C_2' . The dot marks the PF_6^- counter anion t_{1u} vibration mode band. Blue squares mark typical dppm $\delta_{(C-H)}$ ligand bands.

IR (cm^{-1}) : 689 (vs), 739 (vs), 785 (s), 831 (vs), 918 (w), 975 (vw), 999 (m), 1028 (w), 1073 (w), 1098 (m), 1140 (vw), 1152 (vw), 1190 (w), 1310 (w), 1335 (vw), 1364 (vw), 1436 (s), 1484 (m), 1575 (vw), 1587 (vw), 2127 (m), 3060 (w).

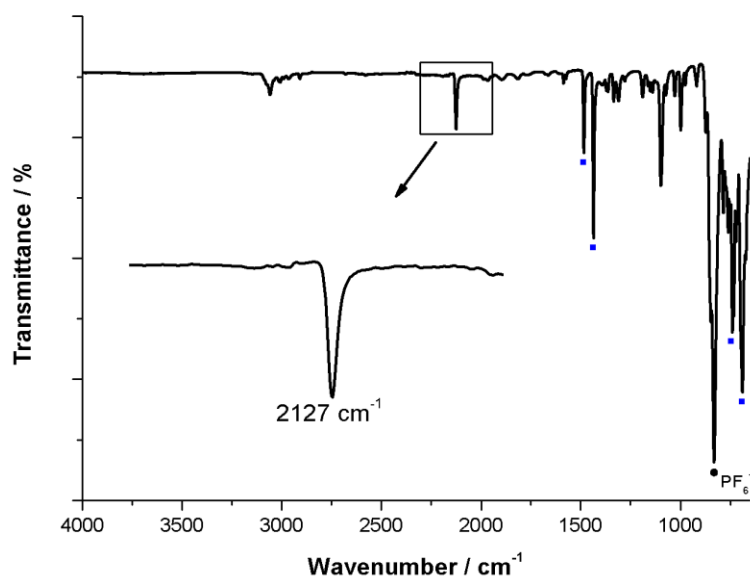


Figure SIII.3 : Infrared spectrum of compound C_3 . The dot marks the PF_6^- counter anion t_{1u} vibration mode band. Blue squares mark typical dppm $\delta_{(C-H)}$ ligand bands.

IR (cm^{-1}) : 689 (vs), 739 (vs), 786 (s), 831 (vs), 919 (w), 975 (vw), 999 (m), 1028 (w), 1073 (w), 1098 (m), 1140 (vw), 1152 (vw), 1191 (w), 1311 (w), 1335 (w), 1364 (vw), 1436 (s), 1484 (m), 1575 (vw), 1587 (vw), 2127 (m), 3060 (w).

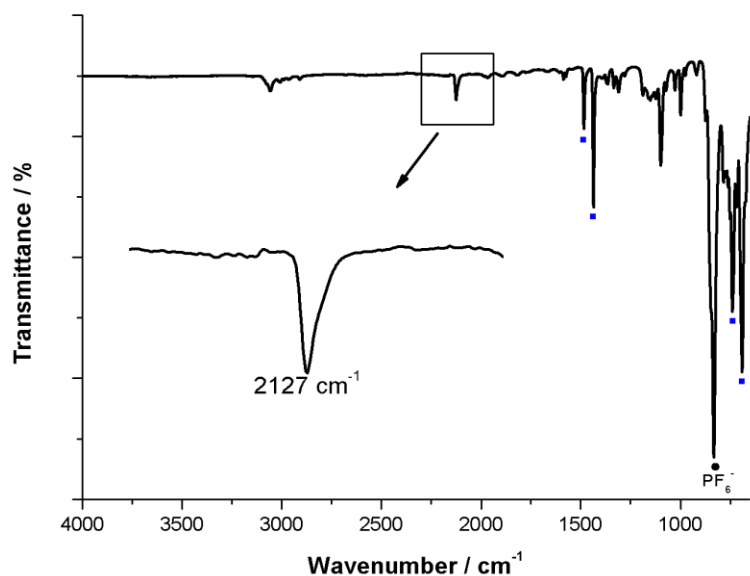


Figure SIII.4 : Infrared spectrum of compound C_4 . The dot marks the PF_6^- counter anion t_{1u} vibration mode band. Blue squares mark typical dppm $\delta_{(C-H)}$ ligand bands.

IR (cm^{-1}) : 690 (vs), 739 (vs), 785 (s), 833 (vs), 919 (w), 975 (vw), 1000 (m), 1027 (w), 1072 (w), 1099 (m), 1141 (vw), 1152 (vw), 1189 (w), 1310 (w), 1335 (w), 1365 (vw), 1436 (s), 1484 (m), 1574 (vw), 1587 (vw), 2127 (m), 3059 (w).

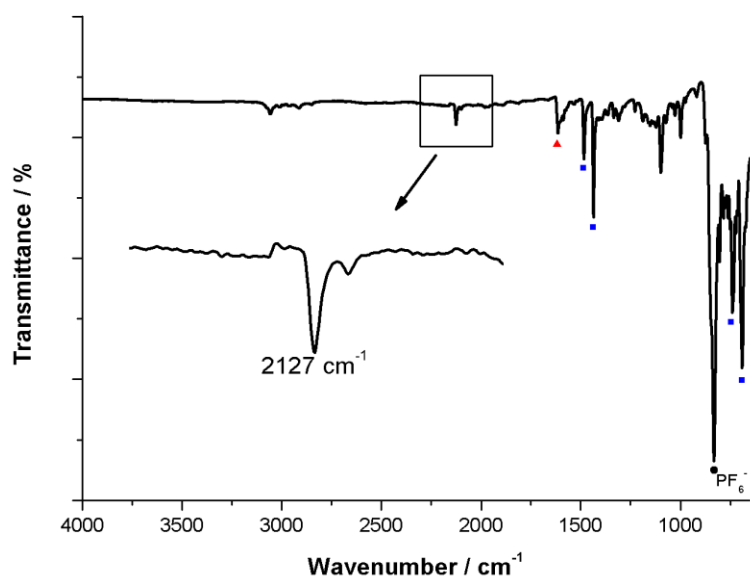


Figure SIII.5 : Infrared spectrum of compound **C₅²**. The dot marks the PF₆⁻ counter anion t_{1u} vibration mode band. Blue squares mark typical dppm δ_(C-H) ligand bands. Red triangles mark **B₅** ligands bands.

IR (cm⁻¹) : 690 (vs), 739 (vs), 785 (s), 832 (vs), 918 (w), 975 (vw), 999 (m), 1027 (w), 1072 (w), 1100 (m), 1140 (vw), 1152 (vw), 1189 (w), 1228 (w), 1310 (w), 1335 (w), 1364 (vw), 1436 (s), 1484 (m), 1574 (vw), 1588 (vw), 1615 (m), 2127 (m), 3059 (w).

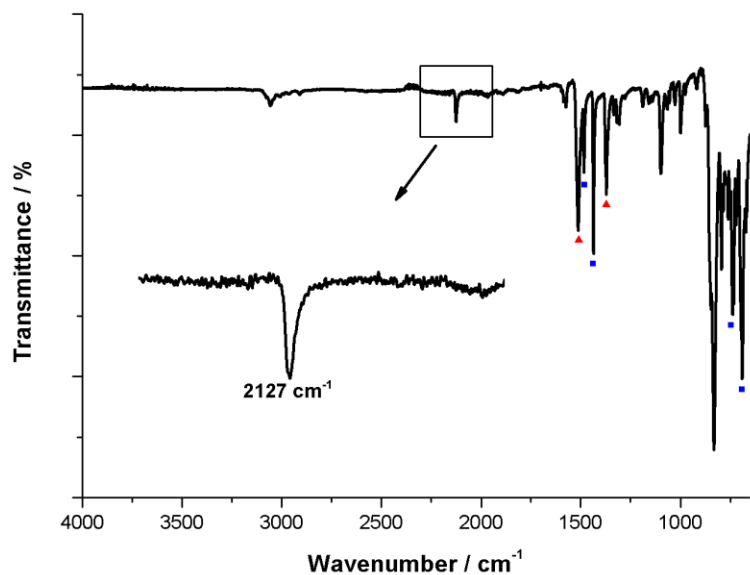


Figure SIII.6 : Infrared spectrum of compound **C₆²**. The dot marks the PF₆⁻ counter anion t_{1u} vibration mode band. Blue squares mark typical dppm δ_(C-H) ligand bands. Red triangles mark **B₆** ligands bands.

IR (cm⁻¹) : 691 (vs), 739 (vs), 794 (s), 832 (vs), 920 (w), 975 (vw), 1000 (m), 1027 (w), 1073 (w), 1098 (m), 1140 (vw), 1152 (vw), 1189 (w), 1307 (w), 1335 (w), 1372 (vw), 1436 (s), 1484 (m), 1513 (s), 1575 (w), 1586 (w), 2127 (m), 3058 (w).

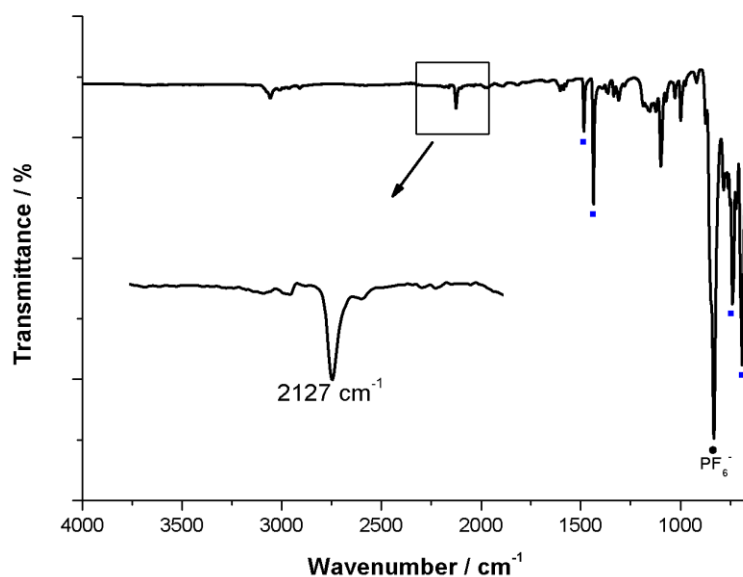


Figure SIII.7 : Infrared spectrum of compound **C7**. The dot marks the PF_6^- counter anion t_{1u} vibration mode band. Blue squares mark typical $\delta_{(\text{C-H})}$ ligand bands.

IR (cm^{-1}) : 690 (vs), 739 (vs), 784 (s), 832 (vs), 919 (w), 975 (vw), 999 (m), 1027 (w), 1072 (w), 1098 (m), 1123 (vw), 1187 (w), 1309 (w), 1335 (w), 1371 (vw), 1436 (s), 1484 (m), 1575 (w), 1587 (w), 2127 (m), 3059 (w).

III-3 Sublimation experiments on polymers C_n

Here are presented ^1H NMR spectra of the residues collected from the cold finger of the sublimation apparatus during experiments conducted on polymers C_1 - C_4 and C_7 . Along the thermal transition of C_5 and C_6 , the linker is not sublimated. Therefore, nothing is collected on the cold finger of the sublimation apparatus. Concerning C_7 , the thermal transition temperature being close to the degradation temperature, only a complex mixture of non-identified degradation residues were collected on the cold finger of the sublimation apparatus.

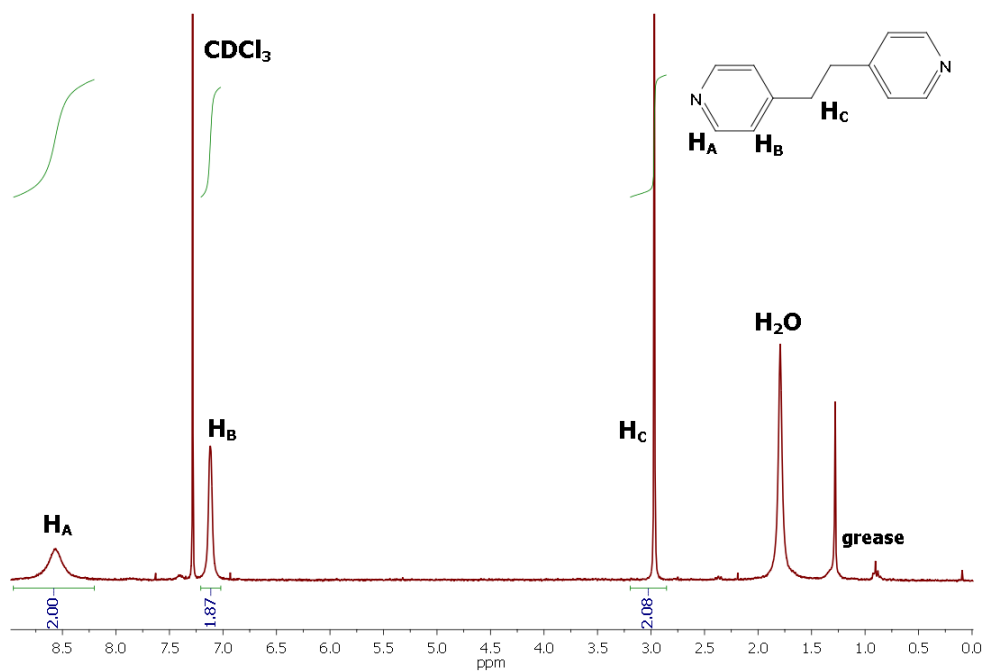


Figure SIII.8 : ¹H NMR spectrum of the linker B₁ residue in CDCl₃ collected on the cold finger of the sublimation apparatus, as the sample C₁ is heated above the transition temperature.

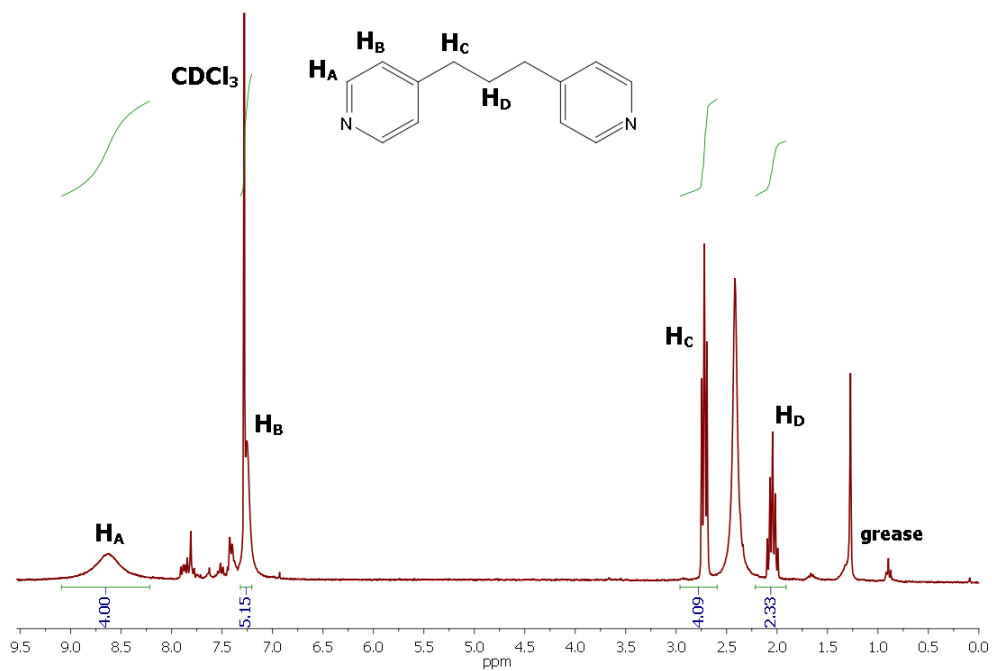


Figure SIII.9 : ¹H NMR spectrum of the linker B₂ residue in CDCl₃ collected on the cold finger of the sublimation apparatus, as the sample C₂ is heated above the transition temperature.

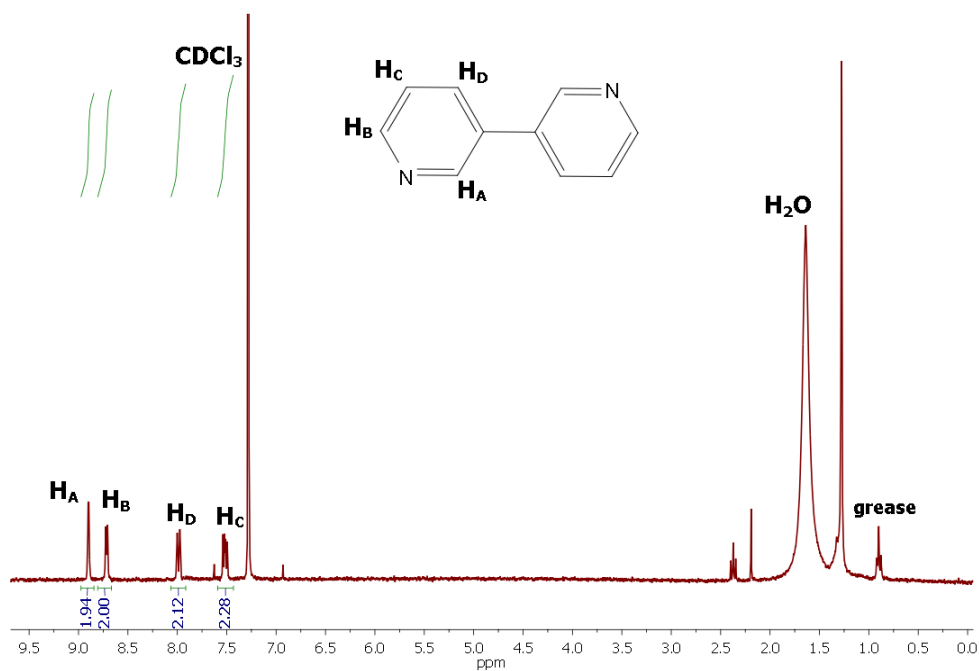


Figure SIII.10 : ^1H NMR spectrum of the linker B_3 residue in CDCl_3 collected on the cold finger of the sublimation apparatus, as the sample C_3 is heated above the transition temperature.

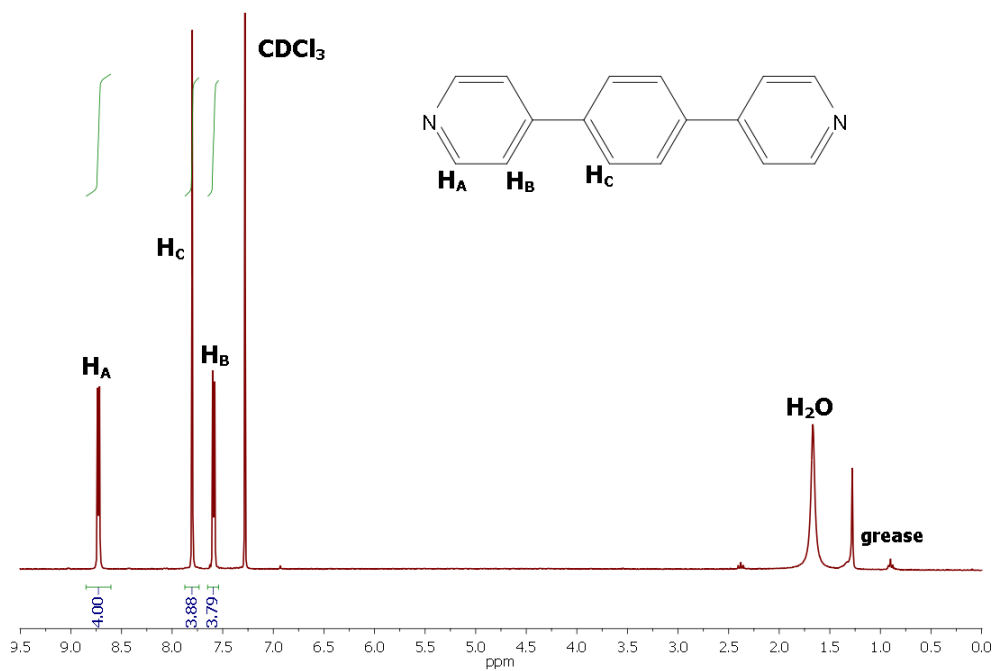


Figure SIII.11 : ^1H NMR spectrum of the linker B_4 residue in CDCl_3 collected on the cold finger of the sublimation apparatus, as the sample C_4 is heated above the transition temperature.

III-4 Photophysical study of phases C_n'

III-4.1 Solid-state UV-visible absorption

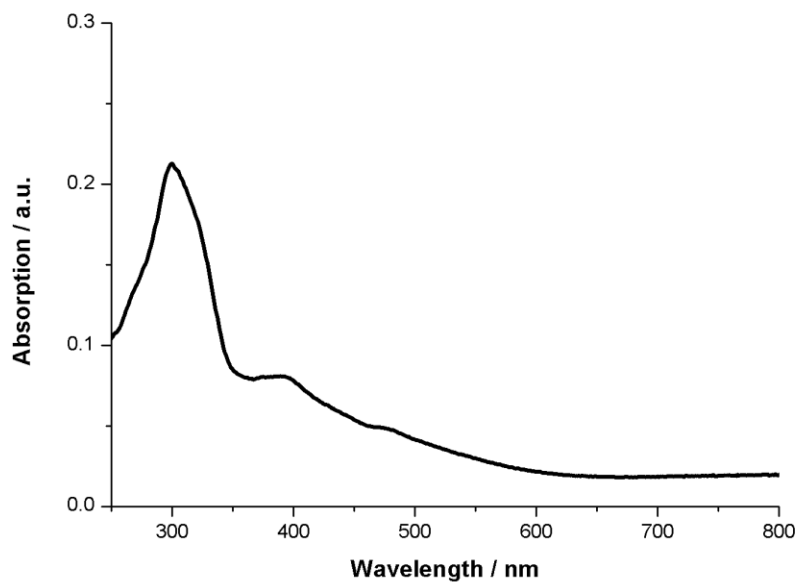


Figure SIII.12 : Solid-state UV-visible absorption spectrum of C₁'.

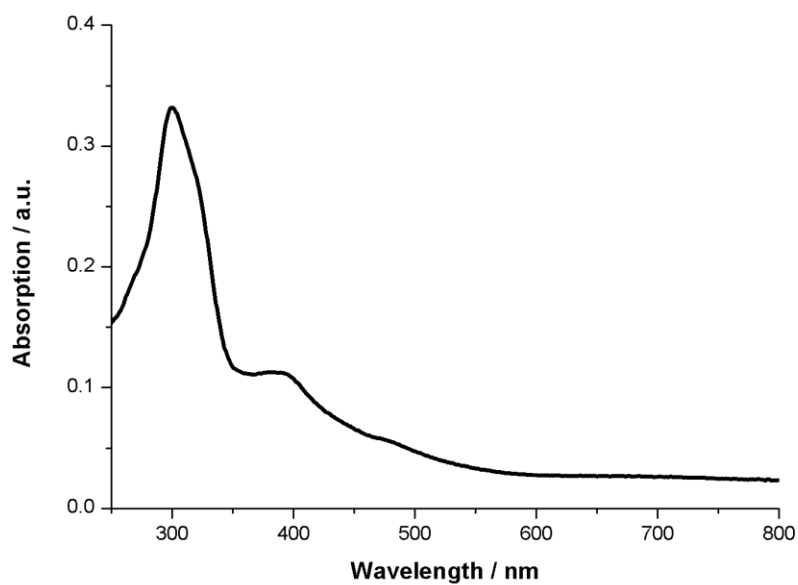


Figure SIII.13 : Solid-state UV-visible absorption spectrum of C₂'.

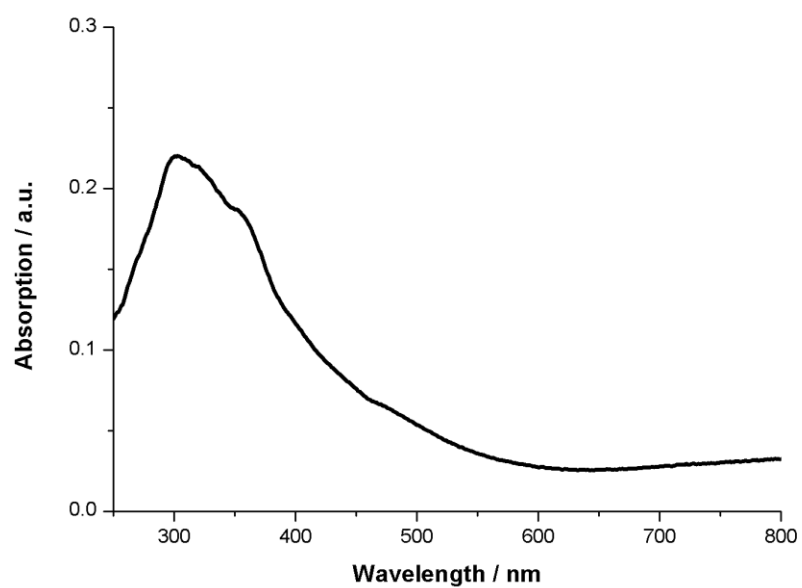


Figure SIII.14 : Solid-state UV-visible absorption spectrum of C3'.

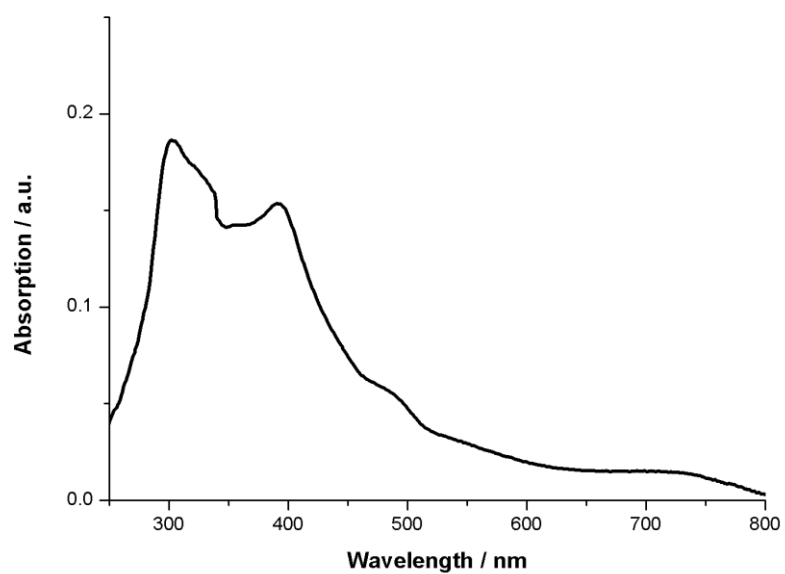


Figure SIII.15 : Solid-state UV-visible absorption spectrum of C4'.

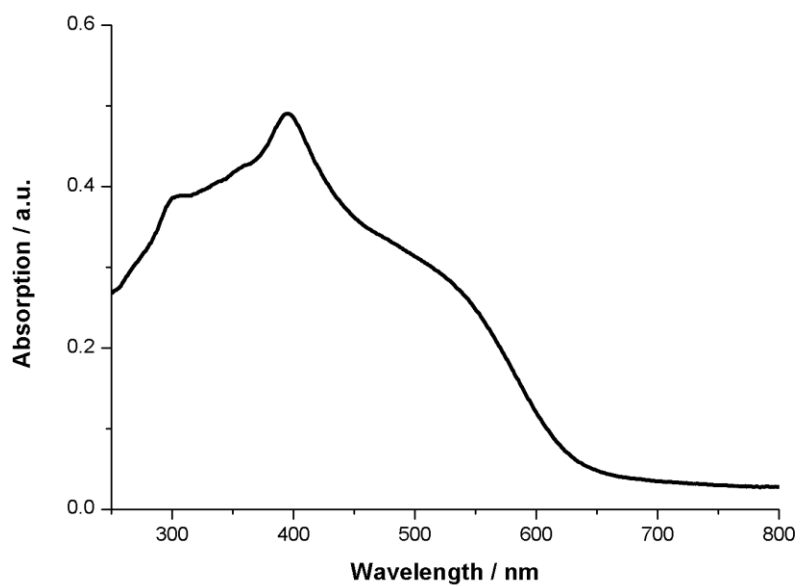


Figure SIII.16 : Solid-state UV-visible absorption spectrum of Cs².

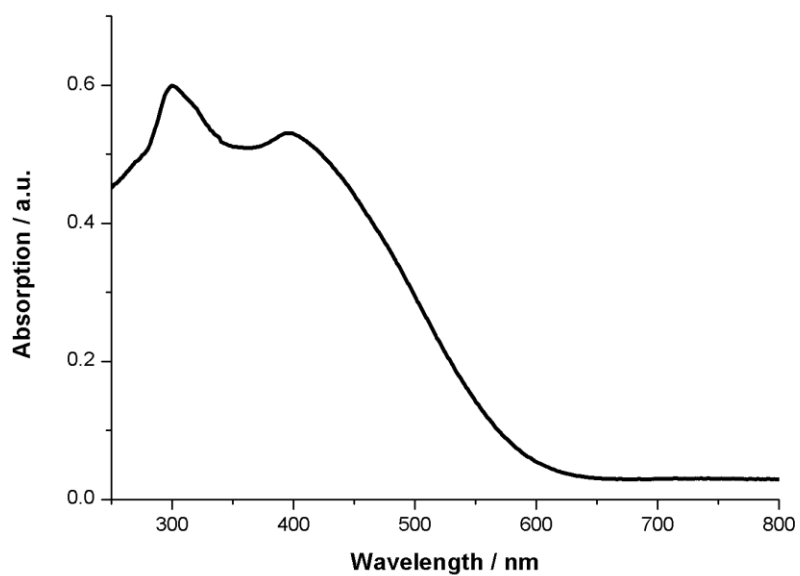


Figure SIII.17 : Solid-state UV-visible absorption spectrum of C₆².

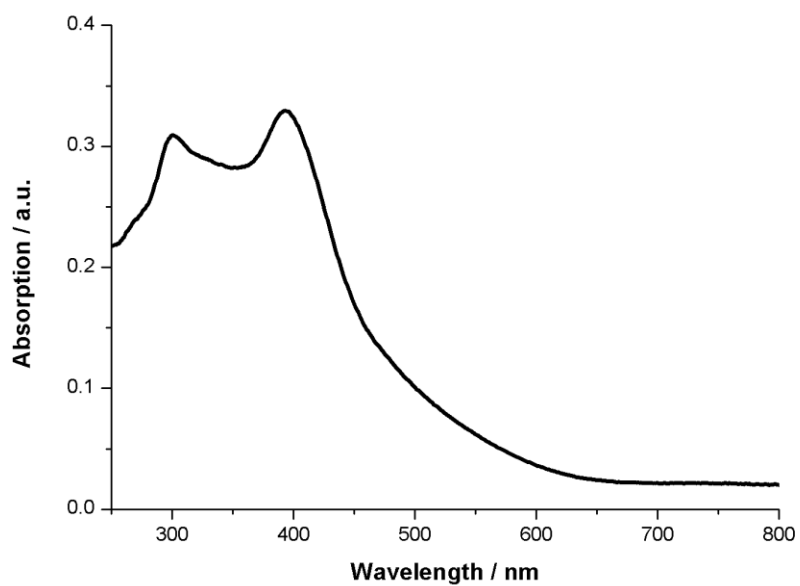


Figure SIII.18 : Solid-state UV-visible absorption spectrum of C_7' .

III-4.2 Solid-state excitation spectrum

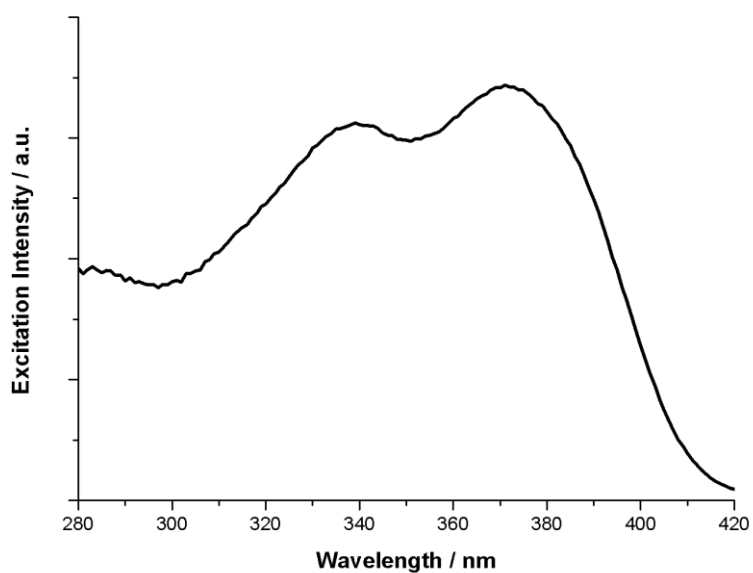


Figure SIII.19 : Solid-state room temperature excitation spectrum of phase C_1' .

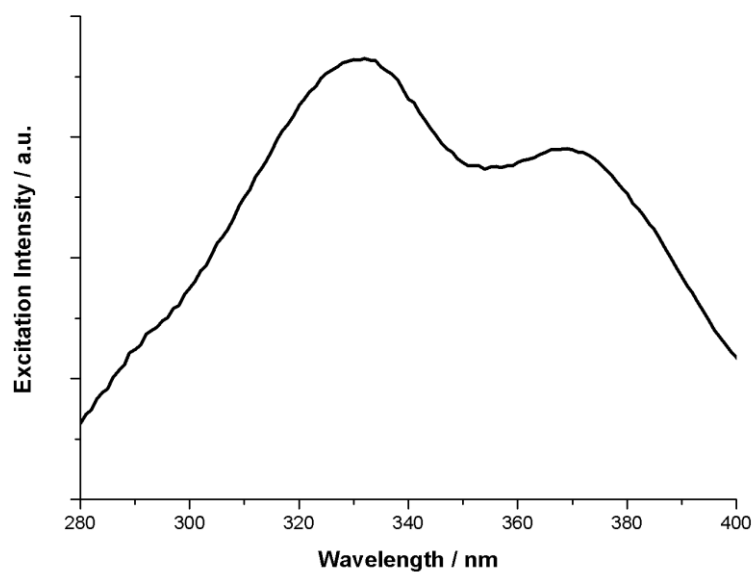


Figure SIII.20 : Solid-state room temperature excitation spectrum of phase C₂'.

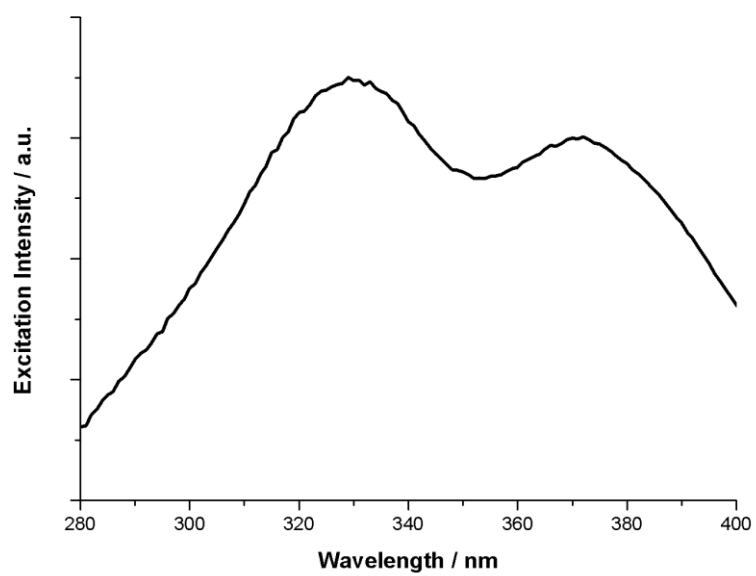


Figure SIII.21 : Solid-state room temperature excitation spectrum of phase C₃'.

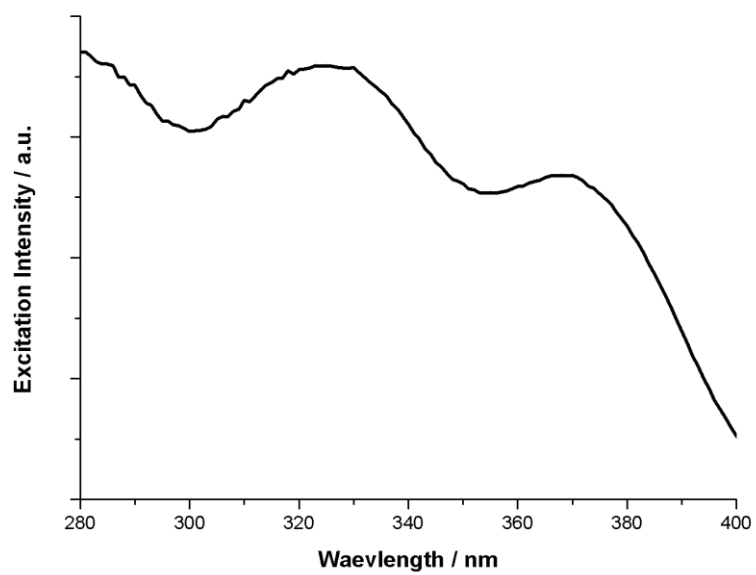


Figure SIII.22 : Solid-state room temperature excitation spectrum of phase C4'.

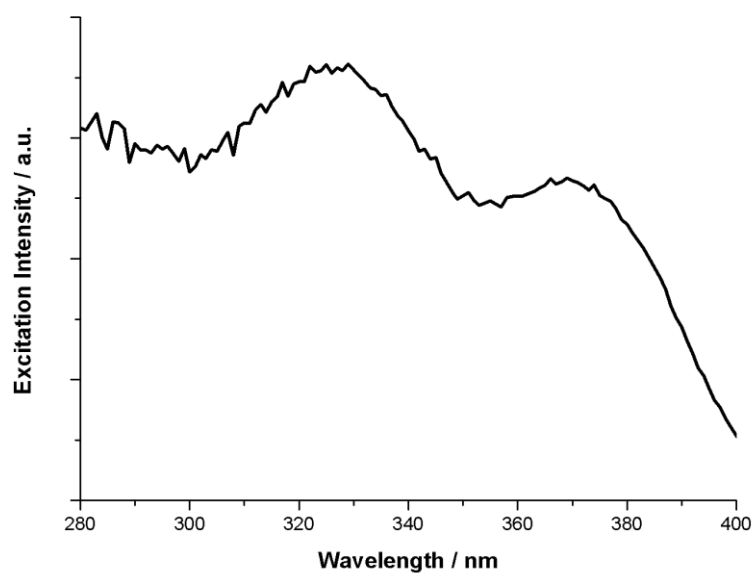


Figure SIII.23 : Solid-state room temperature excitation spectrum of phase C5'.

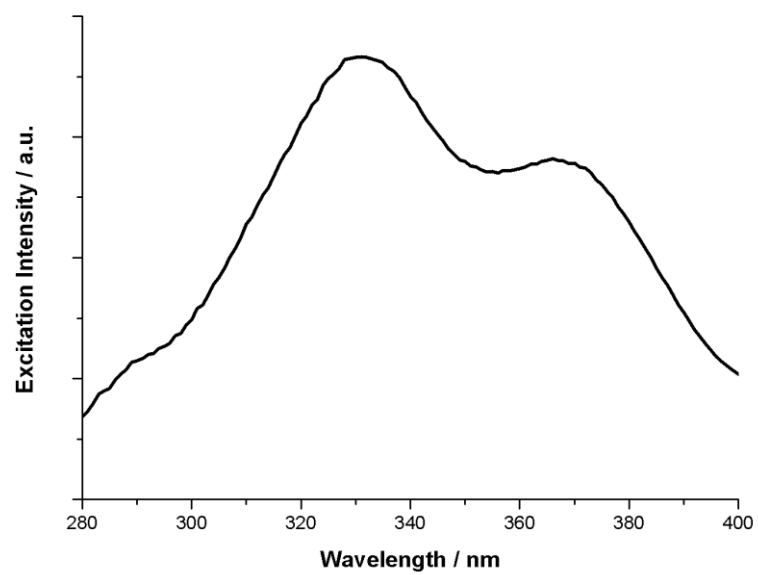


Figure SIII.24 : Solid-state room temperature excitation spectrum of phase C6'.

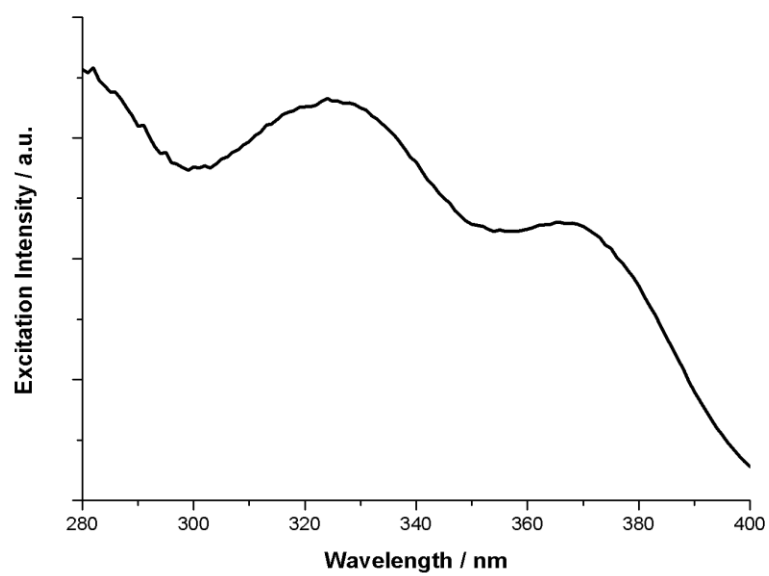


Figure SIII.25 : Solid-state room temperature excitation spectrum of phase C7'.

III-4.3 Temperature dependant emission spectrum

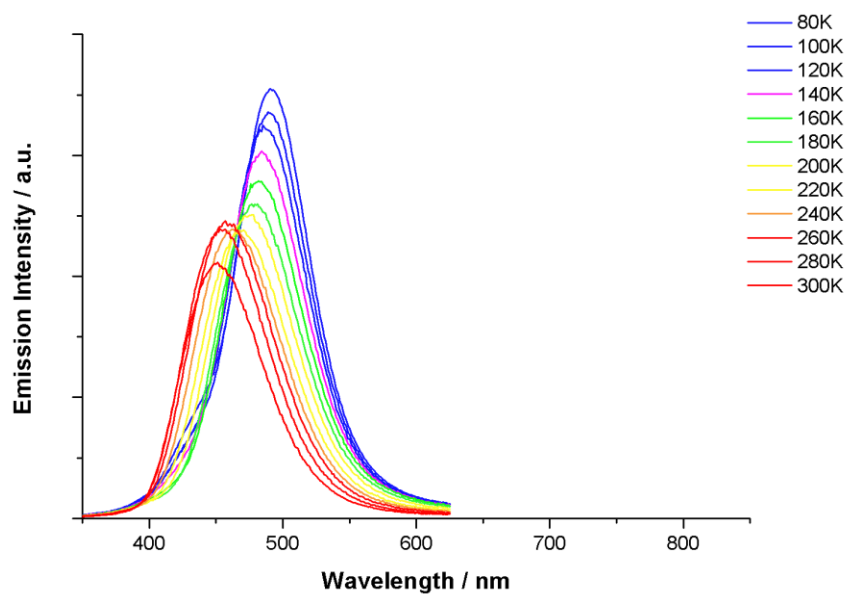


Figure SIII.26 : Temperature dependence of the emission spectrum of transited phase C₁.

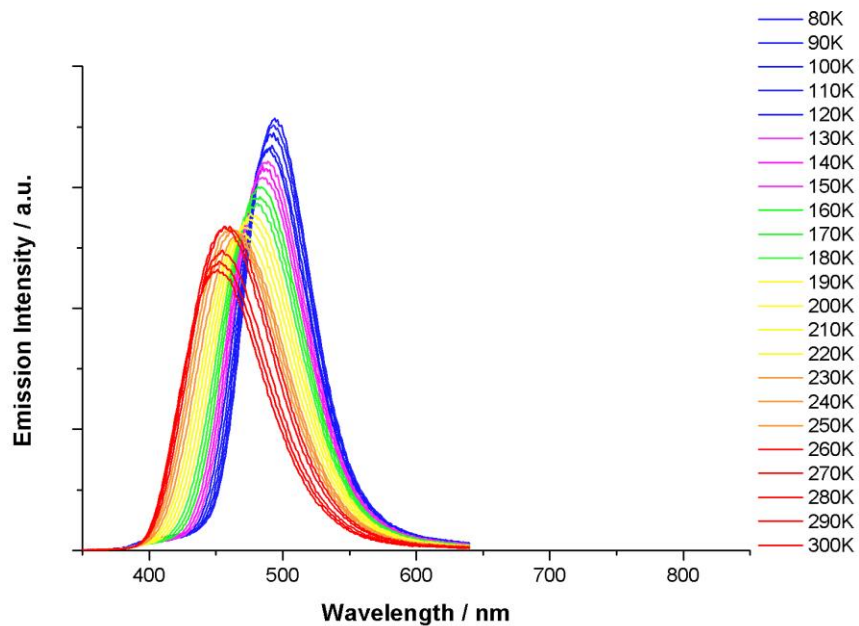


Figure SIII.27 : Temperature dependence of the emission spectrum of transited phase C₂.

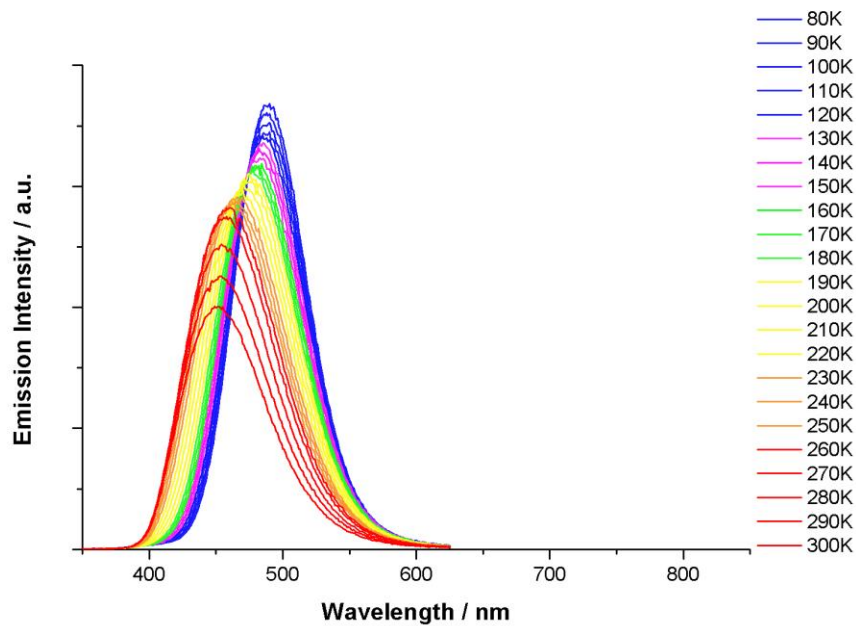


Figure SIII.28 : Temperature dependence of the emission spectrum of transited phase C₃'.

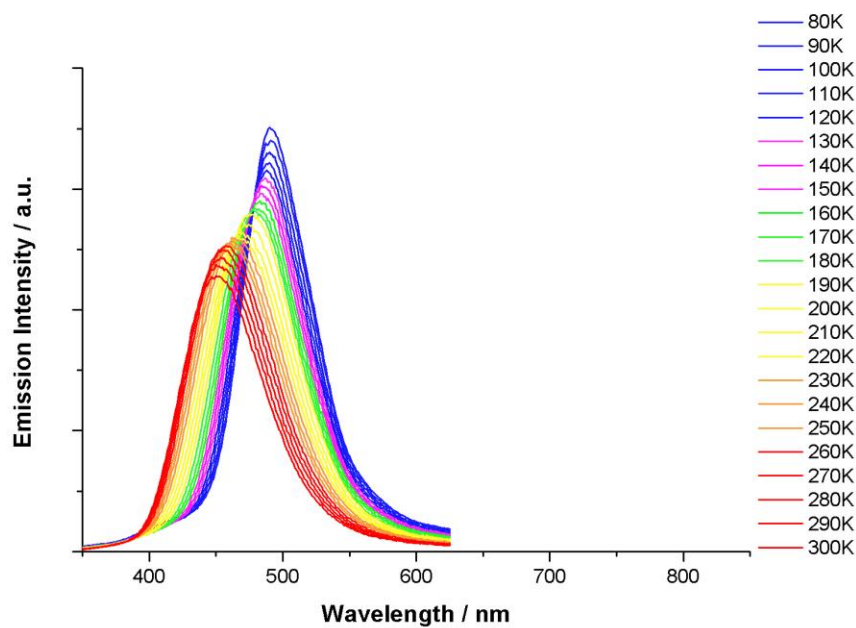


Figure SIII.29 : Temperature dependence of the emission spectrum of transited phase C₄'.

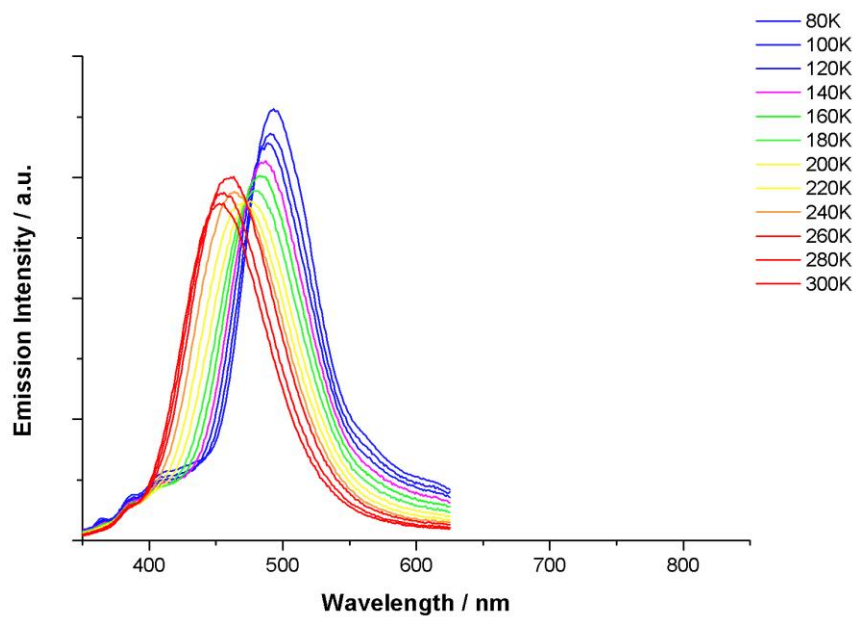


Figure SIII.30 : Temperature dependence of the emission spectrum of transited phase Cs'.

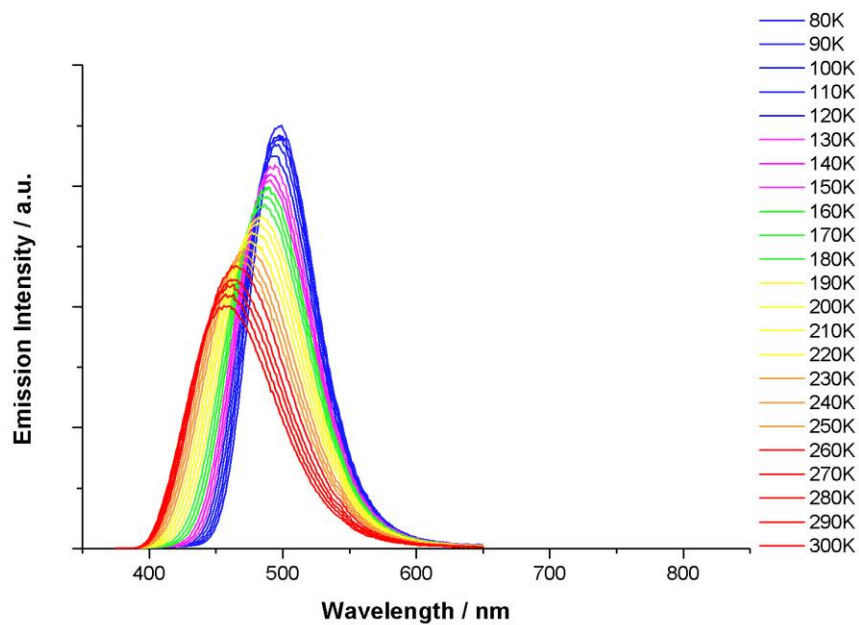


Figure SIII.31 : Temperature dependence of the emission spectrum of transited phase C6'.

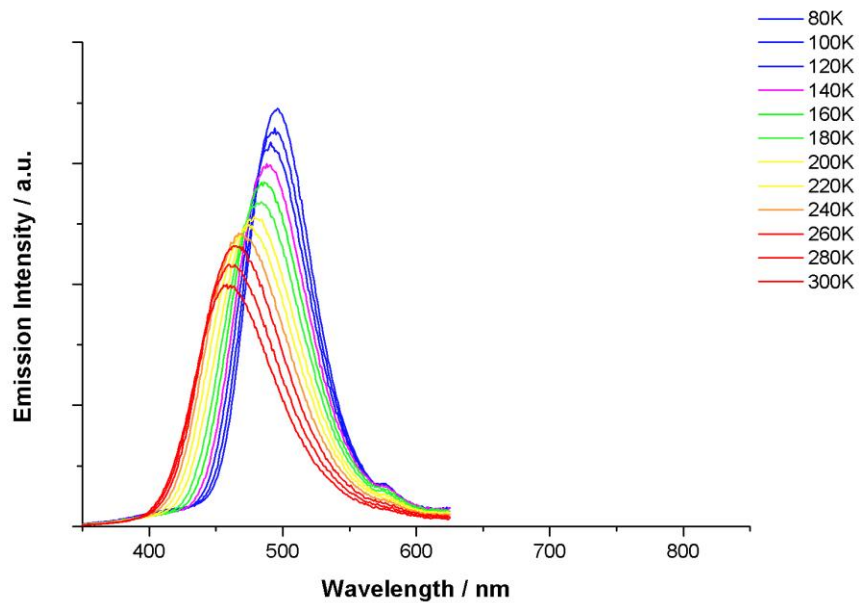


Figure SIII.32 : Temperature dependence of the emission spectrum of transited phase C7'.

III-4.4 Temperature dependence of the decay times of the excited states

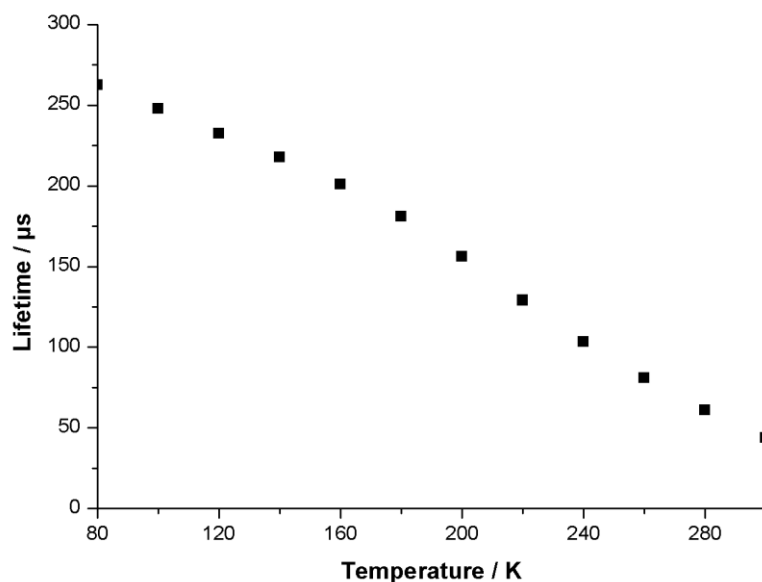


Figure SIII.33 : Variation of the lifetime of the excited state depending of the temperature of transited phase C1'.

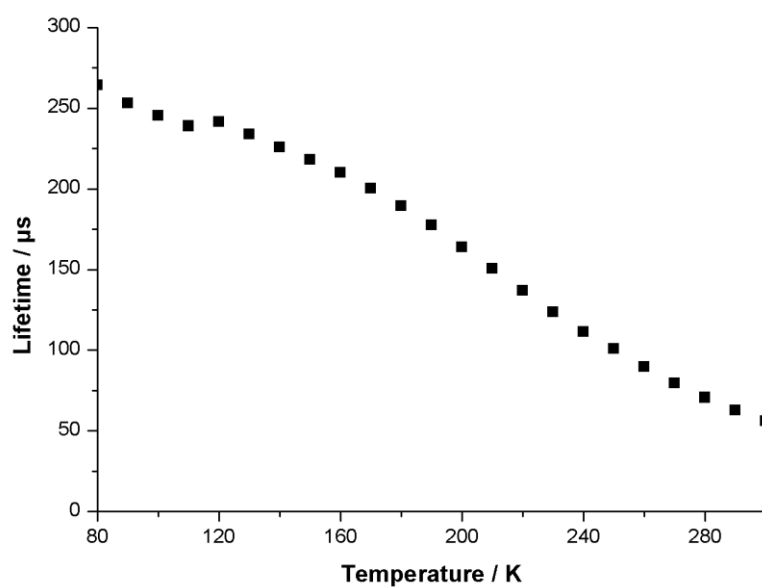


Figure SIII.34 : Variation of the lifetime of the excited state depending of the temperature of transited phase C_2' .

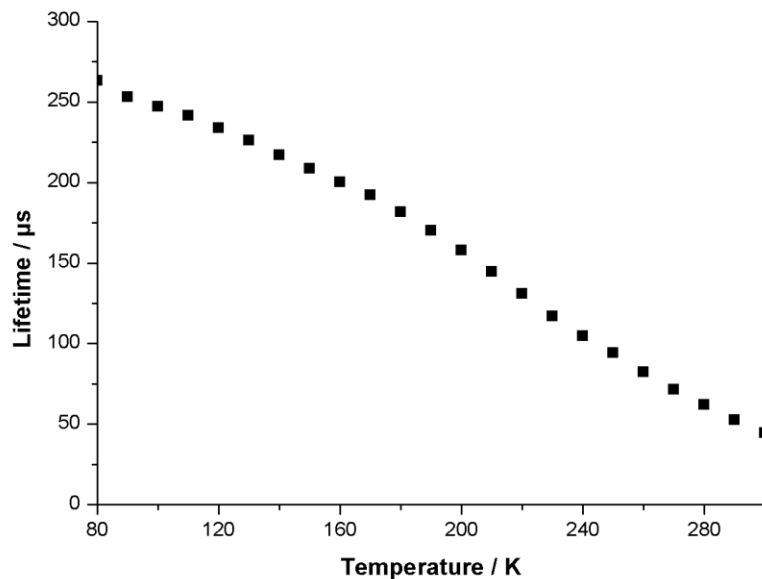


Figure SIII.35 : Variation of the lifetime of the excited state depending of the temperature of transited phase C_3' .

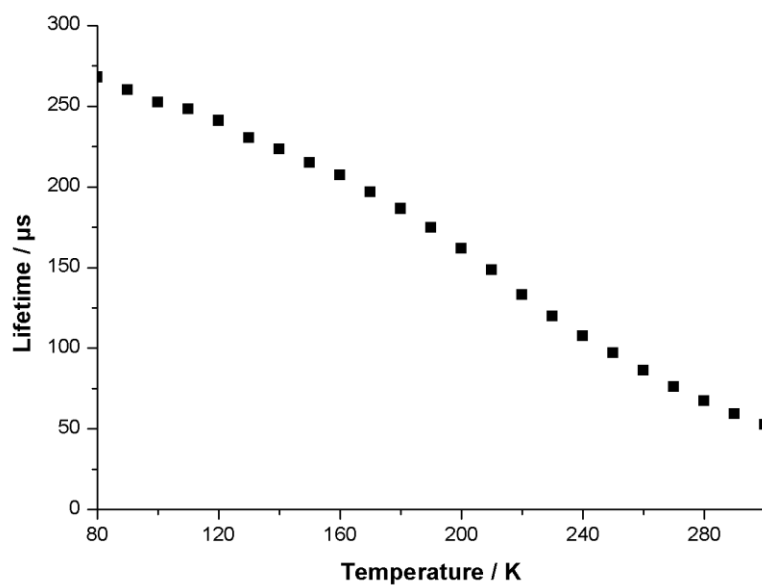


Figure SIII.36 : Variation of the lifetime of the excited state depending of the temperature of transited phase C₄'.

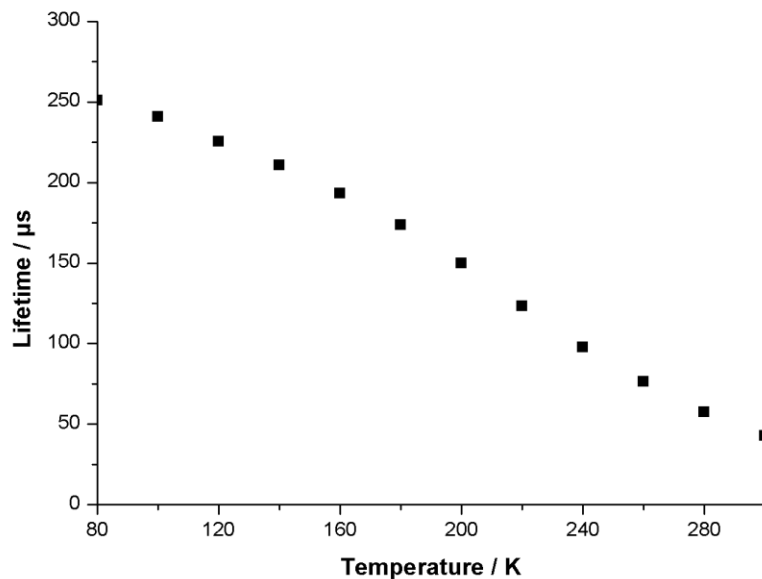


Figure SIII.37 : Variation of the lifetime of the excited state depending of the temperature of transited phase C₅'.

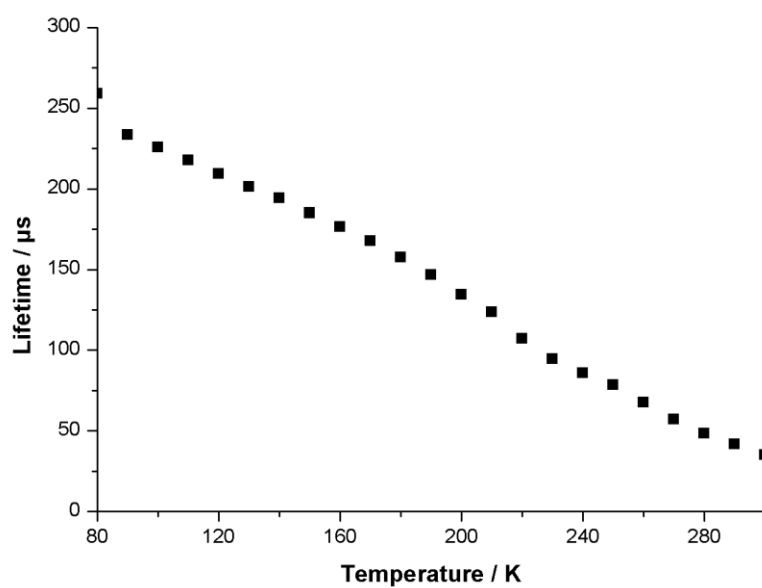


Figure SIII.38 : Variation of the lifetime of the excited state depending of the temperature of transitioned phase C_6' .

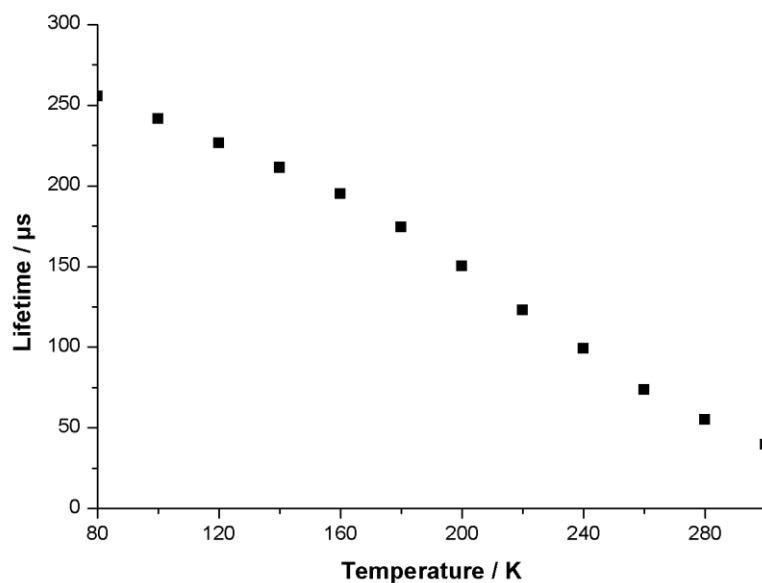


Figure SIII.39 : Variation of the lifetime of the excited state depending of the temperature of transitioned phase C_7' .

III-5 Powder X-ray diffraction of phases C_n '

III-5.1 Powder X-ray diffraction of initial polymers C_n

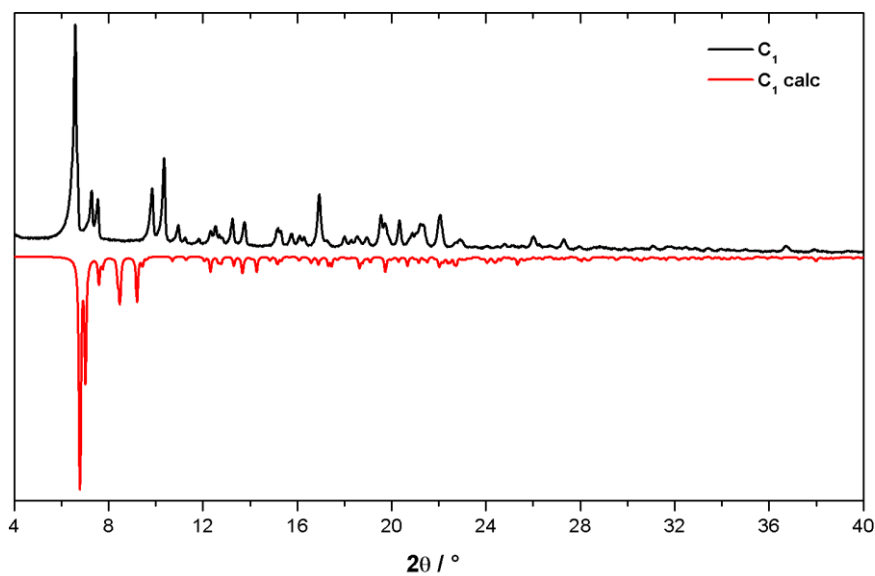


Figure SIII.40 : Comparison between the PXRD diagram of C_1 (black) and the calculated diagram from the crystallographic data (red).

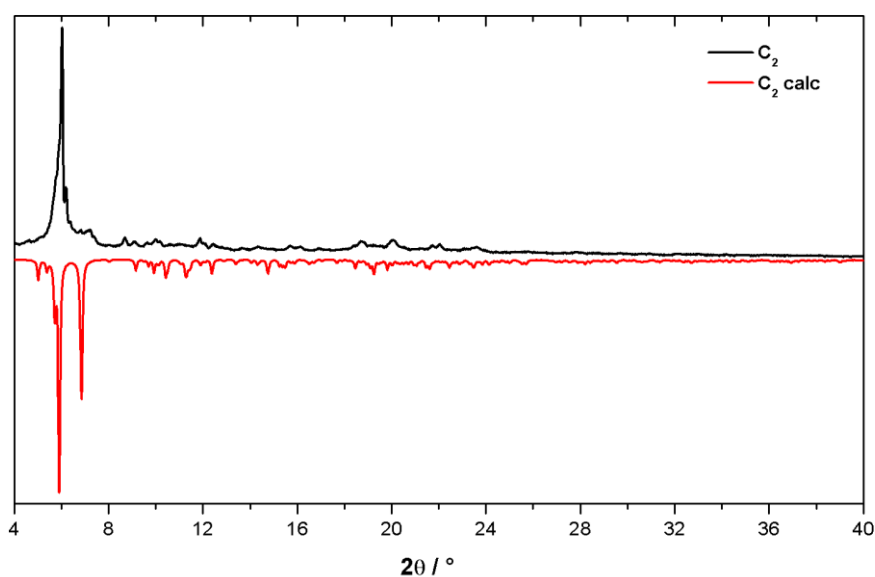


Figure SIII.41 : Comparison between the PXRD diagram of C_2 (black) and the calculated diagram from the crystallographic data (red).

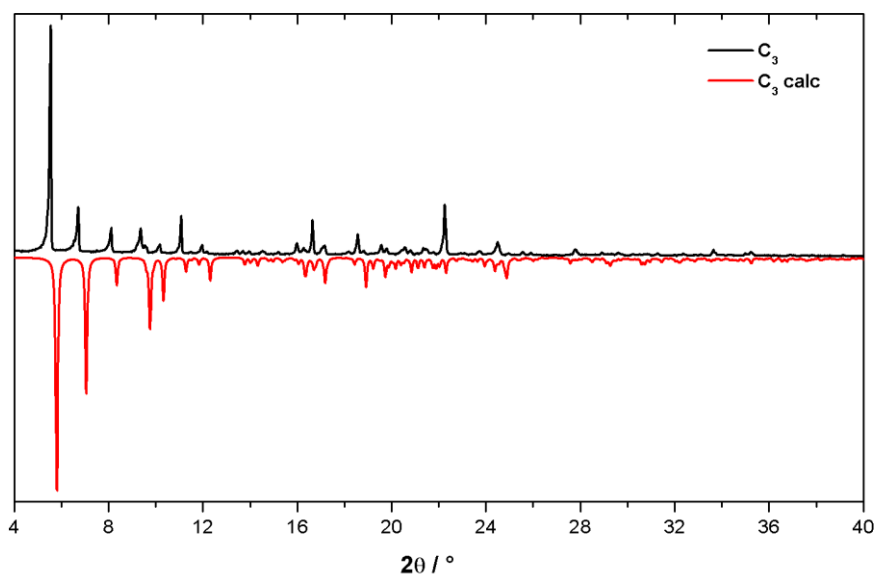


Figure SIII.42 : Comparison between the PXRD diagram of C₃ (black) and the calculated diagram from the crystallographic data (red).

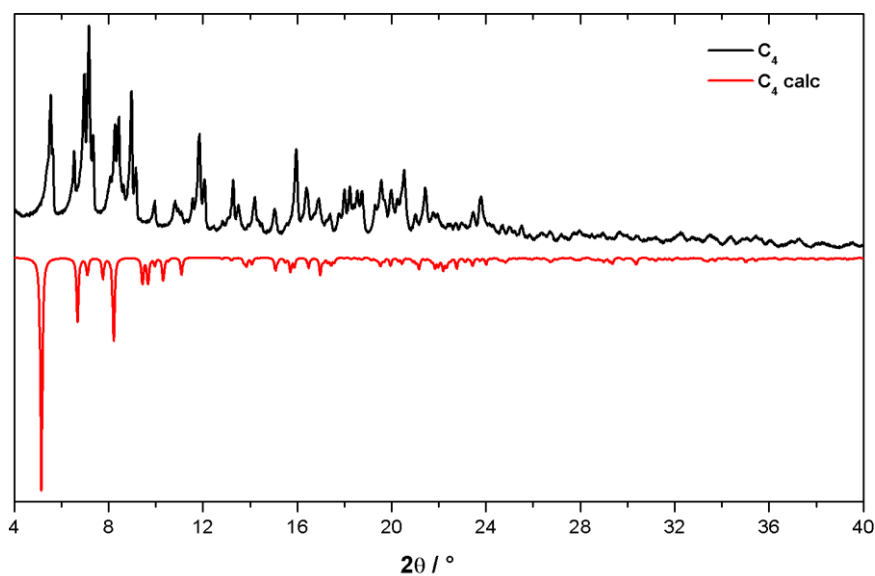


Figure SIII.43 : Comparison between the PXRD diagram of C₄ (black) and the calculated diagram from the crystallographic data (red).

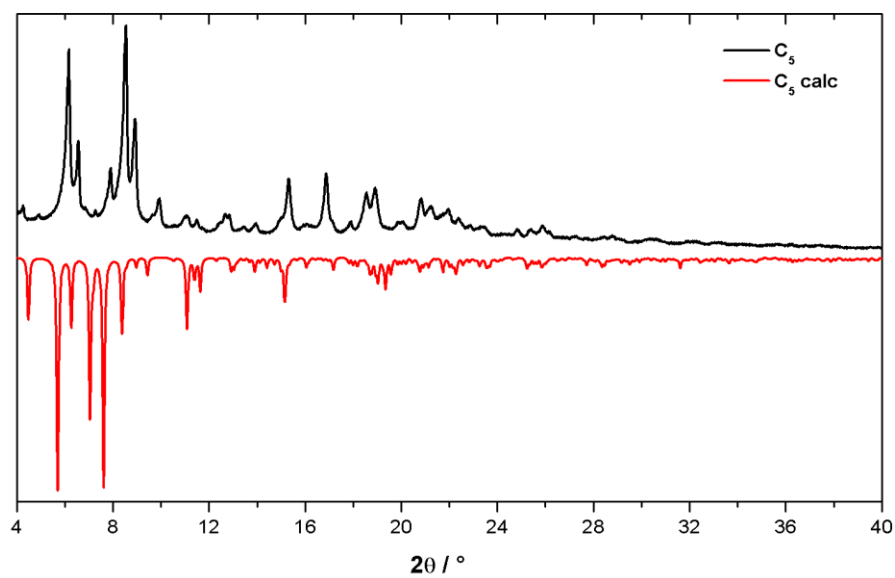


Figure SIII.44 : Comparison between the PXRD diagram of C₅ (black) and the calculated diagram from the crystallographic data (red).

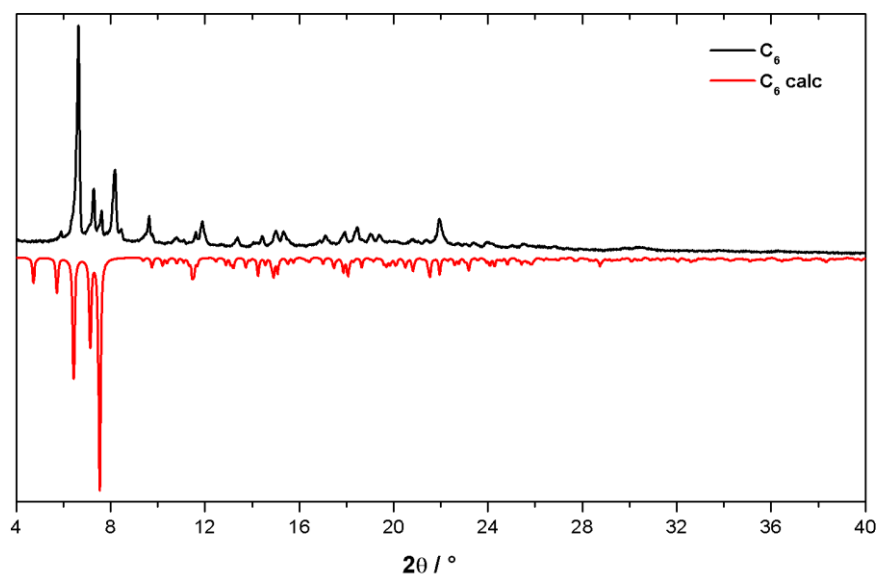


Figure SIII.45 : Comparison between the PXRD diagram of C₆ (black) and the calculated diagram from the crystallographic data (red).

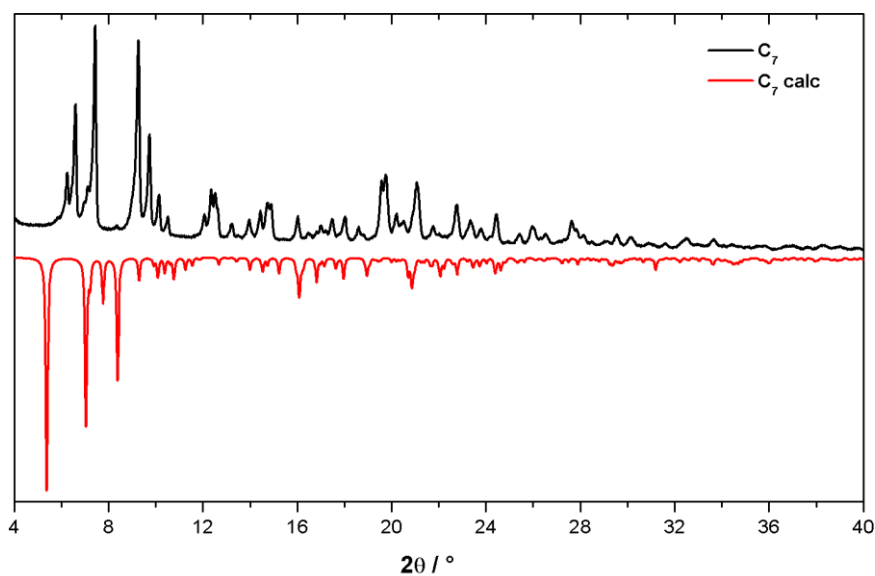


Figure SIII.46 : Comparison between the PXRD diagram of C_7 (black) and the calculated diagram from the crystallographic data (red).

III-5.2 Powder X-ray diffraction of transitioned phases A' and C_n'

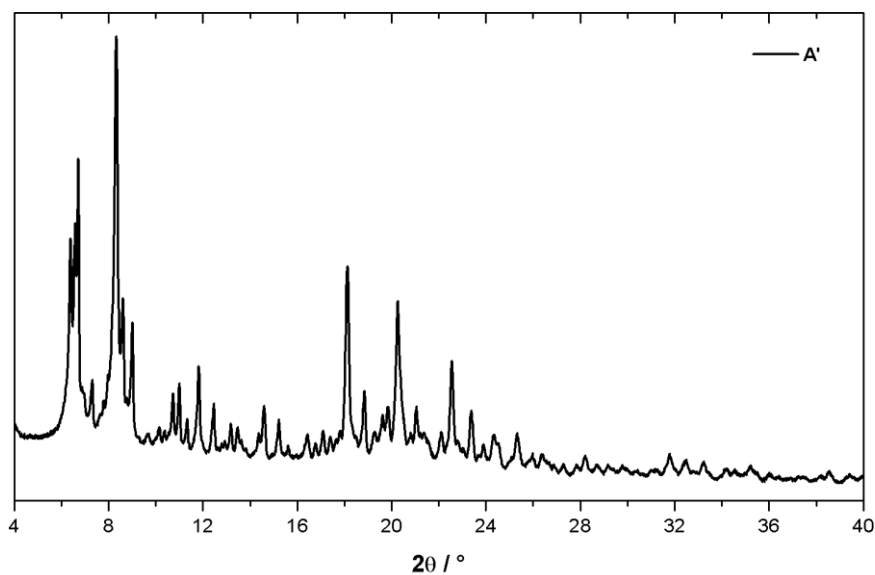


Figure SIII.47 : Powder X-ray diffraction diagram of phase A' .

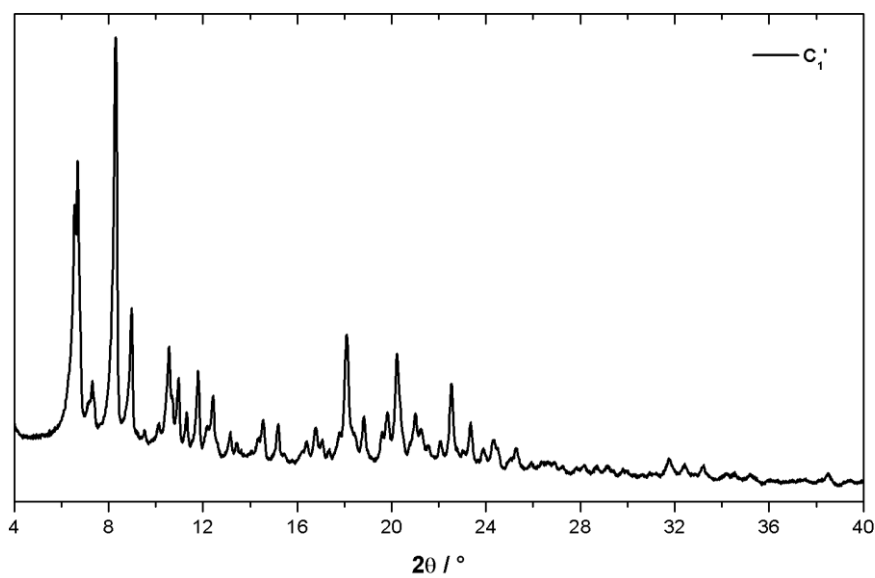


Figure SIII.48 : Powder X-ray diffraction diagram of phase C₁'.

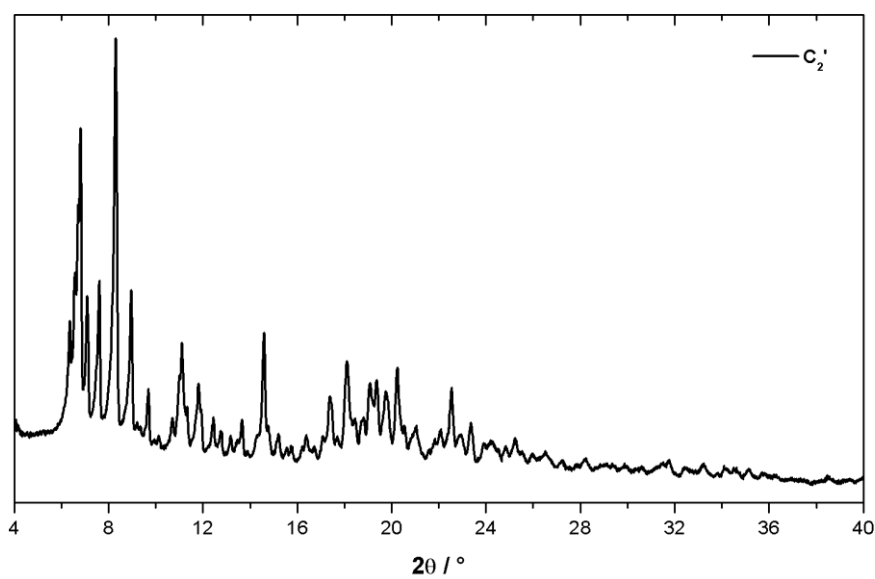


Figure SIII.49 : Powder X-ray diffraction diagram of phase C₂'.

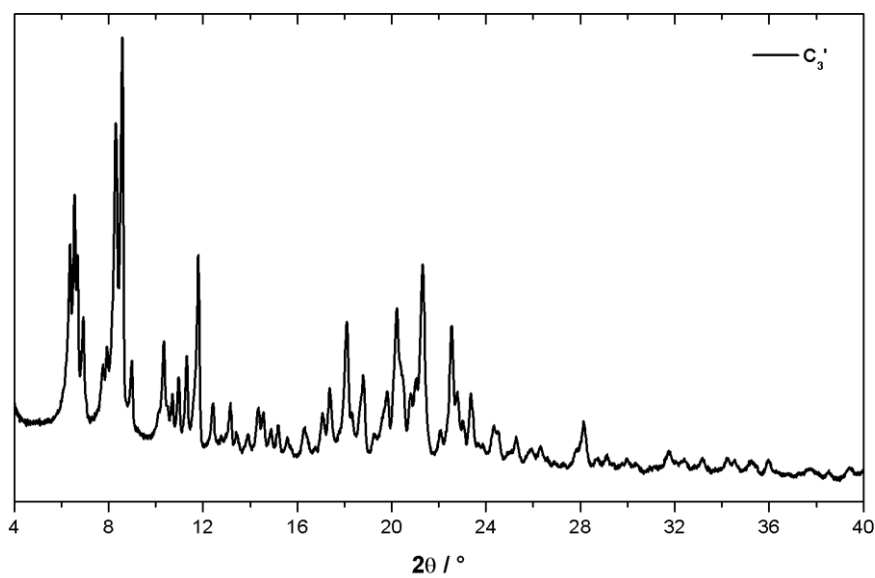


Figure SIII.50 : Powder X-ray diffraction diagram of phase C₃'.

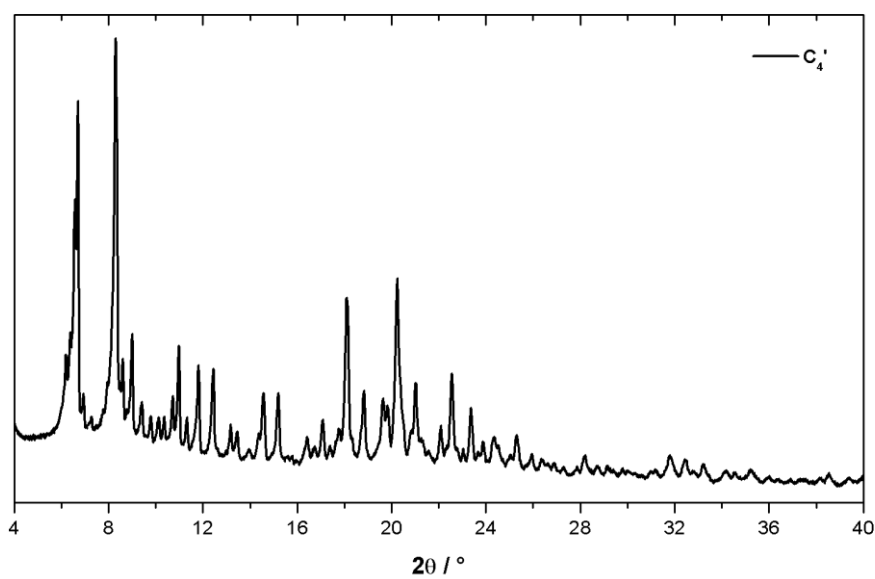


Figure SIII.51 : Powder X-ray diffraction diagram of phase C₄'.

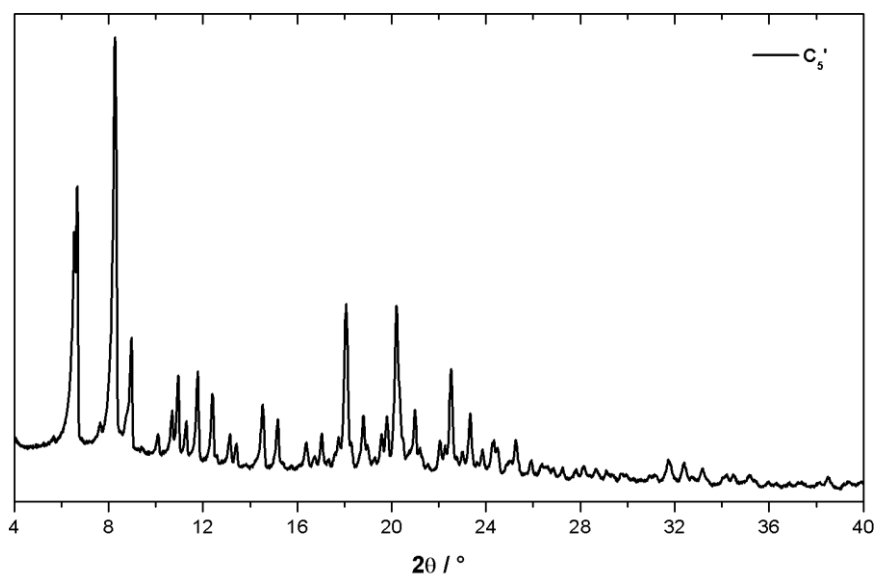


Figure SIII.52 : Powder X-ray diffraction diagram of phase C₅'.

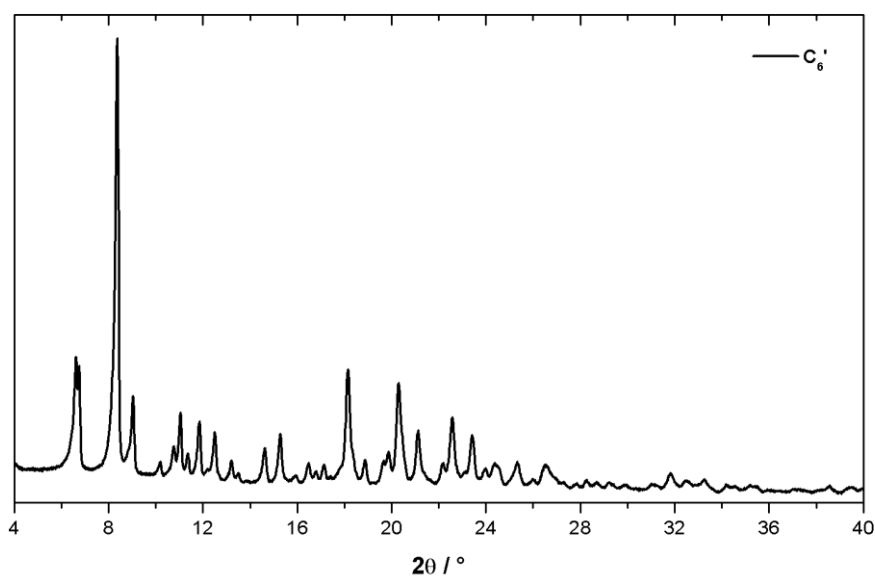


Figure SIII.53 : Powder X-ray diffraction diagram of phase C₆'.

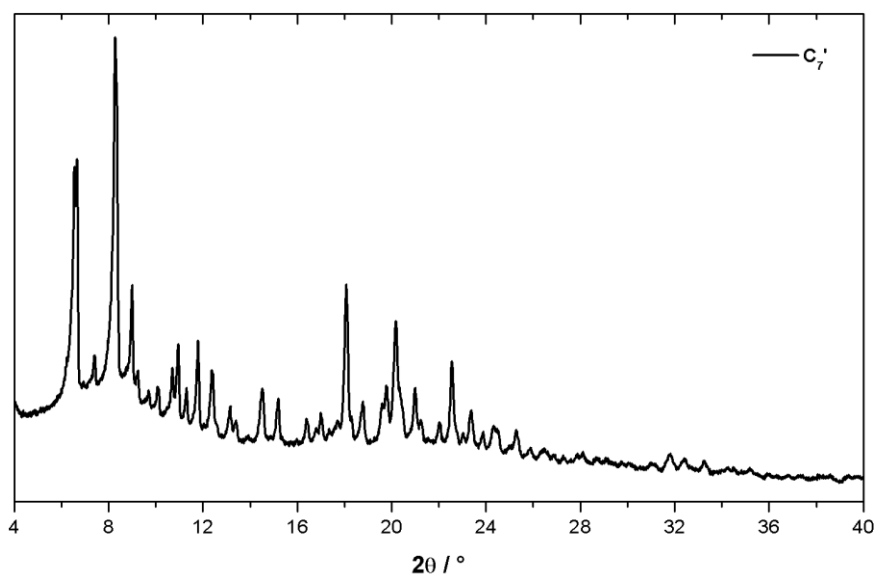


Figure SIII.54 : Powder X-ray diffraction diagram of phase C7'.

III-5.3 Temperature dependant powder X-ray diffraction of precursor A and polymers C₂, C₃ and C₆.

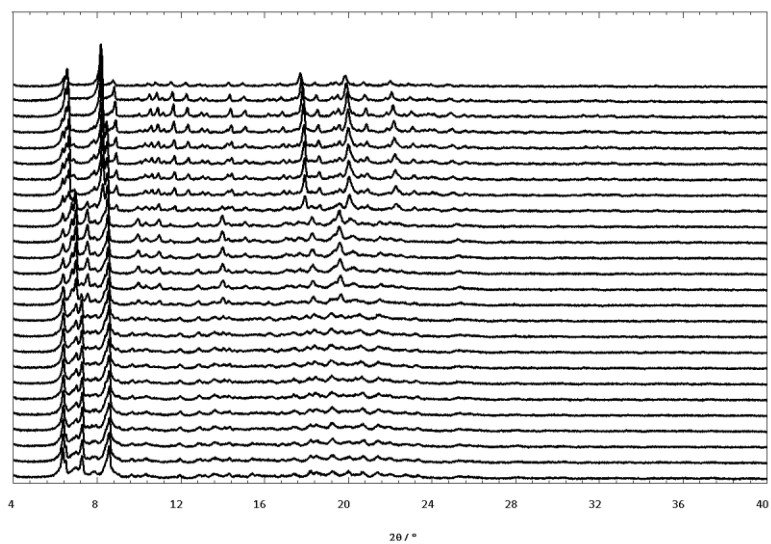


Figure SIII.55 : TD-PXRD measurement of precursor A from 30 to 280 °C, in 10 °C increments.

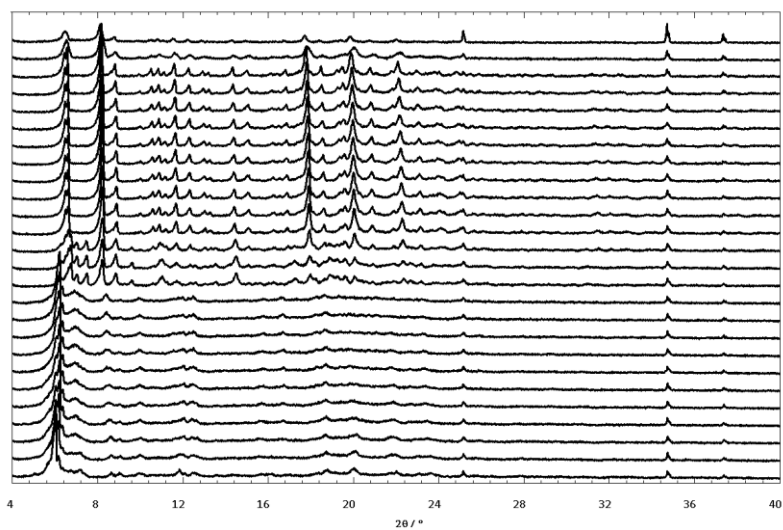


Figure SIII.56 : TD-PXRD measurement of polymer C₂ from 30 to 280 °C, in 10 °C increments.

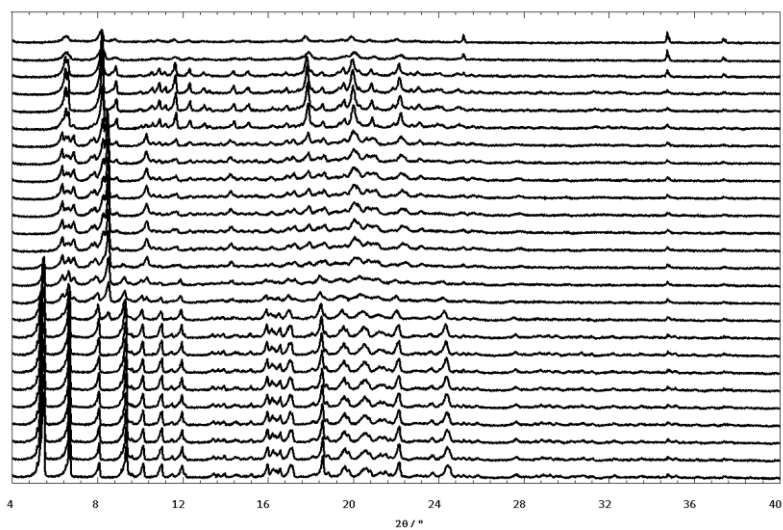


Figure SIII.57 : TD-PXRD measurement of polymer C₃ from 30 to 280 °C, in 10 °C increments.

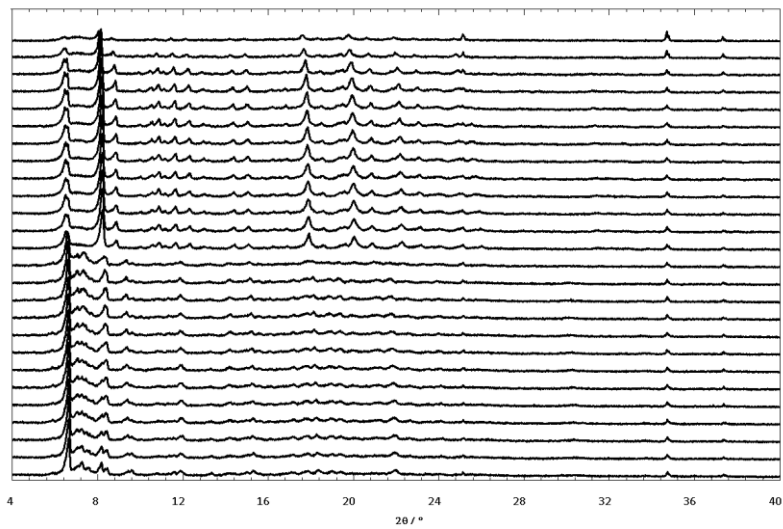


Figure SIII.58 : TD-PXRD measurement of polymer C₆ from 30 to 280 °C, in 10 °C increments.

III-6 TGA-DTA measurements performed on transited phases

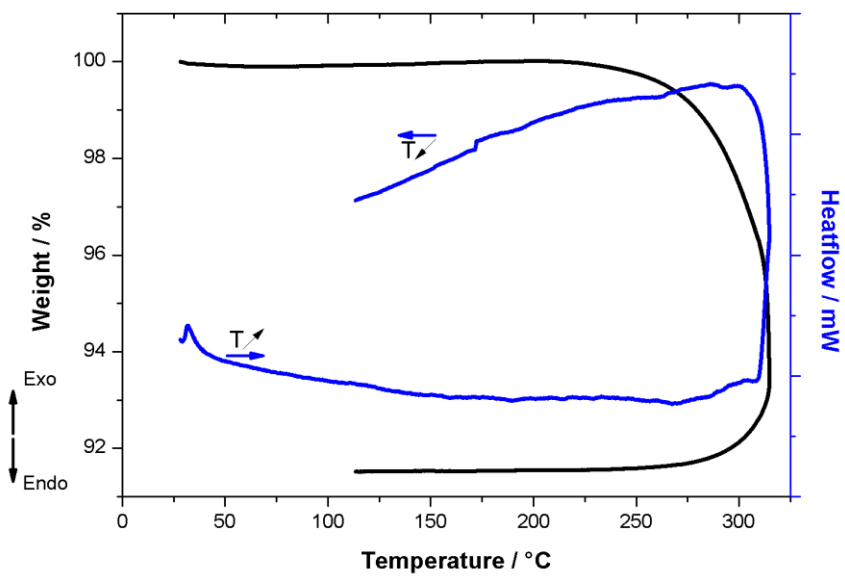


Figure SIII.59 : TGA-DTA analysis of transited phase C₁' until 300 °C and record of the return to room temperature.

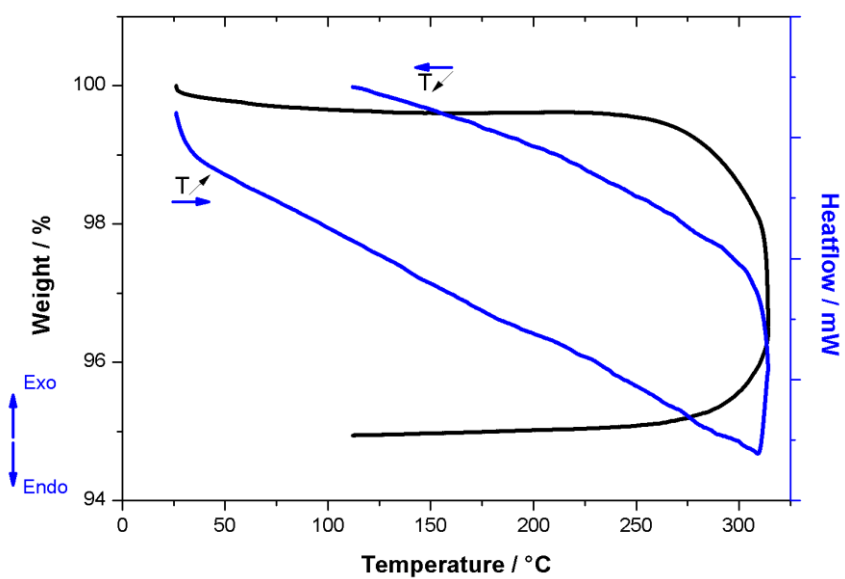


Figure SIII.60 : TGA-DTA analysis of transited phase C₂' until 300 °C and record of the return to room temperature.

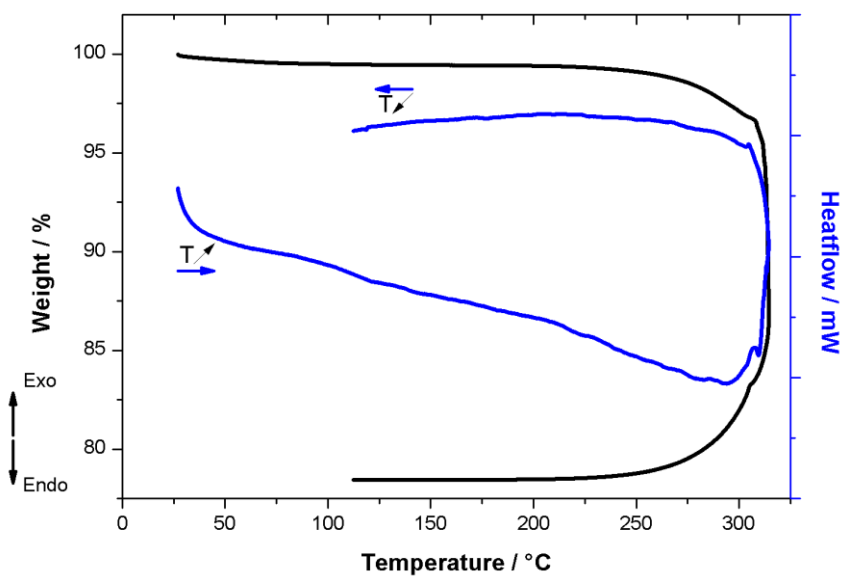


Figure SIII.61 : TGA-DTA analysis of transited phase C₃' until 300 °C and record of the return to room temperature.

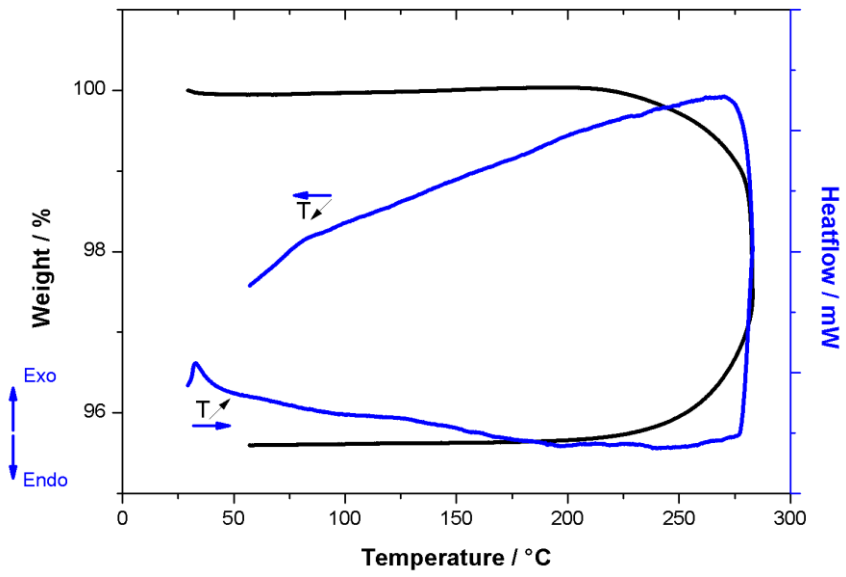


Figure SIII.62 : TGA-DTA analysis of transited phase C₄' until 300 °C and record of the return to room temperature.

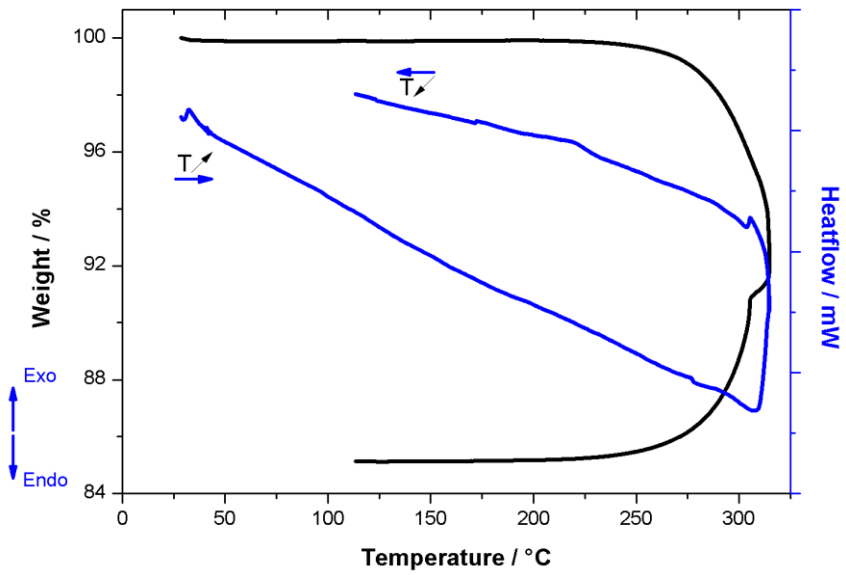


Figure SIII.63 : TGA-DTA analysis of transited phase C₅' until 300 °C and record of the return to room temperature.

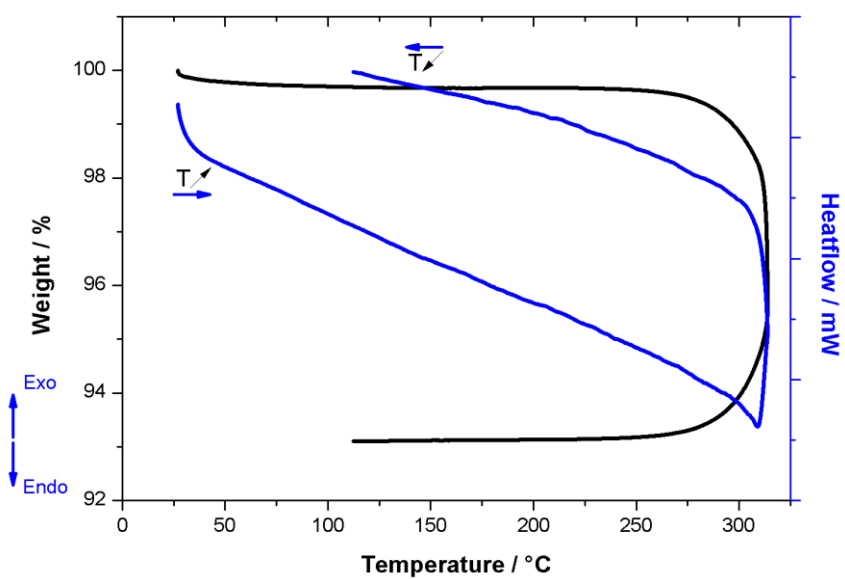


Figure SIII.64 : TGA-DTA analysis of transited phase C_6' until 300 °C and record of the return to room temperature.

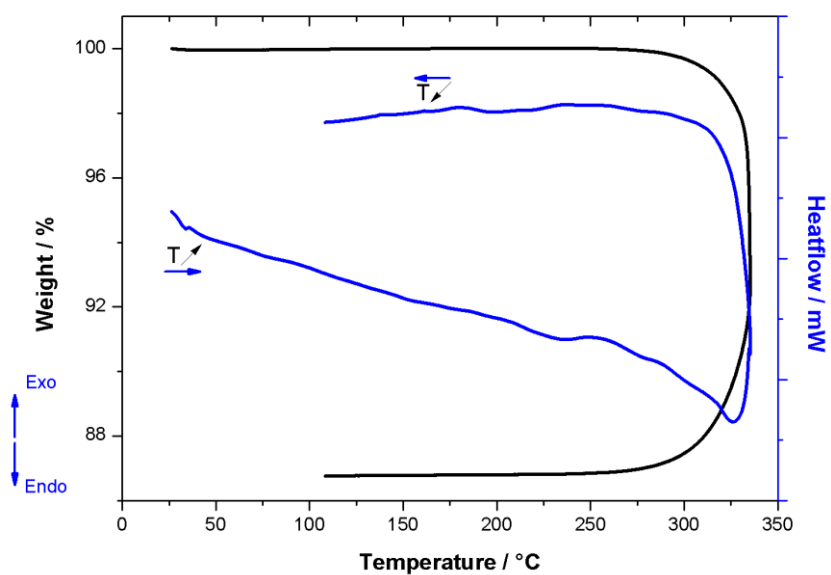


Figure SIII.65 : TGA-DTA analysis of transited phase C_7' until 300 °C and record of the return to room temperature.

III-7 Measurements conducted on the regenerated phase $C_6'D_{CM}$

The regenerated phase $C_6'D_{CM}$ was obtained by submerging the sample of thermally transited phase C_6' in 3 ml of dichloromethane. The solution was stirred manually with a glass rod for five minutes to allow for the complete regeneration of the transited phase. The regenerated phase was then filtered on a paper filter out of the solution. After drying under air, the regenerated phase $C_6'D_{CM}$ consists of a pale yellow polycrystalline powder emitting under UV light excitation ($\lambda_{ex} = 365$ nm) a yellow-orange luminescence.

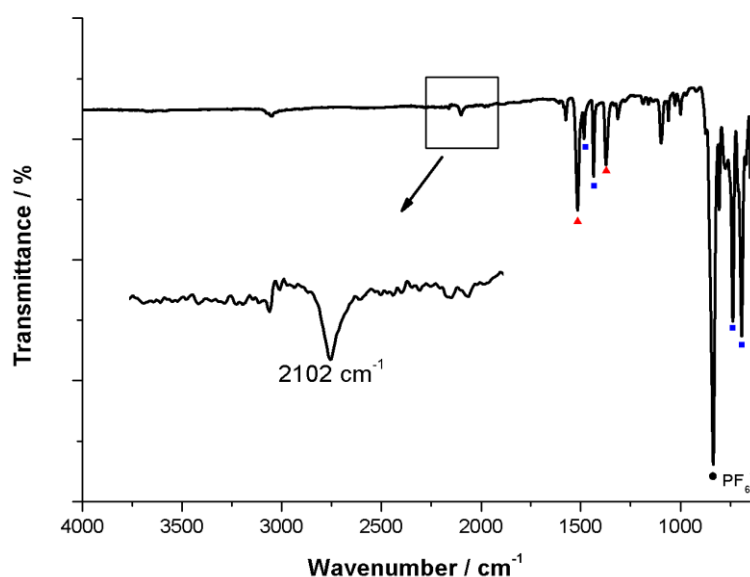


Figure SIII.66 : Infrared spectrum of regenerated phase $C_6'D_{CM}$. The dot marks the PF_6^- counter anion t_{1u} vibration mode band. Blue squares mark typical dppm $\delta_{(C-H)}$ ligand bands. Red triangles mark B_6 ligands bands.

IR (cm^{-1}) : 692 (s), 737 (vs), 777 (s), 835 (vs), 972 (vw), 1000 (w), 1027 (w), 1060 (w), 1097 (m), 1162 (vw), 1189 (vw), 1279 (vw), 1315 (w), 1374 (m), 1436 (m), 1484 (m), 1516 (s), 1575 (m), 1586 (w), 2102 (m), 3052 (w).

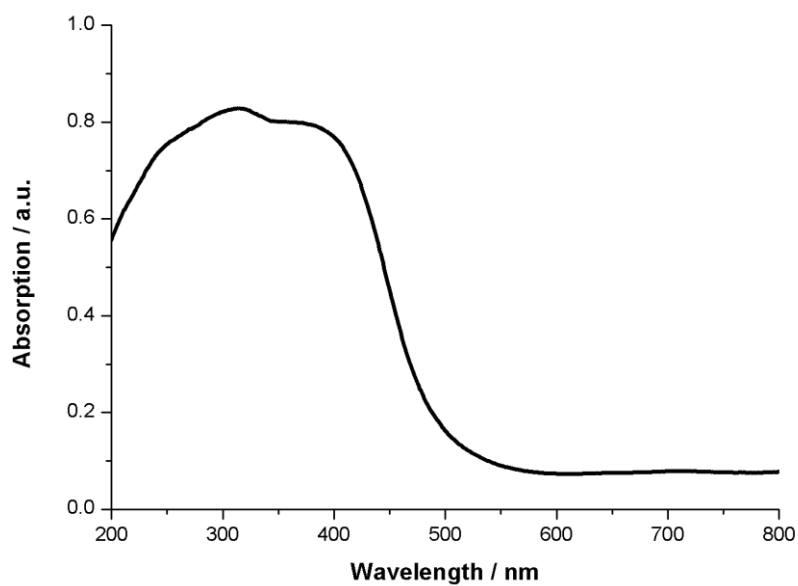


Figure SIII.67 : Solid-state UV-visible absorption spectrum of regenerated phase $C_6'DCM$.

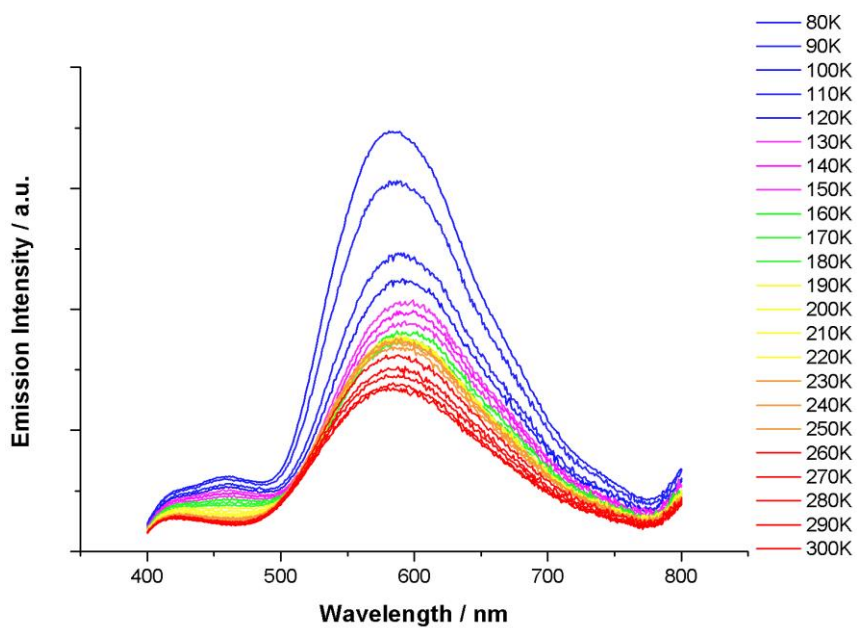


Figure SIII.68 : Temperature dependence of the emission spectrum of regenerated phase $C_6'DCM$.

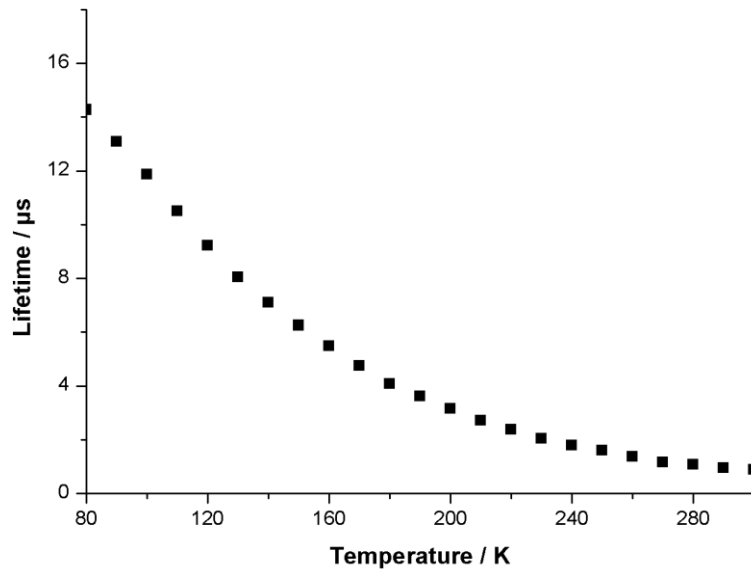


Figure SIII.69 : Variation of the lifetime of the excited state depending of the temperature of regenerated phase $\text{C}_6'\text{DCM}$.

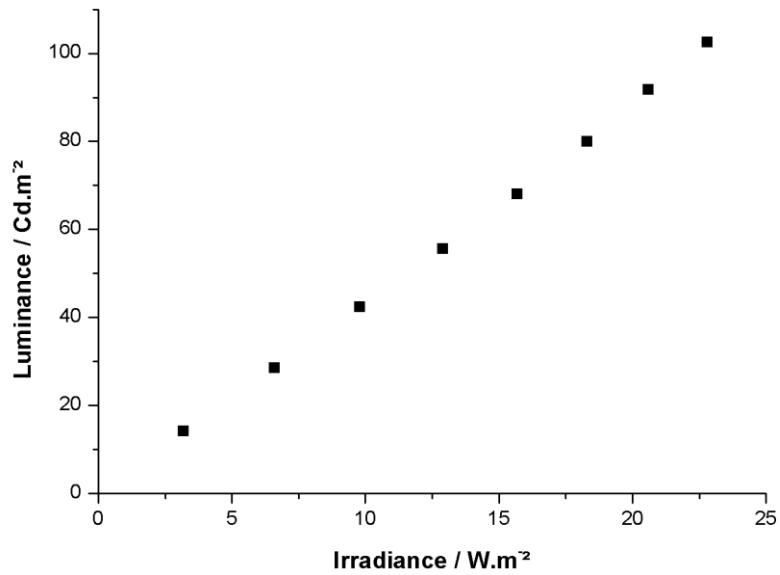


Figure SIII.70 : Variation of the luminance of regenerated phase $\text{C}_6'\text{DCM}$ depending on the irradiance.

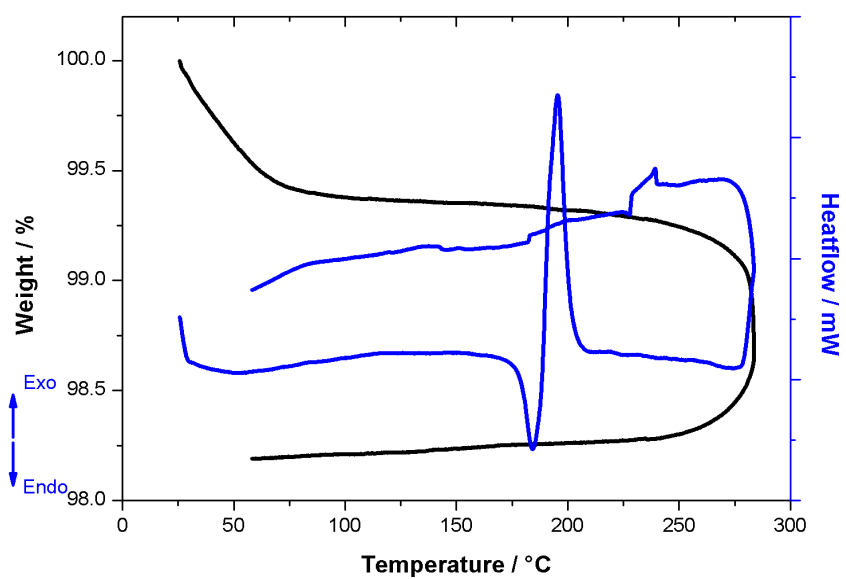


Figure SIII.71 : TGA-DTA analysis of regenerated phase $C_6'DCM$ until 300 °C and record of the return to room temperature.

IV-Appendix to chapter IV :

IV-1 Synthesis of tetrametallic metallacycles D_x

Synthesis of deivative D_{Cl} :

To a dichloromethane solution (10 ml) of [Cu(CH₃CN)₄]PF₆ (0.040 g, 0.11 mmol) and CuCl (0.011 g, 0.11 mmol) was added a dichloromethane solution (5 ml) of dppm (0.085 g, 0.22 mmol). This solution was stirred for 1 hour. A dichloromethane solution (5 ml) of 3,3'-bipyridine (0.017 g, 0.11 mmol) was added to the crude solution. The stirring was stopped and the solution was left undisturbed overnight at room temperature. The solution was filtered over cotton and was left upon n-pentane vapor diffusion to obtain the product C_{Cl} after crystallization.

The final product after filtration on paper filter was a pure colorless crystalline powder obtained with a yield of 66% (0.087 g, 0.035 mmol). This powder emits under UV-Vis excitation ($\lambda_{\text{lamp}} = 365\text{nm}$) an eye-perceived light blue luminescence.

¹H NMR (300 MHz, CD₂Cl₂, ppm): δ 3.44 (broad s, 8H, PCH₂P), 6.97 (t, 4H, ¹J(H-H) = 9 Hz, H_{3,3'}bipyridine), 7.02-7.42 (broad m, 80H, H_{arom}dppm), 7.59 (d, 4H, ¹J(H-H) = 9 Hz, H_{3,3'}bipyridine), 8.40 (broad s, 4H, H $\alpha_{3,3'$ bipyridine), 8.48 (s, 2H, H $\alpha_{3,3'$ bipyridine).

³¹P{¹H} NMR (121 MHz, CD₂Cl₂, ppm): δ = -8.77 (s, P_{dppm}), -144.38 (sept, ¹J(P-F) = 708 Hz, PF₆⁻).

IR (cm⁻¹): 690 (vs), 737 (vs), 766 (s), 788 (s), 832 (vs), 931 (vw), 1002 (w), 1028 (w), 1096 (m), 1196 (w), 1245 (vw), 1280 (vw), 1308 (vw), 1351 (w), 1434 (s), 1484 (m), 1588 (w), 3057 (w)

Synthesis of deivative D_{Br} :

To a dichloromethane solution (10 ml) of [Cu(CH₃CN)₄]PF₆ (0.040 g, 0.11 mmol) and CuBr (0.016 g, 0.11 mmol) was added a dichloromethane solution (5 ml) of dppm (0.085 g, 0.22 mmol). This solution was stirred for 1 hour. A dichloromethane solution (5 ml) of 3,3'-bipyridine (0.017 g, 0.11 mmol) was added to the crude solution. The stirring was stopped and the solution was left undisturbed overnight at room temperature. The solution was filtered

over cotton and was left upon n-pentane vapor diffusion to obtain the product **C_{Br}** after crystallization.

The final product after filtration on paper filter was a pure colorless crystalline powder obtained with a yield of 84% (0.116 g, 0.05 mmol). This powder emits under UV-Vis excitation ($\lambda_{\text{lamp}} = 365\text{nm}$) an eye-perceived light blue luminescence.

^1H NMR (300 MHz, CD_2Cl_2 , ppm): $\delta = 3.28$ (broad s, 4H, PCH_2P), 3.51 (broad s, 4H, PCH_2P), 6.95 (t, 4H, $^1\text{J}(\text{H-H}) = 7$ Hz, $\text{H}_{3,3'}$ bipyridine), 7.07-7.48 (broad m, 80H, $\text{H}_{\text{arom dppm}}$), 7.67 (d, 4H, $^1\text{J}(\text{H-H}) = 7$ Hz, $\text{H}_{3,3'}$ bipyridine), 8.43 (broad s, 4H, $\text{H}\alpha_{3,3'}$ bipyridine), 8.54 (s, 4H, $\text{H}\alpha_{3,3'}$ bipyridine).

$^3\text{P}\{^1\text{H}\}$ NMR (121 MHz, CD_2Cl_2 , ppm): $\delta = -8.84$ (s, P_{dppm}), -144.44 (sept, $^1\text{J}(\text{P-F}) = 707$ Hz, PF_6^-).

IR (cm^{-1}): 690 (vs), 737 (vs), 766 (s), 788 (s), 832 (vs), 931 (vw), 1002 (w), 1028 (w), 1096 (m), 1196 (w), 1245 (vw), 1280 (vw), 1308 (vw), 1351 (w), 1434 (s), 1484 (m), 1588 (w), 3057 (w)

Synthesis of deivative **D_I** :

To a dichloromethane solution (10 ml) of $[\text{Cu}(\text{CH}_3\text{CN})_4]\text{PF}_6$ (0.04 g, 0.11 mmol) and CuI (0.021g, 0.11 mmol) was added a dichloromethane solution (5 ml) of dppm (0.085 g, 0.22 mmol). This solution was stirred for 1 hour. A dichloromethane solution (5 ml) of 3,3'bipyridine (0.017 g, 0.11 mmol) was added to the crude solution. The stirring was stopped and the solution was left undisturbed overnight at room temperature. The solution was filtered over cotton and was left upon n-pentane vapor diffusion to obtain the product **C_I** after crystallization.

The final product after filtration on paper filter was a pure colorless crystalline powder obtained with a yield of 60% (0.085 g, 0.03 mmol). This powder emits under UV-Vis excitation ($\lambda_{\text{lamp}} = 365\text{nm}$) an eye-perceived light blue luminescence.

^1H NMR (300 MHz, CD_2Cl_2 , ppm) : $\delta = 3.40$ (broad s, 4H, PCH_2P), 3.62 (broad s, 4H, PCH_2P), 6.97 (t, 4H, $^1\text{J}(\text{H-H}) = 6$ Hz, $\text{H}_{3,3'}$ bipyridine), 7.02-7.47 (broad m, 80H, $\text{H}_{\text{arom dppm}}$), 7.69 (d, 4H, $^1\text{J}(\text{H-H}) = 6$ Hz, $\text{H}_{3,3'}$ bipyridine), 8.46 (broad s, 4H, $\text{H}\alpha_{3,3'}$ bipyridine), 8.56 (s, 4H, $\text{H}\alpha_{3,3'}$ bipyridine).

$^{31}\text{P}\{^1\text{H}\}$ NMR (121 MHz, CD_2Cl_2 , ppm) : $\delta = -9.81$ (s, P_{dppm}), -144.40 (sept, $^1J(\text{P-F}) = 708$ Hz, PF_6^-).

IR (cm^{-1}): 690 (vs), 737 (vs), 766 (s), 788 (s), 832 (vs), 931 (vw), 1002 (w), 1028 (w), 1096 (m), 1196 (w), 1245 (vw), 1280 (vw), 1308 (vw), 1351 (w), 1434 (s), 1484 (m), 1588 (w), 3057 (w)

Synthesis of the polymer described in part IV-4 :

A dichloromethane solution (10 ml) of $[\text{Cu}(\text{CH}_3\text{CN})_4]\text{PF}_6$ (0.0147 g, 0.04 mmol), CuBr (0.0113, 0.08 mmol) and bis(diphenylphosphinomethyl)phenylphosphine (dpmp, 0.040 g, 0.08 mmol) was prepared and stirred for one hour. A dichloromethane solution (5 ml) of 2,4,6-tri(4-pyridyl)-1,3,5-triazine (**B₆** linker) (0.0123 g, 0.04 mmol) was added to the crude solution. The stirring was stopped and the solution was left at room temperature. After a week, the final product was obtained as a polycrystalline orange crystals and recovered out of the solution by filtration over a paper filter and after drying is obtained as a pure orange polycrystalline powder obtained. This air-stable powder emits under UV excitation ($\lambda_{\text{ex}} = 365$ nm) an eye-perceived deep red light luminescence.

IV-2 Infrared spectroscopy study

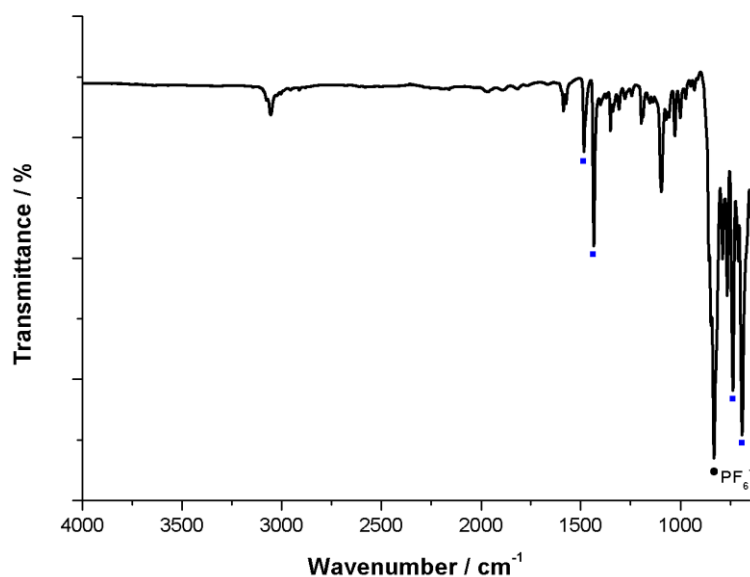


Figure SIV.1 : Infrared spectrum of compound **DCl**. The dot marks the PF_6^- counter anion t_{1u} vibration mode band. Blue squares mark typical dppm $\delta_{(\text{C-H})}$ ligand bands.

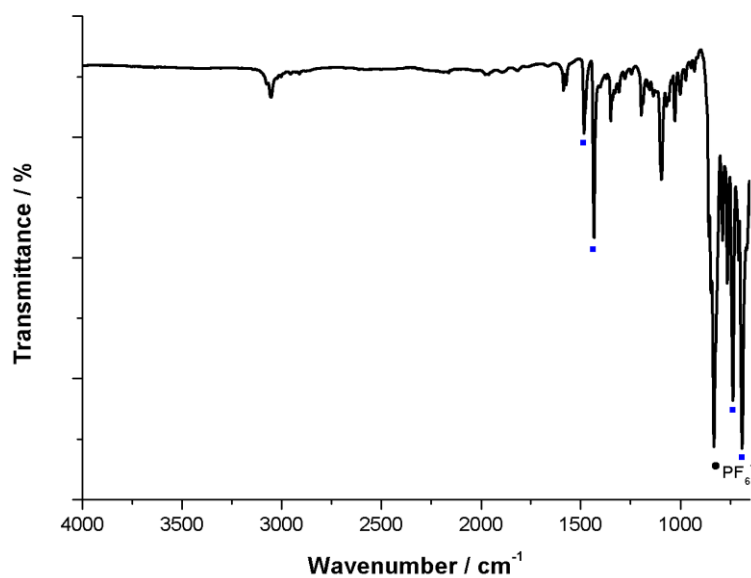


Figure SIV.2 : Infrared spectrum of compound **D_{Br}**. The dot marks the PF_6^- counter anion t_{1u} vibration mode band. Blue squares mark typical dppm $\delta_{(\text{C-H})}$ ligand bands.

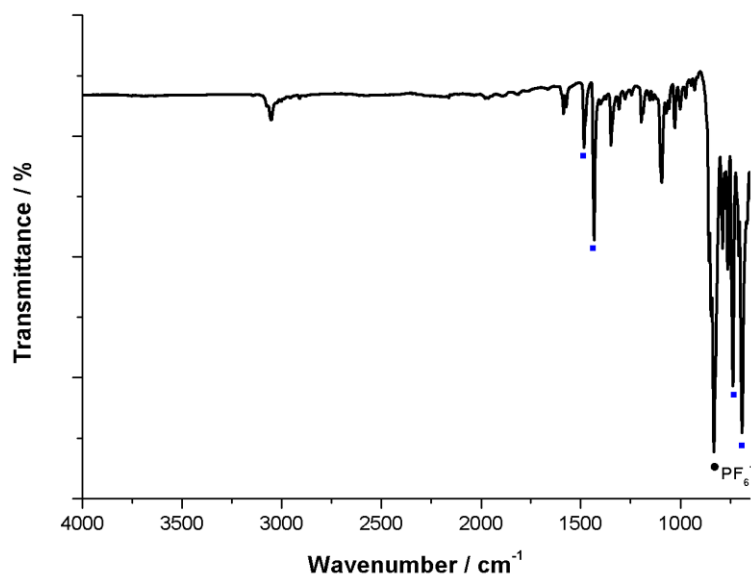


Figure SIV.3 : Infrared spectrum of compound **D_{Cl}**. The dot marks the PF_6^- counter anion t_{1u} vibration mode band. Blue squares mark typical dppm $\delta_{(\text{C-H})}$ ligand bands.

IV-3 X-ray crystallographic study

IV-3.1 Molecular structure of compounds D_x

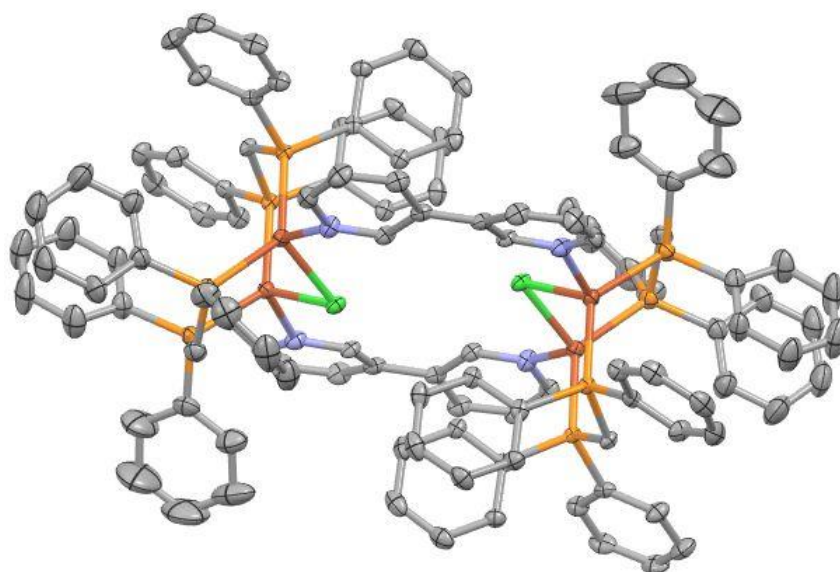


Figure SIV.4 : ORTEP views of the molecular structure of the dicationic derivative D_{Cl} . Hydrogen atoms, hexafluorophosphate counter-anions and included CH_2Cl_2 solvent molecules have been omitted for clarity. Atoms color codes: dark orange : copper, light orange : phosphorus, grey : carbon, blue : nitrogen, light green : chlorine

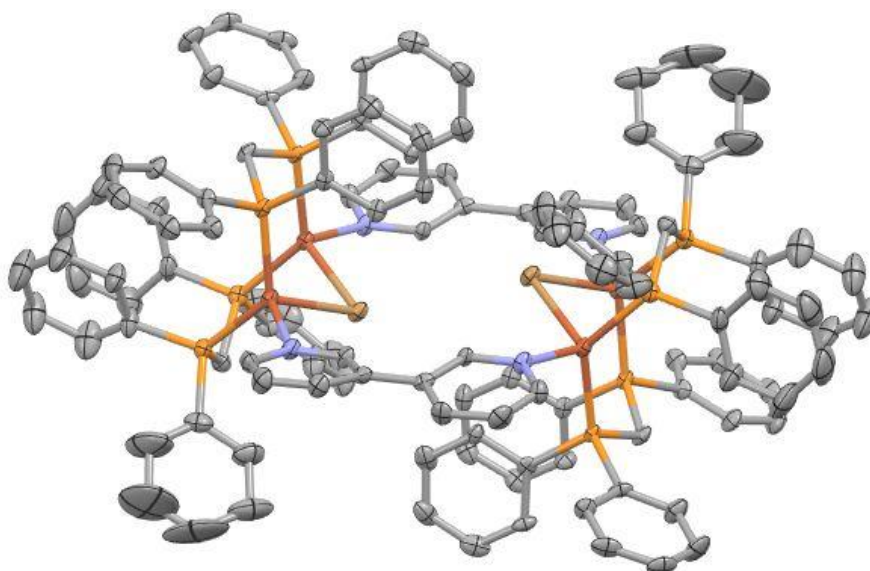


Figure SIV.5 : ORTEP views of the molecular structure of the dicationic derivative D_{Br} . Hydrogen atoms, hexafluorophosphate counter-anions and included CH_2Cl_2 solvent molecules have been omitted for clarity. Atoms color codes: dark orange : copper, light orange : phosphorus, grey : carbon, blue : nitrogen, brown : bromine.

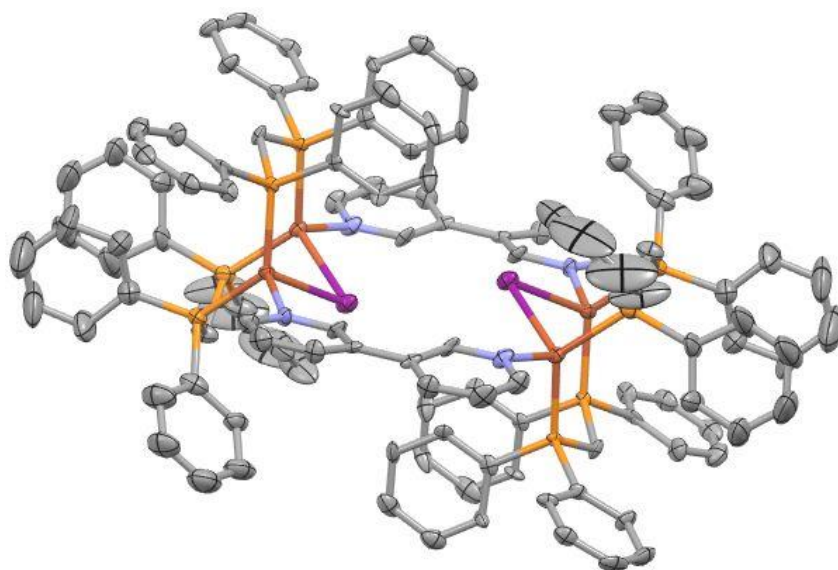


Figure SIV.6 : ORTEP views of the molecular structure of the dicationic derivative **D₁**. Hydrogen atoms, hexafluorophosphate counter-anions and included CH₂Cl₂ solvent molecules have been omitted for clarity. Atoms color codes: dark orange : copper, light orange : phosphorus, grey : carbon, blue : nitrogen, violet : iodine.

IV-3.2 Crystallographic tables of compounds **D_x**

	D_{Cl}	D_{Br}	D_I
Molecular formula	C ₁₂₀ H ₁₀₄ Cl ₂ Cu ₄ F ₁₂ N ₄ P ₁₀ (C ₁₃₀ H ₁₁₂ Cl ₂₂ Cu ₄ F ₁₂ N ₄ P ₁₀)	C ₁₂₀ H ₁₀₄ Br ₂ Cu ₄ F ₁₂ N ₄ P ₁₀ (C ₁₃₀ H ₁₁₂ Br ₂ Cl ₂₀ Cu ₄ F ₁₂ N ₄ P ₁₀)	C ₁₂₀ H ₁₀₄ I ₂ Cu ₄ N ₄ P ₈ (C ₁₃₂ H ₉₈ I ₂ Cl ₂₄ Cu ₄ F ₁₂ N ₄ P ₁₀)
CCDC number	2074606	2074608	2074607
Molecular weight	2464.83 (3302.00)	2553.75 (3390.92)	2357.79 (3636.60)
a (Å)	14.113(2)	14.182(3)	14.308(2)
b (Å)	14.181(2)	14.237(3)	14.297(2)
c (Å)	18.602(2)	18.585(3)	18.459(2)
α (°)	87.110(4)	87.431(6)	68.401(6)
β (°)	69.039(4)	69.448(5)	87.648(5)
γ (°)	84.128(4)	84.493(6)	85.231(6)
V (Å³)	3458.0(8)	3497.2(12)	3498.7(3)
Z	1	1	1
D_c (g.cm⁻³)	1.184 (1.586)	1.213 (1.610)	1.119 (1.726)
Crystal system	Triclinic	Triclinic	Triclinic
Space group	P-1	P-1	P-1
Temperature (K)	150(2)	150(2)	150(2)
Wavelength Mo-Kα (Å)	0.71069	0.71069	0.71069
Crystal size (mm)	0.35 x 0.28 x 0.11	0.45 x 0.11 x 0.09	0.16 x 0.11 x 0.07
μ (mm⁻¹)	0.819 (1.215)	1.343 (1.734)	1.171 (1.682)
F(000)	1260 (1668)	1296 (1704)	1194 (1806)
θ limit (°)	2.02 – 27.57	2.19 – 27.63	2.17 – 27.55
Index ranges hkl	-18 < h < 18 -17 < k < 18 -24 < l < 24	-18 < h < 18 -18 < k < 15 -24 < l < 24	-18 < h < 18 -17 < k < 18 -23 < l < 23
Reflections collected	70583	55169	56861
Independent reflections	15920	15866	15846
Reflection [I>2σ(I)]	12697 (12710)	12432 (12827)	10279 (10872)
Data/restraints/parameters	15920 / 0 / 719 (15920 / 0 / 854)	15866 / 0 / 709 (15966 / 0 / 854)	15846 / 0 / 622 (15846 / 0 / 875)
Goodness of fit on F²	1.088 (1.058)	1.088 (1.042)	1.105 (0.988)
Final R indices [I>2σ(I)]	R ₁ = 0.0680 (0.0891) wR ₂ = 0.1995 (0.2353)	R ₁ = 0.0852 (0.1127) wR ₂ = 0.2290 (0.2853)	R ₁ = 0.0857 (0.1143) wR ₂ = 0.2219 (0.2866)
R indices (all data)	R ₁ = 0.0802 (0.1082) wR ₂ = 0.2210 (0.2568)	R ₁ = 0.1009 (0.1329) wR ₂ = 0.2418 (0.3035)	R ₁ = 0.1188 (0.1607) wR ₂ = 0.2413 (0.3248)
Largest diff peak and hole (e Å⁻³)	1.483 and -1.383 (2.209 and -1.730)	2.452 and -1.635 (4.816 and -1.559)	2.247 and -1.797 (3.434 and -1.857)

Table SIV.1 : Crystallographic data of compounds **D_{Cl}**, **D_{Br}** and **D_I**. Data presented are after squeeze treatment. Data before squeeze treatment are given in brackets.

IV-4 Photophysical study of metallacycles D_x

IV-4.1 Solid-state UV-visible absorption of compounds D_x

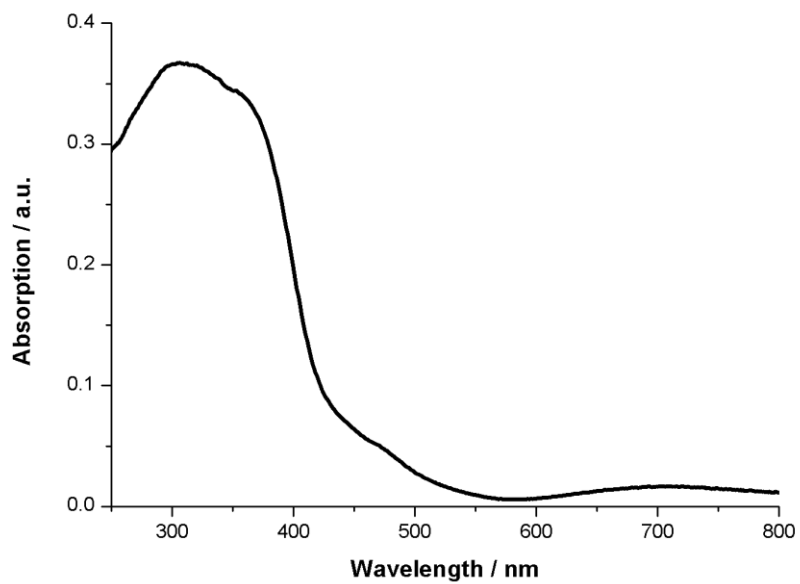


Figure SIV.7 : Solid-state UV-visible absorption spectrum of D_{Cl} .

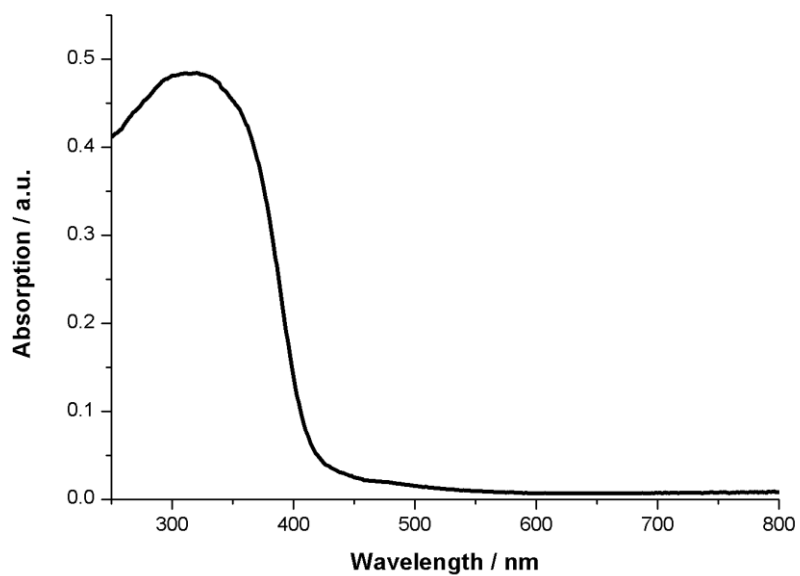


Figure SIV.8 : Solid-state UV-visible absorption spectrum of D_{Br} .

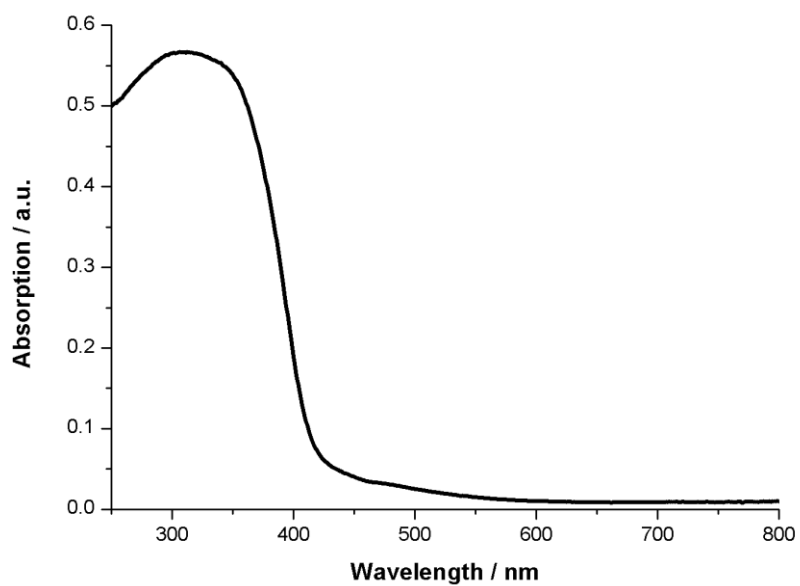


Figure SIV.9 : Solid-state UV-visible absorption spectrum of **D1**.

IV-4.2 Solid-state excitation spectrum of compounds **D_x**

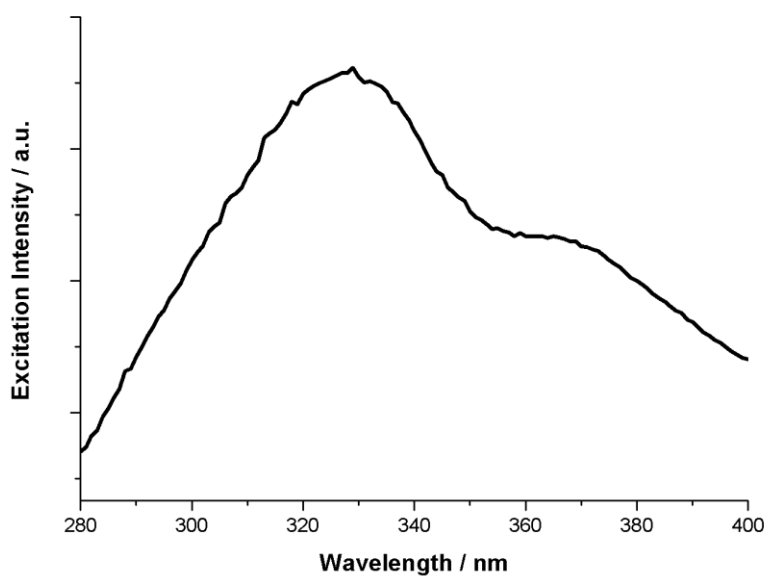


Figure SIV.10 : Solid-state room temperature excitation spectrum of **D1**.

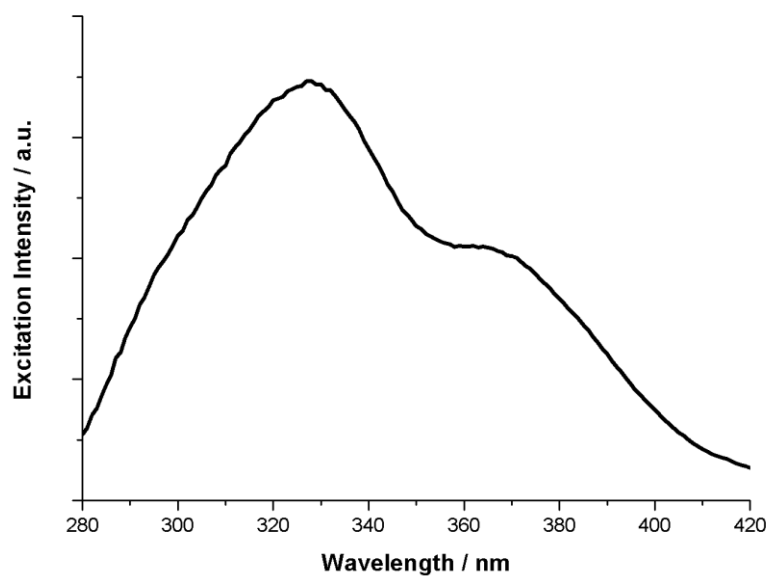


Figure SIV.11 : Solid-state room temperature excitation spectrum of **DBr**.

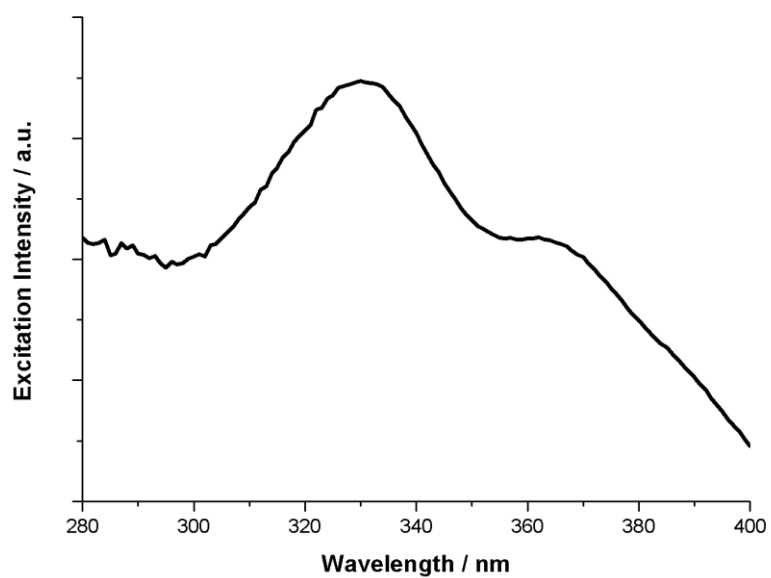


Figure SIV.12 : Solid-state room temperature excitation spectrum of **Df**.

IV-4.3 Solid-state temperature dependant emission spectra of compounds **D_x**

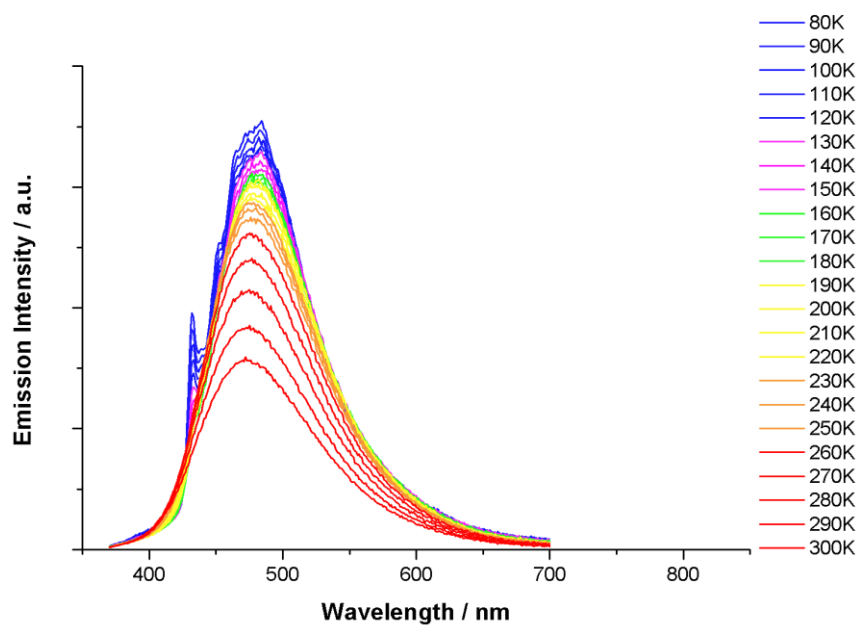


Figure SIV.13 : Temperature dependence of the emission spectrum of compound **D_{Cl}**.

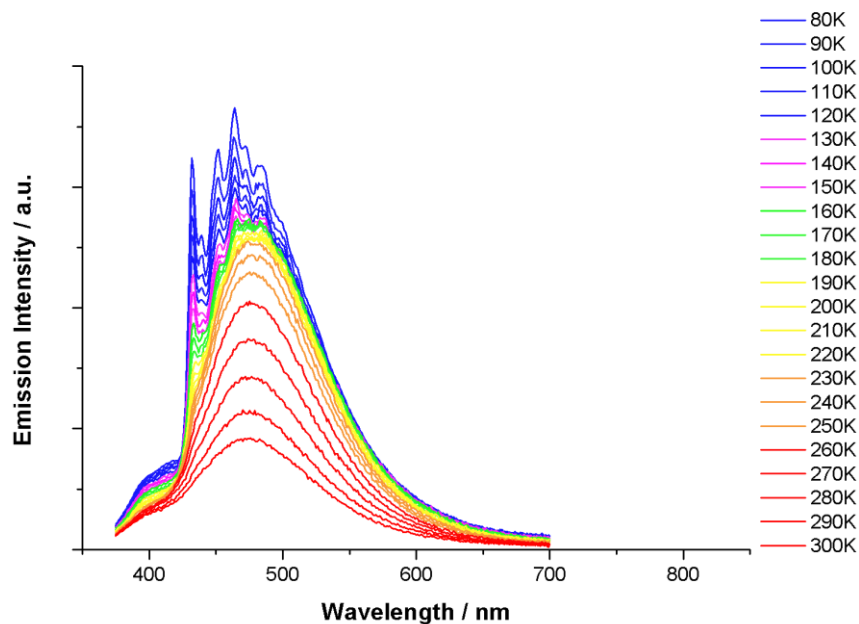


Figure SIV.14 : Temperature dependence of the emission spectrum of compound **D_{Br}**.

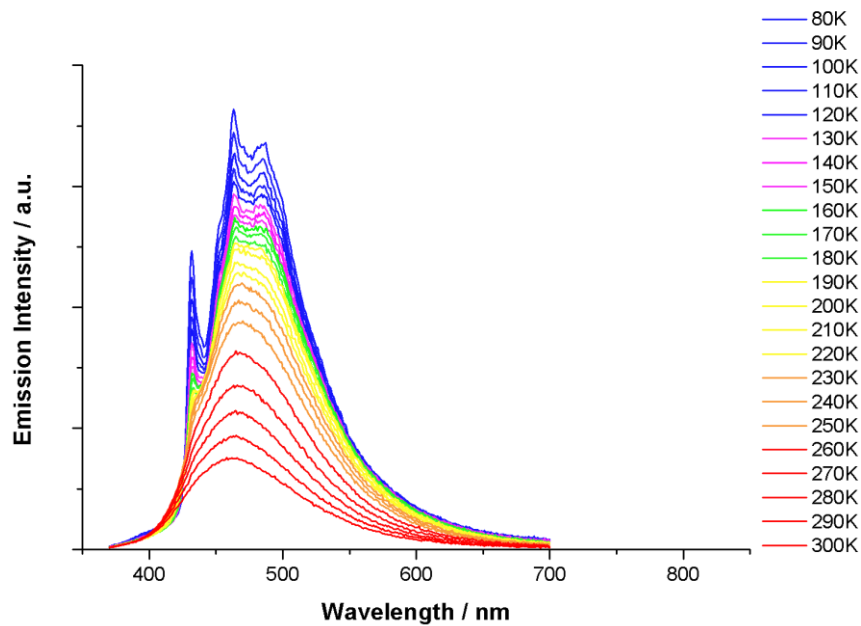


Figure SIV.15 : Temperature dependence of the emission spectrum of compound **D₁**.

IV-4.4 Temperature dependence of the decay times of the excited states of compounds **D_x**

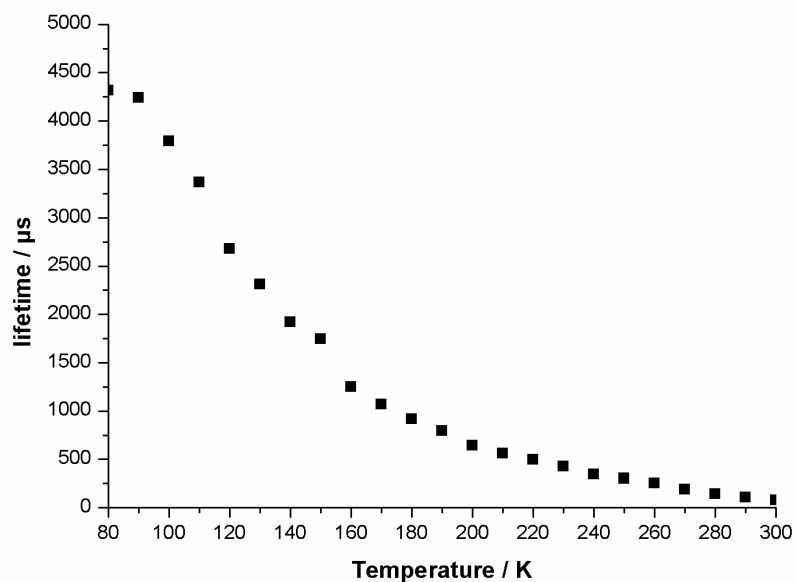


Figure SIV.16 : Variation of the lifetime of the excited state depending on the temperature of metallacycle **DCl**.

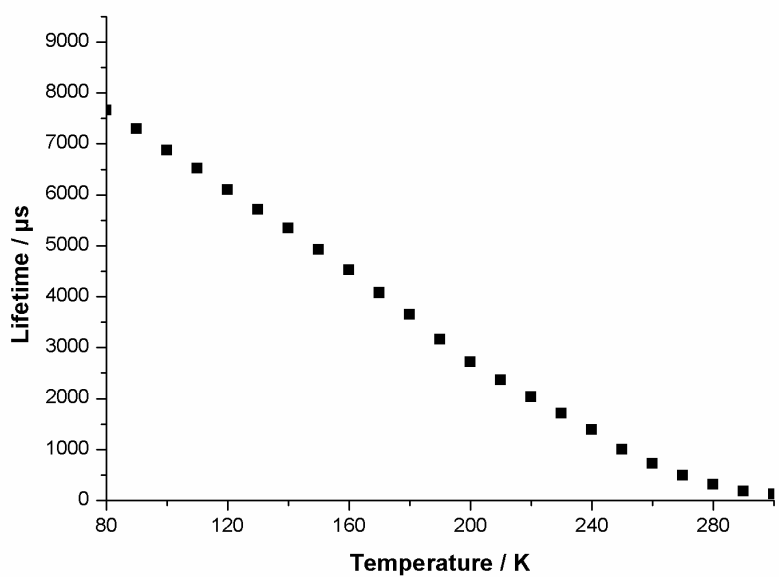


Figure SIV.17 : Variation of the lifetime of the excited state depending of the temperature of metallacycle D_{Br} .

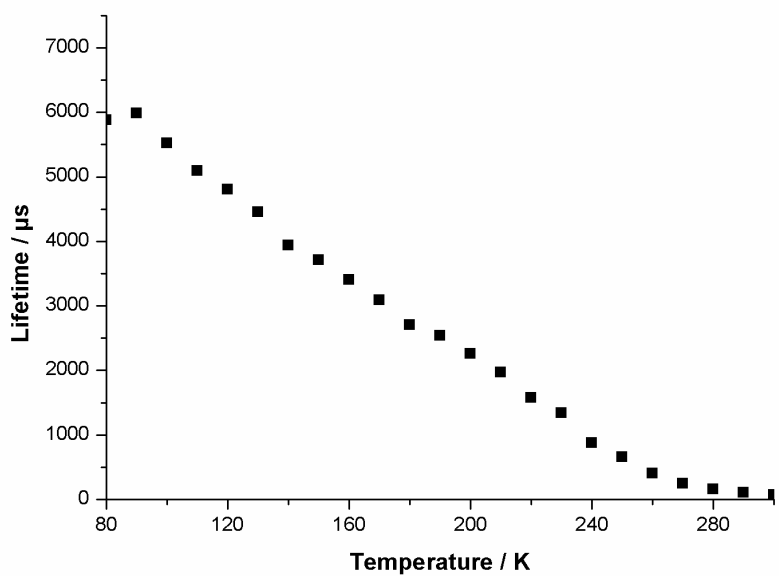


Figure SIV.18 : Variation of the lifetime of the excited state depending of the temperature of metallacycle D_f .

IV-5 TGA-DTA measurements performed on metallacycles D_x

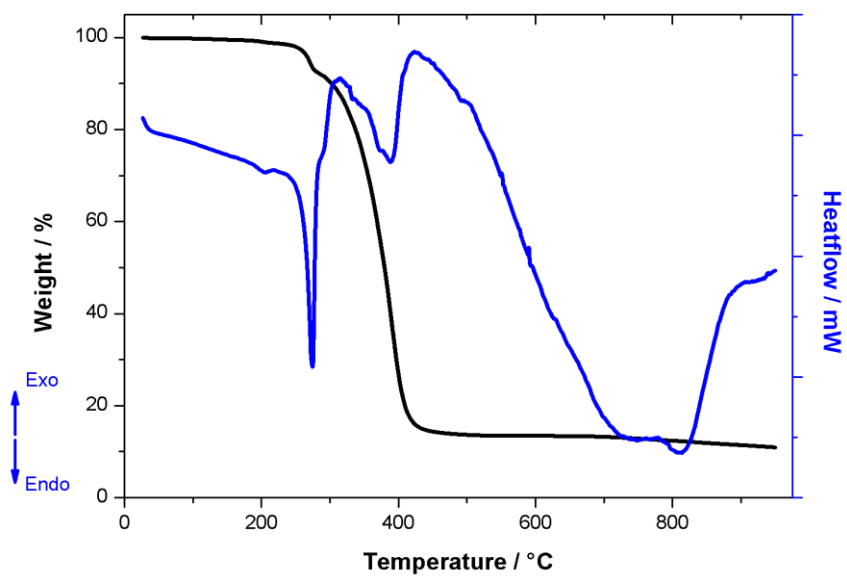


Figure SIV.19 : TGA-DTA analysis of compound D_{Cl1} until 950 °C.

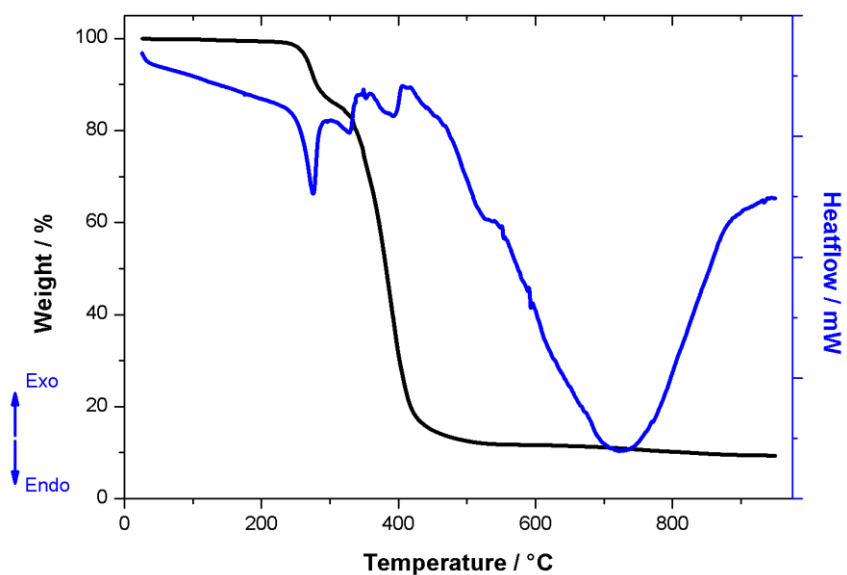


Figure SIV.20 : TGA-DTA analysis of compound D_{Br1} until 950 °C.

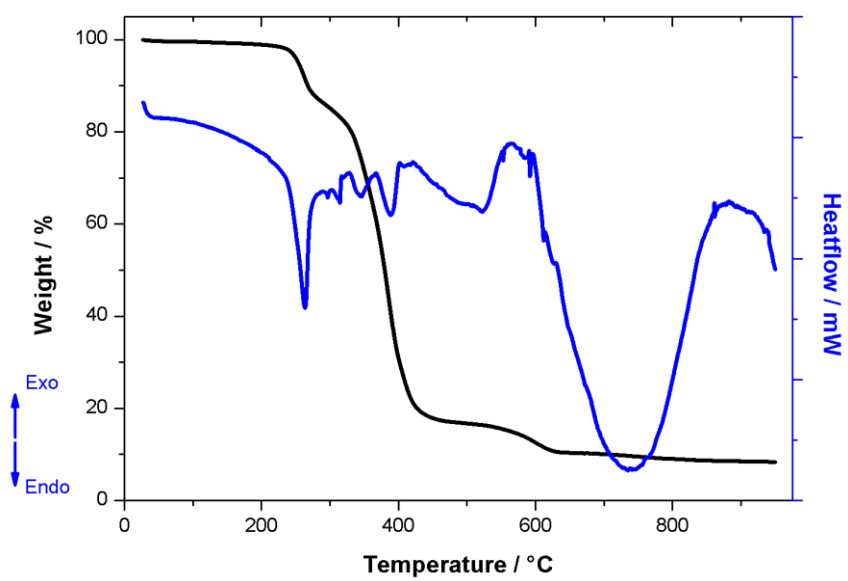


Figure SIV.21 : TGA-DTA analysis of compound **D_I** until 950 °C.

References :

1. Appel, R.; Geisler, K.; Schöler, H.-F., Über ein neues Darstellungsverfahren und eine ungewöhnliche Spaltung der Methylenbis(diorganylphosphane) durch Alkalimetalle. *Chem. Ber.* **1979**, *112* (2), 648-653.
2. Evariste, S.; Khalil, A. M.; Moussa, M. E.; Chan, A. K.-W.; Hong, E. Y.-H.; Wong, H.-L.; Le Guennic, B.; Calvez, G.; Costuas, K.; Yam, V. W.-W.; Lescop, C., Adaptive Coordination-Driven Supramolecular Syntheses toward New Polymetallic Cu(I) Luminescent Assemblies. *J. Am. Chem. Soc.* **2018**, *140* (39), 12521-12526.
3. Otwinowski, Z.; Minor, W., Processing of X-ray diffraction data collected in oscillation mode. In *Methods of Enzymology*, Carter, C. W.; Sweet, R. M., Eds. Academic Press: New York, 1997; Vol. 276, pp 307-326.
4. Altomare, A.; Burla, M. C.; Camalli, M.; Casciarano, G. L.; Giacovazzo, C.; Guagliardi, A.; Moliterni, A. G. G.; Polidori, G.; Spagna, R., SIR97: a new tool for crystal structure determination and refinement. *J. Appl. Crystallogr.* **1999**, *32*, 115-119.
5. Sheldrick, G. M. *SHELX97, Program for the Refinement of Crystal Structures*, University of Göttingen, Germany, 1997.
6. Spek, A. L., Single-crystal structure validation with the program *PLATON*. *J. Appl. Crystallogr.* **2003**, *36*, 7-13.
7. van der Sluis, P.; Spek, A. L., BYPASS: an effective method for the refinement of crystal structures containing disordered solvent regions. *Acta Crystallogr. A* **1990**, *A46* (194-201).

AVIS DU JURY SUR LA REPRODUCTION DE LA THESE SOUTENUE

Titre de la thèse:

New Supramolecular assemblies based on Cu(I) ion bearing and irreversible thermal transition of their solid state luminescence

Nom Prénom de l'auteur : MOUTIER FLORENT

Membres du jury :

- Monsieur KOSHEVOY Igor
- Madame PERRUCHAS Sandrine
- Monsieur LESCOP Christophe
- Monsieur SCHEER Manfred
- Madame COSTUAS Karine
- Monsieur CALVEZ Guillaume

Président du jury : *COSTUAS Karine*

Date de la soutenance : 23 Novembre 2022

Reproduction de la these soutenue

- Thèse pouvant être reproduite en l'état
 Thèse pouvant être reproduite après corrections suggérées

Fait à Rennes, le 23 Novembre 2022

Signature du président de jury

Le Directeur,


Vincent BRUNIE


K. COSTUAS

Titre : Nouveaux assemblages supramoléculaires de l'ion Cu(I) présentant une transition thermique irréversible de leurs propriétés de luminescence à l'état solide

Mots clés : Chimie supramoléculaire, polymères de coordination, matériaux luminescents, ion Cu(I)

Résumé : Les travaux de cette thèse s'inscrivent dans l'optique de la synthèse de nouveaux assemblages supramoléculaires luminescents en utilisant un précurseur à base d'ions Cu(I) et de fragments cyanure possédant des propriétés photophysiques attractives. La première partie de ces travaux concerne l'obtention de nouveaux polymères de coordination 1D en faisant réagir le précurseur avec des ligands polytopiques à terminaison pyridine, ainsi que l'étude approfondie de leurs propriétés photophysiques d'émission. La seconde partie de la thèse concerne l'obtention de nouveaux métallacycles supramoléculaires luminescents ne contenant pas de fragments cyanure au sein de leur structure moléculaire. Le premier chapitre sert d'introduction au cont-

exte dans lequel s'inscrit la thèse. Le chapitre II rend compte de l'obtention de sept nouveaux polymères de coordination luminescents qui présentent des propriétés photophysiques variées, attribuées à la présence de divers processus de relaxation radiative. L'étude de la stabilité thermique révèle la présence d'une transition thermique irréversible à haute température entraînant un changement drastique de leur luminescence. Les propriétés photophysiques de ces nouvelles phases, ainsi que la possibilité d'une régénération de l'une d'elle sont étudiées dans le chapitre III. Le chapitre IV rend compte de l'obtention de trois métallacycles tétramétalliques pontés par des ions halogénures et présentant une luminescence basée sur le ligand connecteur.

Title : New supramolecular assemblies based on Cu(I) ion bearing an irreversible thermal transition of their solid state luminescence

Keywords : Supramolecular chemistry, coordination polymers, luminescent materials, Cu(I) ion

Abstract : The work presented in this thesis is done in the context on the synthesis of new supramolecular luminescent assemblies using a Cu(I) ion based precursor bearing cyano moieties possessing attractive photophysical properties. The first part of this work deals with the obtention of new one-dimensional coordination polymers by the reaction of the precursor with pyridyl capped polytopic linkers and the thorough study of their luminescent properties. The second part of this work describes the obtention of new luminescent supramolecular metallacycles which do not possess a cyanide fragment in their molecular structure. The first chapter of this thesis serves as an introduction to the context of this work. In chapter II, the synthesis of seven new 1D coordination

polymers displaying various photophysical properties is discussed. The origin of such variety is attributed to the presence of different radiative relaxation processes despite the observed similarities of their molecular structure. The study of the thermal stability of these polymers reveals the presence of an irreversible thermal transition property leading to a drastic change of the luminescence at high temperature. The photophysical properties of these new transitioned phases and the possibility of the regeneration of one of those phases are studied in chapter III. Chapter IV reports the synthesis of three new tetrametallic metallacycles, bridged by halides ions and displaying a luminescence attributed to a connecting ligand centered origin of emission.